STUDIES ON ANIONIC GEMINI SURFACTANTS AS CORROSION INHIBITORS ON AZ31 MAGNESIUM ALLOY

Thesis

Submitted in partial fulfillment of the requirements for the degree of

DOCTOR OF PHILOSOPHY

By

GURURAJ ACHARYA M

DEPARTMENT OF CHEMISTRY

NATIONAL INSTITUTE OF TECHNOLOGY KARNATAKA

SURATHKAL, MANGALORE - 575 025

May, 2022

DECLARATION

I hereby *declare* that the Research Thesis entitled "**STUDIES ON ANIONIC GEMINI SURFACTANTS AS CORROSION INHIBITORS ON AZ31 MAGNESIUM ALLOY**" which is being submitted to the **National Institute of Technology Karnataka Surathkal,** in partial fulfillment of the requirements for the award of the Degree of **Doctor of Philosophy** in **Chemistry** is a *bonafide report of the research work carried out by me*. The material contained in this Research Thesis has not been submitted to any University or Institution for the award of any degree.

M. Gururaj

GURURAJ ACHARYA M
Register Number: 165012CY16F02
Department of Chemistry

Place: NITK - SURATHKAL
Date: 06/06/2022

CERTIFICATE

This is to *certify* that the Research Thesis entitled **"STUDIES ON ANIONIC GEMINI SURFACTANTS AS CORROSION INHIBITORS ON AZ31 MAGNESIUM ALLOY"** submitted by **GURURAJ ACHARYA M** (Register Number: 165012CY16F02) as the record of the research work carried out by him, is *accepted as the Research Thesis submission* in partial fulfillment of the requirements for the award of degree of **Doctor of Philosophy.**

Dr. A. Nityananda Shetty

Research Guide

06/06/2022

Chairman – DRPC

HEAD, DEPARTMENT OF CHEMISTRY
National Institute of Technology Karnataka
Surathkal, Srinivasnagar
MANGALORE - 575 025, D.K.

ACKNOWLEDGEMENT

I will bring my deepest thank to my advisor **Dr. Adka Nityananda Shetty**, Department of Chemistry, NITK, who supported me over years to pursue a Ph.D. degree in Corrosion Lab, NITK. He would like to use all his patience, knowledge without reservations to me, to allow me to become a knowledgeable person in aqueous corrosion in these five years. I would like to also thank my RPAC members **Dr. Sib Sankar Mal** and **Dr. Shashi Bhushan Arya** who continuously gave suggestions and improvements on my research through my progress meetings.

I am grateful to **Dr. Udaya Kumar Dalimba**, Head, Department of Chemistry, National Institute of Technology Karnataka, Surathkal for providing me with the required experimental facilities of the department. I am thankful to the faculty of the Department of Chemistry, National Institute of Technology Karnataka, Surathkal, **Dr. A. C. Hegde**, **Dr. B. R. Bhat, Dr. D. K. Bhat**, **Dr. A. M. Isloor**, **Dr. D. R. Trivedi**, **Dr. Beneesh P. B**, **Dr. D. Chakraborty**, **Dr. Saikat Dutta, Dr. Vijayendra Shetti and Dr. Lakshmi** for their support.

I will bring my special thanks to **Dr. V. Aranganathan,** and **Dr. Kavyashree Keremane** for their support in my research. I also would like to thank **Dr. K. Ramesh,** Dept. of Chemistry, IITH, **Dr. Keyur Raval,** and **Mrs. Priyanka Bhat,** Dept of Chemical Engineering, for helping me in characterizations.

It is a pleasure to thank my fellow research scholars, **Dr. Prakashaiah B G** and **Dr. Sudarshan Shetty,** and all others for making my stay at NITK during research a memorable one. I would like to thank all the **non-teaching staff**, Department of Chemistry NITK, for their assistance in the laboratory.

Finally, I would like to thank my parents **Shri M. R. Acharya** and **Smt. Mohini**, my sister **Mrs. Shwetha** and all my teachers for their immense support throughout my life. Your understanding allows me to focus on my personal and professional life. I would also like to thank my professors from my college. I Thank the supreme who kept me on the right path and showered blessings all the way.

GURURAJ ACHARYA M

ABSTRACT

The magnesium alloys are considered to be the best structural materials, because of their advantageous strength to weight ratio. But, the limitation in their real field applications lies in the fact that magnesium alloys are highly susceptible for corrosion. Hence understanding the corrosion of AZ31 alloy and developing the measures to combat the same are crucial.

In the present studies, the corrosion behaviour of AZ31 alloy was investigated by electrochemical methods in sodium chloride and sodium sulphate media of different concentrations at different temperatures and followed by its inhibition studies. The corrosion rate was monitored by potentiodynamic polarization technique and electrochemical impedance spectroscopy along with SEM-EDX, and XPS. The synthesized inhibitors were subjected to theoretical studies as well. The blank corrosion studies were performed at various medium concentrations, pH and temperatures. The results revealed a trend of higher corrosion rate associated with higher medium concentration, lower pH and higher temperature.

Five different long chain anionic Gemini surfactants namely, DB, DH, DO, DC and DD were synthesized and tested as corrosion inhibitors for AZ31 alloy. The calculated activation and thermodynamic parameters have been recorded in the thesis. The inhibitors were predominantly physisorbed with partial chemisorption. The adsorption of the surfactant on the surface of AZ31 alloy obeyed Langmuir adsorption isotherm. The studied surfactants were found to function as mixed-type inhibitors. The surfactants were more efficient at lower temperatures. The efficiencies of the surfactants decreased in the order: DD>DC>DO>DH>DB and this has been accredited to the reduction of chain length. The proposed mechanism attributed the cathodic inhibition to the blockage of the reaction spots by chemisorbed acetates. The anodic inhibition resulted from the compaction of porous film by precipitated magnesium-inhibitor salts.

Keywords: AZ31 alloy, Corrosion, Inhibitor, Anionic Gemini surfactant, Impedance.

CONTENTS

Page No.

LIST OF FIGURES

LIST OF TABLES

NOMENCLATURE

Abbreviations	**Nomenclature**
CPE	Constant phase element
DC	Direct Current
EDTA	Ethylenediamine tetraacetic acid
EDX	Electron dispersive x-ray analysis
EIS	Electrochemical impedance spectroscopy
EW	Equivalent weight of the corroding material
Fig	Figure
HF	High frequency
LF	Low frequency
MF	Medium frequency
OCP	Open circuit potential
SCC	Stress Corrosion Cracking
SCE	Saturated calomel electrode
SEM	Scanning electron microscopy
DB	Sodium 2,2'-(5,14-dibutyl-6,13-dioxo-5,8,11,14-tetraazaoctadecane-8,11-diyl)diacetate
DH	Sodium 2,2'-(7,16-dihexyl-8,15-dioxo-7,10,13,16-tetraazadocosane-10,13-diyl)diacetate
DO	Sodium 2,2’-(9,18-dioctyl-10,17-dioxo-9,12,15,18-tetraazahexacosane-12,15-diyl)diacetate
DC	Sodium 2,2’-(11,20-didecyl-12,19-dioxo-11,14,17,20-tetraazatriacontane-14,17-diyl)diacetate
DD	Sodium 2,2’-(13,22-didodecyl-14,21-dioxo-11,14,17,20-tetraazatetratriacontane-16,19-diyl)diacetate
XPS	X-ray photoelectron spectroscopy

LIST OF SYMBOLS

Symbol	Definition
T	Absolute temperature
E_a	Activation energy
ω	Angular frequency
N	Avagadro's number
W_i	Atomic weight of the i^{th} element in the alloy
β_c	Cathodic Tafel slope
R_{ct}	Charge transfer resistance
C_{inh}	Concentration of the inhibitor
Y_0	Constant phase element constant
B	Constant
K	Constant
i_{corr}	Corrosion current density
$i_{corr(inh)}$	Corrosion current density in the presence of inhibitor
E_{corr}	Corrosion potential
υ_{corr}	Corrosion rate
ρ	Density of the corroding material
C_{dl}	Double layer capacitance
E_0	Electrode potential for zero current at equilibrium
$\Delta H^{\#}$	Enthalpy of activation
$\Delta S^{\#}$	Entropy of activation
i_o	Exchange current density
R_f	Film resistance
F	Faraday constant
ΔG	Free energy change
ω_{max}	Frequency at which imaginary part of the impedance has a maximum
R	Gas constant
Z''	Imaginary part impedance
Z_{mod}	Impedance modulus
η	Inhibition efficiency
R^2	Linear regression coefficient
ε	Local dielectric constant
f_i	Mass fraction of the i^{th} element in the alloy
n	Number of electrons in a reaction
χ	Number of water molecules replaced per molecule of adsorbed inhibitor
R_{hf}	Overall resistance associated with higher frequency capacitive loop

$R_{hf(b)}$	Overall resistance associated with higher frequency capacitive loop in the absence of the inhibitor
$R_{hf(inh)}$	Overall resistance associated with higher frequency capacitive loop in the presence of the inhibitor
θ_{max}	Phase maximum
φ	Phase shift
h	Plank's constant
R_p	Polarization resistance
Z'	Real part of impedance
R_{dif}	Resistance associated with electrolyte diffusion
E^0	Rest potential
ΔH^0_{ads}	Standard enthalpy of adsorption
ΔS^0_{ads}	Standard entropy of adsorption
R_s	Solution resistance
θ	Surface coverage
d	Thickness of the film
t	Time
n_i	Valence of the i^{th} element of the alloy

CHAPTER-1

INTRODUCTION

CHAPTER 1

INTRODUCTION

Corrosion is the disastrous attack on a metal by its surroundings through a chemical or electrochemical reaction. About one-quarter of the world's annual steel production is destroyed by corrosion. On certain occasions, the chemical attack goes with physical weakening, as depicted by the accompanying terms: errosion-corrosion, corrosive wear, or fretting corrosion. Few insist that the statement must be restricted to metals, but many corrosion engineers had considered both metals and non-metals for the solution of a given problem. Non-metals are not considered for this definition of corrosion. Plastics may expand or crack, wood may split or decay, stones may erode, and Portland concrete may spoil away, yet the term corrosion, here, is confined to chemical substances attacking metals. For example, iron railroad tracks show little less rusting over the years than 18-8 stainless steel that is badly attacked in hours by polythionic acid (Sastri 1998).

Although many other metals form their oxides when corrosion occurs, corrosion of iron or iron-based alloys, with their corrosion products, largely of hydrous ferric oxides is called "rusting".

The three main bases for the significance of corrosion are economics, safety, and conservation. In order to suppress the impact of corrosion, scientists aim to reduce material losses, as well as the go with economic losses, that result from the corrosion of metallic materials and installations such as pipings, tanks, metal components of machines, ships, bridges, marine structures, and so on.

Indirect losses are highly laborious to assess, yet, the direct losses such as replacing corroded structures and machinery or their components, such as condenser tubes, mufflers, pipelines, and metal roofing, including the necessary labor cost amount to a large amount of money. Examples of indirect losses are shutdown, loss of product, loss of efficiency, and contamination of products. Another important concern is the world's supply of metal resources. The rapid industrializations of many countries indicate that the competition for the price of metal resources will increase. Due to corrosion, useful metal properties such as malleability, ductility, electrical conductivity, and also surface appearance are lost (Fontana 2005).

1.1 DAMAGE DUE TO CORROSION

A few of the major effects of corrosion are listed below. However, corrosion is desirable in some cases. For example, aircraft and other machines use chemical milling and chemical machining. Excess metal is dissolved for an uncovered surface that is been exposed to acids. This process is economical and is used when the conventional method cannot be reached to some parts of the machine.

- **Appearance**: The automobile vehicles are painted for better appearance and rust-free surfaces. Machines corrode and badly get rusted when equipments are kept in a plant over the years, and that would showcase poor impression on the observer.
- **Maintenance and operating costs**: Substantial savings can be made in many types of industrial plants through the use of corrosion-resistant materials of construction. One example is the waste acid recovery plant operated for several months was stopped until a serious corrosion problem was solved. The application of cathodic protection can reduce corrosion rates in existing underground pipelines.
- **Plant shutdowns**: Frequently plants are shut down or part of a process in an industry is stopped because of unexpected corrosion failures. Sometimes these shutdowns are caused by corrosion that involves no change in process conditions, but occasionally they are caused by changes in operating procedures erroneously regarded as incapable of increasing the severity of the corrosive conditions. For example, to increase the production of a chemical compound, a company decided to lower the temperature of the cooling medium in a heat-exchanger system and the time required per batch decreased. But, induced higher stresses in the metal. Stress corrosion cracking (SCC) of the vessels occurred quickly, and the plant was shut down with production delayed for some time.

  Corrosion monitoring of an industrial plant process helps prevent unexpected plant shutdown.

- **Contamination of product**: In many case studies, the price of the product is directly related to its purity and quality. Free from contamination is an important factor in the manufacture and handling of transparent plastics, dyes, foods, drugs, and semiconductors. One of the examples in this case is manufacture and transporting of concentrated hydrogen peroxide or hydrazine in which case, a very small amount of corrosion, which introduces certain metal ions into the solution, may cause catalytic decomposition of the product.
- **Loss of valuable products**: No particular concern is attached if slight leakage of acid to the drainage system, but the loss of material in huge amount requires immediate corrective action. Slight losses of uranium compounds or solutions are hazardous and can be very costly. In such cases, utilization of more expensive designs and better materials of construction are well warranted.
- **Effects on safety and reliability**: The handling of toxic materials such as HF, radioactive substances, and chemicals at high temperatures and pressures demands the use of construction materials that minimize corrosion failures. Stress corrosion of a metal wall separating the fuel and oxidizer in a missile could cause premature mixing, which could result in a loss of a huge amount of money.

  Corrosion plays a vital part in medical metals used by orthopedics, such as hip joints, screws, plates, and heart valves. Reliability is, of course, of paramount importance here (Fontana 2005) (Uhlig 2011).

1.2 ELECTROCHEMICAL THEORY OF CORROSION

As per this hypothesis, corrosion of metals take place due to the formation of anodic and cathodic regions on the same metal surface or when two different metals are in contact with one another in the presence of a conducting medium. At the anodic region, the metal undergoes oxidation, forming the oxidized product and liberating electrons. At the cathodic area, a reduction reaction takes place. The constituents of the corrosion medium undergo reduction at the cathode. The oxidation reaction at the anodic region and the reduction reaction at the cathodic region must continue simultaneously at the same rate to maintain electroneutrality. The electrons generated by the anodic reactions migrate to the cathodic region, constituting the corrosion current and the electrons are consumed in the cathodic process. The metal ions formed at the anode and the anions formed at the cathode diffuse towards each other through the conducting medium and form a corrosion product somewhere in between the anode and the cathode (Fontana 2005).

Corrosion reactions

At the anodic region: The metal that gets converted into ions with the liberation of electrons.

$$\mathrm{M} \rightarrow M^{n+} + n^{e-} \tag{1.1}$$

At the cathodic region**:** Depending on the nature of the corrosion medium/environment the following reactions may take place at the cathode.

1. Hydrogen evolution**:** $2H^{+} + 2e^{-} \rightarrow H_2 \uparrow$ (1.2)
2. Hydrogen evolution in neutral**:** $2H_2O + 2e^{-} \rightarrow 2OH^{-} + H_2 \uparrow$ (1.3)
3. Oxygen reduction (acid solutions): $O_2 + 4H^{+} + 4e^{-} \rightarrow 2H_2O$ (1.4)
4. Oxygen reduction (neutral or basic solutions): $O_2 + 2H_2O + 4e^{-} \rightarrow 2H_2O$(1.5)
5. Metal ion reduction: $M^{3+} + e^{-} \rightarrow M^{2+}$ (1.6)

1.3 CLASSIFICATION OF CORROSION

The corrosion process can be classified based on various perspectives. Based on the temperature conditions at which the corrosion takes place, it is distinguished as low-temperature and high-temperature corrosion. Another classification is a direct chemical attack and electrochemical corrosion. They are also known as dry corrosion and wet corrosion, respectively, as they take place in the absence and presence of moisture or conducting medium (Fontana 2005).

1.3.1 Forms of corrosion

Based on the appearance of the corroded surface by visual examination, the different types of corrosion have been classified into eight types. The eight types are as follows (Fontana 2005):

1.3.1.1 Uniform attack

Uniform corrosion is a loss of material distributed uniformly over the entire surface exposed to the corrosive environment. Metals in contact with strong acids are sometimes subjected to uniform corrosion. The material becomes thinner and breaks eventually. For example, a sheet-iron roof will show essentially the same degree of rusting over its entire outside surface. It is also called general overall corrosion, represents the greatest destruction of metal on a large basis.

1.3.1.2 Crevice corrosion

It is caused by a difference in oxygen availability between two sites on a passive metal that leads to the formation of an electrochemical cell. A selective attack within cracks and at other sites of poor oxygen access is frequently observed.

The most common is oxygen differential aeration corrosion. This occurs when the oxygen supply is less in crevice than on the surface layer. In lower oxygen levels, it forms an anode. The metal surface that is exposed to air moisture forms a cathode.

1.3.1.3 Filliform corrosion

It is a special type of crevice corrosion, occuring under protective films, and for this reason, it is often referred to as filliform corrosion. An example of this type of corrosion is the attack of enameled or lacquered surfaces of food and beverage cans that have been exposed to the atmosphere. Filliform corrosion is an unusual type of attack, since it does not weaken or destroy metallic components but only affects surface appearance.

1.3.1.4 Pitting corrosion

It is observed on passive metals in presence of certain anions (in particular chloride) when the potential exceeds a critical value. This process typically produces cavities with diameters on the order of several tens of micrometers. Pitting is a form of extremely localized attack that results in holes in the metal. These holes may be small or large in diameter, but in most cases, they are relatively small. Pits are sometimes isolated or so close together that they look like a rough surface. Pitting is particularly vicious because it is a localized and intense form of corrosion, and failures often occur with extreme suddenness. For example, iron buried in the soil corrodes with the formation of shallow pits, whereas stainless steels immersed in seawater characteristically corrode with the formation of deep pits.

1.3.1.5 Intergranular corrosion

Intergranular corrosion is a selective attack of grain boundaries. Often, it is related to thermal treatments that lead to preferred precipitation of phases at grain boundaries. The alloy disintegrates (grain fall out) and/or loses its strength. It can be caused by impurities at the grain boundaries, enrichment of one of the alloying elements, or depletion of one of these elements in the grain-boundary area.

1.3.1.6 Errosion corrosion

It is the result of an electrochemical reaction combined with a material loss by mechanical wear due to the impingement of solids or a fluid. The increase in the rate of depletion or attack on material because of relative movement between a corrosive fluid and the metal surface is called errosion corrosion. Usually, this movement is very fast, and abrasion is involved. Metal is removed from the surface as dissolved ions. Erosion corrosion is characterized in appearance by grooves, gullies, waves, and valleys and usually exhibits a directional pattern.

1.3.1.7 Stress corrosion

It results from the combined action of corrosion and of mechanical stress. It manifests itself by crack formation at stress levels well below the ultimate tensile strength of a material. During stress-corrosion cracking, the metal or alloy is virtually unattacked over most of its surface, while fine cracks progress through it. This cracking phenomenon can have serious consequences since it can occur at stresses within the range of typical design stress.

1.3.1.8 Hydrogen damage

Hydrogen can cause several corrosion problems. Hydrogen embrittlement is a problem with high-strength steels, titanium, and some other metals. Hydrogen blistering can occur when hydrogen enters steel as a result of the reduction reaction on a metal cathode. Single-atom nascent hydrogen atoms then diffuse through the metal until they meet with another atom, usually at inclusions or defects in the metal. The resultant diatomic hydrogen molecules are then too big to migrate and become trapped.

Hydrogen blistering is not restricted to installations containing high-pressure hydrogen gas. A corrosion reaction involving the reduction of protons, for example during pickling of steel, can also be responsible for this type of damage (Sastri 1998).

1.4 FACTORS INFLUENCING CORROSION RATE

Numerous factors impact the rate of corrosion. These factors are classified into two main groups, as related to the nature of the metal, and the nature of the environment or corrosion medium (Gadag and Shetty 2010).

1.4.1 Nature of the metal

The nature of a metal or an alloy significantly influences the corrosion rate, irrespective of the corrosion medium. Some of the properties of the metal, which potentially influence the mechanism as well as the corrosion rate are explained below.

1.4.1.1 Purity of the metal

A pure metal is safer against corrosion than its alloy which is a commercial counterpart. Yet, the metals of most elevated virtues are costly and precisely weak, confining their utilization. During the production and when they are subjected to different metallurgical processes to enhance their properties, they develop inhomogeneities in them. These may include the formation of inclusions, different crystallographic orientations, grain and grain boundaries, different phases, scatches, etc. These changes will initiate and stimulate the corrosion.

1.4.1.2 Electrode potential of metal

The standard electrode potential is the benchmark to decide the tendency of a metal to undergo corrosion. The metal with lower electrode potential is more susceptible for corrosion than a noble metal with a higher electrode potential. Thus, metals like magnesium and zinc with lower electrode potential are less resistant to corrosion than noble metals like platinum and gold with high electrode potential. But there are exceptions to this pattern as seen with metals like aluminium, because of surface passivation. The coupling of two metals with a small difference in their electrode potentials will minimize the risk of corrosion.

1.4.1.3 Hydrogen overvoltage on the metal surface

The metal with lower hydrogen overvoltage on its surface is more susceptible to corrosion when the cathodic reaction which is an evolution of hydrogen gas. Lower hydrogen overvoltage facilitates the easy release of hydrogen gas. Consequently, cathodic reaction becomes faster, which, in turn makes the anodic reaction faster. The higher the hydrogen overvoltage lesser is the corrosion rate.

1.4.1.4 Relative areas of the anodic and cathodic region

The rate of corrosion is impacted by the relative areas of the cathodic and anodic regions. If a small anodic region is in contact with a large cathodic region, then the electrons are consumed at a faster rate at the cathodic region, forcing the anodic dissolution of the metal to proceed with the maximum optimum rate and thus increasing the corrosion rate.

1.4.1.5 Nature of the corrosion product

The nature of the corrosion product formed on the surface decides whether the rate of corrosion is high or low. The corrosion product formed like metal oxide may act as a protective film. If the oxide layer, which forms on the surface, is highly insoluble and non-porous in nature with low ionic and electronic conductivity, then that type of products layer effectively prevents further corrosion, by acting as a barrier between the metal surface and corrosion medium. On the other hand, if the corrosion product is unstable, porous, and soluble, it increases corrosion.

1.4.2 Environmental factors

The nature of the corrosive medium has an equivalent effect on the rate of metal corrosion as that of the nature of metal. Some of the environmental factors which have a significant effect on the corrosion rate are explained below.

1.4.2.1 Temperature

Corrosion rate increases with an increase in the temperature of the corrosion medium. This is because of the increase in the conductance of the medium with the increase in temperature.

1.4.2.2 pH of medium studies

The pH of the medium influences the rate of cathodic reaction by affecting the availability of H^+ ions for the cathodic reactions. Therefore, a decrease in pH increases the rate of corrosion. Amphoteric metals such as aluminium, lead, and zinc are the exceptions, which undergo significant corrosion at higher pH values of the medium also.

1.4.2.3 Humidity

It is observed that corrosion rate increases with an increase in humidity of the environment. The presence of moisture provides conducting medium for the formation of a galvanic cell, thus facilitating corrosion of metal.

1.4.2.4 Presence of impurities

The presence of certain impurities in the environment increases the corrosiveness of the medium. For instance, pollutants like SO_2 combine with the dampness in the condition, forming sulphuric acid. Increased acidity brings about a rise in the corrosion rate of the metals.

1.4.2.5 Electrical conductivity of medium

Corrosion rate increases with the increase in the conductivity of the medium. Higher the conductivity quicker will be the movement of ions between the cathodic and anodic regions, increasing the rate of corrosion. It is because of the higher electrical conductivity that ocean water is more corrosive than freshwater.

1.4.2.6 Presence of oxygen and oxidizers

It is seen that the effect of oxidizer additions or the presence of oxygen on corrosion rate depends on both the medium and the metal involved in the system. The corrosion rate may be increased by the addition of oxidizers, oxidizers may not affect the corrosion rate, or a very complex behavior may be observed.

Knowing the basic characteristics of a metal/metal alloy and the medium to which it is exposed, it is possible to predict in many instances the effect of oxidizer additions.

1.4.2.7 Effect of velocity

The effects of velocity on corrosion rate are, like the effects of oxidizer additions, complex and depend on the characteristics of the metal and the environment to which it is exposed. For corrosion processes that are controlled by activation polarization, agitation and velocity do not affect the corrosion rate. If the corrosion process is under cathodic diffusion control, then agitation increases the corrosion rate.

1.4.2.8 Effect of Concentration of medium

Many materials that exhibit passivity effects are only negligible affected by wide changes in corrosive concentration. Similarly, few other materials show the same behavior except that at very high corrosive concentrations, the corrosion rate increases rapidly.

1.4.2.9 Polarization of anodic and cathodic regions

Polarization of cathode or anode decreases the rate of corrosion. If anodic polarization takes place, the tendency of the metal to undergo oxidation decreases, decreasing the rate of corrosion. Anodic polarization results from the accumulation of metal ions formed at the anode and/or due to the passivation of the anode surface. Cathodic polarization is either due to the activation polarization or due to the concentration polarization resulting from the decelerated diffusion of cathodic reactants.

1.5 THERMODYNAMICS OF CORROSION

Thermodynamics, the science of energy change, has been widely applied to corrosion studies for many years. Below, the principles applicable to corrosion phenomena and their limitations are reviewed (Sastri 1998).

1.5.1 Concept of free energy

The free-energy change accompanying an electrochemical reaction can be calculated by the following equation:

$$\Delta G = -nFE \qquad (1.7)$$

where ΔG is the free-energy change, n is the number of electrons involved in the reaction, F is the Faraday constant, and E is the cell potential.

Therefore, for a given corrosion reaction to take place, the cell potential should be positive. The cell potential is taken as the difference between the potentials of two half-cell reactions. Assuming hydrogen evolution as a reaction at the cathode, the following relations are obtained.

$$E_{cell} = E\left(\frac{H^+}{H_2}\right) - E(M^{n+}/M) \tag{1.8}$$

It follows that metals with negative standard electrode potential, electrochemical cell potential will be positive and thus the process of corrosion occurs (ΔG= -ve). Corrosion will not occur unless the reaction of metal oxidation (anodic metal dissolution) is spontaneous.

1.5.2 Application of thermodynamics to corrosion

The applications of thermodynamics to corrosion phenomena have been further generalized using potential-pH plots. These are frequently called Pourbaix diagrams, after M. Pourbaix who first suggested their use (Pourbaix 1974).

The main uses of these diagrams are (1) predicting the spontaneous direction of reactions, (2) estimating the composition of corrosion products, and (3) predicting the environmental changes that will prevent or reduce corrosive attacks.

The Pourbaix diagram for the pure magnesium-water system at 25 °C is shown in Fig. 1.1 (Pourbaix 1974). As shown by the diagram, magnesium is susceptible to corrosion under potentials more positive than - 2.37 V (E° of magnesium) and pH below 10.5. A narrow corrosion immune region exists at potentials more negative than the standard electrode potential of magnesium. The passive region exists at highly alkaline conditions (pH>10.5), which favor the formation of magnesium hydroxide precipitation.

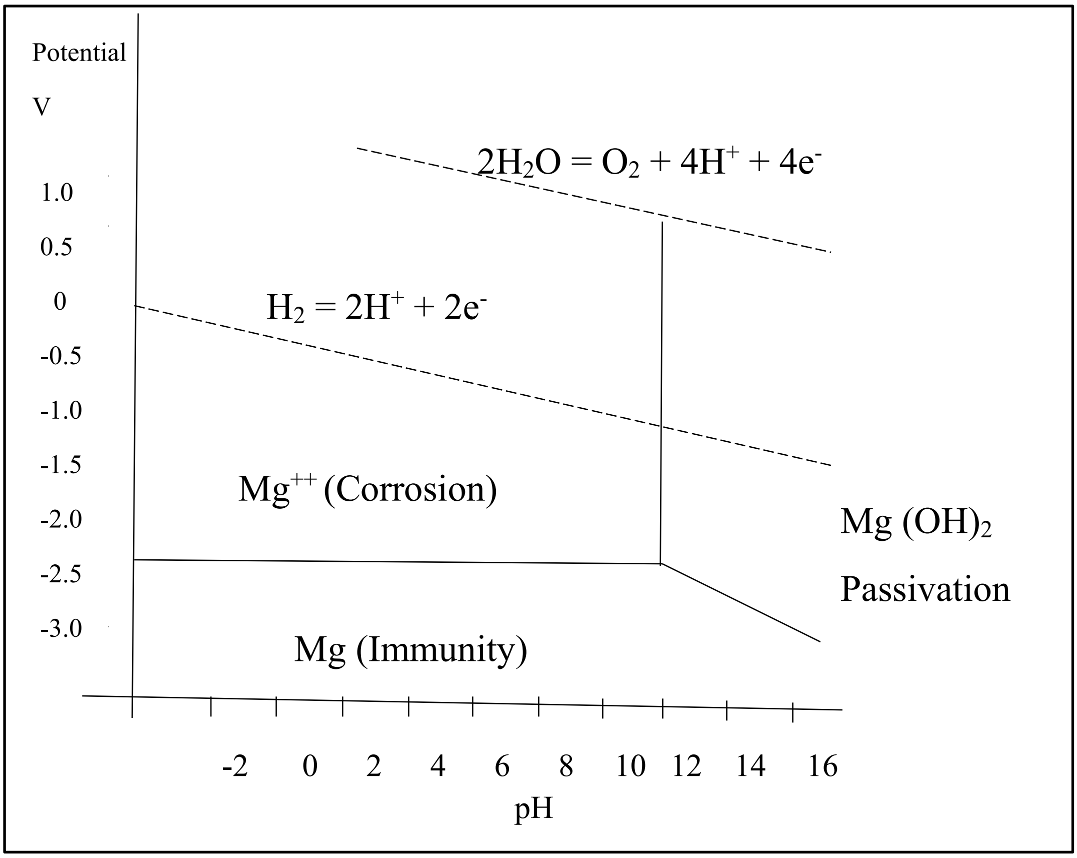

Fig. 1.1: Pourbaix diagram of magnesium and water system at 25 °C, showing the theoretical domains of corrosion, immunity, and passivation (Pourbaix 1974).

1.6 CORROSION KINETICS

Corrosion kinetics deals with the rate of the corrosion reaction, which in turn is dependent on the rate of the reactions taking place at the anodic and cathodic regions. The kinetics of the reaction taking place on the electrode surface is dependent on the electrode potential. Thus, electrode kinetics is the investigation of reaction rates at the interface between an electrode and a fluid. The study of electrode kinetics has made conceivable advances in the perception of corrosion and the functional estimation of corrosion rates. The understanding of corrosion, forms by superimposing electrochemical fractional procedures was created by Wagner and Traud (Tsai et al. 1998). Some of the significant factors related with the electrode kinetics are presented in this part.

1.6.1 Polarization

Electrode polarization can be defined as the extent of deviation of electrode potential from equilibrium value, resulting from a net current flowing from or to the electrode surface. An electrochemical reaction is said to be polarized when the reaction is retarded by chemical, physical or environmental factors. Hence polarization is also referred to as reaction inertia. Electrode polarization reduces the overall potential difference between two half cells. Hence decreases the electrochemical corrosion. The degree of polarization is called overvoltage or overpotential given by the following equation:

$$Overvoltage = E - E_0 \tag{1.9}$$

where E is the electrode potential for some condition of current flow and E_0 is the electrode potential for zero current flow at equilibrium (also termed as the open circuit potential (OCP), corrosion potential, rest potential).

Depolarizers added to the corrosion medium increase corrosion rate. Chelating ligands act as anodic depolarizers and oxidizers like ferric ions or O_2 act as cathodic depolarizers (McCafferty 2010).

1.6.1.1 Activation polarization

Activation polarization usually is the controlling factor during corrosion in a media that contains a high concentration of active species. Activation polarization refers to an electrochemical process that is controlled by the slowest step of the reaction sequence taking place at the metal-electrolyte interface. In other words, activation polarization is caused by a slow reaction of the electrode because the reaction at the electrode requires activation energy. Both anodic and cathodic reactions can be under activation polarization. A reaction for which an activation polarization predominates is referred to as 'activation controlled'.

1.6.1.2 Concentration polarization

Concentration polarization refers to an electrochemical process controlled by the diffusion in the electrolyte bulk rather than at the interface. Concentration polarization is said to be cathodic when the electrons accumulate at the cathodic interface due to the slow diffusion of the reducing species from the bulk electrolyte to the cathode surface. Anodic polarization arises due to the slow diffusion of metal ions from the anodic interface into the bulk electrolyte. Cathodic concentration polarization usually is the controlling factor during corrosion in a media that contains a scarce amount of reducible species or oxidizers (e.g. diluted acids and aerated salt solution). Any electrochemical process where agitation leads to an increased rate of reaction is controlled by concentration polarization.

1.6.1.3 Ohmic Polarization

Electrolyte solutions have relatively lower conductivities in comparison with metals, particularly in dilute solutions. The potential drop due to the resistance of the electrolyte solution is referred to as ohmic polarization. In corrosion systems, if the metal surface is secured with paint or other protecting materials or the electrode has high resistance, they also contribute to ohmic polarization.

1.6.1.4 Exchange current density

Exchange current density is the rate of exchange reactions or redox reactions expressed in terms of current density, for electrochemical equilibria involving the participation of electrons. At equilibrium,

$$r_{ox} = r_{red} = \frac{i_0}{nF} \qquad (1.10)$$

where r_{ox} and r_{red} are the equilibrium oxidation and reduction rates and i_o is the exchange current density; n and F are no of electrons involved and Faraday in coulombs.

Some factors influencing the exchange current density are mentioned below.

- Ratio of the concentration of oxidized to reduced species at the electrodes.
- Temperature of the medium. Higher the temperature higher will be $\boldsymbol{i_o}$.
- Electrode surface roughness. The greater the roughness of the electrode surface, more will be the surface area, hence the higher will be $\boldsymbol{i_o}$. Example: platinized platinum has higher $\boldsymbol{i_o}$ for hydrogen evolution than platinum.

1.6.1.5 Mixed potential theory

The concepts utilized in the mixed-potential theory were known in the 19th century. The concepts of this theory were formally presented by Wagner and Traud in 1938. This theory consists of two postulates:

1. Two or more partial redox reactions are involved in an electrochemical reaction.
2. In an electrochemical reaction, there can not be any net accumulation of electric charge.

The first postulate is self-evident, as electrochemical reactions are made up of at least two half-cell reactions of oxidation and reduction. The second postulate is similar to the statement of the law of conservation of charge. That is, a metal immersed in an electrolyte can not immediately collect an electric charge. From this, it follows that during the corrosion of an electrically detached metal sample, the total rate of oxidation must be equal to the rate of reduction (Fontana 2005).

1.7 ELECTROCHEMICAL CORROSION TESTING

Corrosion testing is divided into three types of classifications: 1) Laboratory tests, 2) Pilot-plant tests, 3) Tests in fields, i.e, on-site tests.

The main justifications for corrosion testing are:

- Evaluation and selection of materials for a specific environment or a given definite application.
- Evaluation of new or old metals or alloys to determine the environments in which they are suitable.
- Control of corrosion resistance of the material or corrosiveness of the environment.
- The study of the mechanisms of corrosion or other research and development purposes. These tests usually involve specialized techniques, precise measurements, and precise control.

Though numerous corrosion testing methods are available, the selection of the method is based on the type of the metal and the form of corrosion. Each of the corrosion testing methods finds its application either in the laboratory or in the on-site field. Among the methods used, only electrochemical methods provide insight into the mechanism of corrosion. As corrosion is electrochemical in its nature, electrochemical testing methods are precise in determining its rate (Barnartt 1969).

The corrosion measurement techniques are classified into two types.

a) DC electrochemical monitoring techniques
b) AC electrochemical monitoring techniques

1.7.1 DC Electrochemical monitoring techniques

These methods include changing the potential of the working electrode and estimating the current delivered as a function of time or potential. When the electrode is polarized, it can cause electrochemical reactions at the electrode surface. The amount of current produced during these reactions is controlled by the kinetics of the reactions and the diffusion of reactants both towards and away from the electrode.

DC polarization technique utilizes a typical three-electrode system. The metal sample under study is made as the working electrode. An inert metal like platinum constitutes the auxiliary electrode. The potential of the working electrode is measured with reference to the reference electrode such as the saturated calomel electrode (Thompson and Payer 1998).

1.7.1.1 Tafel Extrapolation Technique

In the Tafel extrapolation method, the working electrode would be immersed in the electrolyte and then allowed to attain the steady-state potential or the OCP using an electrochemical workstation. On attaining the OCP, the system will be drifted away from its steady-state both anodically and cathodically to the OCP. A plot of the logarithm of corrosion current density against the potential thus obtained is called the Tafel plot. The straight line of anodic and cathodic branches are extrapolated such that their intersection point defines OCP at Y-axis and corrosion current density (i_{corr}) at the X-axis. However, to ensure accuracy, the linear region at least ±50 mV from the OCP and one decade of linearity is considered to ensure good accuracy in the measurements. The corrosion potential (E_{corr}) is a thermodynamic parameter that is specific to the sample and i_{corr} is a kinetic parameter that is directly proportional to the rate of corrosion. The anodic and cathodic Tafel slopes or constants are referred to as β_a and β_c, respectively. A representative Tafel extrapolation is depicted in Fig. 1.2.

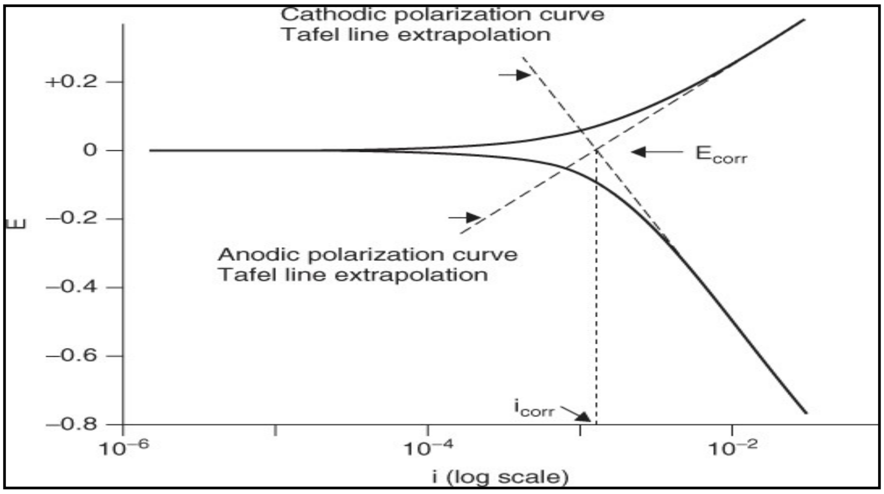

Fig. 1.2: Potentiodynamic polarization curves.

Kinetically controlled electrochemical reaction of an isolated half-cell obeys Tafel equation (1.11).

$$i = i_0\, e^{\left(\frac{2.3(E-E_0)}{\beta}\right)} \qquad (1.11)$$

where, i is the electrode current density of the reaction, i_0 is exchange current density, E is the electrode potential, E_0 is the equilibrium potential, β is the Tafel constant for a given reaction expressed in units of volts/decade. The combined Tafel equations for both the anodic and cathodic reactions of a corroding system generate the Butler-Volmer equation (2).

$$i = i_a + i_c = i_{corr}\left[e^{[2.3(E-E_0)]/\beta_a]} - e^{\left[-\frac{2.3(E-E_0)}{\beta_c}\right]}\right] \qquad (1.12)$$

where, βa and βc are Tafel constants for the linear portion of anodic and cathodic Tafel branches up to 1 decade of current, respectively. Tafel constants are related to electrode kinetic parameters and are useful in the valuation of polarization resistance (Rp) as described by the Stern-Geary Equation below (3).

$$R_p = \frac{\beta_a \beta_c}{2.3\, i_{corr}(\beta_a+\beta_c)} \qquad (1.13)$$

The rate of corrosion is determined by the equation below (1.14).

$$\upsilon_{corr}\ (mmy^{-1}) = \frac{(K \times i_{corr} \times E.W)}{\rho} \tag{1.14}$$

where, constant K=0.00327 mm g μA^{-1} cm^{-1} y^{-1}, defining the unit of corrosion rate mm y^{-1}, i_{corr} is the corrosion current density expressed in μA cm^{-2}, $E.W$ is the equivalent weight of the corroding specimen, ρ is the density of corroding specimen.

Advantages of Tafel extrapolation technique

• A rapid corrosion monitoring technique as compared to the conventional weight-loss method of analysis.

• Greater accuracy in determining corrosion rate, even at extremely low corrosion rates.

• Continuous corrosion monitoring in industries is facilitated by the Tafel polarization method.

Disadvantages

• The test electrode can be polarized only a limited number of times because some degree of electrode surface roughening occurs with each polarization.

• The method can be applied only to systems containing one reduction process since the Tafel region is distorted if more than one reduction process occurs.

• The system gets disturbed due to polarization of material under test by several hundred mV from corrosion potential.

1.7.2 AC electrochemical monitoring techniques

1.7.2.1 Electrochemical impedance spectroscopy (EIS)

The electrochemical interfaces are best understood when viewed from an impedance standpoint. The impedance studies of corroding systems help to characterize and analyze complex interfaces (Niu and Lee 2000). The impedance is the AC equivalent of DC resistance (*R*). It is the resistance offered by a circuit to the flow of AC. In impedance tests, a sinusoidal electrochemical (current or potential) perturbation considered with reference to a suitable DC condition is impressed on the system. Most corrosion investigations involve the application of a small amplitude voltage excitation which is centered on the corrosion potential and which encompasses a wide range of frequencies. Such a multiple frequency stimulation enables computation of electrode capacitance and rates of various electrochemical reactions. Small amplitude stimulation is preferred to achieve a linear or pseudo-linear response from the system. In a linear (or pseudo-linear) system, the output will be a current sinusoid at the same frequency but shifted in phase as shown in Fig. 1.3.

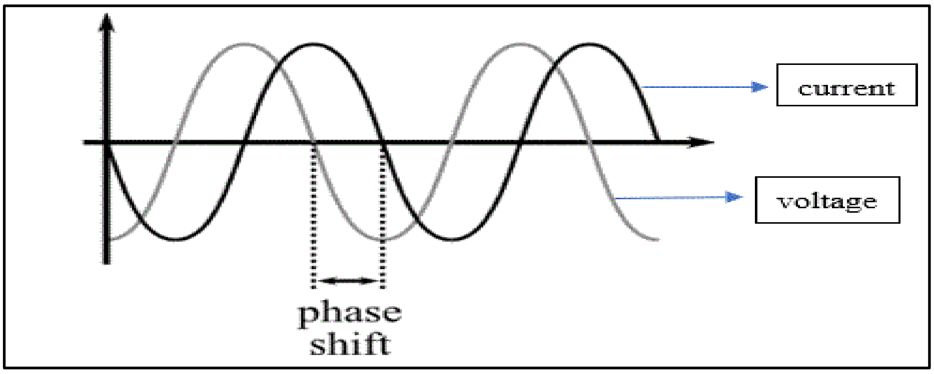

Fig. 1.3: Schematic representations of a pattern of waves.

An expression similar to Ohm's law gives the impedance (*Z*) of the system as the ratio of potential to current both expressed as functions of time, as represented in the equation below

$$Z = \frac{E_t}{I_t} = \frac{E_0(sin\omega t)}{I_0(sin\omega t + \varphi)} = Z_0 \frac{(sin\omega t)}{(sin\omega t + \varphi)} \qquad (1.15)$$

where E_t and I_t are the potential and current at time t, E_o and I_o are the amplitude of potential and current signals, ω is the radial frequency, Z_o is the magnitude of the impedance and ϕ is the phase shift.

However, the impedance ($Z_{(\omega)}$) for practical convenience is expressed in terms of real Z' (ω) and imaginary Z"(ω) components in cartesian coordinates as given in equation (1.16):

$$Z(\omega) = Z'(\omega) + Z"(\omega) \tag{1.16}$$

The impedance data are interpreted by developing different plots like Nyquist and Bode plots. On plotting Z' along X-axis and Z" along Y-axis, Nyquist plot will be obtained. A plot of log (Z_o) along Y-axis and log (f) (frequency) along X-axis yields Bode magnitude plot, whereas Bode phase angle plot is obtained by plotting ϕ along Y-axis against log (f) taken along X-axis. On a Nyquist plot, the impedance is symbolized as a vector, the length of which corresponds to the magnitude Z_o and the angle with which the vector remains inclined to the X-axis is equivalent to ϕ. A foremost drawback of Nyquist plots is that the exact frequency at which any data point is recorded remains disguised. The Bode plots however compensate for this limitation. Representative impedance plots are shown in Fig. 1.4.

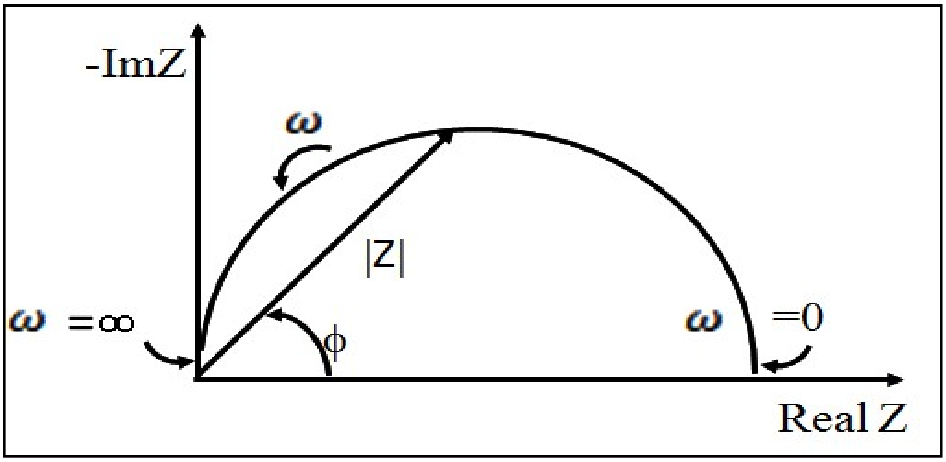

Fig. 1.4: A representative Nyquist plot.

The interpretation of impedance data is often achieved through simulation of the experimentally acquired impedance behavior with that of a suitable theoretical 'equivalent electrical circuit'.

Most of these equivalent electrical circuit models comprise various combinations of common electrical elements like resistors, capacitors, and inductors. An equivalent electrical circuit chosen for the fitment of impedance data should be such that a property related to the physical electrochemistry of the system is reflected in each of the elements in the model (Greene et al. 1961). The Nyquist plot shows a semicircle, with increasing frequency in a counter-clockwise direction as shown in Fig 1.4. At very high frequency, the imaginary component -Z" disappears, leaving only the solution resistance R_s. At very low frequency, -Z" again disappears, leaving a sum of R_s and the Faradaic reaction resistance or polarization resistance (R_p). The Faradaic reaction resistance is inversely proportional to the corrosion rate. R_s measured at high frequency can be subtracted from the sum of R_p and R_s.

The advantages of EIS studies are as follows:

- Non-destructive method of analysis as it operates in OCP (open circuit potential).
- Operational at extremely low corroding rates and low conductivity system.

Shortcomings of EIS are as listed below:

- A complicated method of analysis and tedious data interpretation.
- EIS alone cannot fetch sufficient data, therefore usually tested along with other measurement techniques like potentiodynamic polarization (Mansfeld et al. 1992, Laisa et al. 2017).

1.8 CORROSION CONTROL

The corrosion types are so various, and the conditions under which corrosion occurs are so different that no single strategy can be utilized to control all conceivable corrosion cases. The decision of a control strategy relies upon several factors, such as the type of the metallic structure, the application for which it is planned, the type of corrosion, and the nature of the overall condition. Some of the significant techniques used are given below (Bradford and Bringas 1993).

1.8.1 Material selection

The selected material should be such that it should be the most economic material exhibiting the best corrosion resistance against the given environment of exposure. Pure metal or nonmetallic should be used whenever possible without compromising the desired output.

1.8.2 Alternation of environment

Changing or altering the corrosive environment gives a flexible way to decrease the corrosion rate. Ordinary changes in the medium that are regularly utilized are (1) bringing down the temperature, (2) reducing the velocity, (3) removing oxygen or oxidizers, and (4) changing the concentration of corrosive. As a rule, these progressions can fundamentally reduce corrosion, yet they should be exercised with care.

1.8.3 Mechanical design

Metallic structures ought to be planned with the end goal that there is the least possibility for any type of corrosion to occur, simultaneously without changing off any mechanical parts. There are many design rules, avoiding heterogeneity and mechanical stress are among the unmistakable ones.

1.8.4 Cathodic Protection

Cathodic protection is accomplished by providing electrons to the metal surface, making it cathodic to encompassing. It is accomplished by the galvanic coupling with a sacrificial anode or by the impressed current technique utilizing an external source of current and an inert anode. The advantage of the cathodic protection method is that the corrosion rate of cathodically protected ensured structure is not simply limited, but reduced to zero.

1.8.5 Anodic Protection

This strategy is relevant just for metals showing the active-passive transition. The metallic structure is passivated and ensured to be an anode utilizing a potentiostat. The potentiostat keeps the metal at a constant potential at which it is passivated.

1.8.6 Surface coatings

Any coating on the surface of the metal, acting as a physical barrier between the metal and the destructive corrosion medium, is useful in metal protection. Metallic, inorganic, and organic coatings have been generally applied on metal surfaces. To be viable as a physical barrier, a surface coating ought to be persistent, uniform, impenetrable, and synthetically inactive to the corrosives and ought to have a sensibly long life.

1.9 CORROSION INHIBITORS

A corrosion inhibitor is a substance that, when added in small amounts to the corrosion environment decreases, the corrosion rate. There are various inhibitor types and classifications. Most inhibitors have been chosen by observational experimentation, and many inhibitors are exclusive in nature.

To qualify as a good inhibitor any chemical must fulfill the following requisites.

- It should be non-toxic, economically cheaper.
- It should be thermally stable and chemically inert.

The most well-known and generally known utilization of inhibitors is their application in vehicle cooling frameworks and evaporator feed water (Sastri 1998).

1.9.1 Evaluation of corrosion inhibition efficiency

Since there might be more than one inhibitor appropriate for a particular application, it is important to assess their ability to inhibit the corrosion on a metal surface. The ability of an inhibitor to protect the metal from corrosion is expressed in terms of its inhibition efficiency and is calculated using equation 1.17.

$$\eta(\%) = \left[\frac{\upsilon_{corr\ uninhib} - \upsilon_{corr\ inh}}{\upsilon_{corr\ uninhib}}\right] \times 100 \qquad (1.17)$$

where, $\upsilon_{corr(uninh)}$ and $\upsilon_{corr(inh)}$ are corrosion rates in uninhibited and hindered conditions individually. The corrosion rates $\upsilon_{corr(uninh)}$ and $\upsilon_{corr(inh)}$ can be determined by any of the standard corrosion testing methods.

1.9.2 Types of inhibitors

Based on the effect of the inhibitors on the anodic reaction, cathodic reaction, or both, the inhibitors are classified as follows:

1.9.2.1 Anodic inhibitor

Anodic inhibitors are those substances that act on the anodic sites. They displace the corrosion potential (E_{corr}) in the positive direction and reduce the corrosion current (i_{corr}), thereby retard the anodic reaction and suppress the corrosion rate. Basically, oxyanions such as chromates, molybdates, tungstates, and antimonates are very effective anodic inhibitors. The anodic inhibitors combine with metal ions formed at the anodic region, forming the sparingly soluble respective salts. These compounds formed are deposited on the anodic sites forming the protective films, which act as barriers between the fresh metal surface and the corrosive medium, thereby preventing the further anodic reaction. Anodic inhibitors are found to be effective only when a sufficient amount of the inhibitor is added to the corrosion medium. When an insufficient quantity of an anodic inhibitor is added, corrosion may be more rather than inhibition.

1.9.2.2 Cathodic inhibitor

Cathodic inhibitors are those substances which act on the cathodic sites and polarize the cathodic reaction. They displace the corrosion potential in the negative direction and reduce the corrosion current, thereby retard the cathodic reaction and suppress the corrosion rate. Cathodic inhibitors may be divided into three categories, viz., (i) those that consume oxygen (deaerators or oxygen scavengers) (ii) those that reduce the area of the cathode, and (iii) those that increase the hydrogen overpotential on the cathode.

1.9.2.3 Mixed inhibitor

These are substances that affect both the cathodic and anodic reactions. Corrosion potential change in such a case is smaller. Mixed type of inhibitors is generally organic compounds that are adsorbed on the metal surface and suppress both the metal dissolution and the reduction reactions (Sastri 1998); (Tizpar and Ghasemi 2006). Based on the mechanism by which the inhibitors act, they are classified as explained as follow:

1.9.2.4 Adsorption-type inhibitors

This is the largest class of inhibiting substances. Usually, these are organic moieties that adsorb on the substrate surface and suppress metal dissolution and reduction reactions. In most cases, it appears that adsorption of inhibitors affect both the anodic and cathodic processes, although in many cases the effect is unequal.

1.9.2.5 Hydrogen-evolution poisons

These are substances such as arsenic and antimony ions, that retards the hydrogen-evolution reaction. As a consequence, these substances are very effective in acid solutions but are ineffective in environments where other reduction processes such as oxygen reduction are the controlling cathodic reactions.

1.9.2.6 Scavengers

They are the ones that act by removing corrosive reagents from the solution. Examples of this type can be sodium sulfite and hydrazine, which remove dissolved oxygen from aqueous solutions as given below

$$2Na_2SO_3 + O_2 \rightarrow 2Na_2SO_4 \qquad (1.18)$$

$$N_2H_4 + O_2 \rightarrow N_2 + 2H_2O \qquad (1.19)$$

1.9.2.7 Oxidizers

These are species such as chromate, nitrate, and ferric salts that also act as inhibitors in many systems. In general, they are primarily used to inhibit the corrosion of metals and alloys that demonstrate active-passive transitions, such as iron and its alloys and stainless steels.

1.9.2.8 Vapor-phase inhibitors

These are similar to the adsorption-type inhibitors and possess a very low vapor pressure. As a consequence, these materials can be used to inhibit atmospheric corrosion of metals without being placed in direct contact with the metal surface. In use, such inhibitors are placed in the vicinity of the metal to be protected, and they are transferred by sublimation and condensation to the metal surface. These inhibitors are usually only effective if used in closed spaces such as inside packages or on the interior of machinery during shipment. It is important to use enough inhibitors, since many inhibiting agents accelerate corrosion, particularly localized attacks such as pitting, when present in small concentrations. To avoid this possibility, inhibitors should be added in excess and their concentration checked periodically.

The mixed inhibitors inhibit the corrosion on the metal surface by one or more of the following mechanisms of inhibition.

- **Physical Adsorption**: Physical adsorption takes place through the electrostatic attraction between the diploes of the inhibitor molecules and the charged metal surface. The physisorption process requires less activation energy and susceptible to desorption at a higher temperatures. Thus the process of physisorption is reversible in nature.
- **Chemisorption**: Adsorption that takes place due to the chemical interaction between the surface atoms of the adsorbent and the atoms of the adsorbate. This type of adsorption is known to be called chemisorption. For example, oxygen is chemisorbed by carbon, and hydrogen is chemisorbed by nickel under suitable conditions. In each case, a stable surface compound, frequently referred to as surface complex, results.
- **Film Formation**: These involve in the dependence of chemical composition, their molecular structure, and their affinities for the metal surface. Because film formation is an adsorption process, the temperature and pressure in the system are important factors. Organic inhibitors will be adsorbed according to the ionic charge of the inhibitor and the charge on the surface (Gräfen et al. 2000).

1.10 MECHANISM OF CORROSION INHIBITIONS

Corrosion inhibitors influence the corrosion rate by controlling either the anodic reaction or the cathodic reaction or both. Some commonly observed mechanisms are presented in the following sections (Saji and Umoren 2020).

1.10.1 Inhibitors for acid solutions

The corrosion of metals in acid solutions can be inhibited by a wide range of substances, such as halide ions, carbon monoxide, and many organic compounds, particularly those containing elements such as nitrogen, sulphur, phosphorus, arsenic, and oxygen. The primary step in the action of inhibitors in acid solutions is to adsorb on the metal surface, which is oxide-free in acid solutions. The adsorbed inhibitor then acts to stop the cathodic/anodic electrochemical corrosion processes.

Inhibitors of corrosion in acid solutions can interact with metals and affect the corrosion reaction in numerous ways, some of which may occur simultaneously. The mechanism of action of an inhibitor may vary with factors such as its concentration, the pH of the acid, the nature of the anion of the acid, the presence of other species in the solution, the extent of the reaction to form secondary inhibitors, and the nature of the metal.

1.10.1.1 Surface charge on the metals

Adsorption may be due to electrostatic attractive forces between ionic charges or dipoles on the adsorbed species and the electric charge on the metal at the metal-solution interface. In solution, the charge on the metal can be expressed by its potential to the zero-charge potential. As the potential of a metallic surface becomes more positive, the adsorption of anions is favored, and as the zero charge potential becomes more negative, the adsorption of cations is favored.

1.10.1.2 The functional group and structure of the inhibitor

Inhibitors can also bond to metal surfaces by electron transfer to the metal to form a coordinate type of link. This process is favored by the presence in the metal of vacant electron orbitals of low energy, such as occurs in the transition metals. Electron transfer from the adsorbed species is favored by the presence of relatively loosely bound electrons, such as may be found in anions, and neutral organic molecules containing lone pair electrons or pi-electron systems associated with multiple, especially triple bonds or aromatic rings. The inhibition efficiency increases as the electron density on the functional group increases in a series of related compounds. This is consistent with the increasing strength of coordinate bonding due to easier electron transfer and hence greater adsorption.

1.10.1.3 Interaction of the inhibitor with water molecules

Adsorption of inhibitor molecules is often a displacement reaction involving the removal of adsorbed water molecules from the surface. During the adsorption of a molecule, the change in interaction energy with water molecules in passing from the dissolved to the adsorbed state forms an important part of the free energy change on adsorption. This has been shown to increase with the increasing size of the hydrocarbon portion of an organic molecule. Thus increasing size leads to the decreasing solubility and increasing adsorbability. This is consistent with the increasing inhibitive efficiency observed at constant concentrations with increasing molecular size in a series of related compounds.

1.10.1.4 Interaction of adsorbed inhibitor species

Lateral interactions between adsorbed inhibitor species may become significant as the surface coverage, and hence the proximity, of the adsorbed species increases. These lateral interactions may be either attractive or repulsive. Interactions occur between molecules containing large hydrocarbon components. As the chain length increases, the increasing van der Waals attractive force between adjacent molecules leads to stronger adsorption at high coverage. Repulsive interactions occur between ions or molecules containing dipoles and lead to weaker adsorption at high coverage.

In the case of ions, the repulsive interaction can be altered to an attractive interaction if an ion of opposite charge is simultaneously adsorbed. In a solution containing inhibitive anions and cations, the adsorption of both ions may be enhanced and the inhibitive efficiency greatly increased compared to solutions of the individual ions. Thus, synergistic inhibitive effects occur in such mixtures of anionic and cationic inhibitors.

1.10.2 Method of inhibition in neutral solutions

Typical inhibitors for near-neutral solutions are the anions of weak acids, some of the most important in practice being chromate, nitrite, benzoate, and borate. Passivating oxide films on metals offer high resistance to the diffusion of metal ions, and the anodic reaction of metal dissolution is inhibited. The action of inhibitive anions on the corrosion of metals in near-neutral solution involves the following important functions:

- Reduction of the dissolution rate of the passivating oxide film
- Prevention of the adsorption of aggressive anions

Inhibition in neutral solutions can also be due to the precipitation of compounds, on a metallic surface, that can form or stabilize protective films. The inhibitor may form a surface film of an insoluble salt by precipitation or reaction. Inhibitors forming film of this type include

- Salts of metals such as zinc, magnesium, manganese, and nickel, which form insoluble hydroxides, especially at cathodic areas, which are more alkaline due to the hydroxyl ions produced by the reduction of oxygen
- Soluble calcium salts, which can precipitate as calcium carbonate in H_2O contaning CO_2, again at cathodic areas where the high pH permits a sufficiently high concentration of carbonate ions
- Polyphosphates in the presence of zinc or calcium, which produce a thin amorphous salt film

These salt films, which are often quite thick and may even be visible, restrict diffusion, particularly of dissolved oxygen to the metal surface. They are poor electronic conductors, and so oxygen reduction does not occur on the film surface (Yohai et al. 2011, Willumeit et al. 2011, Chou et al. 2019, Awad and Turgoose 2004).

1.11 MAGNESIUM AND ITS ALLOYS

Magnesium alloys are low-density materials with high strength to weight ratio. It is considered as a prominent material for inner closure for war ships, etc., but are limited in a wide practical application by their low corrosion resistance to the attack of electrolyte aqueous solutions. Among the structural metals, magnesium is the lightest, with a density of 1.74 g/cm^3, which is nearly two-thirds that of aluminum. Magnesium alloys are often named after the synthetic method used for their manufactures, like cast alloys and wrought alloys. Despite being the lightest, the utility of magnesium alloys in weight-sensitive applications remains a challenge owing to their vulnerability to corrosion, high-temperature creep, and flammability. Over the years all these limitations have been overcome to some extent by new alloy development using the inclusion of alloying elements that counteract these undesirable properties (Gupta and Ling 2011, Wagner et al. 2003).

1.11.1 Applications of magnesium alloys

The magnesium alloys have good demand as basic materials in structural applications, particularly in weight-critical applications. Some of the important are summarized as follows.

1.11.1.1 Application in the transport industry

Many car parts are made up of magnesium alloys. Even though they were first used in racing vehicles, later magnesium alloys parts are being used in commercial vehicles also. Magnesium-based materials are used in gearbox housing steering wheels, fuel tank cover, seat frame, airbag housing, etc (Luo and Sachdev 2012).

1.11.1.2 Military applications

The aircraft fitted with magnesium alloy parts were used during World War II. The H-19 Chickasaw helicopter, a US Army helicopter built-in 1951, contains 17% (by weight) of magnesium, a record level during its time. Examples of "military magnesium" include artillery guns, light weight personnel carrier, military aircraft like Eurofighter Typhoon, F16 and intercontinental ballistic missiles (Mathaudhu and Nyberg 2016).

1.11.1.3 Medical applications

Magnesium alloys are used in bio-implant materials. The density of Mg alloys is close to that of natural bone (1.8-2.0 g/cm^3) and is lower than the competing titanium alloys. Mg alloys have a high mechanical strength compared to ceramic or polymeric biomaterials and possess greater fracture toughness. Mg ion participates naturally in human metabolism, it is the fourth most abundant cation in the human body; hence magnesium is biocompatible and nontoxic at moderate levels (Gu and Zheng 2010).

1.11.1.4 Applications in electronics

For the user, portability is highly anticipated of the electronic devices. As compared to plastic electronic materials, magnesium alloys are not only light-weight but also have better heat transfer and the ability to protect against electromagnetic and radiofrequency interferences. The magnesium components currently found in electronic devices include the housing of cell phones, digital cameras, computers, laptops, digital projectors, media players, etc.

1.11.1.5 Applications in sports

The popularity of Mg alloys as structural materials for sports equipments is not surprising considering their enviable properties such as low density, their ease of machining which facilitates the creation of complex shapes, good properties of cushioning and shock absorption, and vibration absorption. The handles of the golf club heads, tennis rackets, and mountain bike bicycle frames are some notable examples of magnesium parts in sports equipment.

1.11.1.6 Other applications

Magnesium alloys find applications in consumer products that must be lightweight for easy portability. Some examples include spectacle frames, binocular parts, and hand-held working tools for mechanical operations.

1.11.2 Magnesium alloy AZ31

AZ31 alloy is an Mg-Al alloy, which has aroused scientific interest over the last two decades. It is made up of 3 wt% of Aluminium, 1 wt% Zinc, 0.35 wt% manganese, and rest with magnesium. From a practical point of view, magnesium is the structural metal of the lowest density, which makes it highly attractive for use in the automotive, aerospace, IT, and electronics industries, as well as in the development of new biomaterials for orthopedic and cardiovascular applications where weight plays a decisive role. AZ31 alloy is a common wrought alloy that has medium strength, weldability, and good strength**.** This particular type of alloy comes in sheet and plate shapes. AZ31 alloy is the most widely used magnesium alloy for applications at or slightly above room temperature. Sheets made from AZ31 have been used for prototype testing for automotive sheet panels. AZ31 sheet has similar hot deep-drawing characteristics as steel and, aluminium sheet. Magnesium alloy brackets with one rib are widely used in aircraft control systems. (Frignani et al. 2012); (Montemor 2014); (Baghni et al. 2004).

Magnesium alloys, though characterized by a low density and interesting mechanical properties, their practical applications are limited due to low corrosion resistance to the attack of aqueous solutions (Frignani et al. 2012), (Cui et al. 2008). Even if the natural magnesium corrosion products (oxides, hydroxides) tend to slow down the corrosion process by chiefly hindering the anodic oxidation reaction, the corrosion rates of these artifacts remain too high for a profitable service life (De Beni 1967), (Frignani et al. 2012). Therefore, to moderate the corrosive attacks, corrosion inhibitors may be proposed, to further decrease the corrosion rate by forming protective films or layers, either by surface adsorption or by reaction with Mg^{2+} ions.

Table 1.1: Physical and mechanical properties of AZ31 alloy.

Parameters	Value
Density (g cm^{-3})	1.8
Melting point (°C)	605-630
Electrical resistivity (ohm m)	9.2E-08
Elongation at break (%)	15
Modulus of elasticity (GPa)	45
Poisson ratio	0.35
Ultimate tensile strength (MPa)	290
Yield strength (MPa)	220

Uses

- AZ31 Mg alloy is best known for its strength, weldability, and low mass density.
- Due to its optimum physical properties and withstanding particular temperatures, it is used to produce mobile phone cases.
- AZ31 alloy is used as aircraft brackets and also used for making the backbone of aircraft as it usually comes in sheets.

- This alloy is also used in the automotive and machine-building industries for making important spare parts.
- The AZ31 Mg alloy is used in orthopedic implantations as it is a biodegradable bio-material.

1.12 LITERATURE REVIEW

1.12.1 Corrosion behavior of pure magnesium and magnesium alloys

The usage of magnesium has been limited due to its poor corrosion resistance. The resistance is very less to corrosion when it has impurities in the alloy or else exposed to strongly concentrated electrolyte species. In some cases, localized corrosion initiates corrosion in magnesium and magnesium alloys, but sometimes it is widespread and shallow. The corrosion morphology of magnesium and magnesium alloys depends on the alloy's chemistry and environmental conditions. For example, localized corrosion occurs in immersed conditions, whereas atmospheric corrosion occurs uniformly in industrial atmospheres. (Tunold et al. 1977), reported that pure magnesium was corroding trans granular and its alloys were corroding uniformly. Also, it was reported that the corrosion of pure magnesium is non-uniform, and that of its alloys are uniform (Ghali et al. 2004).

It has been thought that there are two main reasons for poor corrosion resistance in magnesium and its alloys (Shaw and Jones 1997). Initially, there is internal galvanic corrosion caused by secondary phases or impurities (Solanki et al. 2017). Secondly, the quasi-passive hydroxide film on magnesium is much less stable than the passive films which form on metals such as aluminum and stainless steels. This quasi-passivity provides only poor pitting resistance for magnesium and magnesium alloys.

The presence of impurities such as iron, nickel, and copper had attacked magnesium alloys mainly in moist conditions. In the presence of a corroding medium, these impurities act as small cathodes, creating micro-cells with the anodic magnesium matrix (Luo and Shinoda 1998).

1.12.2 Corrosion inhibitors for magnesium and magnesium alloys

Large number of chemical compounds have been synthesized and investigated for their capability to inhibit corrosion of magnesium alloys in different media. These compounds include inorganic and organic and even the combinations of the two. Some of the best inhibitors are reported in the literature along with certain essential details are listed in Table 1.1.

Table 1.2: Eminent corrosion inhibitors for magnesium and magnesium alloys.

S.No	Inhibitor	Medium	Alloys used	Remarks	References
1	Imidazole based ionic liquids	NaCl	AZ31	Follows the Langmuir adsorption isotherm, green and sustainable	(Marya et al. 2006)
2	Sodium dodecylbenzenesulfonate (SDBS)	NaCl	AZ31 alloy	Inhibition efficiency of 0.008 $mol^{-1}L^{-1}$ SDBS was more than 90%, Langmuir adsorption isotherm, a mixed-type inhibitor.	(Li et al. 2009)
3	Cerium(III) salts	NaCl	AM60	Formation of a thicker and more compact resistive film on the alloy sample.	(Heakal et al. 2012)
4	Sodium salt of N-lauroylsarcosine, N-lauroyl-N-methyltaurine, dodecylbenzensulphonic acid, or sodium lauryl sulphate	NaCl and Na_2SO_4	AZ31	DBS is the most effective, precipitated layer formed, Langmuir adsorption	(Frignani et al. 2012)
5	Stearate, palmitate, and myristate	NaCl and Na_2SO_4	ZE41	Mixed type inhibition, efficiency up to 88%, obeys Langmuir adsorption	(Dinodi and Shetty 2014)
6	Sodium alginate	NaCl	AZ31	The maximum inhibition efficiency is 90.00%, at a sodium alginate	(Dang et al. 2015)

				concentration of 500 ppm.	
7	2-Hydroxy-acetophenone	Na_2SO_4, $NaHCO_3$, and NaCl	AZ91D	Below 50 ppm, the inhibition efficiency increases with the increase of in inhibitor concentration, however, with a further increase in inhibitor concentration, the inhibition efficiency decreases.	(Hu et al. 2015)
8	N,N-bis (salicylidene)-2-hydroxy-1, 3-propanediamine Schiff base	HCl	Magnesium bar	Acts as mixed-type corrosion inhibitor	(Bezaatpour and Basharnavaz 2016)
9	Sodium dodecylbenzene sulphonate (SDBS) by the addition of trisodium phosphate and sodium benzoate	Ethylene glycol	Mg-Al-Zn alloy	Predominant anodic action, Langmuir adsorption isotherm, Efficiency: 91.8%	(Medhashree and Shetty 2018)
10	Methyl-cellulose polysaccharide	HCl	Magnesium Metal	The inhibition action follows both Langmuir and Freundlich adsorption isotherms.	(Hassan and Ibrahim 2021)

1.12.3 Strategies used for corrosion control of AZ31 magnesium alloy

The literature reveals various attempts to combat AZ31 alloy corrosion, but, the use of inhibitors has been overlooked.

Table 1.3: Strategies for corrosion control of AZ31 alloy.

Method opted	Outcome	References
Mg-Si thin film deposition	The amorphous Mg-Si film showed superior anti-seizure properties to the crystalline one because of higher hardness and Young's modulus.	(Yamaguchi et al. 2006)
Calcium phosphate coating	The coatings significantly decreased the degradation rate of the original Mg alloy, indicating that the Mg alloy with calcium phosphate coating was a promising degradable bone material.	(Cui et al. 2008)
Nanostructured cerium oxide film	Treated magnesium alloy exhibited a higher corrosive resistance than the untreated magnesium alloy.	(Ishizaki et al. 2011)
Anodised in the ionic liquid (IL) trihexyl(tetradecyl)phosphonium bis(2,4,4-trimethylpentyl) phosphinate	Film stability and corrosion protection of the AZ31 alloy increased when surfaces were anodized after an acid pickling pre-treatment in a mixture of nitric and phosphoric acid.	(Latham et al. 2012)
45S5 Glass-ceramic coatings	It was found that optimized 45S5 glass-ceramic coatings could slow down the degradation rate and decrease the mass loss of the magnesium alloy substrate from 78.04% to 2.31% in the 7th day test, showing a good anti-	(Huang et al. 2013)

	corrosion property in a certain period.	
Schiff base	Potentiodynamic polarization curves showed that Schiff base AC inhibited both anodic and cathodic reactions at all concentrations, which indicated that it was a mixed type inhibitor.	(Thirugnanaselvi et al. 2014)
Tin Al coatings	The corrosion current density of the TinAl-coated AZ31 Mg alloy decreased from 1.066×10^{-5} A/cm^2 of the control sample to 4.321×10^{-7}A/cm^2, a reduction of more than one order of magnitude	(Wang et al. 2014)
Hydrotalite film	There were optimum values of pH, the temperature of the coating bath, and immersion time for the film formation process to achieve the best quality and corrosion resistance of the hydrotalcite film	(Chen et al. 2015)
Coated with polycaprolactone (PCL) nano-fibrous layer	Nano-fibrous PCL coating combined with prior acid treatment found to be a promising method to tailor degradation rate with enhanced bioactivity of Mg alloys	(Hanas et al. 2016)
A hydrid coating composed of dicalcium phosphate dihydrate (DCPD) and poly(lactic-co-glycolic acid) (PLGA)	The deposition time influenced the morphology and structure of the DCPD coating and consequently affected the corrosion resistance of	(Li et al. 2016)

	both the DCPD and DCPD/PLGA coated samples.	
Fluoride conversion layer (hydrofluoric acid solution and poly (L-lactic acid) (PLLA) film was prepared by spin-coating the PLLA solution)	The composite PLLA/MgF_2 coating outperformed either of the solely applied coatings with respect to anticorrosion and adhesion properties.	(Wang and Guo 2016)
Coating DCPD	The resistance polarization was 43 times higher than non-coated.	(Zhao et al. 2016)
An inner silane-TiO_2 coating while the top layer was composed of chitosan	The top-most biopolymer layers did not have a detrimental effect on the barrier properties of the silane-TiO_2 coating. the corrosion mechanisms of AZ31 provided promising insights into their control via a multilayered coating.	(Cordoba et al. 2019)
$Mn(NO_3)_2{\cdot}4H_2O$, $Co(NO_3)_2{\cdot}6H_2O$, and polyvinyl alcohol (PVA).	Results demonstrated that the AZ31 Mg alloy sample treated by Ce-Mn-PVA showed the highest corrosion resistance. A denser Ce film with lower crack was precipitated on the sample treated by Ce-Mn-PVA conversion coating.	(Liu et al. 2021)

1.12.4 Surfactants as corrosion inhibitors

Surfactants are surface-active agents. They contain a hydrocarbon chain that points towards the metal surface phase and a hydrophilic head that points towards the aqueous phase. The amphiphilic nature of surfactant molecules creates an affinity for adsorption at interfaces such as metal/metal oxide–water interface. The adsorption of surfactant on metals and metal oxides creates a barrier that can inhibit corrosion. The properties of surfactant and the interaction of surfactant with metal or metal oxide and the surrounding solution environments determine the level of adsorption and corrosion inhibition (Fuchs-Godec 2009; Kellou-Kerkouche et al. 2008).

Surfactant inhibitors often contain either a nitrogen or sulphur atom as part of the functional group of the molecule. Very commonly, the nitrogen atom is part of a hydrocarbon chain, and its unshared pair of electrons commonly forms a bond with metal substrates. This type of bonding often leads to bonds that are classified as chemical bonds that lead to the ‘‘chemisorption”. This type of adsorption makes it difficult for these molecules to be displaced by reactants or to allow exposure of the metal surface to the environment at the adsorption site. However, it should be noted that most metals used in corrosive environments have metal oxide surfaces that interact with surfactants differently than metals (Zhu et al. 2017).

The hydrophilic functional groups of surfactant molecules strongly prefer interaction with polar entities such as water, metals ions, and other ions. Generally, surfactants adsorb on the metal surface, block the active sites exposed to corrosive media, and thereby reduce corrosion attack.

The hydrophobic portion, which is nonpolar, strongly prefers interaction with hydrophobic entities such as the hydrocarbon phase. Therefore, surfactant molecules are prone to adsorb at and cover the surfaces/interfaces, such as air-liquid surface and liquid-solid interface, to escape from a polar solvent such as water by associating and packing hydrocarbon chains together.

Metal and metal oxide surfaces are hydrophilic. Consequently, the functional group in surfactant molecules is attracted to surfaces of metals and metal oxides. Thus, there is a driving force for surfactant adsorption on metal and metal oxide surfaces that orients the surfactant with the hydrophilic group at the solid interface and the hydrophobic hydrocarbon chain directed out into the solution, thereby creating a hydrophobic surface. This driving force causes surfactant molecules to aggregate on surfaces. If sufficient surfactant is present in solution a second layer or multiple layers of surfactant, may be adsorbed, creating a variety of adsorbed structures (Zhu et al. 2017); (Sun et al. 2018); (Aiad et al. 2010).

A broadly used corrosion control strategy is to utilize natural surfactant inhibitors, a significant number of which are surfactants with hydrophilic and hydrophobic molecules. One example of a surfactant molecule of homologous benzalkonium (BAC), hexadecyl trimethyl ammonium bromide (C_{16}, $C_{16}Cl$, or $C_{16}BzCl$), C_{16} has an N-based aromatic functional group which is hydrophilic, and a hydrophobic hydrocarbon tail with 16 linear CH_2 and CH_3 sections. This anomalous nature of surfactants determines their interactions with surfaces and interfaces.

Surfactant particles must adsorb to act as corrosion inhibitors. Adsorption relies upon the organization of the arrangement, the convergence of the adsorbate, the connection of the adsorbate with the surface, the properties of the surface and the adsorbate, and the electrochemical capacity of the surface. The sorts of natural particle adsorption are normally chemisorption, physisorption, electrostatic adsorption, and pi-bond orbital connections that have both physisorption and chemisorption properties. Inhibitors are additionally arranged into proton acceptors, electron acceptors, and mixed molecules.

Table 1.4: Surfactants as corrosion inhibitors

Surfactants	Material	Medium	references
Alkanediyl-α,ω-bis-(dimethylalkyl ammonium bromide)	Iron	HCl	(El Achouri et al. 2001)
Dodecyl benzene sulphonate	Aluminium	HCl	(Abd El Rehim et al. 2003)
Quaternaryammonium salts, three cationic surfactants and two non-ionic surfactants	Zinc	KOH	(Bereket et al. 2006)
Natrium 1,4-bis(2-etylhexyl) sulphosuccinate	Zinc	KOH and NaCl	(Branzoi et al. 2008)

Benzoylmethyl benzimidazolium hexafluoroantimonate	Mild Steel	HCl	(Nahlé et al. 2012)
Butanediyl 1,4-bis(dimethyl cetylammonium bromide), pentanediyl 1,5 - bis (dimethyl cetylammonium bromide) and hexanediyl 1,6 - bis (dimethyl cetylammonium bromide)	Mild steel	20% formic acid	Mobin and Masroor 2012
Benzyl triethylammonium chloride	Carbon steel	HCl	(Idris et al. 2013)
Non ionic surfactants	Carbon steel	Oil well water	(Migahed et al. 2013)
Anionic surfactants	ZE41	NaCl and Na_2SO_4	(Dinodi and Shetty 2014)
Non toxic cationic gemini surfactants	Mild steel	HCl	(Mobin et al. 2017)
Sodium dodecyl sulfate	AZ91	NaCl	(Liu et al. 2018)
Cationic clevelable surfactants	Stainless steel AISI 304	HCl	(Pakiet et al. 2019)
Trimeric cationic pyrdinium surfactants	Carbon steel	Oil well water	(Shaban et al. 2020)

1.13 SCOPE AND OBJECTIVES OF THE PRESENT WORK

1.13.1 Scope of the work

Magnesium alloys, with low density and good mechanical properties, have the potential for their applications in diverse fields. But their uses are limited by their low corrosion resistances (Frignani et al. 2012, Cui et al. 2008). Even if the natural magnesium corrosion products (oxides, hydroxides) tend to slow down the corrosion process by chiefly hindering the anodic oxidation reaction, the corrosion rates remain too high for a profitable service life (De Beni 1967, Li et al. 2009). Therefore, to moderate the corrosive attacks, corrosion inhibitors may be proposed. For example, substances that should further decrease the corrosion current in a wider potential interval by forming far more protective films or layers maybe by surface adsorption or by reaction with Mg^{2+} ions.

The AZ31 alloy is one of the most important magnesium alloys with aluminium. Due to its low density and good mechanical properties, this structural material offers considerable potential for applications in the aerospace and transport manufacturing industries. The AZ31 alloy is used in the aircraft industry to produce flat parts with ribs, such as brackets. Though it has very good points to be considered in many fields, it is highly susceptible to corrosion in salt mediums. So far, researchers have concentrated on sol-gel treatment, coatings with organic materials etc., for corrosion prevention on AZ31 alloy. These techniques have certain drawbacks. The surface coats or films (electroplated, organic, and sol-gel) show mediocre adhesion to the alloy surface. The inhibitor addition has been popular for other alloys as an effective and economical approach for corrosion mitigation. However, the usage of inhibitors for AZ31 is quite less explored (Ishizaki et al. 2011). It can be thought that for any magnesium used technology to be triumphant, the use of efficient, green, and economic corrosion mitigation measures are indispensable. Hence the development of corrosion inhibitors for AZ31 which meet the above-laid requirements is needed now.

1.13.2 Objectives

- To study the corrosion behavior of magnesium AZ31 alloy in different media such as sodium chloride and sodium sulfate at different concentrations and solution temperatures.
- To establish the influence of pH of the media on corrosion behavior of magnesium alloy AZ31.
- To synthesize and use some organic surfactants as inhibitors and investigate their inhibition efficiency on AZ31 alloy in sulfate medium and chloride medium.
- To carry out corrosion inhibition experiments at different temperatures to evaluate the activation parameters for the corrosion process.
- To evaluate the thermodynamic parameters for the adsorption of inhibitors, and to propose the mechanism for the inhibition of AZ31 alloy corrosion, in sulfate and chloride medium.
- To correlate the theoretical DFT studies of the inhibitors with the experimental observations

1.14 OUTLINE OF THE THESIS

The thesis has been divided into four chapters. The contents of each of the chapters are summarized as follows.

Chapter 1 presents some basic aspects of corrosion, corrosion measurement techniques, corrosion control methods, and fundamental aspects of corrosion inhibitors. This chapter additionally underlines the importance of magnesium alloys as the modern auxiliary materials for weight-delicate applications. The literature survey on the corrosion of magnesium and its alloy and its inhibition has been included in the chapter. At the end of the chapter, the scope and objectives of the present work are stated.

Chapter 2 deals with the experimentation part. The methodology embraced for the preparation of the test specimen and the electrolyte medium has been explained. The section additionally presents the operative details identified with the electrochemical strategies utilized along with the calculations that have permitted to obtain the numerical results of the current work.

Chapter 3 is on results and discussions, offering an in-detail depiction of the full outcomes obtained in the study with graphical and numerical interpretations. This section fundamentally is an endeavor to explain the electrochemical behavior and corrosion inhibition of AZ31 alloy based on the investigation.

Chapter 4 sums up the work included in the thesis and lists the conclusions drawn based on experimental evidences and discussions.

CHAPTER-2

MATERIALS AND METHODS

CHAPTER 2

MATERIALS AND METHODS

2.1 MATERIALS

The investigations were performed on AZ31 Mg alloy specimen. The elemental composition of the AZ31 Mg alloy sample is given in Table 2.1.

Table 2.1: Composition of the specimen (in terms of weight%)

Elements	Weight %
Al	2.96
Zn	0.83
Mn	0.43
Si	0.004
Cu	0.004
Ni	<0.001
Fe	0.002
Mg	Balance

Preparation of test materials

Rectangular sheet-like test coupons were cut from the plate and fixed with epoxy resin so that, the area exposed to the medium was 0.69 cm^2. These coupons were cleaned according to standard metallographic practice, such as belt grinding followed by abrading on emery sheet, and further polishing over polishing-wheel with alumina to get a mirror finish, degreased with acetone, washed with double distilled water, and dried before immersing in the corrosion medium.

2.2 MEDIA

The media used for the investigations were sodium chloride and sodium sulfate solutions at five different concentrations.

2.2.1 Preparation of standard sodium chloride solution

Standard solutions of sodium chloride having concentrations of 0.05 M, 0.1 M, 0.15 M, 0.2 M, and 0.25 M were prepared by dissolving grade sodium chloride in double distilled water.

2.2.2 Preparation of standard sodium sulfate solution

Standard solutions of sodium sulfate having concentrations of 0.05 M, 0.1 M, 0.15 M, 0.2 M, and 0.25 M were prepared by dissolving analytical grade sodium sulfate in double distilled water.

2.2.3 Preparation of chloride and sulfate media with differing pH

The corrosion behaviour was characterized by immersing the alloy specimen in solutions of different concentrations of chloride and sulfate media. The concentrations of chloride and sulfate were kept at 0.05 M, 0.1 M, 0.15 M, 0.20 M, and 0.25 M. The pH of the solutions was adjusted to the desired values of 3, 5, 7, 9, and 11 by the addition of diluted solutions of HCl and NaOH. The chloride and sulfate solutions were prepared by dissolving analytical grade sodium chloride and sodium sulfate in distilled water.

2.3 INHIBITORS

The inhibitors, anionic Gemini surfactants, sodium 2,2'-(5,14-dibutyl-6,13-dioxo-5,8,11,14-tetraazaoctadecane-8,11-diyl)diacetate (DB), sodium 2,2'-(7,16-dihexyl-8,15-dioxo-7,10,13,16-tetraazadocosane-10,13-diyl)diacetate (DH), sodium 2,2’-(9,18-dioctyl-10,17-dioxo-9,12,15,18-tetraazahexacosane-12,15-diyl)diacetate (DO), sodium 2,2’-(11,20-didecyl-12,19-dioxo-11,14,17,20-tetraazatriacontane-14,17-diyl)diacetate (DC), sodium 2,2’-(13,22-didodecyl-14,21-dioxo-11,14,17,20-tetraazatetratriacontane-16,19-diyl)diacetate (DD) were synthesized as follows.

R (dibutylamine, dihexylamine, dioctylamine, didecylamine and didodecylamine) of about 16 mmol and EDTA anhydride (8 mmol) suspended in CH_3OH (50 mL) were reacted for 22 h at 40-45 °C.

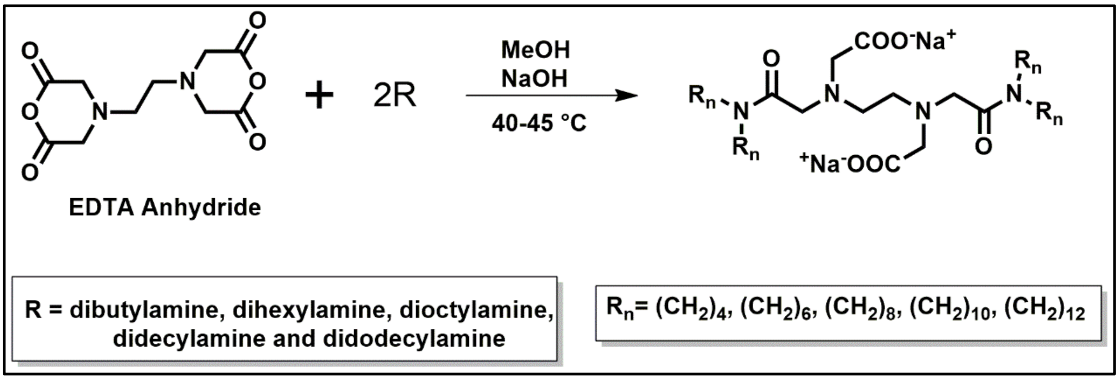

SCHEME 1: **Synthesis of anionic Gemini surfactants**

The anhydride particles progressively disappeared as the reaction progressed. After cooling the sample to room temperature, the remaining particles were filtered off. The reaction mixture was evaporated to give yellowish oil. Acetone was then added until a white solid precipitated. The precipitate was filtered off and was further purified by dissolution in $CHCl_3$ and precipitation in acetone, to yield a white powder, Finally, the intermediate product was neutralized with sodium hydroxide (1 M aq, 2 equivalents), and the obtained solution was freeze-dried to give Gemini surfactant in quantitative yield as a colorless, hygroscopic powder. The anionic Gemini surfactants synthesized were characterized using ^{1}H-NMR (Bruker NMR spectrometer (400 MHz) with $CDCl_3$ as solvent and tetramethyl silane (TMS) as internal reference standard), FT-IR (Bruker, USA FT-IR spectrophotometer), and LC-MS (Agilent chromatography-mass spectrometer). The spectra are presented in Fig. 2.1 to Fig. 2.15.

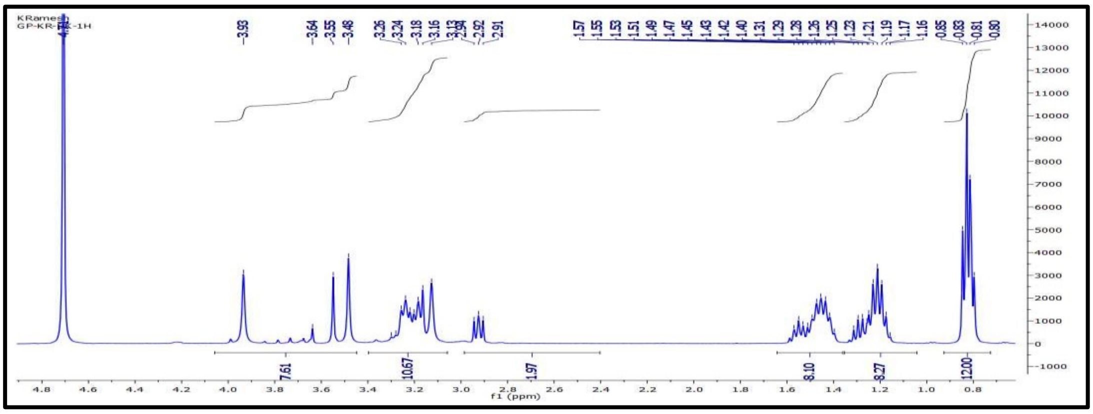

Fig. 2.1: ^{1}H-NMR spectrum of DB-based surfactant.

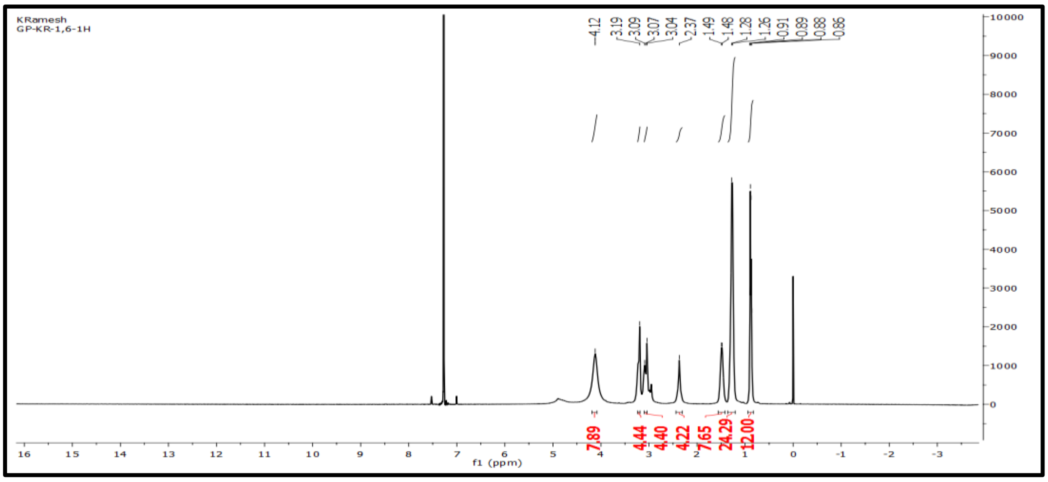

Fig. 2.2: ^{1}H-NMR spectrum of DH-based surfactant.

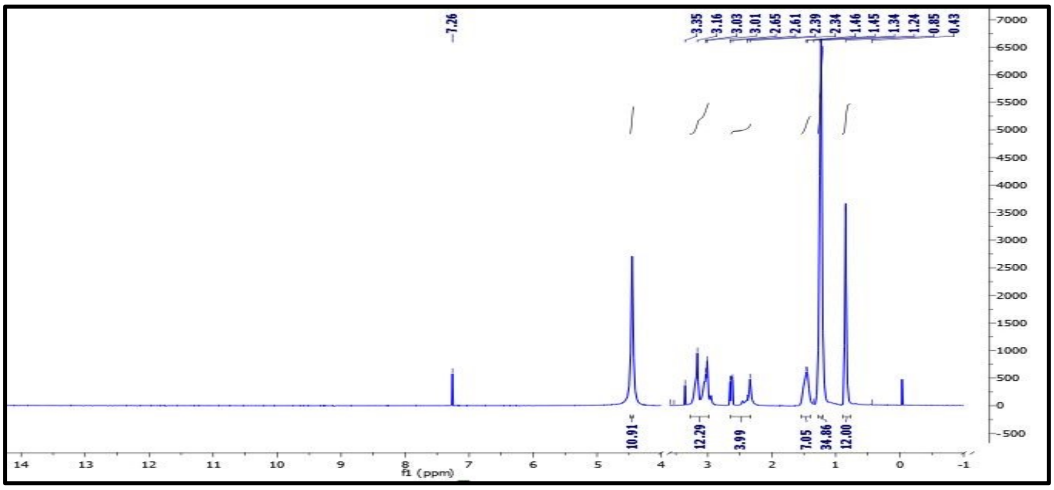

Fig. 2.3: ^{1}H-NMR spectrum of DO-based surfactant.

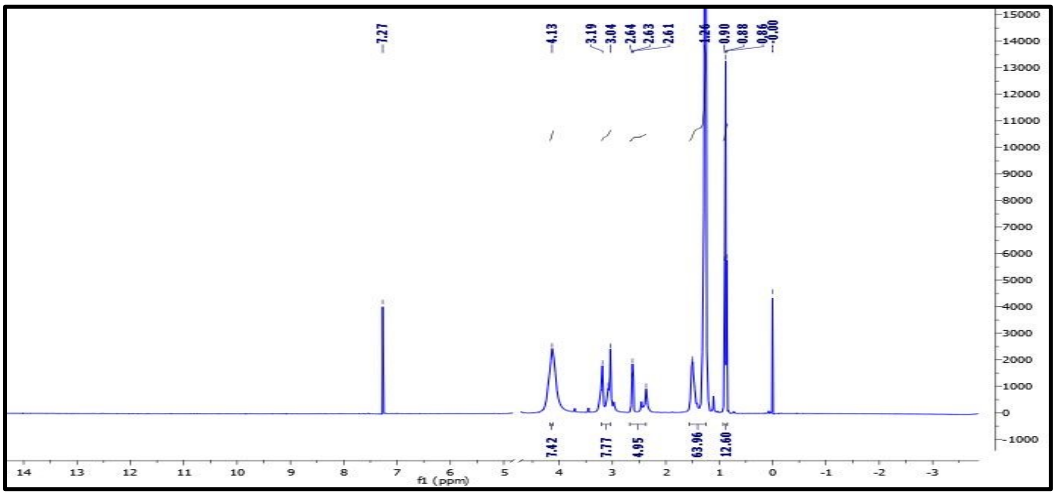

Fig. 2.4: ^{1}H-NMR spectrum of DC-based surfactant.

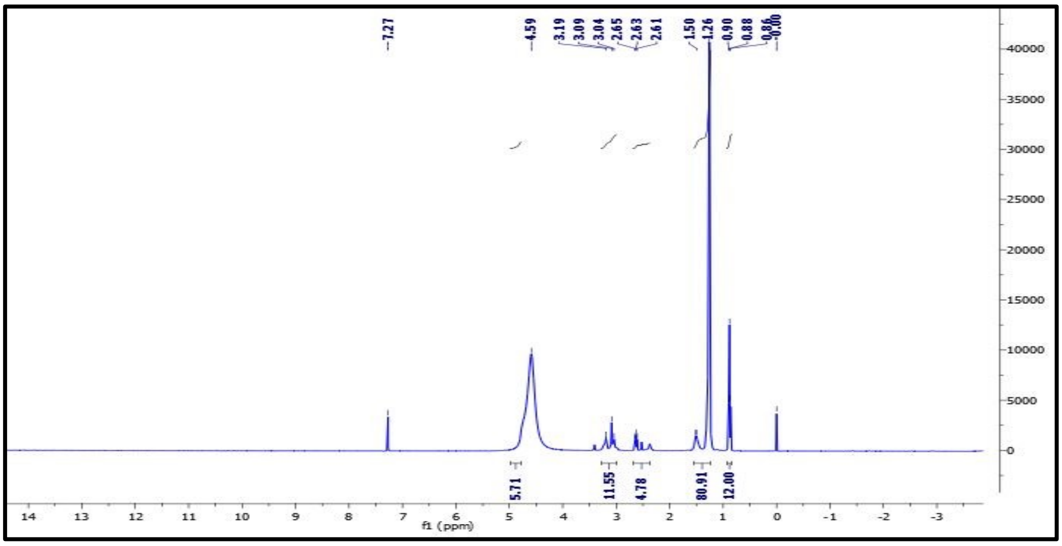

Fig. 2.5: ^{1}H-NMR spectrum of DD-based surfactant.

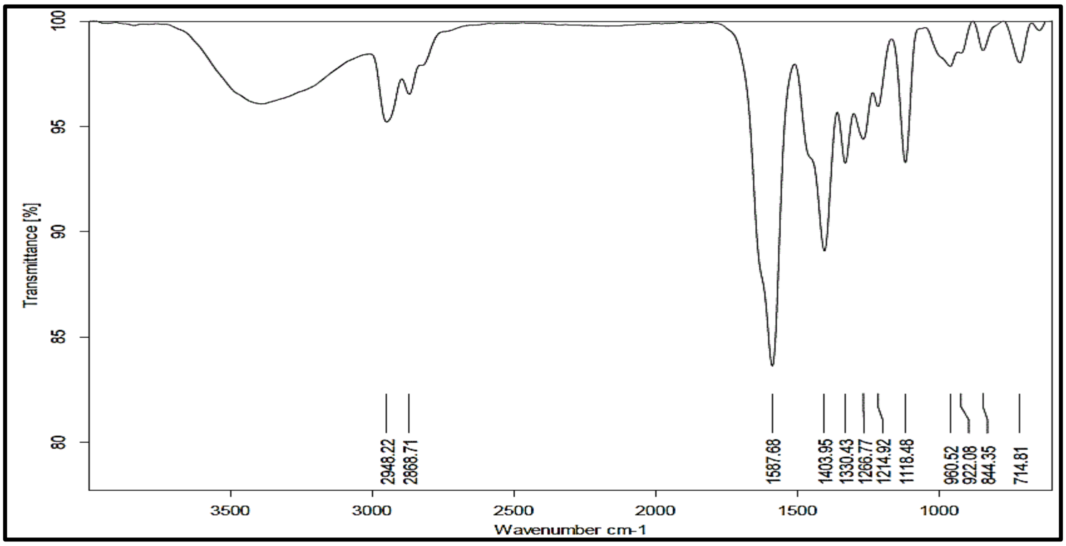

Fig. 2.6: FT-IR spectrum of DB-based surfactant.

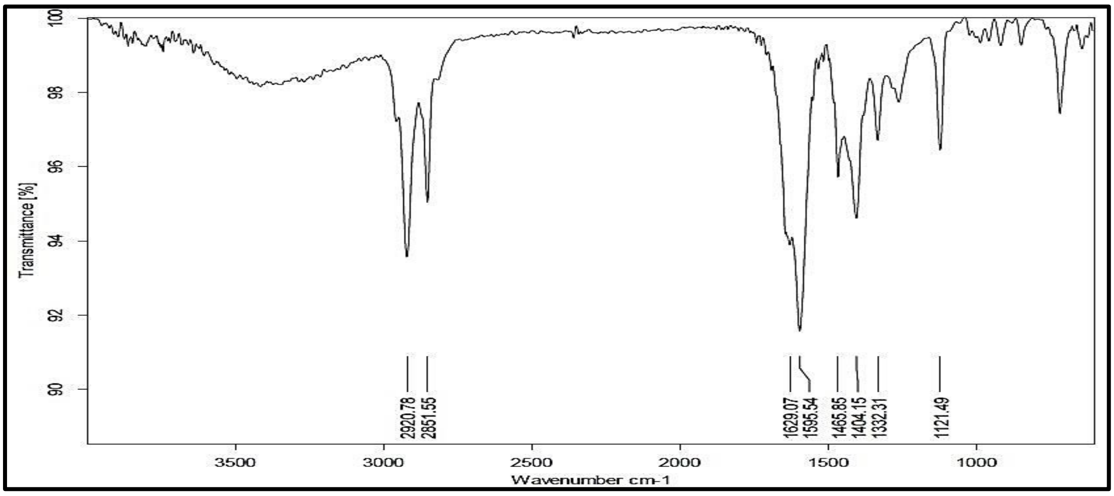

Fig. 2.7: FT-IR spectrum of DH-based surfactant.

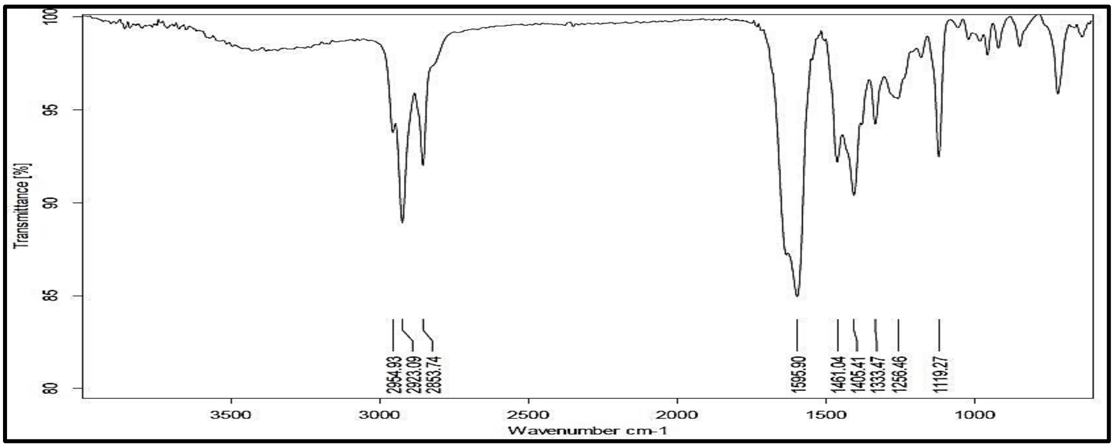

Fig. 2.8: FT-IR spectrum of DO-based surfactant.

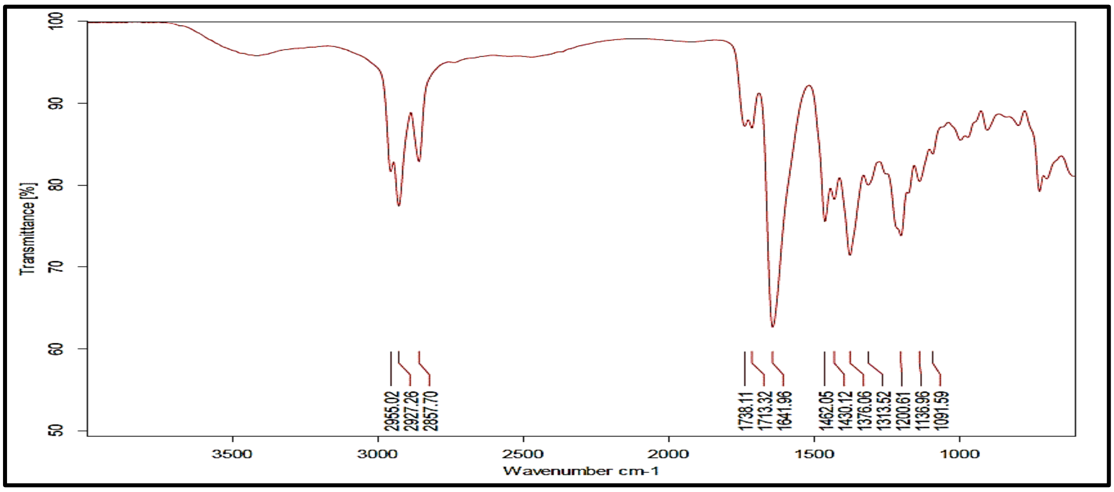

Fig. 2.9: FT-IR spectrum of DC-based surfactant.

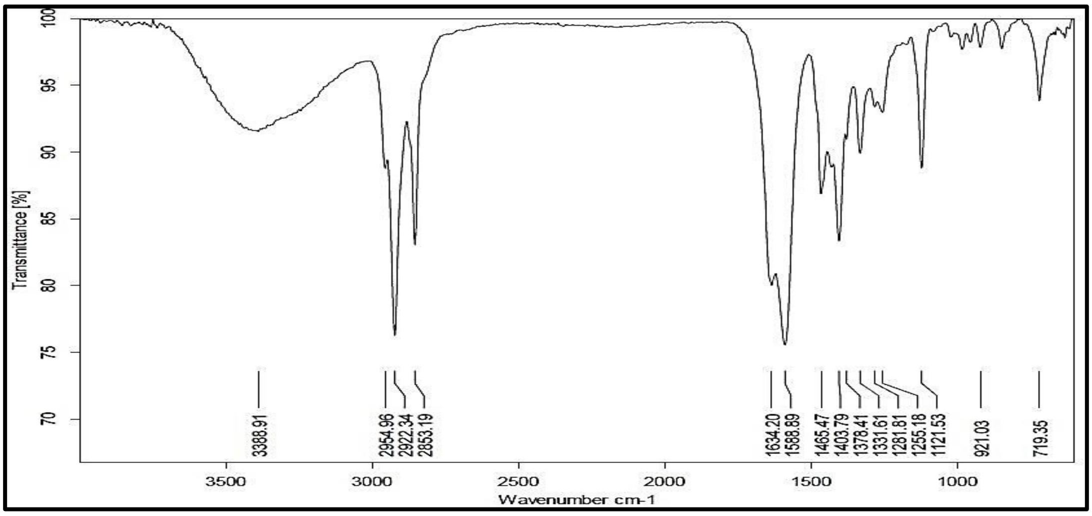

Fig. 2.10: FT-IR spectrum of DD-based surfactant.

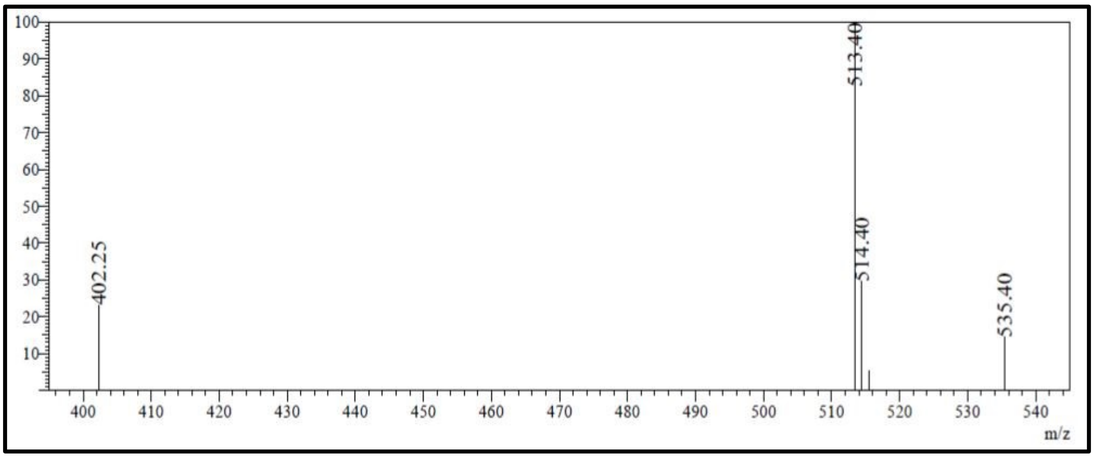

Fig. 2.11: LC-MS of DB-based surfactant.

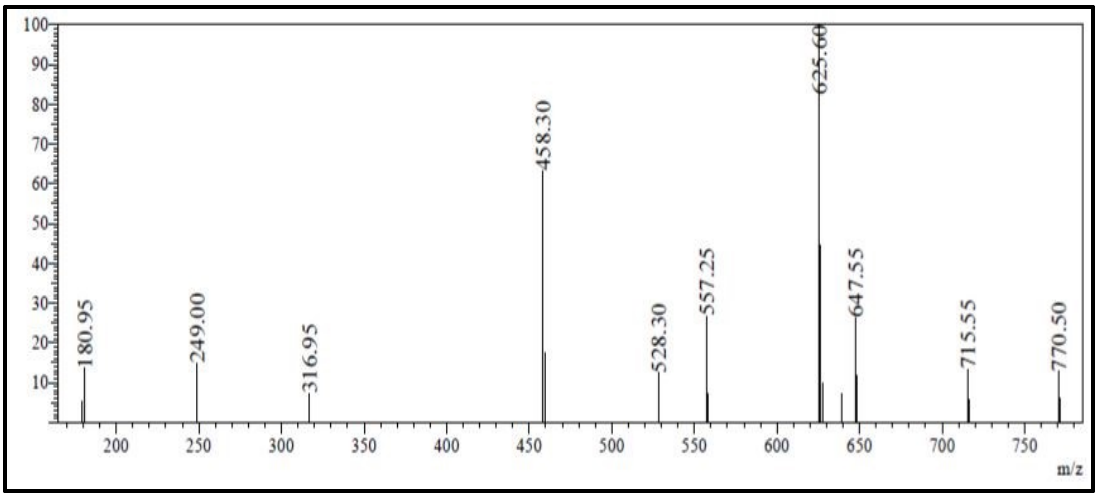

Fig. 2.12: LC-MS of DH-based surfactant.

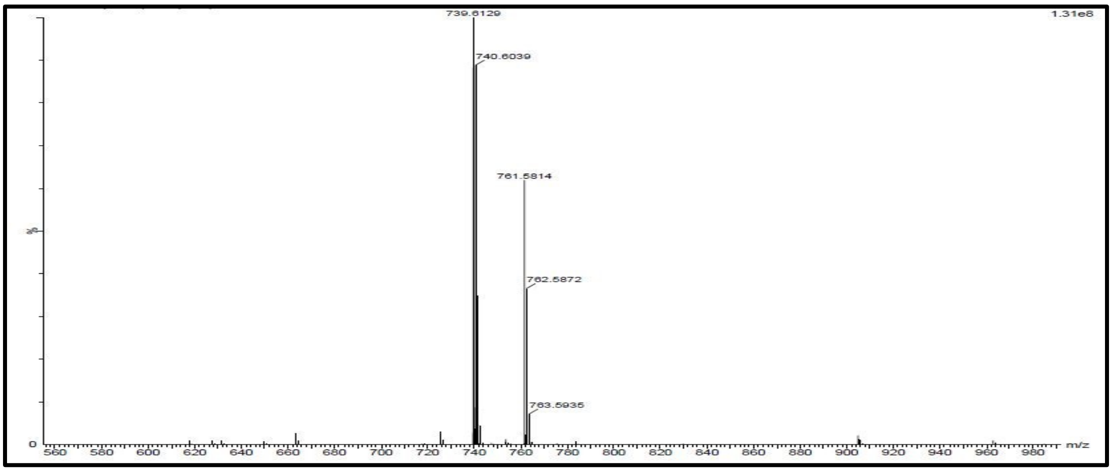

Fig. 2.13: LC-MS of DO-based surfactant.

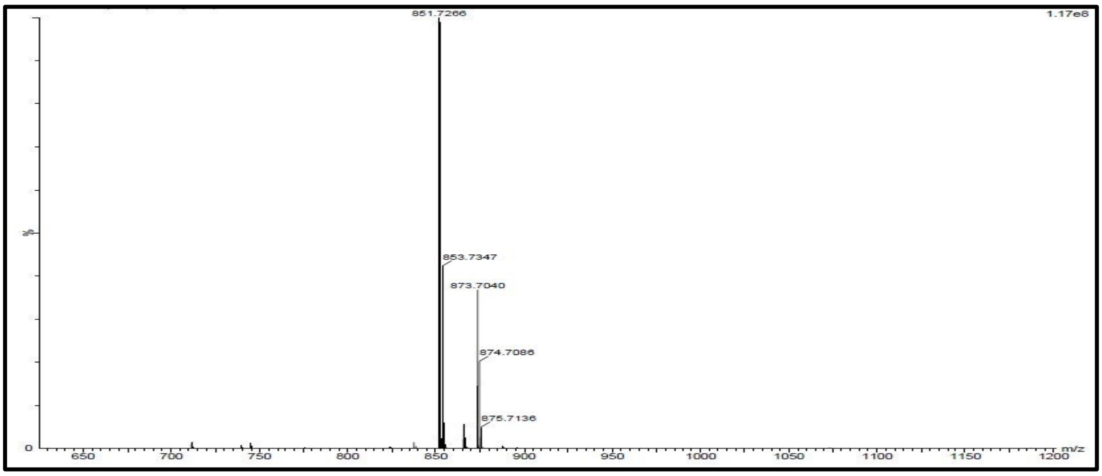

Fig. 2.14: LC-MS of DC-based surfactant.

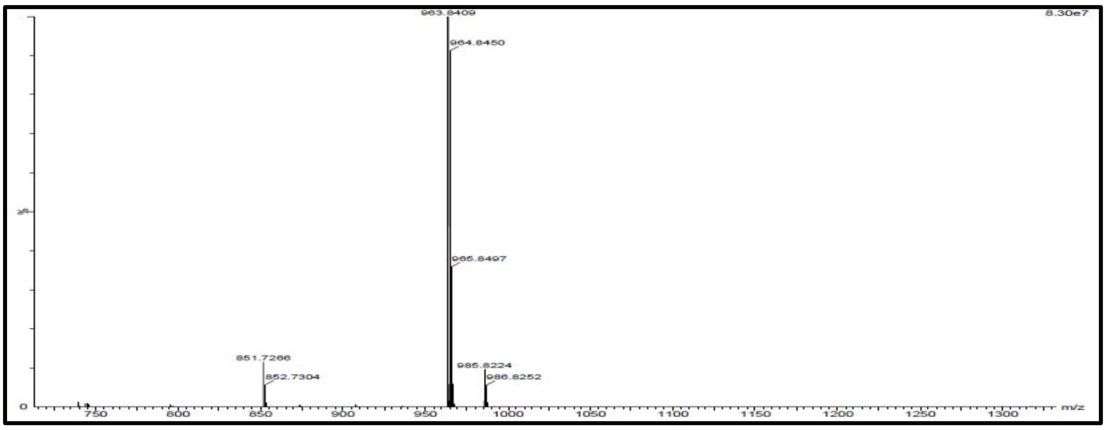

Fig. 2.15: LC-MS of DD-based surfactant.

2.4 METHODS

2.4.1 Electrochemical techniques

Electrochemical measurements were carried out using an electrochemical work station, Gill AC having ACM instrument Version 5 software. A conventional three-electrode system with a Pyrex glass cell was employed, with the AZ31 alloy specimen as the working electrode, a platinum counter electrode, and a saturated calomel electrode (SCE) as the reference electrode. All the values of potential reported are referred to the SCE. The polarization studies were carried out immediately after the EIS studies on the same exposed electrode surface without any additional surface treatment.

2.4.1.1 Electrochemical impedance spectroscopy (EIS) studies

Well-polished AZ31 alloy specimen coupon was exposed to the corrosion medium and allowed to establish steady-state open-circuit potential (OCP). Impedance measurements were performed at the open circuit potential (OCP) by the application of a periodic small amplitude (10 mV) ac voltage signal over a wide spectrum of frequencies ranging from 100 kHz to 0.01 Hz. The impedance data were analyzed using Nyquist and Bode plots. In all the above measurements, at least three similar results were considered and their average values have been reported.

2.4.1.2 Potentiodynamic polarization studies

The potentiodynamic current potential curves (Tafel curves) were recorded by polarizing the specimen to −250 mV cathodically and + 250 mV anodically, relative to the OCP at a scan rate of 1 mV s^{-1}. The potentiodynamic polarization parameters were deduced by the Tafel extrapolation technique on the polarization plots.

2.4.2 Surface analysis

2.4.2.1 Scanning electron microscopy (SEM) analysis

The surface morphology of the freshly polished surface and the corroded surface of the AZ31 alloy, in the corrosive media were analyzed through the SEM images recorded using JEOL JSM-6380LA analytical scanning electron microscope. The surface composition of the fresh surface and corroded surface were determined from their corresponding EDX spectra.

2.4.2.2 X-ray photoelectron spectrum

The corrosion product analysis was carried out by recording the X-ray photoelectron spectra of the corroded alloy surface using ULVAC-PHI, Inc; Model: PHI5000 Version Probe III spectrometer with Al K-α X-ray source.

2.4.2.3 DFT

The ground state geometry and electronic distribution of the synthesized inhibitor surfactant molecules were determined with Density Functional Theory (DFT) simulations using the Turbomole 7.2v software package. The further optimization of the geometry was done with the help of software-generated C1 point group symmetry via the B3LYP program and here, the basic set def-TZVPP was used for all the calculations. The parameters of the investigated surfactants, such as the energy of the molecule (E), the energy of the highest occupied molecular orbital (E_{HOMO}), the energy of the lowest unoccupied molecular orbital (E_{LUMO}), energy gap (ΔE), chemical hardness (η), softness (σ), ionization potential (I_p), electron affinity (E_A), electronegativity (χ), and dipole moment (μ), were calculated.

2.5 CALCULATIONS

2.5.1 Computation of corrosion rate

The corrosion current density (i_{corr}) values were deduced from the extrapolation of cathodic Tafel branches of the potentiodynamic polarization curves to the corrosion potential as the anodic curves did not have well-defined Tafel regions. The experimentally determined i_{corr} values were used in the calculation of corrosion rate (υ_{corr}) using the equation mentioned below.

$$Corrosion\ rate\ (\upsilon_{corr}) = K\frac{i_{corr}}{\rho}EW \qquad (2.1)$$

where, K is 3.27×10^{-3}, a constant that defines the unit for the corrosion rate, i_{corr} is the current density in A cm^{-2}, ρ is the density in g cm^{-3} and EW is the equivalent weight of the alloy. The equivalent weight for the alloy was calculated from the following equation (Dean 1999).

$$EW = \frac{1}{\Sigma \frac{n_i f_i}{W_i}} \qquad (2.2)$$

where, f_i is the mass fraction of the i^{th} element in the alloy, W_i is the atomic weight of the i^{th} element in the alloy and n_i is the valence of the i^{th} element of the alloy. The values of fi, Wi, and ni, of four major elements present in AZ31, are listed in Table 2.2.
The substitution of the values in equation 2.2, gives the equivalent weight of the AZ31 alloy as 12.12.

Table 2.2: The valence, weight fraction, and atomic weight of major elements present in AZ31 alloy.

Element	n_i	f_i	W_i
Mg	2	95.78	24.30
Al	3	2.96	26
Zn	2	0.83	65.38
Mn	2	0.43	54.93

2.5.2 Calculation of inhibition efficiency

The inhibition efficiency (η) was evaluated as a function of surface coverage (θ) and the relation between the two is presented in the following equation.

$$\eta(\%) = \theta \times 100 \qquad (2.3)$$

The value of θ was deduced from the results of electrochemical measurements. The i_{corr} values obtained from the Tafel polarization studies and values of polarization potential (R_p) obtained from EIS measurements were used separately in the evaluation of θ, as per the equations presented below.

$$\theta = \frac{i_{corr(b)} - i_{corr(inh)}}{i_{corr(b)}} \qquad (2.4)$$

where, $i_{corr(b)}$ and $i_{corr(inh)}$ signify the corrosion current densities in the absence and presence of inhibitors, respectively.

The value of θ was evaluated from the values of R_{hf} values using equation 2.5.

$$\theta = \frac{R_{hf(inh)} - R_{hf(b)}}{R_{hf(inh)}} \qquad (2.5)$$

where, $R_{hf(inh)}$ and R_{hf} signify the polarization resistances obtained in the presence and absence of inhibitors, respectively.

2.5.3 Evaluation of activation parameters

The activation parameters for the corrosion of AZ31 were calculated by measuring the corrosion rates at different temperatures. The activation parameters included apparent activation energy (*Ea*), apparent enthalpy of activation ($\Delta H^{\#}$) and entropy of activation ($\Delta S^{\#}$). Arrhenius law equation (Eq 2.6) was used for the calculation of *Ea* and the transition state equation (Eq.2.7) was employed for the calculation of $\Delta H^{\#}$ and $\Delta S^{\#}$.

$$\upsilon_{corr} = Ae^{\frac{-E_a}{RT}} \qquad (2.6)$$

where A is the proportionality constant which is dependent on the type of the metallic material, T is absolute temperature, R is the universal gas constant and υ_{corr} is corrosion rate. The slope of the straight lines was used in the deduction of E_a (slope= $-E_a/R$).

Transition state equation:

$$\upsilon_{corr} = \frac{RT}{Nh} e^{\frac{\Delta S^{\#}}{R}} e^{\frac{\Delta H^{\#}}{RT}} \qquad (2.7)$$

where h is plank's constant and N is Avogadro's number. The parameters $\Delta H^{\#}$ and $\Delta S^{\#}$ were calculated, respectively, from the slope (slope = $-\Delta H^{\#}/R$) and intercept (intercept = $\ln (R/Nh) + \Delta S^{\#}/R$) values of the straight lines obtained from the plots of $\ln (\upsilon_{corr}/T)$ versus ($1/T$).

2.5.4 Calculation of thermodynamic parameters

The calculation of the thermodynamic parameters for the adsorption of inhibitor were based on a suitable adsorption isotherm model with which the system under the study showed the best agreement. An adsorption isotherm is defined as a graphical representation showing the variation of extent of adsorption with pressure at a given constant temperature. For the adsorption occurring at solution/solid interface, the concentration of the adsorbate (inhibitor) can be considered as the equivalent of pressure. The mathematical expression for the adsorption isotherms highlights an equilibrium relation between inhibitor concentrations on the metal surface and that in bulk solution. Hence the adsorption isotherms are applicable to the systems where the inhibition is the consequence of surface coverage brought about by the inhibitor on adsorption. Some of the adsorption isotherms commonly verified to explain corrosion inhibition, their mathematical expressions, and verification plots are presented in Table 2.3.

The parameters in Table 2.3 are as follows:

Table 2.3: List of adsorption isotherms.

Name	Isotherm	Verification Plot
Langmuir	$\theta/(1-\theta) = \beta.C$	C/θ vs C
Frumkin	$[\theta/(1-\theta)]e^{f\theta} = \beta.C$	θ vs log C
Bockris-Swinkels	$\theta/(1-\theta)^n.[\ \theta + n(1-\theta)]^{n-1}/n^n = C.e^{-\beta}/55.4$	$\theta/(1-\theta)$ vs log C
Temkin	$\theta = (1/\mathrm{f})\ln K.C$	θ vs log C
Virial Parson	$\theta.e^{2f\theta} = \beta.C$	θ vs $\log(\theta/C)$
Flory Huggins	$\log(\theta/C) = \log nK + n\log(1-\theta)$	$\log(\theta/C)$ vs $\log(1-\theta)$
El – Awady	$\log[\theta/(1-\theta)] = \log K + y\log C$	$\log[\theta/(1-\theta)]$ vs log C

θ is the surface coverage, $\beta = \Delta G/2.303RT$, where ΔG is free energy change of adsorption, R – gas constant, T- temperature, C is inhibitor concentration in bulk electrolyte, χ represents size ratio or the number of water molecules replaced per molecule of adsorbed inhibitor, f is the inhibitor interaction parameter (0 implies no interaction; positive value implies attraction; negative value implies repulsion) and K and y are constants.

The C and θ values were graphically fitted in the adsorption isotherms to get the linear relationship between them and regression coefficients (R^2) were compared. The standard free energy of adsorption (ΔG°_{ads}) was calculated using the following expression.

$$\Delta G^\circ_{ads} = -RT \ln \left[\frac{55\times\theta}{C(1-\theta)}\right] \qquad (2.8)$$

where C is the inhibitor concentration expressed in mol.dm^{-3} and 55.5 in mol dm^{-3} is the molar concentration of water in solution.

The standard enthalpy of adsorption (ΔH°_{ads}) and standard entropy of adsorption (ΔS°_{ads}) were evaluated by making use of a rearranged form of the Gibbs Helmholtz equation, as shown below.

$$\Delta G^\circ_{ads} = \Delta H^\circ_{ads} - T\Delta S^\circ_{ads} \qquad (2.9)$$

As per Equation 2.9, straight lines were obtained on graphically plotting the variation of ΔG°_{ads} with T. The slope and the intercept of the lines were, respectively, equal to ΔS°_{ads} and ΔH°_{ads}.

CHAPTER-3

RESULTS AND DISCUSSIONS

CHAPTER 3

RESULTS AND DISCUSSION

3.1 CORROSION BEHAVIOR OF AZ31 ALLOY IN AQUEOUS SALT SOLUTIONS

3.1.1 Potentiodynamic polarization measurements

The corrosion behavior of AZ31 alloy was investigated in sodium chloride and sodium sulfate media of different concentrations, at different temperatures by potentiodynamic polarization method. Fig. 3.1 represents the potentiodynamic polarization curves for the corrosion of AZ31 alloy in sodium chloride and sodium sulfate media. Similar curves have been obtained at other temperatures also.

It is seen from Fig. 3.1 that the polarization curves are shifted to the higher current density region, indicating an increase in the corrosion rate with the increase in chloride and sulfate concentration in the corrosion media. The anodic polarization curves represent the anodic oxidation of the magnesium alloy, while the cathodic curves represent the hydrogen evolution through the reduction of water at the cathode. The anodic curves show the inflection points, characterized by two different slopes, indicating a kinetic barrier effect, possibly due to the deposition of a surface film of magnesium hydroxide, followed by its dissolution at higher anodic potential (CHENG et al. 2009). It is also observed from Fig. 3.1 that there is no significant change in the overall shapes of the Tafel branches with the varying salt concentration in the corrosion media, indicating that medium concentration only alters the rate, without altering the mechanism of corrosion reaction. Such kinds of results have been reported by Nandini et al. (2014) (Dinodi and Shetty 2014) for ZE41 alloy and by Wang et al. (2010) for Mg-Al-Pb alloy. The corrosion current density (i_{corr}) was deduced by extrapolating the cathodic branch of the polarization curves to the OCP. The electrochemical polarization parameters like corrosion potential (E_{corr}), corrosion current density (i_{corr}), and cathodic slope (β_c) were obtained from the curves. Equation (Eq. (3.1)) given below was used to determine corrosion rate in mm y^{-1} (Standard 2006).

$$v_{corr}(mm\ y^{-1}) = \frac{K \times i_{corr} \times EW}{\rho} \qquad (3.1)$$

where constant K = 0.00327, defines the unit of corrosion rate (mm y^{-1}), i_{corr} is the corrosion current density in µA cm^{-3}, ρ is the density of the corroding material and EW is the equivalent weight of the alloy.

The potentiodynamic polarization parameters, including corrosion potential (E_{corr}), corrosion current (i_{corr}), cathodic slopes (β_c), and corrosion rate (υ_{corr}) are summarized in Tables 3.1 and 3.2 for the corrosion of AZ31 alloy in NaCl and Na_2SO_4 media, respectively. It is evident from the data in Tables 3.1 and 3.2, that the corrosion rate increases with the increase in the concentration of chloride/sulfate in the corrosion medium. These ions are corrosive towards magnesium and its alloys because they tend to cause surface film breakdown by the dissolution of the deposited corrosion product, thereby increasing the anodic dissolution of the alloy.

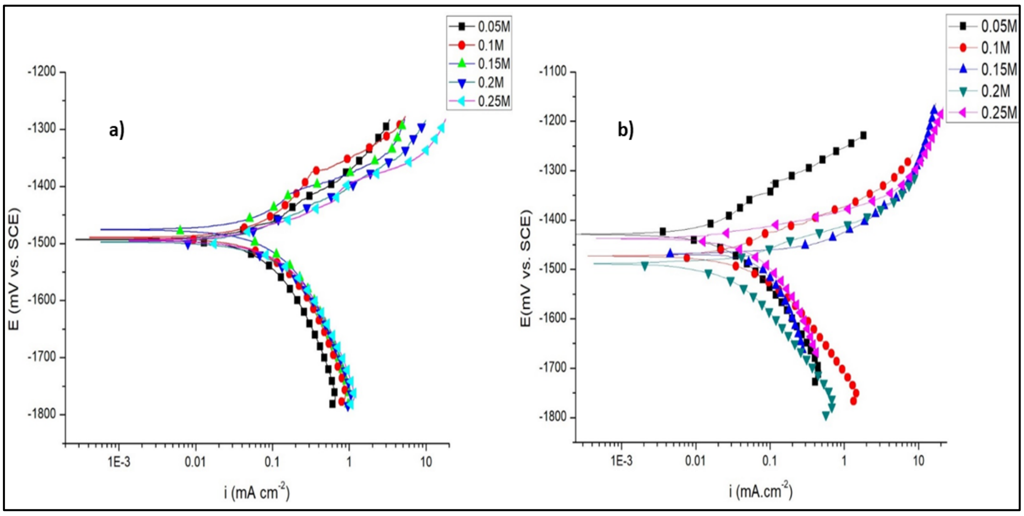

Fig. 3.1: Potentiodynamic polarization curves for the corrosion of AZ31 alloy in different concentrations of a) NaCl medium at 50 °C and b) Na_2SO_4 medium at 40 °C.

3.1.2 Electrochemical impedance spectroscopy studies

The electrochemical impedance spectra in the form of Nyquist plots for the corrosion of AZ31 alloy in NaCl and Na_2SO_4 solutions of different concentrations, at 50 °C and 40 °C are presented in Fig. 3.2, respectively. Similar plots were obtained at other temperatures also.

All the Nyquist plots consist of two capacitive loops at the higher and the medium frequencies, and the beginning of an inductive loop at the lower frequency region. The higher frequency (*hf*) semicircle corresponds to the charge transfer of corrosion process and oxide film effects, and the medium frequency (*mf*) semicircle corresponds to the mass transport (diffusion of magnesium ions) through the corrosion product layer of $Mg(OH)_2$. The relaxation of surface adsorbed species like $Mg(OH)^+$ and $Mg(OH)_2$ is considered to be the genesis of the lower frequency (*lf*) inductive loop. Though there are different versions of interpreting the impedance of magnesium alloy corrosion processes, the current explanation has been one of the most adopted (Mathieu et al. 2002; Song and Atrens 2007; Ardelean et al. 2008; Frignani et al. 2012). It is observed from Fig. 3.2 that the diameter of the capacitive loops decreases with the increase in the concentrations of chloride ions and sulfate ions, respectively, implying that the corrosion rate increases with an increase in the concentrations of these ions.

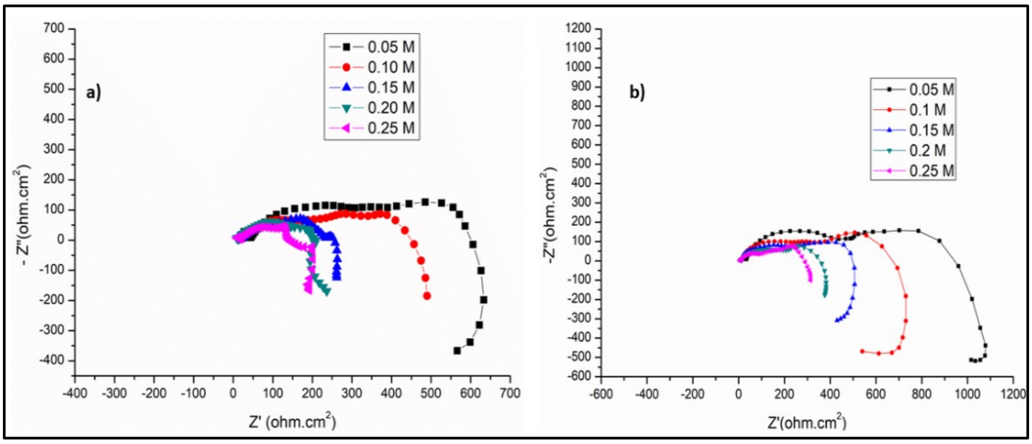

Fig. 3.2: Nyquist plots for the corrosion of AZ31 alloy in different concentrations of a) NaCl medium at 50 °C and b) Na_2SO_4 medium at 40 °C.

The impedance parameters obtained are derived from simulation analyses. The impedance data points excluding the *lf* inductive loop can be analyzed using an equivalent electrical circuit (EEC) along with the representative simulation plot as shown Fig. 3.3. The entire impedance studies were carried out using simulation analyses to obtain the parameters, and the measurement error was kept below 5%. The *hf* region of the impedance spectra can be simulated by a series of two parallel resistance – constant phase element (R-CPE) networks; consisting of the charge transfer resistance (R_{ct}) in parallel with the double layer CPE (Q_{dl}) and the surface film resistance (R_f) in parallel with the CPE (Q_f) of the film. The *mf* response can be simulated with a parallel network of resistance (R_{dif}) with the CPE (Q_f) of the film. The *mf* response can be simulated with a parallel network of resistance (R_{dif}) and CPE (Q_{dif}) associated with the diffusion (Fletcher 1994). The constant phase element (Q_{dl}) is substituted for the ideal capacitive element in order to account for the inhomogeneity and porosity of the electrode surface (Mansfeld et al. 1992).

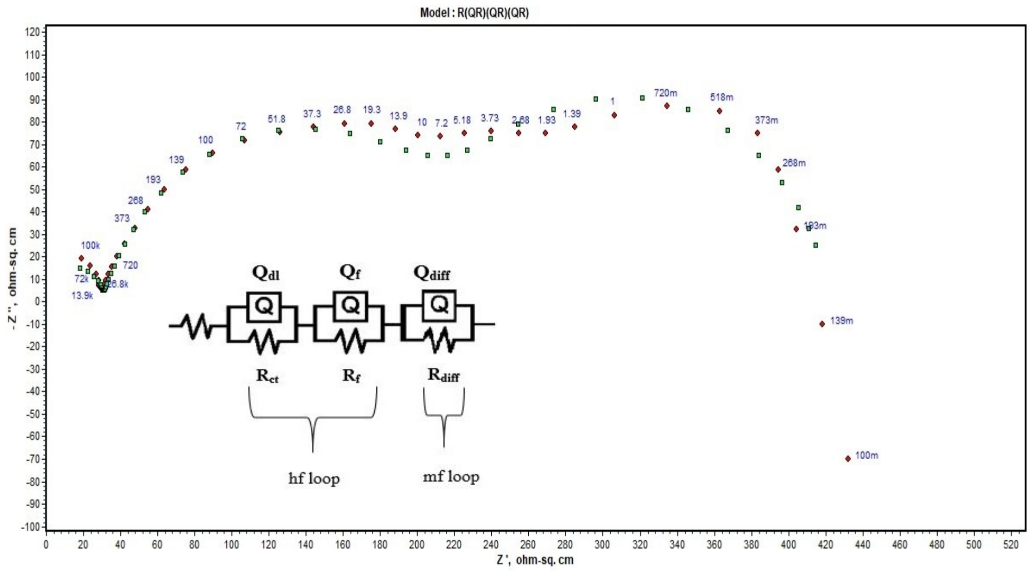

Fig. 3.3: Simulation curve and electrical equivalent circuit used for the simulation of experimental data for the corrosion of AZ31 alloy in 0.20 M NaCl medium.

The impedance of the constant phase is given by the following equation (Dinodi and Nityananda Shetty 2013):

$$Z_Q = Y_0^{-1}(j\omega)^{-n} \tag{3.2}$$

where Y_0 is the CPE constant, ω represents the angular frequency (in rad s^{-1}), $j^2 = -1$ is the imaginary number and n is a CPE exponent which measures the heterogeneity or roughness of the surface. The value of n is given by ($-1 \leq n \leq 1$); and the CPE simulates an ideal capacitor when $n = 1$, an ideal inductor for $n = -1$, and an ideal resistor for $n = 0$. The capacitance is deduced from the CPE using the following equation (Pebere et al. 1990):

$$C = Y_0(\omega_{max})^{n-1} \tag{3.3}$$

where, ω_m^n is the frequency at which the imaginary part of the impedance (Z") has a maximum.

The values of electrochemical impedance parameters are listed in Tables 3.3 and 3.4 for the corrosion of AZ31 alloy in NaCl medium and Na_2SO_4 medium, respectively. The impedance value is inversely related to the corrosion rate. The decrease in the values R_{hf} with the increase in the concentration of chloride and sulfate ions indicates the increase in the corrosion rate. The trend is in line with the one observed in the case of potentiodynamic polarization studies. The trend can be explained by taking into account of the tendency of anions like sulfate and chloride to destabilize the $Mg(OH)_2$ surface film by dissolution when they are present in higher concentrations in the corrosion media, thereby negating the partial protection provided by the surface film of the corrosion product.

3.1.3 Influence of temperature

The effect of temperature on the corrosion of AZ31 alloy in the chloride and the sulfate media of different concentrations were evaluated by measuring the corrosion rates at different temperatures. Fig. 3.4 shows the potentiodynamic polarization curves for the corrosion of AZ31 alloy at different solution temperatures, in 0.25 M NaCl and 0.15 M Na_2SO_4 solutions. The Nyquist plots for the same are shown in Fig. 3.5.

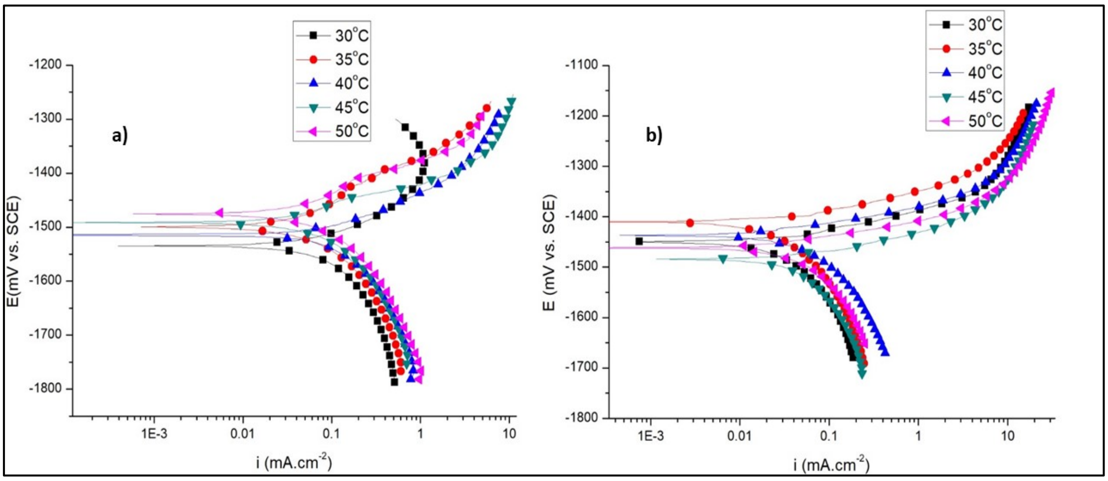

Fig. 3.4: Potentiodynamic polarization curves for the corrosion of AZ31 alloy in a) 0.25 M NaCl and b) 0.15 M Na_2SO_4 at different temperatures.

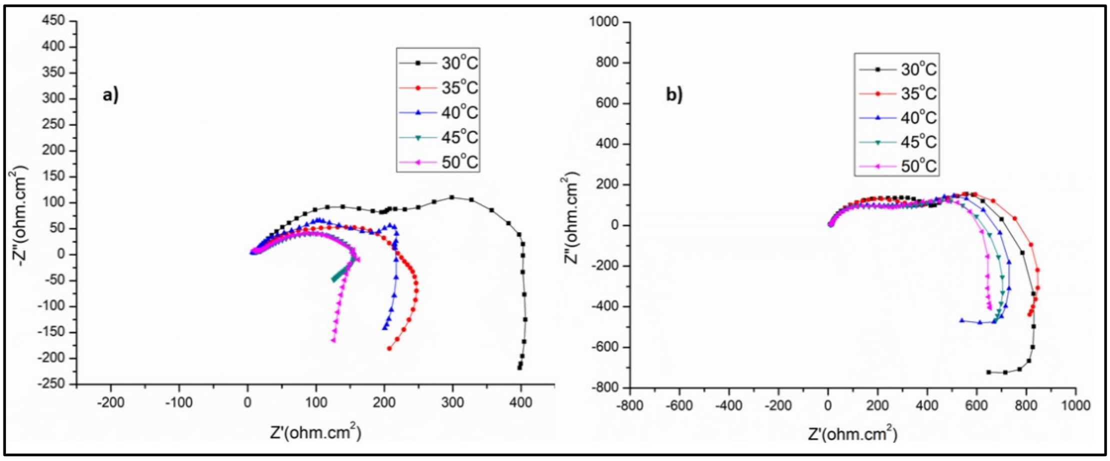

Fig. 3.5: Nyquist plots for the corrosion of AZ31 alloy in a) 0.25 M NaCl and b) 0.15 M Na_2SO_4, at different temperatures.

It can be observed from Fig. 3.5 that the increase in medium temperature makes the polarization curves to shift towards a higher current density region and capacitive loops in the Nyquist plots to decrease its diameter, both of which signify an increase in the rate of corrosion. The influence of temperature is rather apparent from the variation in the electrochemical parameters enlisted in Table 3.3, Table 3.4, wherein both sodium chloride and sodium sulfate media, at any concentration, the rate of AZ31 corrosion increases with the increase in the temperature. Furthermore, at any specific medium concentration, the thickness and the protective performance of the surface film are optimal at lower temperatures, as precisely reflected by the combination of values; smaller C_f, and larger R_f, which is observed only at lower temperatures.

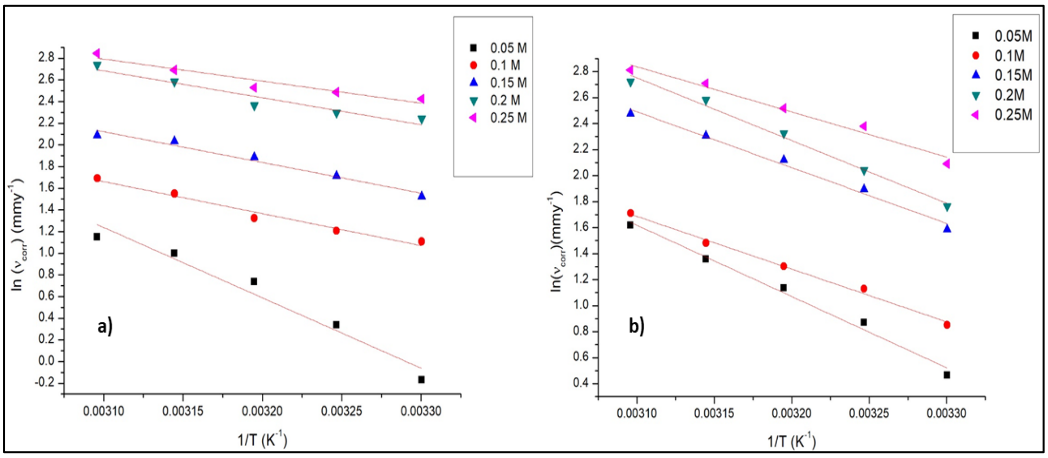

Fig. 3.6: Arrhenius plots for the corrosion of AZ31 alloy in a) NaCl and b) Na_2SO_4 media.

The activation energy corresponds to the energy barrier for the occurrence of corrosion. The continuous decrease in E_a with the increased ionic concentration of the media as seen in Table 3.5 and Table 3.6, points out that the corrosion of AZ31 is energetically more feasible in concentrated media (Baghni et al. 2004).

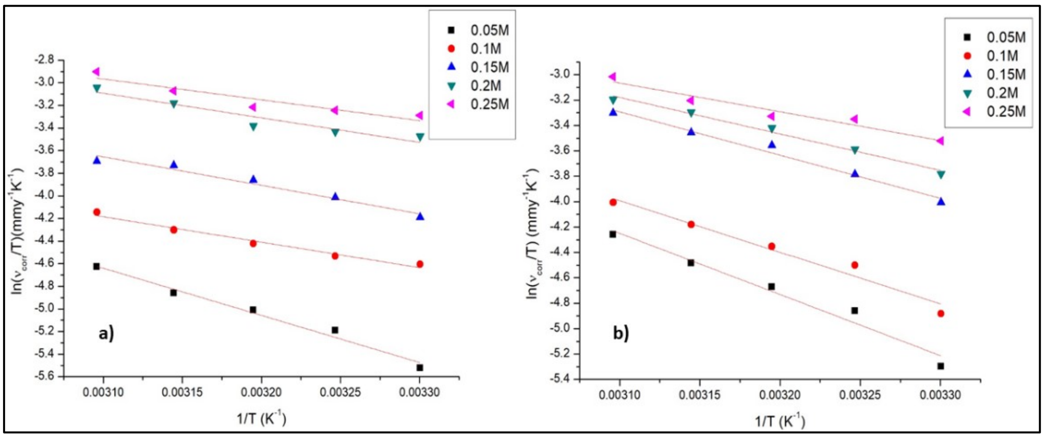

Fig. 3.7: ln(v_{corr}/T) vs. 1/T plots for the corrosion of AZ31 alloy in a) NaCl and b) Na_2SO_4 media.

The pattern of variation of $\Delta H^{\#}$ values is identical to that of activation energy. The negative values of $\Delta S^{\#}$ suggest a decrease in the randomness of the system which could be the consequence of the association of the reactants during the formation of the activated complex in the rate-determining step of corrosion (Bentiss et al. 2005).

The study of corrosion in a range of temperatures is good in some ways; not only does it establish the impact of temperature on the corrosion rate but also facilitates the evaluation of activation parameters pertaining to the alloy dissolution. Arrhenius law equation (Eq. 2.7) and transition state equation (Eq. 2.8) as stated in the previous chapter, were utilized for the determination of activation energy (E_a), the enthalpy of activation ($\Delta H^{\#}$), and entropy of activation ($\Delta S^{\#}$). Arrhenius plots for the corrosion of AZ31 alloy specimen in sodium chloride and sodium sulfate media are represented in Fig. 3.6. The ln(υ_{corr}/T) versus ($1/T$) plots for the same are shown in Fig. 3.7.

3.1.4 Mechanism of AZ31 alloy corrosion

3.1.4.1 Anodic dissolution of magnesium and negative difference effect [NDE]

The corrosion behavior of magnesium and its alloys is accompanied by high hydrogen evolution and the reaction rate increases with the increase in the anodic polarization. This is called a negative difference effect (Song et al. 1998). Many models have been suggested to explain this effect. The removal of a protective film surface with anodic polarization must make up the diminution of the cathodic current density by anodic polarization.

The chosen medium NaCl and Na_2SO_4 for the present study are both near-neutral solutions, where the cathodic reaction of corrosion dominates and where the corrosion happens due to the hydrogen evolution through electrochemical reduction of water as shown below.

$$2H_2O + 2e^- \rightarrow H_2 + 2OH^- \qquad (3.5)$$

However, the anodic oxidation of magnesium dissolution has remained complex. The oxidation and the corresponding corrosion of magnesium in an aqueous solution can be represented by the following reactions (Baghni et al. 2004):

$$Mg \rightarrow Mg^{+} + e^{-} \tag{3.6}$$

$$Mg \rightarrow Mg^{2+} + 2e^{-} \tag{3.7}$$

The steady-state working potential of magnesium is about –1.5 V, even though the standard electrode potential of magnesium is –2.38 V. The change in potential is due to the formation of $Mg(OH)_2$ film on the surface of the alloy (Mathieu et al. 2002). However, this hydroxide layer is discontinuous and only partially covers the alloy surface, without effectively protecting the alloy surface. The anodic dissolution of magnesium and its alloys involve two oxidation processes. At more active potentials of about –2.78 V (vs SCE) magnesium undergoes oxidized to monovalent magnesium ion (Mg^{+}) and at slightly higher potentials of about –1.56 V (vs SCE), magnesium undergoes oxidation to a divalent magnesium ion (Mg^{2+}), in parallel with the former oxidation (Lopez and Natta 2001). The monovalent magnesium ion is unstable and undergoes oxidation to divalent magnesium ion through a series of reactions involving unstable intermediates like magnesium hydride as shown in equations below:

$$Mg^{+} + 2H^{+} + 3e^{-} \rightarrow MgH_2 \tag{3.8}$$

$$Mg^{2+} + 2OH^{-} \rightarrow Mg(OH)_2 \tag{3.9}$$

$$2Mg^{+} + 2H_2O \rightarrow Mg^{2+} + Mg(OH)_2 + H_2 \tag{3.10}$$

The involvement of intermediates like monovalent magnesium ions during AZ31 corrosion is substantiated by the appearance of the inductive loops at the lower frequency region in the Nyquist plots. The secondary oxidation eventually produces hydrogen (evolved via chemical oxidation) and magnesium hydroxide as represented in the eqn. 3.10 (Song and Atrens 1999).

Thus, during corrosion of magnesium and its alloy in an aqueous solution, the hydrogen evolution takes place in both cathode and anode, respectively, through electrical reduction and chemical oxidation of Mg^+ and Mg^{2+}. The product formed by corrosion, i.e., $Mg(OH)_2$ precipitates and forms over the corroding magnesium surface as a film. The film is very feeble and thin with a Pilling Bedworth ratio of 0.84 (Zhao et al. 2008). The efficacy of the surface film to protect the underlying metal is believed to be inadequate and hence the magnesium hydroxide surface film has been termed as partially protective where the corrosion reactions continue unabatedly within the defects of the film (Nordlien et al. 1997).

Many different ways have been put forward to clarify negative difference effects in the literature review of the introduction; such as 1) univalent magnesium ion (Mg^+) model, (2) eroding and tearing away of cathodic secondary phase particles due to micro galvanic corrosion, (3) hydride model, (4) feeble protective film model. These models try to discuss the NDE in their aspects. The univalent magnesium ion model and hydride model corroborate the chemical evolution of hydrogen. The second aspect of NDE explains that the untimely and accelerated anodic dissolution results due to the breakdown and dissolution of the surface film at higher anodic overvoltages as predicted by the partially protective film model.

3.1.4.2 Microgalvanic corrosion of AZ31 alloy

AZ31 is a wrought alloy, where its microstructure is pivotal in the corrosion of its alloy. The microstructure of AZ31 alloy consists of the α-Mg matrix, distributed with the secondary β-phase, comprising of intermetallic compound $Mg_{17}Al_{12}$. The secondary β-phase is cathodic to the Mg matrix and is with a good passive behavior over a broad range of pH (CHENG et al. 2009). However, the role of β-phase in the corrosion process depends upon its size and distribution (Dinodi and Nityananda Shetty 2013). When the grain size of magnesium alloy is small and the mass fraction of β- phase is high, the distribution of the β-phase on the α-Mg matrix is continuous; providing corrosion protection by a barrier layer effect. On the other hand, when the grain size is larger and the β-phases cannot cover the α-phase completely, galvanic corrosion results with the α-phase acting as anode and undergoing corrosion.

The corrosion product, $Mg(OH)_2$, precipitates over the α-Mg matrix and this surface film is only partially selective as the continuity of the film is interrupted by the presence of the secondary phase. In addition, the secondary oxidation results in the chemical liberation of hydrogen gas at the anode. This rapid liberation of hydrogen gas at the anodic sites causes the breakdown of the surface film at higher anodic overvoltage and accounts for the inflection in an anodic branch of Tafel plots (Nordlien et al. 1997).

Choi (Choi and Pyo 2016) investigated the corrosion of several magnesium alloys in aqueous salt solutions and have highlighted the difference between the corrosion rates obtained from the Tafel extrapolation (short-term method) and other non-electrochemical methods like hydrogen evolution studies and weight-loss measurements (long-term methods). In Tafel measurements, the corrosion rate determination is based upon the rate of electron transfer or the current density. The polarization measurements when performed soon after the immersion of the alloy in the electrolyte give instantaneous corrosion rates. The corrosion rates were examined using hydrogen evolution studies for exposure periods until a steady state was obtained. Considering the dynamic nature of the interface of corroding alloy, the immediate and steady-state corrosion rates are meant to differ as to the surface topography and the corroding area continuously change with time (Lv et al. 2014; King et al. 2014; Chen et al. 2019). The potentiodynamic polarization measurements for AZ31, even when performed after the attainment of the steady-state, might differ from those obtained through hydrogen evolution tests and other techniques, considering the features of negative difference effect. Since magnesium corrosion is only partly electrochemical, hydrogen is evolved both electrically through cathodic reduction and chemically through secondary oxidation; the rate of evolution of hydrogen calculated from the hydrogen evolution studies might overestimate the actual rate of alloy corrosion. The discrepancy with the results of weight loss measurements is because of the after-effects of micro-galvanic corrosion, where the cathodic intermetallic particles fall out of the alloy due to accelerated dissolution across the particle boundary. Such undermining and falling away of the cathodic particles results in a weight loss that is larger than that arising solely from the electrochemical metal alloy dissolution.

3.1.4.3 Influence of ionic concentration and temperature

The response of the AZ31 alloy towards the changes in the environmental factors like ionic concentration or temperature to a great measure is influenced by the surface film properties, especially the film stability. The dissolution of the film layer exposes the naked alloy surface to the electrolyte, resulting in an accelerated attack. The protective performance of the surface film is primarily dependent on the electrolyte type. The anions like chloride and sulfate which act as pitting agents bring about the dissolution of the surface film by transforming magnesium hydroxide into soluble salts of magnesium chloride and magnesium sulfate respectively (CHENG et al. 2009). The outcome of this surface film dissolution paves way for an increase in the corrosion rate of the AZ31 alloy as there is an increase in the concentration of ionic media.

Normally chloride will be significantly more corrosive than sulfate for both Mg and Al (Zhao et al. 2008a). In the NaCl environment, the adsorption of the chloride ions on the Mg surface effectively changes $Mg(OH)_2$ to soluble $MgCl_2$, thus destroying the compactness of the corrosion product film and resulting in pitting corrosion (Song and Atrens 1999). It is expected that magnesium dissolution and hydrogen evolution rates in NaCl medium should be higher than that in Na_2SO_4 medium and the experimental results in the present study are consistent with the trend expected. The chloride ions not only increase the solubility of magnesium oxide or magnesium hydroxide surface film significantly, its combination with metallic magnesium, weakens the bonds among the metallic atoms and quickens their take-off from their original position to form the intermediate species Mg^{+} (Jia'an et al. 2017). Also, in the presence of sulfate ions Mg-Al alloys form $MgAl_2(SO_4)_4.22H_2O$ as per the following equation (3.11):

$$Mg^{2+} + 2Al^{3+} + 4SO_4^{2-} + 22H_2O \rightarrow MgAl_2(SO_4)_4.\ 22H_2O \qquad (3.11)$$

The so formed $MgAl_2(SO_4)_4$. $22H_2O$, as a corrosion product gets deposited on the surface of the alloy, due to its lower solubility, forming a semi-permeable film on the alloy surface. This decreases the penetration of sulfate ions. Also, sulfate ion is bigger than chloride ions in size, and hence, less prone to drill through the film. Thus, both these factors reduce the penetration of sulfate ions to the fresh alloy surface (Iwanaga et al. 2004).

The corrosion rate of AZ31 alloy from the results of this study shows that the increase in the corrosion rate is accompanied by an increase in temperature. The temperature effects can be assigned to the increase in the dissolution of the surface film and decreased hydrogen overvoltage. The solubility of $Mg(OH)_2$ increases with the increase in the temperature and hence a higher solution temperature promotes greater dissolution of the surface film. The increase in temperature is also known to increasingly reduce the hydrogen overvoltage which makes the cathodic hydrogen evolution and the alloy corrosion occur easily.

3.1.5 Surface morphology

The SEM images were used to compare the morphology of the alloy surfaces under un-corroded and corroded conditions. EDX was employed to evaluate the compositions of the respective alloy surfaces. The SEM image of the freshly polished surface of AZ31 alloy is shown in Fig.3.8 The microstructure of the alloy, as evident from the SEM image, consists of randomly distributed sub-micron sized β-phase in the main body of the α-phase. The average grain size was obtained to be 2.8 μm. The EDX spectra (Fig. 3.9) of the freshly polished surface shows the presence of the constituent elements of the alloy. The SEM image of the alloy surface immersed in 0.1 M, 0.15 M, 0.20 M, and 0.25 M NaCl medium for 3 h is shown in Fig. 3.10. The EDX spectra of the alloy surface immersed in 0.25 M NaCl is shown in Fig. 3.11. The SEM image of the alloy in 0.1 M, 0.15 M, 0.20 M, and 0.25 M Na_2SO_4 and EDX spectra of the alloy surface after immersion in 0.2 M Na_2SO_4 medium for 3 h are presented in Figs. 3.12 and 3.13, respectively. The SEM images of the alloy surfaces clearly show the deterioration in the presence of the corrosive media;

the microstructure is hardly visible hinting at the deposition that occurred on the surface as a film. The appearance of predominant oxygen on the alloy surface due to the presence of corrosion product, $Mg(OH)_2$ on the surface.

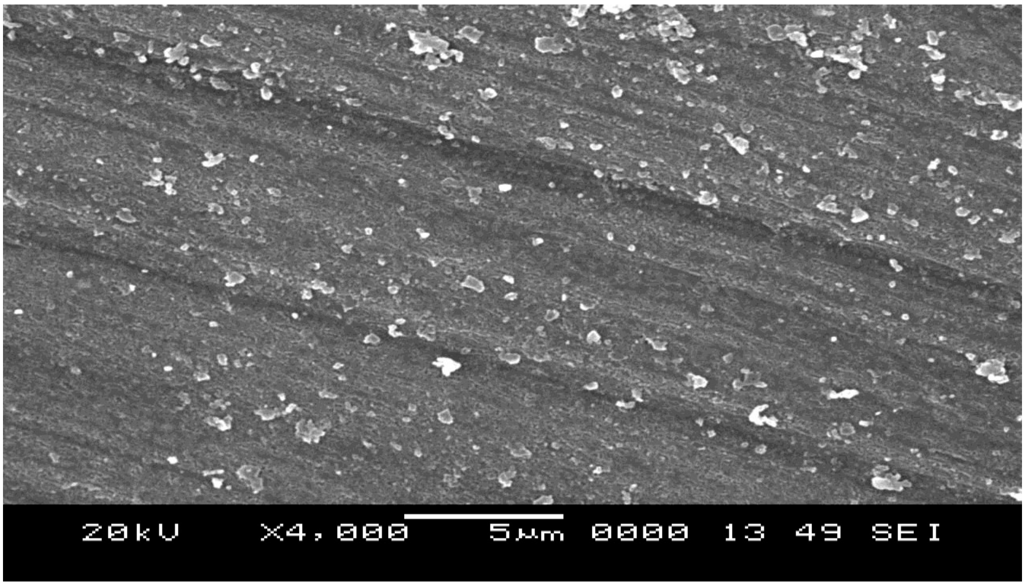

Fig. 3.8: SEM image of freshly polished uncorroded surface of AZ31 alloy.

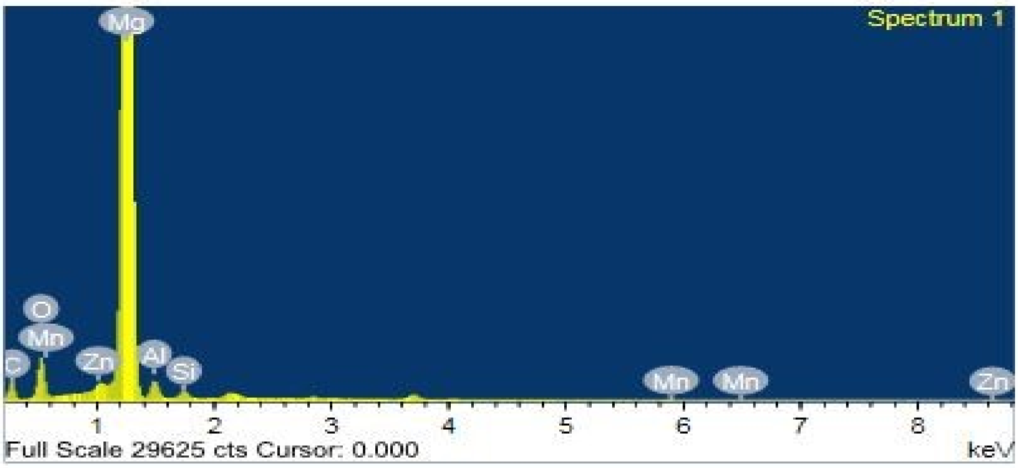

Fig. 3.9: EDX spectrum of freshly polished uncorroded surface of AZ31 alloy.

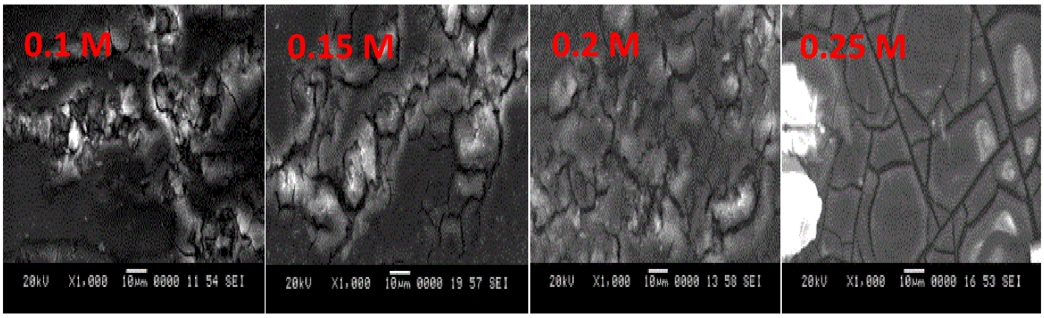

Fig. 3.10: SEM images of AZ31 alloy immersed for 3 hours in NaCl solutions of different concentrations at 30 °C.

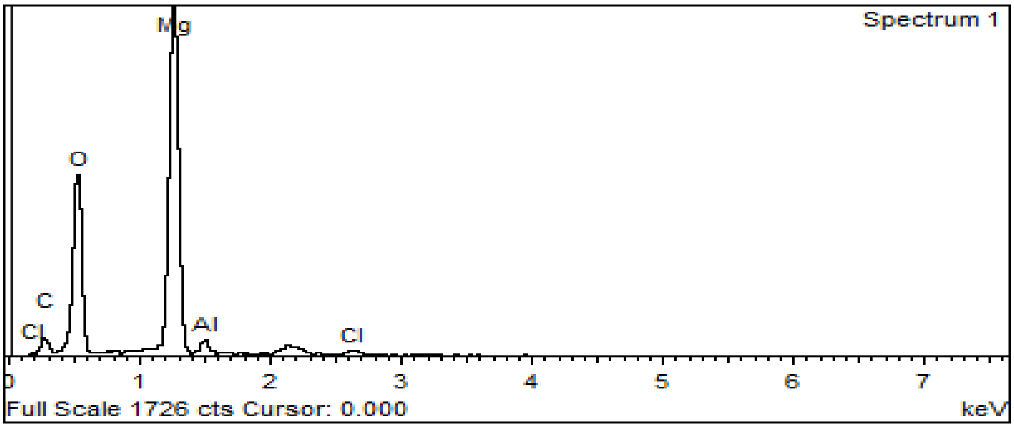

Fig. 3.11: EDX spectrum of AZ31 alloy immersed in 0.25 M NaCl for 3 h at room temperature.

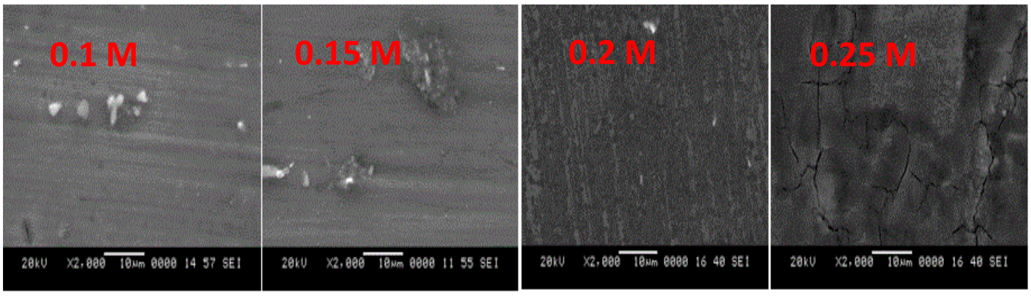

Fig. 3.12: SEM images of AZ31 alloy immersed for 3 hours in Na_2SO_4 solutions of different concentrations at 30 °C.

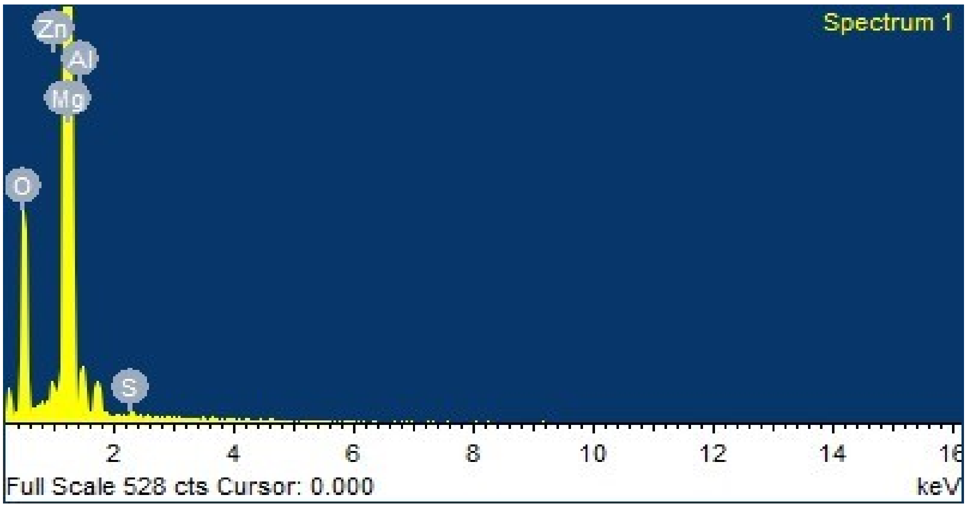

Fig. 3.13: EDX spectrum of AZ31 alloy immersed in 0.20 M Na_2SO_4 for 3 h at room temperature.

3.1.6 Summary

- The environmental factors like temperature, concentrations of sulfate and chloride ions in the corrosion media and temperature have a significant influence on the rate of corrosion of magnesium alloy AZ31.
- The corrosion rate of AZ31 alloy increases with the increase in temperature and ionic concentration.
- The results for electrochemical studies in combination with surface analysis confirm the formation of $Mg(OH)_2$ film on the corroding alloy surface.
- The $Mg(OH)_2$ surface film is partially protective due to imperfections like breaks and non-uniformity. Higher ionic concentrations and temperatures further destabilize the surface film possibly by dissolution and increase the corrosion rate.
- The corrosion kinetics follows Arrhenius law.
- The rate of corrosion of the alloy is higher in the chloride medium than in the sulfate medium.

Table 3.1: Electrochemical polarization parameters for the corrosion of AZ31 alloy in NaCl media at different temperatures.

Concentration (mol dm^{-3})	Temperature (^{o}C)	E_{corr} vs SCE (mV)	i_{corr} (μA cm^{-2})	$-\beta_c$ (mV dec^{-1})	v_{corr} (mm y^{-1})
0.05	30	-1514	70.10	99	1.51
	35	-1490	112.81	122	2.43
	40	-1500	168.06	129	3.62
	45	-1503	183.38	134	3.95
	50	-1493	197.77	140	4.26
0.1	30	-1483	154.03	135	3.34
	35	-1489	171.58	141	3.73
	40	-1502	210.77	165	4.54
	45	-1516	225.52	162	4.90
	50	-1490	235.47	173	5.11
0.15	30	-1537	233.52	150	5.03
	35	-1500	333.34	155	7.18
	40	-1515	455.90	168	9.82
	45	-1491	478.65	170	10.31
	50	-1475	567.33	194	12.22
0.2	30	-1500	432.55	189	9.40
	35	-1485	457.04	214	9.93
	40	-1483	489.13	181	10.63
	45	-1511	687.77	211	14.75
	50	-1497	709.98	198	15.43
0.25	30	-1526	520.41	190	11.31
	35	-1515	553.44	192	12.03
	40	-1488	577.18	188	12.54
	45	-1510	706.61	209	15.22
	50	-1494	792.81	206	17.23

Table 3.2: Electrochemical polarization parameters for the corrosion of AZ31 alloy in Na_2SO_4 media at different temperatures.

Concentration (mol dm^{-3})	Temperature (°C)	E_{corr} vs SCE (mV)	i_{corr} (µA cm^{-2})	$-\beta_c$ (mV dec^{-1})	v_{corr} (mm y^{-1})
0.05	30	-1483	63.33	93	1.37
	35	-1470	110.24	110	2.39
	40	-1502	164.74	125	3.58
	45	-1465	179.03	154	3.89
	50	-1481	190.03	144	4.13
0.1	30	-1522	71.20	117	1.54
	35	-1528	157.60	134	3.42
	40	-1485	191.24	140	4.15
	45	-1481	202.70	150	4.40
	50	-1456	208.41	157	4.53
0.15	30	-1457	218.14	138	4.74
	35	-1457	322.28	142	7.00
	40	-1469	445.19	151	9.67
	45	-1446	461.63	158	10.03
	50	-1448	546.62	170	11.88
0.2	30	-1505	235.63	152	5.12
	35	-1493	354.34	158	7.70
	40	-1489	470.87	164	10.23
	45	-1472	542.13	172	11.78
	50	-1480	672.86	197	14.62
0.25	30	-1451	372.80	147	8.10
	35	-1411	497.12	158	10.80
	40	-1438	516.71	170	11.23
	45	-1486	583.03	190	12.67
	50	-1463	727.89	201	15.82

Table 3.3: Electrochemical impedance parameters for the corrosion of AZ31 alloy in NaCl media at different temperatures.

Concentration (mol dm^{-3})	Temperature (^{o}C)	R_{hf} (Ω cm^2)	R_f (Ω cm^2)	R_{dif} (Ω cm^2)	C_{dl} (μF cm^{-2})	C_f (μF cm^{-2})
0.05	30	580	296	225	138	177
	35	550	255	207	153	181
	40	422	231	184	161	188
	45	340	191	150	170	192
	50	318	160	131	171	198
0.1	30	507	232	209	166	172
	35	380	192	168	181	179
	40	366	173	142	191	183
	45	351	152	115	195	185
	50	301	139	108	200	191
0.15	30	358	170	144	172	115
	35	301	161	121	184	128
	40	288	150	113	197	133
	45	225	128	100	201	140
	50	130	88	73	218	147
0.2	30	170	109	95	193	191
	35	166	97	79	190	199
	40	158	90	70	212	210
	45	125	78	58	220	219
	50	103	73	52	243	232
0.25	30	201	115	99	205	195
	35	150	107	85	217	205
	40	141	98	72	221	222
	45	105	81	68	230	223
	50	99	70	55	248	239

Table 3.4: Electrochemical impedance parameters for the corrosion of AZ31 alloy in Na_2SO_4 media at different temperatures.

Concentration (mol dm^{-3})	Temperature (^{o}C)	R_{hf} (Ω cm^2)	R_f (Ω cm^2)	R_{dif} (Ω cm^2)	C_{dl} (µF cm^{-2})	C_f (µF cm^{-2})
0.05	30	609	471	412	159	102
	35	510	367	303	176	129
	40	477	333	288	201	146
	45	450	350	275	225	151
	50	412	354	252	261	168
0.1	30	460	343	319	201	188
	35	432	322	293	224	191
	40	403	254	227	249	225
	45	387	193	160	269	237
	50	373	209	161	278	241
0.15	30	434	420	383	244	167
	35	463	300	280	278	169
	40	380	230	201	299	180
	45	273	237	200	307	188
	50	245	200	178	321	200
0.2	30	301	226	171	269	179
	35	287	224	190	287	186
	40	259	192	163	301	191
	45	236	203	167	321	201
	50	218	187	159	333	219
0.25	30	392	301	280	320	240
	35	350	250	221	333	259
	40	201	114	96	345	267
	45	180	109	80	359	280
	50	170	100	64	389	308

Table 3.5: Activation parameters for the corrosion of AZ31 alloy in different concentrations of NaCl.

Concentration (mol dm^{-3})	E_a (kJ mol^{-1})	$\Delta H^{\#}$ (kJ mol^{-1})	$\Delta S^{\#}$ (J mol^{-1} K^{-1})
0.05	34.00	34.66	-128.69
0.10	24.55	20.97	-162.88
0.15	23.57	18.70	-174.42
0.20	20.67	18.08	-167.27
0.25	16.94	15.30	-175.67

Table 3.6: Activation parameters for the corrosion of AZ31 alloy in different concentrations of Na_2SO_4.

Concentration (mol dm^{-3})	E_a (kJ mol^{-1})	$\Delta H^{\#}$ (kJ mol^{-1})	$\Delta S^{\#}$ (J mol^{-1} K^{-1})
0.05	44.17	40.04	-108.74
0.10	39.64	33.78	-126.03
0.15	35.65	28.33	-137.09
0.20	35.21	23.87	-149.98
0.25	24.39	18.81	-164.69

3.2 INFLUENCE OF pH ON THE CORROSION OF AZ31 ALLOY IN AQUEOUS SALT SOLUTIONS

3.2.1 Potentiodynamic polarization measurements

The potentiodynamic polarization curves for the corrosion of AZ31 alloy in 0.1 M NaCl and 0.1 M Na_2SO_4 at pH 3, 5, 7, 9, and 11 are presented in Fig. 3.14. Similar plots were obtained in solutions of other concentrations with respect to NaCl and Na_2SO_4. The influence of the medium pH plays an important role in the corrosion of AZ31. The potentiodynamic polarization curves for the corrosion of AZ31 alloy in solutions of different pH show that the polarization curves shift to the higher current density region, implying an increased corrosion rate as the medium pH decreases from highly alkaline (pH=11) to highly acidic (pH=3) conditions (Acharya and Shetty 2019). The cathodic branches of the polarization curves were extrapolated to the open circuit potential to obtain the corrosion current density (i_{corr}), as the anodic curves do not possess distinct Tafel regions.

The results summarised in Table 3.7 and Table 3.8 indicate that a higher corrosion rate is associated with a lower medium pH in all the corrosion media containing different concentrations of chloride ions or sulfate ions. Also, the corrosion rate increases with the increase in the concentrations of both chloride ions and sulfate ions at all the pH conditions studied. Although few authors like Zhao (Zhao et al. 2008) have studied E_{corr} associated with higher corrosion rate for alloys like ZE41 alloy, this behavior cannot be judged as a phenomenon for all magnesium alloys, since many studies carried, shows no such direct relation between $E_{corr,}$ β_c and corrosion rate.

The stability of metallic magnesium and its corrosion product magnesium hydroxide ($Mg(OH)_2$) as a function of the potential and pH of aqueous solutions is shown in the potential-pH plot in the introduction part of the thesis.

The anodic reaction involves the dissolution of magnesium and the cathodic reaction is the hydrogen evolution by the reduction of water. The liberation of hydrogen leads to the increase in the pH of the medium, lowering the solubility of Mg^{2+} and precipitating it as $Mg(OH)_2$, creating a surface layer on the alloy. The so formed corrosion product $Mg(OH)_2$ is stable only in alkaline conditions as shown in pourbaix diagram, with pH value above 10.5. Thermodynamically $Mg(OH)_2$ is unstable at pH values below 10.5, but still magnesium can develop a partial $Mg(OH)_2$ film on the surface of the metal in acidic conditions if the dissolution rate of $Mg(OH)_2$ is slower than the rate of its formation. Also, due to the cathodic reaction of hydrogen generation, an alkaline pH zone develops at the electrode interface, which facilitates $Mg(OH)_2$ precipitation and film formation, even when the bulk pH is acidic (Zhao et al. 2008).

By understanding the mechanism, the observed trend of the increased corrosion rate of AZ31 alloy with the decreasing pH value at every chloride and sulfate medium concentration can be justified. There is a reduced attack on the magnesium alloy surface in alkaline conditions, where $Mg(OH)_2$ surface film is highly stable and protective. Lowering medium pH increases the solubility of the surface film, accounting for the increased corrosion rate observed in the acidic media. The corrosion rate observed in the basic media, is quite significant, though small. The $Mg(OH)_2$ surface film formed on the surface of the alloy is thin with a Pilling-Bedworth ratio ~0.81 (Song and Atrens 2007) and the formed protective film is only partial and is incapable of completely covering the underlying alloy surface. Thus, the corrosion reactions take place predominantly at the breaks and imperfections of the film (Gao and Liang 2007).

The stability of the surface film also depends on the pH value of the corrosion medium. A higher pH value solution usually makes the surface film more passive. In solutions of higher pH, there is a higher concentration of OH^- available to compete with chloride ions or sulfate ions to adsorb onto the film surface, and to repel more of these anions out of the film/solution interface. This decreases the influence of the chloride ions and sulfate ions on the film.

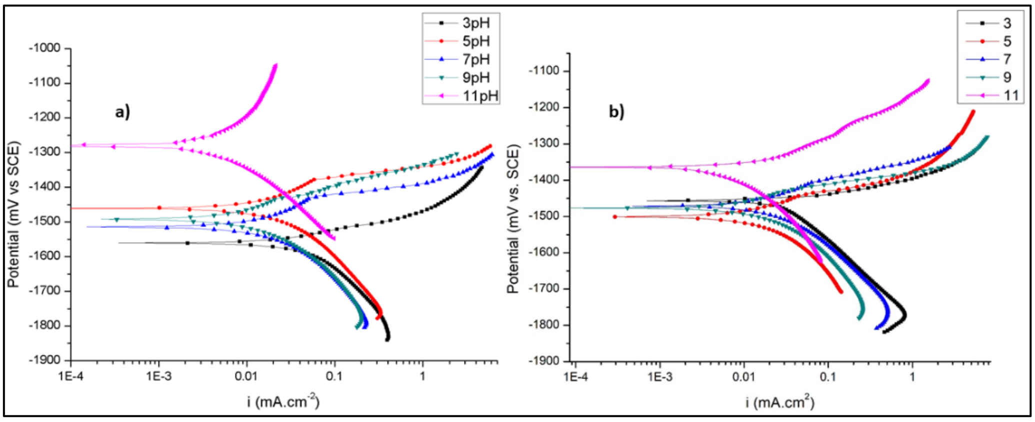

Fig. 3.14: Potentiodynamic polarization curves for the corrosion of AZ31 alloy in a) 0.1 M NaCl and b) 0.1 M Na_2SO_4 solutions of different pH at 30 °C.

3.2.2 Electrochemical impedance spectroscopy

Fig. 3.15 presents the electrochemical impedance spectra in the form of Nyquist plots for the corrosion of AZ31 alloy at different pH conditions in 0.1 M sodium chloride medium and 0.1 M sodium sulfate medium. Similar curves were obtained in other concentrations of chloride and sulfate media.

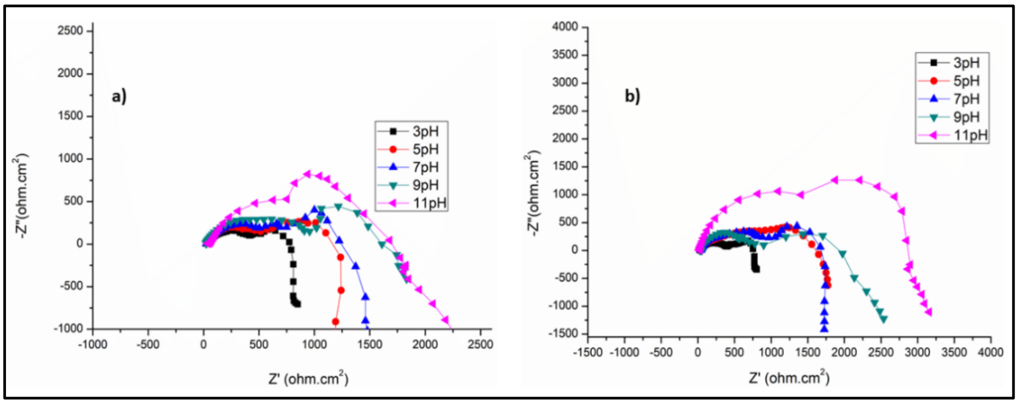

Fig. 3.15: Nyquist plots for the corrosion of AZ31 alloy in a) 0.1 M NaCl and b) 0.1 M Na_2SO_4 solutions of different pH at 30 °C.

The decrease in the diameter of the capacitive loop denotes the increased corrosion rate with the decrease in the pH of the media. respectively. The results of EIS measurements are summarized in Table 3.9 and Table 3.10 for sodium chloride media and sodium sulfate media, respectively. The results of EIS measurements are in line with those of potentiodynamic polarization measurements.

3.2.3 Scanning electron microscopy

The surface morphology of the alloy is often helpful in estimating the effect of a corrosive pH medium on the alloy surface. The surface morphology of the corroded alloy specimens under different conditions was analyzed by recording the SEM images of their surfaces. The SEM image and the corresponding EDX spectrum of the freshly polished surface of AZ31 alloy is shown in Fig. 3.16**.** The SEM images of AZ31 alloy surfaces after their corrosion in 0.2 M in NaCl medium of pH 3,7 and 11 for 3 h at 30 °C are shown in Fig. 3.17. The corresponding EDX spectrum is shown in Fig. 3.18. The SEM images of AZ31 alloy surface after their corrosion in 0.2 M Na_2SO_4 with pH 3, 7, and 11 are shown in Fig. 3.19. The corresponding EDX spectrum is presented in Fig. 3.20. The surface appears more deteriorated in the acidic pH, relatively less deteriorated in the neutral pH, and least deteriorated in the basic pH. These observations are in line with the observations of electrochemical studies.

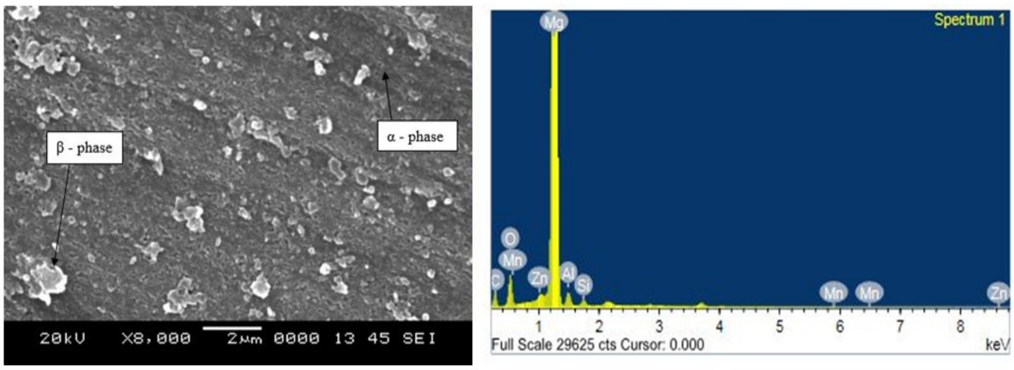

Fig. 3.16 : SEM image and EDX spectrum of freshly polished AZ31 alloy.

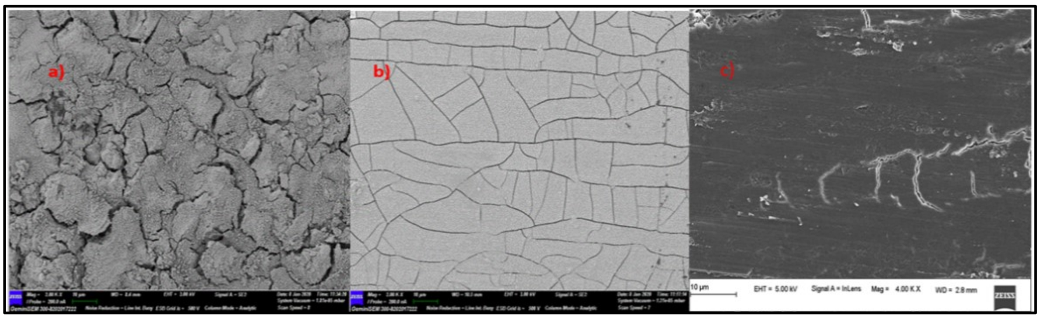

Fig. 3.17: SEM image of AZ31 alloy immersed in 0.2 M NaCl medium at 30 °C for 3 h at a) pH 3, b) pH 7 and c) pH 11.

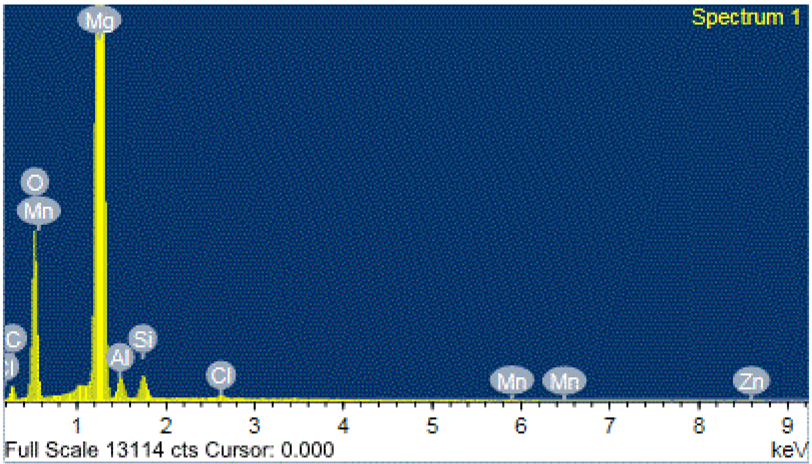

Fig. 3.18: EDX spectrum of AZ31 alloy immersed in 0.2 M NaCl of pH 7 for 3 h at 30 °C.

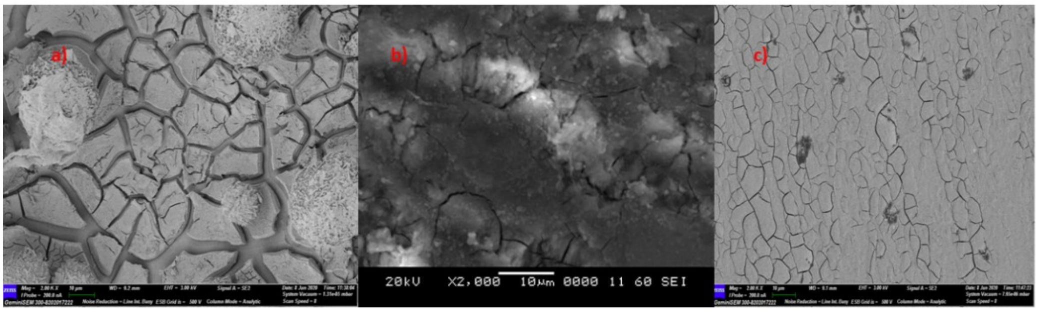

Fig. 3.19: SEM image of AZ31 alloy immersed in 0.2 M Na_2SO_4 medium at 30 °C for 3 h at a) pH 3, b) pH 7 and c) pH 11.

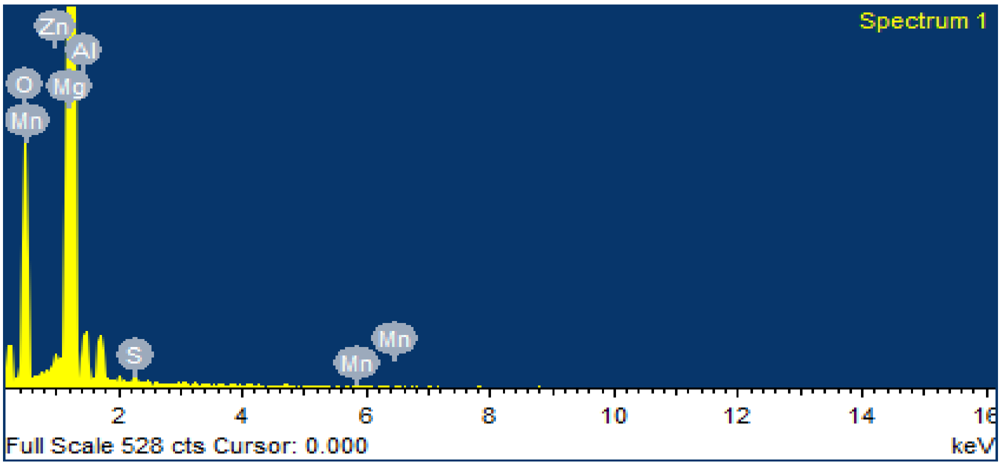

Fig. 3.20: EDX spectrum of AZ31 alloy immersed in 0.2 M Na_2SO_4 of pH 7 for 3 h at 30 °C.

3.2.4 Summary

- The corrosion of magnesium alloy AZ31 in Na_2SO_4 and NaCl solutions is strongly influenced by the medium pH.
- A higher corrosion rate is associated with a higher sulfate and chloride ion concentration at each pH and with a lower pH at each sulfate ion and chloride ion concentration, respectively.
- In the studied range of pH the highest rate of corrosion was exhibited by NaCl and Na_2SO_4 solution at pH value 3, and the lowest corrosion rate at pH value of 11.

Table 3.7: Electrochemical polarization parameters for the corrosion of AZ31 alloy in NaCl media of different pH and concentrations at 30 °C.

Concentration (mol dm^{-3})	pH	E_{corr} vs SCE (mV)	i_{corr} (µA cm^{-2})	$-\beta_c$ (mV dec^{-1})	v_{corr} (mm y^{-1})
0.05	3	-1503	163.88	257	3.53
	5	-1476	40.31	293	0.89
	7	-1496	36.67	288	0.79
	9	-1470	24.60	256	0.53
	11	-1302	11.14	262	0.24
0.10	3	-1560	182.41	285	3.97
	5	-1461	152.23	297	3.32
	7	-1514	139.73	295	3.04
	9	-1491	43.46	269	0.94
	11	-1281	14.29	224	0.31
0.15	3	-1484	216.26	279	4.71
	5	-1483	209.19	280	4.55
	7	-1492	226.59	291	4.62
	9	-1506	90.99	300	1.96
	11	-1419	41.08	234	0.90
0.20	3	-1476	369.07	266	8.04
	5	-1473	274.06	281	5.97
	7	-1482	214.01	238	4.67
	9	-1491	136.65	271	2.84
	11	-1416	106.24	257	2.31
0.25	3	-1490	930.06	286	20.27
	5	-1470	382.03	301	8.33
	7	-1506	207.07	253	4.68
	9	-1477	135.10	321	2.91
	11	-1448	114.67	229	2.47

Table 3.8: Electrochemical polarization parameters for the corrosion of AZ31 alloy in Na_2SO_4 media of different pH and concentrations at 30 °C.

Concentration (mol dm^{-3})	pH	E_{corr} vs SCE (mV)	i_{corr} (µA cm^{-2})	$-\beta_c$ (mV dec^{-1})	v_{corr} (mm y^{-1})
0.05	3	-1495	158.67	224	3.45
	5	-1503	131.48	239	2.86
	7	-1490	113.10	202	2.46
	9	-1462	101.03	233	2.20
	11	-1423	7.42	208	0.16
0.10	3	-1457	169.05	232	3.68
	5	-1492	160.52	231	3.49
	7	-1471	125.43	233	2.76
	9	-1477	110.03	252	2.73
	11	-1361	19.03	225	0.41
0.15	3	-1486	309.18	149	6.75
	5	-1494	115.69	247	2.52
	7	-1522	177.77	279	3.87
	9	-1468	173.02	245	3.77
	11	-1465	33.89	208	0.73
0.20	3	-1508	332.32	238	7.24
	5	-1474	196.30	258	4.28
	7	-1480	187.78	264	4.09
	9	-1447	179.72	200	3.91
	11	-1422	40.39	237	0.87
0.25	3	-1505	551.28	212	12.01
	5	-1462	464.53	253	10.12
	7	-1569	396.26	218	8.63
	9	-1580	315.50	266	6.80
	11	-1398	43.17	288	0.93

Table 3.9: Electrochemical impedance parameters for the corrosion of AZ31 alloy in NaCl media of different pH and concentrations at 30 °C.

NaCl Concentration(M)	pH	R_{hf} (Ω cm^2)	R_f (Ω cm^2)	C_{dl} (μF cm^{-2})	C_f (μF cm^{-2})
0.05	3	362	247	441	442
	5	639	530	425	261
	7	1423	969	210	197
	9	1469	1040	59	184
	11	2750	1945	179	109
0.10	3	507	385	914	805
	5	758	625	626	654
	7	842	667	427	354
	9	1030	946	193	312
	11	1099	900	158	127
0.15	3	508	470	654	623
	5	623	521	467	387
	7	799	629	443	294
	9	971	843	334	138
	11	1020	931	201	134
0.20	3	480	306	858	846
	5	594	335	304	361
	7	728	407	301	323
	9	900	608	201	214
	11	956	752	216	214
0.25	3	432	193	886	622
	5	532	337	703	311
	7	646	357	624	268
	9	836	779	440	235
	11	904	846	221	206

Table 3.10: Electrochemical impedance parameters for the corrosion of AZ31 alloy in Na_2SO_4 media of different pH and concentrations at 30 °C.

Na_2SO_4 concentration(M)	pH	R_{hf} (Ω cm^2)	R_f (Ω cm^2)	C_{dl} (µF cm^{-2})	C_f (µF cm^{-2})
0.05	3	854	406	446	848
	5	1206	847	324	587
	7	1287	990	306	139
	9	1495	1038	193	104
	11	2150	1545	179	89
0.10	3	816	664	658	836
	5	880	707	491	199
	7	968	767	336	193
	9	1157	870	103	164
	11	1290	989	101	141
0.15	3	793	688	377	837
	5	870	720	197	199
	7	906	835	195	139
	9	1049	855	156	110
	11	1151	955	201	149
0.20	3	747	614	279	719
	5	828	726	253	572
	7	890	760	156	471
	9	1002	881	164	145
	11	1090	900	159	146
0.25	3	649	488	311	965
	5	757	613	284	809
	7	862	678	382	342
	9	952	847	169	232
	11	1050	950	163	153

3.3 SODIUM 2,2'-(5,14-DIBUTYL-6,13-DIOXO-5,8,11,14-TETRAAZAOCTADECANE-8,11-DIYL)DIACETATE (DB) AS CORROSION INHIBITOR ON AZ31 MAGNESIUM ALLOY IN SODIUM CHLORIDE AND SODIUM SULFATE SOLUTIONS

3.3.1 Potentiodynamic polarization measurements

Potentiodynamic polarization curves for the corrosion of AZ31 magnesium alloy in 0.1 M NaCl and 0.1 M Na_2SO_4 solution in the presence of different concentrations of DB, at 50 °C are shown in Fig. 3.21. Similar plots were obtained in the other five concentrations each of NaCl and Na_2SO_4 at different temperatures studied.

The potentiodynamic polarization parameters such as corrosion potential (E_{corr}), corrosion current density (i_{corr}), cathodic Tafel slope (β_c) were calculated from the Tafel plots in the presence of different concentrations of DB at different temperatures and are summarized in Tables 3.11 to 3.20.

In general, according to the results presented in Tables 3.11 to 3.20 and also from polarization curves in Fig. 3.21, the corrosion current density (i_{corr}) decreases significantly even on the addition of a small concentration of DB compound, and the inhibition efficiency (η%) increases with the increase in the inhibitor concentration on the AZ31 magnesium alloy. The corrosion current density (i_{corr}) values were obtained by the extrapolation of cathodic branches of the polarization plots. It can be observed that both the cathodic and anodic reactions are suppressed with the addition of DB, which suggested that the inhibitor exerted an efficient inhibitory effect both on the anodic dissolution of metal and on the cathodic hydrogen liberation reaction (Li et al. 2009). Inhibition efficiency increases with the increase in the inhibitor concentration up to an optimum value. Thereafter the increase in the inhibitor concentration resulted in a negligible increase in inhibition efficiency.

As the concentration of the inhibitor increases from 0.0008 M to 0.0025 M, it is noticed that the corrosion current shifts slightly towards a lower current density. This indicates that the inhibitor promotes the passivation of AZ31 magnesium alloy through adsorption and decreases corrosion rate. The increase in the inhibition efficiency with the increase in inhibitor concentration is attributed to the increased surface coverage by the inhibitor molecules as the concentration is increased (Zhao et al. 2008).

It is seen from the Tables, that the value of β_c does not change significantly with the increase in DB concentration, which indicates that the addition of DB does not change the mechanism of cathodic hydrogen evolution. The small change in β_c value suggests that the DB gets adsorbed on the metal surface and the addition of the inhibitor hinders the corrosive attack on the AZ31 magnesium alloy (Zeng et al. 2014).

It can also be seen from the Tables, that there is no appreciable shift in the corrosion potential value (E_{corr}) on the addition of DB to the corrosion medium and also on increasing the concentration of DB. If the displacement in corrosion potential is less than ±85 mV with respect to corrosion potential of the blank, then it is said to be mixed type inhibitor (Dinodi and Nityananda Shetty 2014); (Cao et al. 2009). Therefore, the DB is considered to be a mixed type inhibitor.

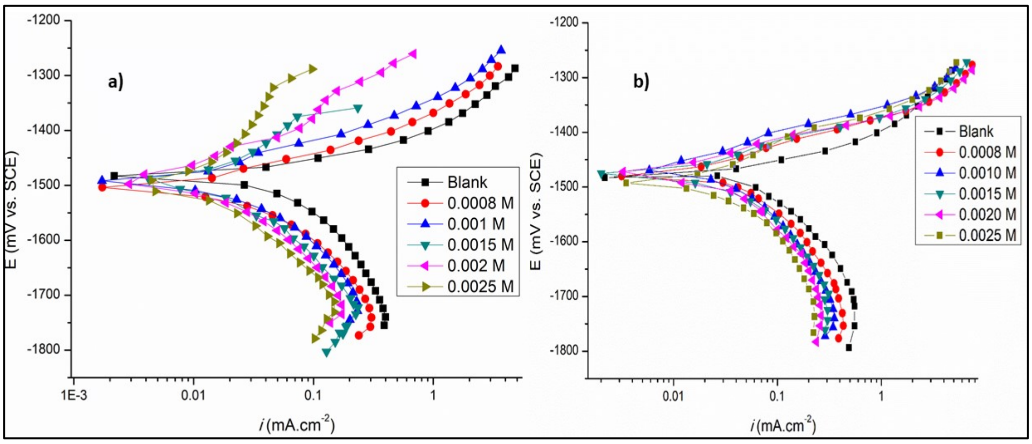

Fig. 3.21: Potentiodynamic polarization curves for the corrosion of AZ31 alloy in the presence of different concentrations of DB in a) 0.1 M NaCl solution and b) 0.1 M Na_2SO_4 solution at 50 °C.

3.3.2 Electrochemical impedance spectroscopy

Nyquist plots for the corrosion of AZ31 magnesium alloy in 0.1 M NaCl and 0.1 M Na_2SO_4 solution in the presence of different concentrations of DB are shown in Fig. 3.22. Similar plots were obtained in other concentrations of NaCl and Na_2SO_4 and also at other temperatures. It can be observed from the figure that the diameter of the semicircle increases with the increase in the concentration of DB, indicating a decrease in the corrosion rate of the alloy sample.

The Nyquist plots display two capacitive semicircles at higher and medium frequencies, the former being much larger than the later, followed by the beginning of an inductive loop at lower frequency region. The higher frequency (*hf*) loop is the result of charge transfer of the corrosion process and surface film effects. The medium frequency (*mf*) semicircle arises as a consequence of diffusion or electrolyte ingress, through the corrosion product layer. The appearance of a lower frequency (*lf*) inductive loop is attributed to the relaxation of intermediates like $Mg(OH)^{+}{}_{ads}$ and $Mg^{+}{}_{ads}$ adsorbed at the metal surface. When compared with the blank the capacitive semicircles appear enlarged in the presence of DB. This is indicative of improved corrosion resistance of AZ31 alloy in DB containing solutions (Dinodi and Shetty 2014); (Song and Atrens 1999); (Mansfeld et al. 1992); (Ardelean et al. 2008).

The electrical equivalent circuit presented in Fig. 3.3 is fitted into the impedance data and the electrochemical impedance parameters were calculated. The electrochemical impedance parameters for the corrosion of AZ31 magnesium alloy in NaCl and Na_2SO_4 media are summarised in Tables 3.21 to 3.30. The inhibitor molecules adsorb along with the interface by replacing previously adsorbed water molecules. As a consequence, the impedance parameters are bound to change upon DB addition, as observed from Tables 3.21 to 3.30. The trend of higher η (%) at higher DB concentration is in close accordance with those obtained from the polarization measurements. On increasing the concentration of DB, R_f, and R_{dif} value increases, whereas C_{dl} and C_f values decline. The increase in R_f signifies that the protection offered by the surface film is magnified to several folds on the addition of DB into the system and R_{dif} is hindrance for the diffusion of ions through the film surface. The diminution in C_{dl} and C_f values can be the outcome of reduction in local dielectric constant and/or increased thickness of the electrical double layer and the surface film, respectively.

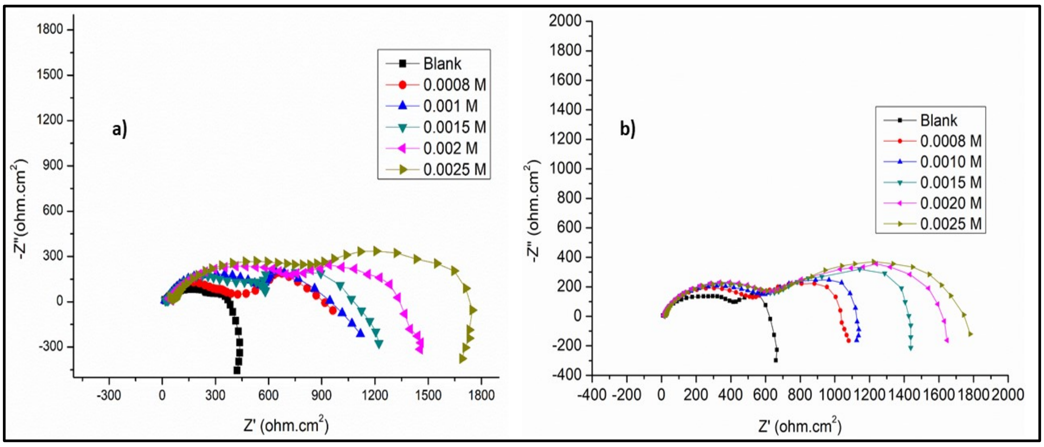

Fig. 3.22: Nyquist plots for the corrosion of AZ31 alloy in the presence of different concentrations of DB in a) 0.1 M NaCl and b) 0.1 M Na_2SO_4 at 50 °C.

The Bode plots of phase angle and amplitude for the corrosion of the AZ31 Mg alloy immersed in 0.1 M NaCl and 0.1 M Na_2SO_4 at 50 °C in the presence of different concentrations of DB, are shown in Fig. 3.23 and Fig. 3.24, respectively. As seen from Bode plots, both the impedance modulus (Z_{mod}) at low frequency and the phase maximum (θ_{max}) at intermediate frequency increase with the increase in DB concentration, which together points out the presence of highly protective surface film formed by the inhibitor, thereby protecting the metal surface from corrosion.

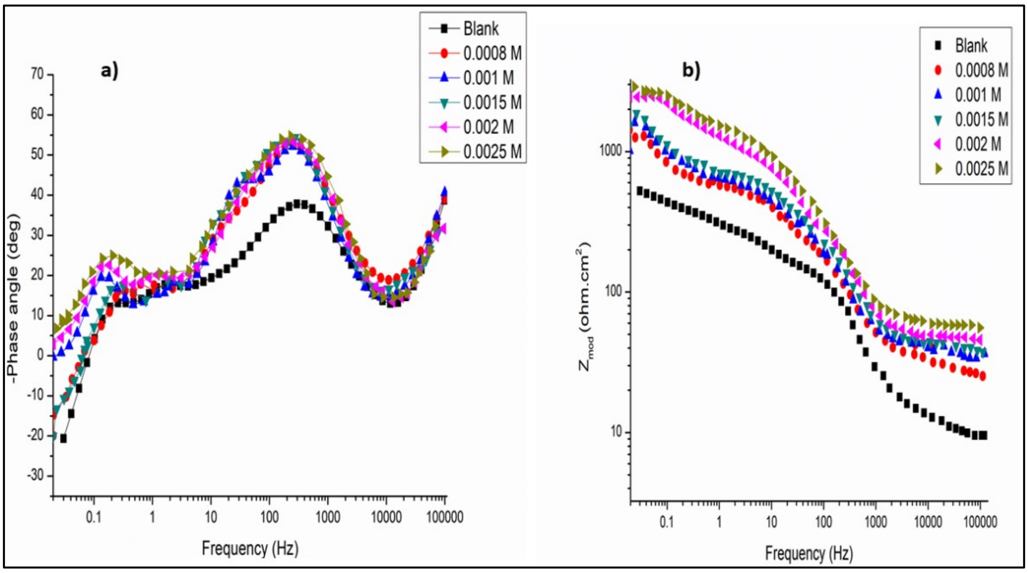

Fig. 3.23: Bode phase angle and amplitude plots for the corrosion of AZ31 alloy in 0.1 M NaCl medium containing different concentrations of DB at 50 °C.

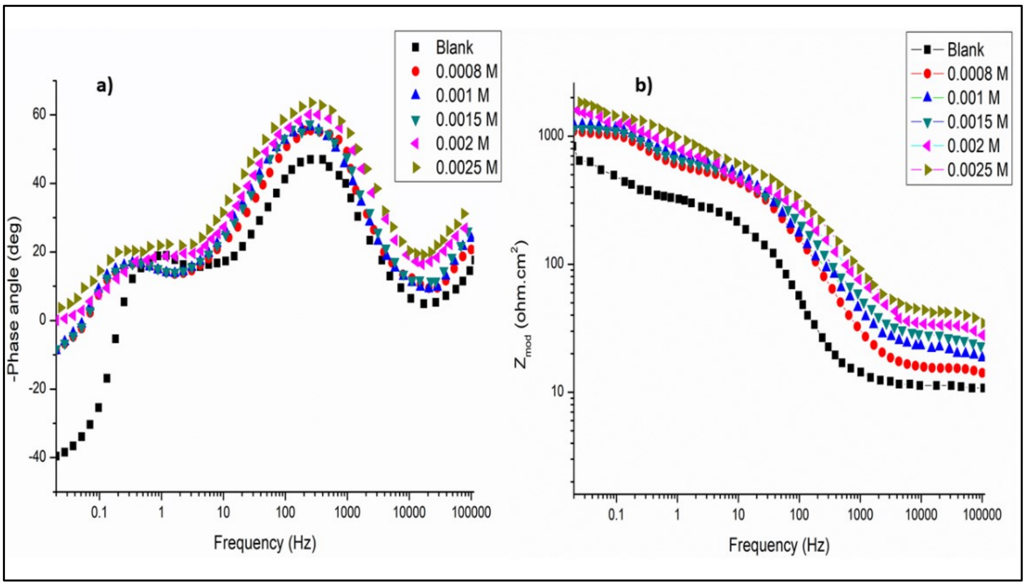

Fig. 3.24: Bode phase angle and amplitude plots for the corrosion of AZ31 alloy in 0.1 M Na_2SO_4 medium containing different concentrations of DB at 50 °C.

3.3.3 Effect of temperature

Studying corrosion at various intervals of temperature facilitates the assessment of important activation parameters. At any particular DB concentration, the efficiency of the studied DB declines with the increase in solution temperature, as seen from the results listed in Table 3.31 and Table 3. 32. This is a distinguishing trait of physisorbed inhibitors, which desorb at higher temperatures (Bentiss et al. 2005). Arrhenius plots for the corrosion of AZ31 alloy specimen in 0.1 M NaCl and 0.1 M Na_2SO_4 having different amounts of DB are presented in Fig. 3. 25.

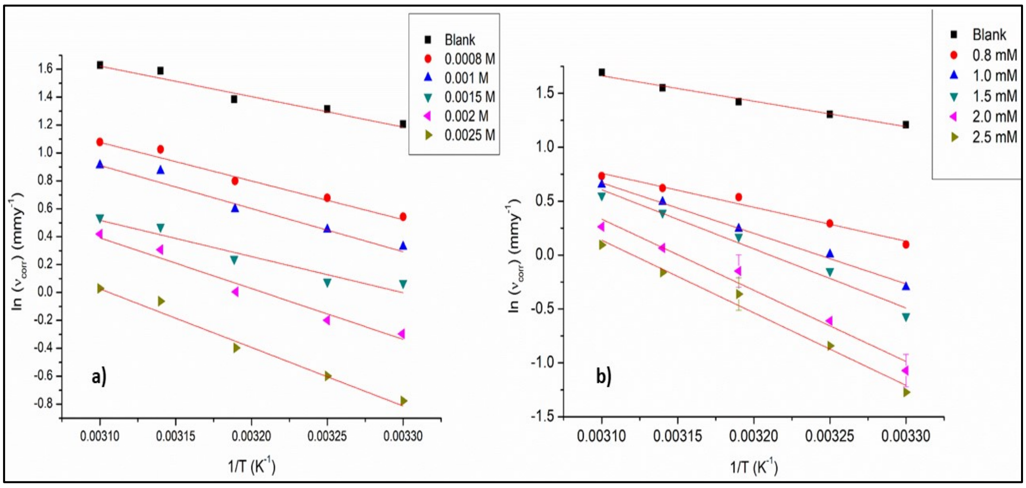

Fig. 3.25: Arrhenius plot for the corrosion of AZ31 magnesium alloy in a) 0.1 M NaCl and b) 0.1 M Na_2SO_4 media in the presence of different concentrations of DB.

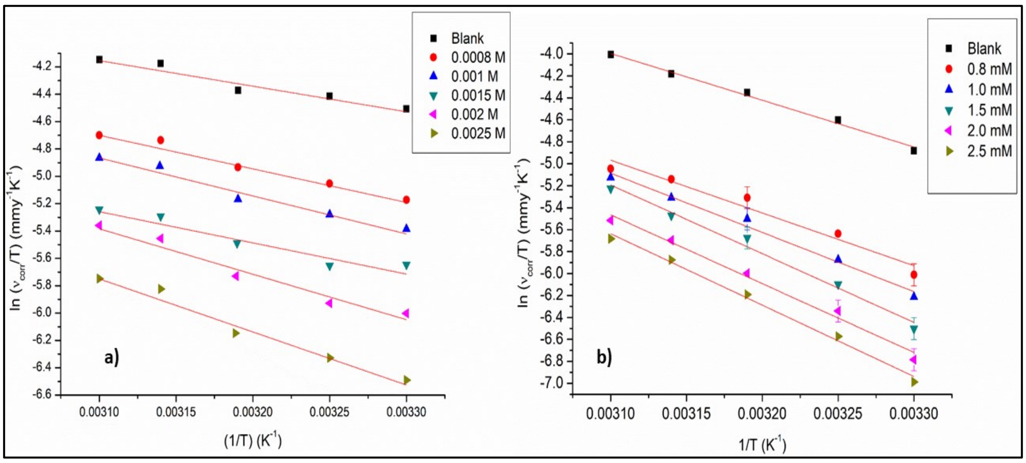

Fig. 3.26: The plots of ln(υ_{corr}/T) vs (1/T) for the corrosion of AZ31 magnesium alloy in a) 0.1 M NaCl and b) 0.1 M Na_2SO_4 media in the presence of different concentrations of DB.

The plots of ln (υ_{corr} /T) versus 1/T for the corrosion of AZ31 magnesium alloy in the presence of different concentrations of DB compound in 0.1 M NaCl and 0.1 M Na_2SO_4 are shown in Fig. 3.26. The activation parameters calculated are summarized in Tables 3.31 and 3.32.

From the data in Table 3.31 and Table 3.32, the following inferences can be drawn. The values of E_a for each DB containing system are greater than E_a of the blank and it gradually increases with the increase in the concentration of DB. E_a is synonymous with the energy barrier for the occurrence of metal corrosion (Schorr and Yahalom 1972). Thus, the presence of DB energetically hinders AZ31 corrosion, most likely by adsorption of the surface film.

The variation of $\Delta H^{\#}$ is similar to that of E_a and the negative values of $\Delta S^{\#}$ suggest the formation of the activated complex involves association with the reduction in the randomness of the system.

3.3.4 Adsorption isotherms

An adsorption isotherm is a graphical representation of variation of extent of adsorption with pressure or concentration of on adsorbate at a given constant temperature. The phenomenon of adsorption plays a vital role during the action of corrosion inhibitors. Hence a thorough knowledge about the adsorption isotherm is a prerequisite in understanding the nature of interactions prevailing between the inhibitor molecules and the metal surface. A metal/electrolyte interface has water molecules adsorbed all along. During inhibitor adsorption, the inhibitor molecules in solution ($Inh_{(sol)}$) replace the previously adsorbed water molecules ($H_2O_{(ads)}$) through a process similar to substitution (Tao et al. 2009), as shown below:

$$Inh_{(sol)} + \chi H_2O_{(ads)} \longrightarrow Inh_{(ads)} + \chi H_2O_{(sol)} \qquad (3.12)$$

where χ is the size ratio corresponding to the number of water molecules replaced upon the adsorption of one inhibitor molecule. χ is specific for an individual inhibitor and is fairly independent of the surface charge on the metal.

Generally, the degree of inhibition brought about by interfacial inhibitors varies as a function of surface coverage (θ). It was attempted to obtain a linear relationship between the values of θ and the concentration of the inhibitor in the solution (C_{inh}) by graphically fitting the parameters to various adsorption isotherms like Langmuir, Temkin, Frumkin, and Flory–Huggins isotherms. The correlation coefficients (R^2) were compared (Wang et al. 2010b). The best fit, however, was achieved with the Langmuir adsorption isotherm, mathematically represented as shown below:

$$\frac{C_{inh}}{\theta} = C_{inh} + (\frac{1}{K}) \tag{3.13}$$

where K is the equilibrium constant for the adsorption-desorption process. Straight lines were obtained on plotting (C_{inh}/θ) versus C_{inh} at all temperatures. Fig. 3.27 represents the Langmuir adsorption isotherms for the adsorption of DB in 0.1 M of NaCl and 0.1 M Na_2SO_4. K was evaluated as the reciprocal of intercept values obtained from the plots. The values of K were substituted in the reaction isotherm equation below to obtain the standard free energy of adsorption.

$$\Delta G°_{ads} = -RTln(55.5XK) \tag{3.14}$$

where 55.5 in mol dm^3 is the molar concentration of water in the solution, R is the universal gas constant and T is the absolute temperature. The standard enthalpy of adsorption ΔH^0_{ads} and standard entropy of adsorption ΔS^0_{ads} were calculated from the plot of $\Delta G°_{ads}$ versus T, by means of thermodynamic relation below:

$$\Delta G°_{ads} = \Delta H^0_{ads} - T\Delta S^0_{ads} \tag{3.15}$$

Tables 3.33 and 3.34 enlist all the calculated thermodynamic parameters for the adsorption of DB on the alloy surface in NaCl and Na_2SO_4. The plots though linear with an average linear regression coefficient (R^2) equal to 0.95, deviate slightly from the ideal Langmuir isotherm, in terms that the slopes are close but not equal to unity. This deviation arises as a consequence of mutual interactions among the adsorbed DB. Such intermolecular interactions among the adsorbate are forbidden as per the assumptions considered for the statistical derivation of the Langmuir equation (Ayawei et al. 2017). The $\Delta G°_{ads}$ values are negative and fall within the range -27 kJ mol^{-1} to -31 kJ mol^{-1}. Generally accepted free energy threshold for physisorption and chemisorption, respectively is -20 kJ mol^{-1} and -40 kJ mol^{-1}. The values obtained in the current study are intermediate hinting that the DB adsorb both physically and chemically. The fact that both $\Delta G°_{ads}$ and inhibition efficiency decrease with the increase in temperature, indicates that the adsorption of DB on the AZ31 alloy surface in NaCl and Na_2SO_4 are not favoured at high temperature and hence can be considered to be predominantly physisorption. The standard adsorption entropy value is negative; indicating that decrease in disordering takes place on going from the reactant to the alloy adsorbed species. This can be attributed to the fact that adsorption is always accompanied by decrease in entropy (Fawzy et al. 2018).

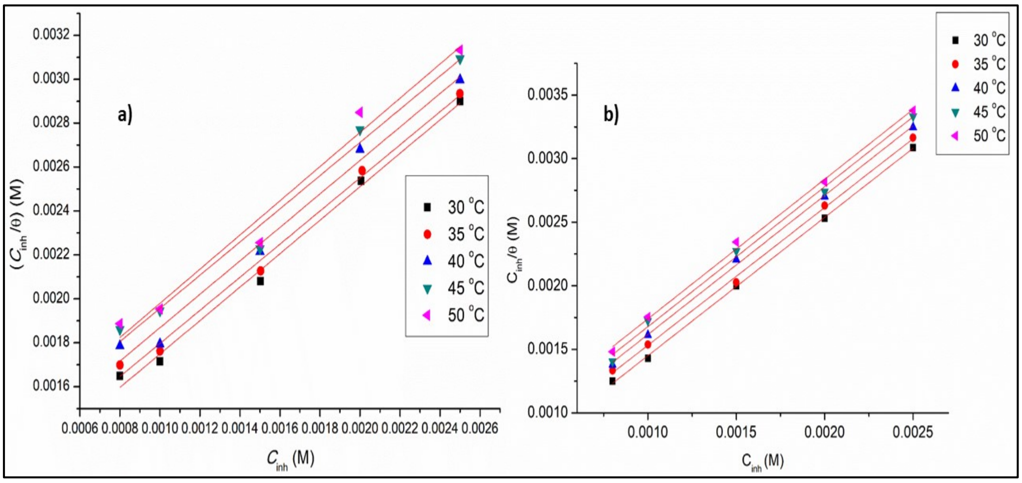

Fig. 3.27: Langmuir adsorption isotherms for the adsorption of DB on AZ31 alloy in a) 0.1 M NaCl medium and b) 0.1 M Na_2SO_4 medium.

3.3.5 Mechanism of corrosion inhibition

Magnesium dissolution in wet environments generally proceeds by an electrochemical reaction with water to produce magnesium hydroxide and molecular hydrogen (H_2), thus magnesium corrosion is relatively insensitive to oxygen concentration.

Generally, the inhibition brought about by chemical inhibitors is attributed to adsorption and barrier film formation at the metal surface. The DB is an anionic surfactant with the carboxylate polar head and long alkyl hydrophobic tail. The DB might physically adsorb through the electrostatic interactions between their anionic head and Mg^{2+} ions trapped within the imperfections of surface film developed over the α-Mg matrix. There certainly is scope for chemisorption as well, at the cathodic phases which are rich in Mn and Zn elements (Zeng et al. 2014); (Hu et al. 2015). Strong covalent bonds might develop from donor–accepter interactions between unshared electron pairs of oxygen in the inhibitor and vacant d-orbitals of Mn or Zn metal atoms, leading to chemisorption of inhibitors. The DB, chemisorbed along cathodic intermetallic phases are likely to inhibit cathodic hydrogen evolution by blocking the active cathodic reaction sites. The physisorbed surfactant, on the other hand, might precipitate as their sparingly soluble magnesium salts within the pores of the film over the α-Mg matrix. The precipitation is favored due to the very low solubility product of magnesium salt of the surfactant and the presence of sufficiently high amounts of dissolved Mg^{2+} ions. The precipitates fill up the pores and densify the surface film. As an overall result, the electrolyte ingress is reduced on the addition of the surfactant. In all likelihood, van der Waals interactions exist between the long alkyl chains of adsorbed surfactant molecules, which causes the adsorption behavior to slightly deviate from the ideal Langmuir behavior. Such mutual interactions further improve the compactness of the modified film. As an added advantage, the modified film even attains certain hydrophobicity which repels the aqueous corrosive solution (Bentiss et al. 2005).

3.3.6 Surface morphology

Fig. 3.28 and Fig. 3.29 present the SEM images and EDX spectra of the AZ31 magnesium alloy surface after the immersion in 0.1 M NaCl and 0.1 M Na_2SO_4 for 3 h at 30 °C, in the presence of DB, respectively. It is noted that the deterioration of the alloy substrate is suppressed in the presence of DB in the NaCl and Na_2SO_4. In the presence of DB inhibitor, the AZ31 alloy is less corroded. The surface observed after the addition of DB inhibitor seems to be more compact and contains fewer cracks in it, supposedly conveying the suppressed corrosion rate. The elements present on the surface of the alloy were ascertained by using the EDX spectra for both when the inhibitor is present in NaCl and Na_2SO_4.

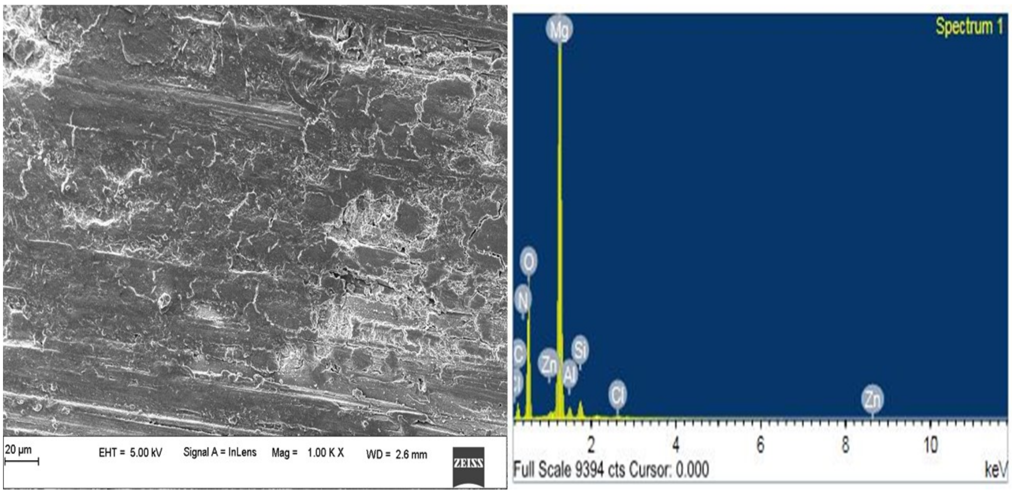

Fig. 3.28: The SEM image and EDX spectrum of AZ31 Mg alloy surface immersed in 0.1 M NaCl medium in the presence of 0.001 M DB for 3 h.

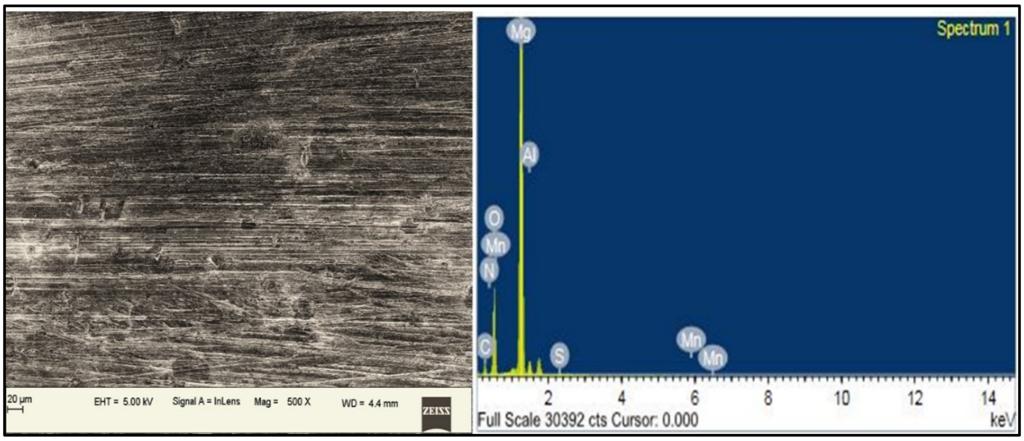

Fig. 3.29: SEM images and EDX spectrum of AZ31 Mg alloy surface immersed in 0.1 M Na_2SO_4 medium in the presence of 0.001 M DB for 3 h.

3.3.7 XPS

Fig. 3.30 and 3.31 shows the XPS survey spectra of AZ31 alloy immersed in 0.01 M NaCl and 0.01 M Na_2SO_4 solution in the presence of DB, respectively. The AZ31 alloy surface consists majorly of Mg, Al, C, O, and N elements in them. Figures 3.32 and 3.33 show the corresponding high-resolution scans for different elements present on the AZ31 alloy surface. The surface of the alloy has high concentrations of O, C, and N, smaller quantities of Al and Mg. The Mg 1s peak was deconvoluted into three peaks corresponding to $Mg(OH)_2$, MgO, and $MgAl_2O_4$ at binding energies 1302.70 eV, 1303.90 eV, and 1304 eV, respectively. The peak associated with Al 2p at ~75 eV is related to $MgAl_2O_4$. The O 1s peak corresponds to MgO at 532.10 eV. C 1s is deconvoluted to give a peak at 284.55 eV which is associated with C-C and C-H of the inhibitor molecule. N 1s peak at 398 eV is related to the N-CH_2 bond in the DB inhibitor. The obtained results show that the surfactant molecules have been adsorbed on the surface of the alloy forming a layer on the surface.

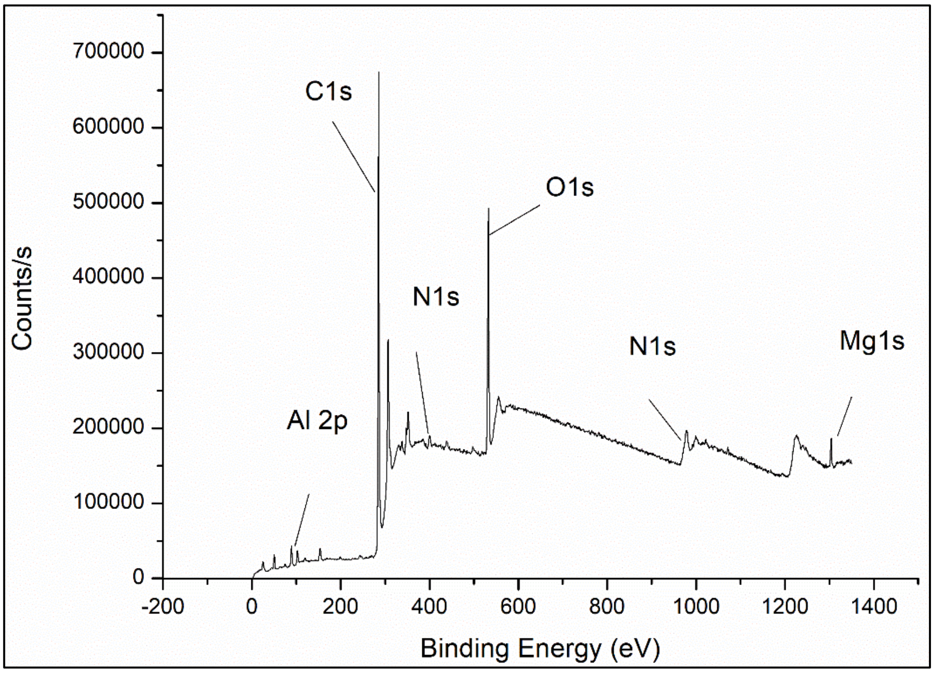

Fig. 3.30: XPS spectra of AZ31 Mg alloy surface immersed in 0.2 M NaCl medium in the presence of 0.001 M DB for 3 h at 30 °C.

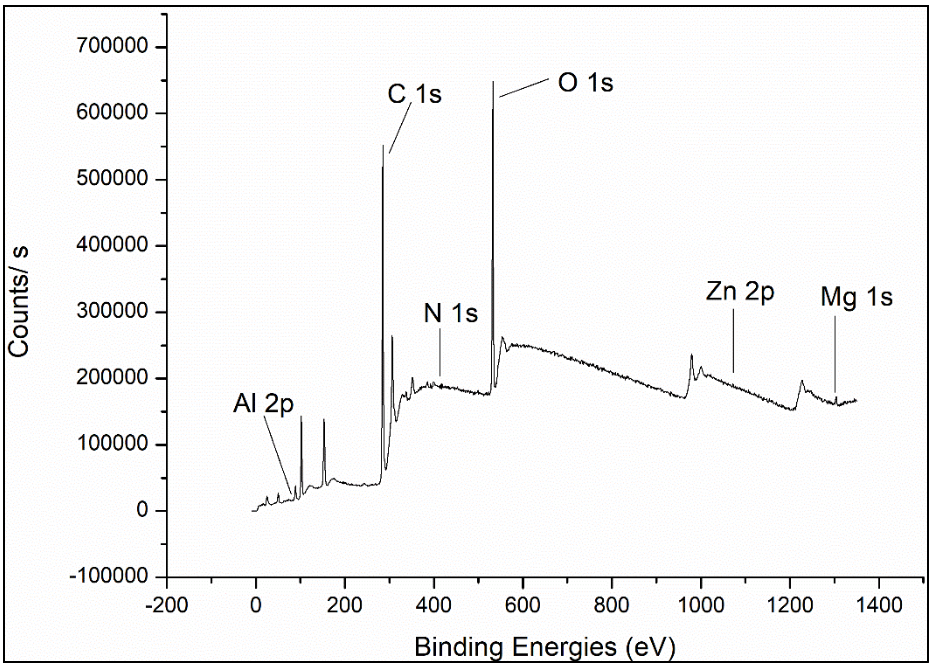

Fig. 3.31: XPS spectra of AZ31 Mg alloy surface immersed in 0.2 M Na_2SO_4 medium in the presence of 0.001 M DB for 3 h at 30 °C.

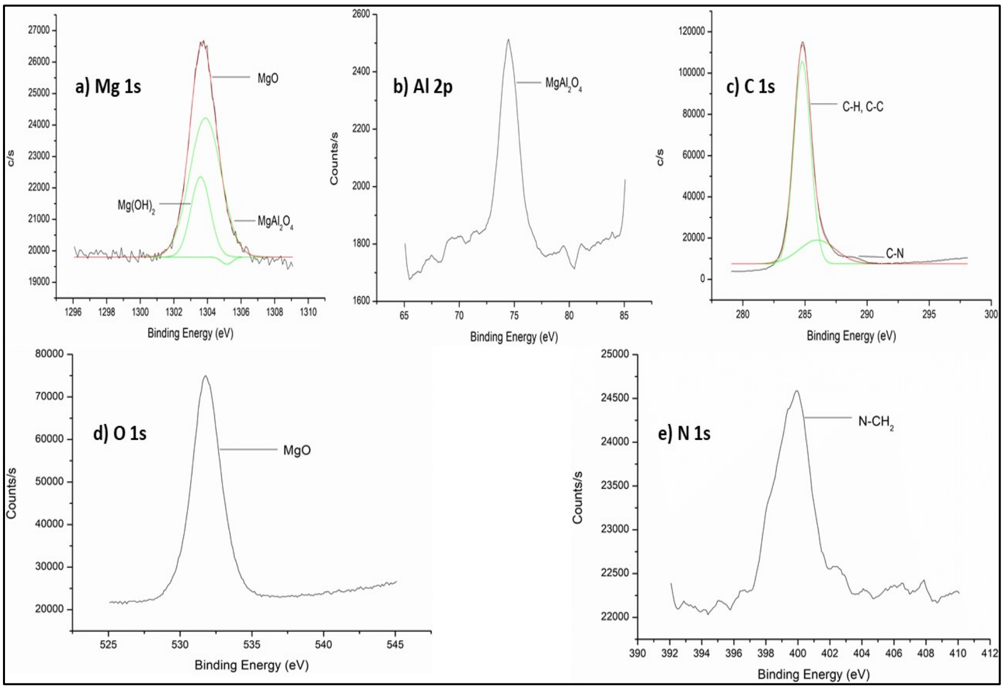

Fig. 3.32: XPS spectra (Mg 2s, Al 2p, C 1s, O 1s and, N 1s) of AZ31 Mg alloy immersed in 0.20 M NaCl medium in the presence of 0.001 M DB for 3 h at 30 °C.

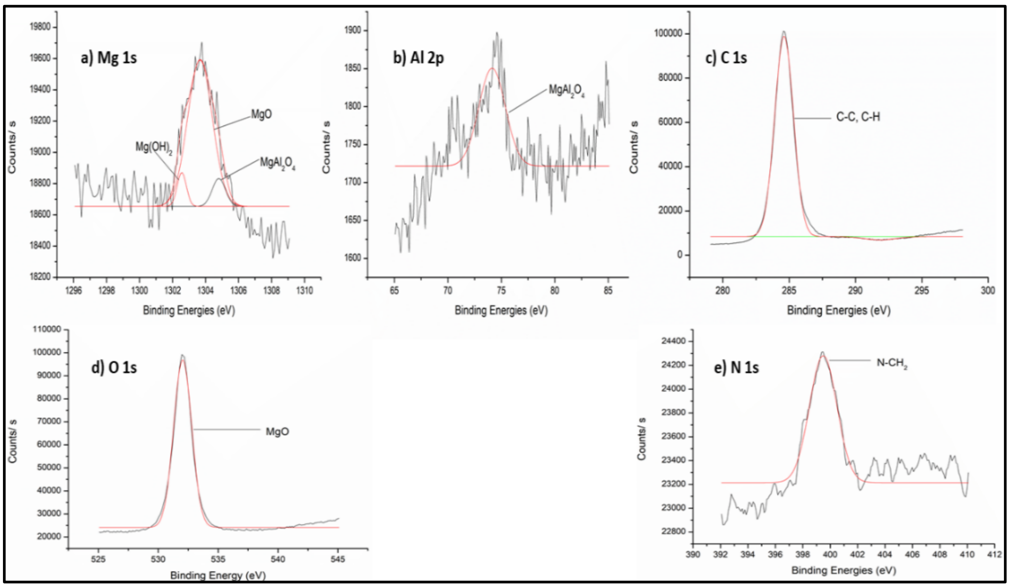

Fig. 3.33: XPS spectra (Mg 2s, Al 2p, C 1s, O 1s and, N 1s) of AZ31 Mg alloy immersed in 0.2 M Na_2SO_4 medium in the presence of 0.001 M DB for 3 h at 30 °C.

3.3.8 DFT

As a consequence of using quantum mechanical methods in theoretical calculations, it is necessary to validate the theoretical approach by comparing experimental data(Liu et al. 2018). The optimized structure for the inhibitor, DB, was obtained using DFT calculations at the B3LYP hybrid functional model with def-TZVP basis set and presented in Fig. 3.34. The energy of the highest occupied molecular orbital (E_{HOMO}), the energy of the lowest unoccupied molecular orbital (E_{LUMO}), energy gap (ΔE), hardness (η), softness (σ), ionization potential (IP), electron affinity (EA), electronegativity (χ), and dipole moment (μ) associated with the corrosion-inhibiting ability of DB (Ćurković et al. 2013)(Kaczerewska et al. 2019)(Gad et al. 2018)(Mejeha et al. 2012)(Lukovits et al. 2001)(Farhat A. Ansari 2010) have been evaluated using DFT. The above-mentioned parameters are presented in Table 3.35.

The structure of the molecule is optimized and the negative value of the total energy (-16.87 KeV) indicates a thermodynamically stable molecule. The E_{HOMO} indicates the ability of the inhibitor molecule to contribute electron pairs.

E_{LUMO} is a measure of electron-accepting ability of the inhibitor. E_{HOMO} value of -1.04 eV for the inhibitor DB, indicates the physical adsorption is the basis for the corrosion inhibition action (Pakiet et al. 2019). The low bandgap energy indicates a higher reactivity of the inhibitor molecules, leading to their ready adsorption on AZ31 alloy surface (H. A. Videla; M. F. L. de Mele; G.Brankevich 1988)(Williams et al. 2013)(Liu et al. 2018). The dipole moment value is the measure of the extent of interaction between charged DB molecules and the charged metal surface. The high value of the dipole moment implies a stronger interaction of DB molecules and the AZ31 alloy surface.

The resistance of the inhibitor to charge transfer and its readiness to receive electrons is indicated by its chemical hardness and softness respectively. The strong tendency of DB to attract electrons from metal shows a higher electronegativity value, which in turn indicates the higher ability to act as a corrosion inhibitor.

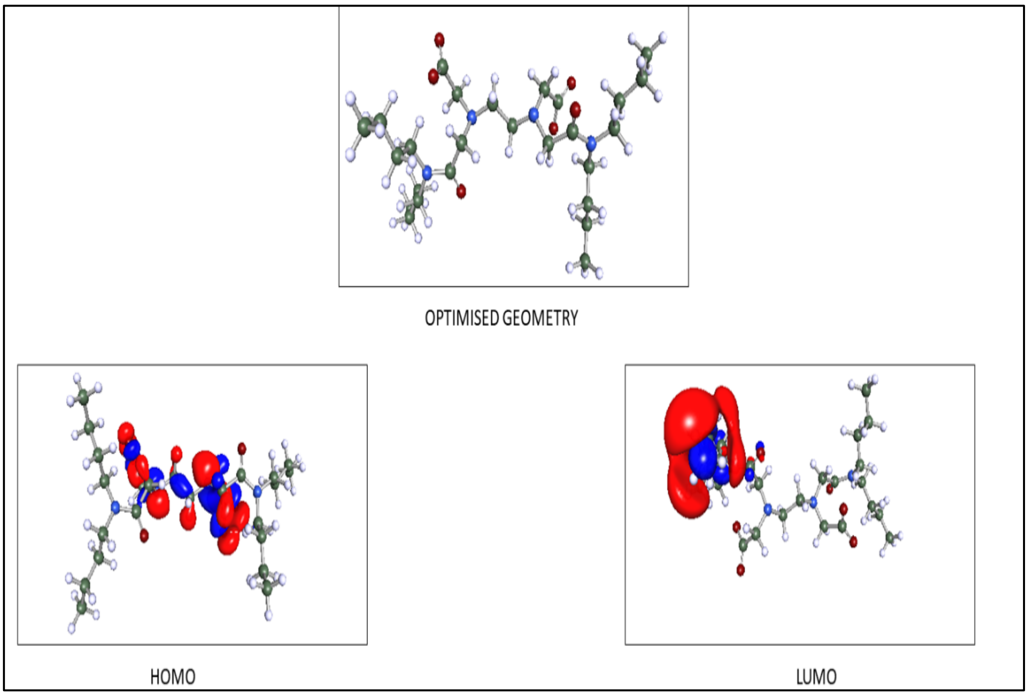

Fig. 3. 34: Optimized structure and the frontier molecular orbital density distribution of the DB molecule.

3.3.9 Summary

- The effect of anionic Gemini surfactant-based inhibitor on the corrosion of AZ31 Mg alloy in NaCl and Na_2SO_4 solutions were investigated.
- The anionic Gemini surfactant DB was successfully synthesized using EDTA and dibutylamine.
- DB effectively inhibits the corrosion of AZ31 alloy in NaCl and Na_2SO_4 solutions.
- As the concentration of inhibitor is increased, the inhibition efficiency increases, and as the temperature increases, the inhibition efficiency decreases.
- The inhibitor appears to be a mixed-type inhibitor and obeys Langmuir adsorption isotherm.
- The inhibitor reacts with Mg^{2+} ions to form the magnesium salt of the inhibitor on the surface of AZ31 alloy to impart corrosion resistance.

Table 3.11: Electrochemical polarization parameters for the corrosion of AZ31 alloy in 0.05 M NaCl solution in the presence of DB at different temperatures.

Inhibitor concentration (mmol dm^{-3})	Temperature (°C)	E_{corr} vs SCE (mV)	i_{corr} (µA cm^{-2})	$-\beta_c$ (mV dec^{-1})	v_{corr} (mm y^{-1})	η (%)
Blank	30	-1514	70.10	99	1.51	-
0.80		-1504	14.39	78	0.31	79
1.00		-1523	10.21	66	0.22	85
1.50		-1518	9.28	68	0.20	86
2.00		-1501	8.35	55	0.18	88
2.50		-1520	5.10	48	0.11	92
Blank	35	-1490	112.81	122	2.43	-
0.80		-1481	37.14	85	0.81	66
1.00		-1505	27.85	79	0.60	75
1.50		-1515	22.74	68	0.49	79
2.00		-1488	19.49	65	0.42	82
2.50		-1497	10.67	58	0.23	90
Blank	40	-1500	168.06	129	3.62	-
0.80		-1497	53.39	89	1.15	68
1.00		-1518	42.24	83	0.91	74
1.50		-1524	34.35	79	0.74	79
2.00		-1530	22.74	67	0.63	82
2.50		-1489	17.64	62	0.38	89
Blank	45	-1503	183.38	134	3.95	-
0.80		-1480	64.53	93	1.39	64
1.00		-1492	46.89	88	1.12	71
1.50		-1512	36.21	79	0.78	80
2.00		-1508	36.21	75	0.78	80
2.50		-1516	25.07	66	0.54	86
Blank	50	-1493	197.77	140	4.26	-
0.80		-1488	77.06	115	1.66	61
1.00		-1507	57.56	99	1.24	70
1.50		-1512	47.35	87	1.02	76
2.00		-1525	41.78	80	0.90	78
2.50		-1489	32.03	74	0.69	83

Table 3.12: Electrochemical polarization parameters for the corrosion of AZ31 alloy in 0.10 M NaCl solution in the presence of DB at different temperatures.

Inhibitor concentration (mmol dm^{-3})	Temperature (°C)	E_{corr} vs SCE (mV)	i_{corr} (µA cm^{-2})	$-\beta_c$ (mV dec^{-1})	v_{corr} (mm y^{-1})	η (%)
Blank	30	-1483	154.03	135	3.34	-
0.80		-1494	79.85	130	1.72	48
1.00		-1489	64.53	126	1.39	58
1.50		-1494	49.67	128	1.07	67
2.00		-1490	35.74	120	0.77	76
2.50		-1497	21.35	119	0.46	86
Blank	35	-1489	171.58	141	3.73	-
0.80		-1489	90.99	140	1.97	47
1.00		-1505	72.88	138	1.57	57
1.50		-1508	50.14	133	1.08	71
2.00		-1513	38.06	134	0.82	78
2.50		-1506	25.53	130	0.55	85
Blank	40	-1502	210.77	165	4.54	-
0.80		-1528	96.10	155	2.07	44
1.00		-1517	77.06	153	1.66	55
1.50		-1503	56.17	150	1.21	67
2.00		-1511	44.10	146	0.95	74
2.50		-1509	28.78	142	0.62	83
Blank	45	-1516	225.52	162	4.90	-
0.80		-1514	129.53	157	2.79	43
1.00		-1525	110.90	148	2.39	51
1.50		-1513	74.28	153	1.60	67
2.00		-1520	63.14	145	1.36	72
2.50		-1507	43.64	140	0.94	80
Blank	50	-1490	235.47	173	5.11	-
0.80		-1494	136.49	157	2.94	42
1.00		-1503	115.60	168	2.49	51
1.50		-1502	79.38	160	1.71	66
2.00		-1509	70.56	166	1.52	70
2.50		-1508	47.81	159	1.03	79

Table 3.13: Electrochemical polarization parameters for the corrosion of AZ31 in 0.15 M NaCl solution in the presence of DB at different temperatures.

Inhibitor concentration (mmol dm^{-3})	Temperature (°C)	E_{corr} vs SCE (mV)	i_{corr} (μA cm^{-2})	$-\beta_c$ (mV dec^{-1})	v_{corr} (mm y^{-1})	η (%)
Blank	30	-1537	233.52	150	5.03	-
0.80		-1503	123.95	121	2.67	46
1.00		-1525	99.81	113	2.15	57
1.50		-1514	79.85	101	1.72	65
2.00		-1500	56.64	95	1.22	75
2.50		-1495	36.21	90	0.78	84
Blank	35	-1500	333.34	155	7.18	-
0.80		-1532	183.38	124	3.95	45
1.00		-1512	146.24	115	3.15	56
1.50		-1508	105.85	103	2.28	68
2.00		-1540	79.85	98	1.72	76
2.50		-1530	53.39	92	1.15	83
Blank	40	-1515	455.90	168	9.82	-
0.80		-1526	255.34	126	5.50	43
1.00		-1529	213.56	119	4.60	53
1.50		-1510	158.31	105	3.41	65
2.00		-1502	123.49	100	2.66	72
2.50		-1518	85.88	96	1.85	81
Blank	45	-1491	478.65	170	10.31	-
0.80		-1475	271.59	131	5.85	42
1.00		-1486	236.77	122	5.10	50
1.50		-1500	165.27	111	3.56	65
2.00		-1514	139.27	104	3.00	70
2.50		-1530	102.13	99	2.20	78
Blank	50	-1475	567.33	194	12.22	-
0.80		-1501	334.27	134	7.20	40
1.00		-1521	285.98	126	6.16	50
1.50		-1503	203.34	115	4.38	64
2.00		-1508	176.42	109	3.80	68
2.50		-1515	129.53	100	2.79	77

Table 3.14: Electrochemical polarization parameters for the corrosion of AZ31 alloy in 0.20 M NaCl solution in the presence of DB at different temperatures.

Inhibitor concentration (mmol dm^{-3})	Temperature (°C)	E_{corr} vs SCE (mV)	i_{corr} (μA cm^{-2})	$-\beta_c$ (mV dec^{-1})	v_{corr} (mm y^{-1})	η (%)
Blank	30	-1500	432.55	189	9.40	-
0.80		-1489	243.27	139	5.24	44
1.00		-1515	190.34	123	4.10	56
1.50		-1522	156.92	110	3.38	64
2.00		-1527	114.20	102	2.46	73
2.50		-1532	79.38	93	1.71	82
Blank	35	-1485	457.04	214	9.93	-
0.80		-1500	262.31	142	5.65	43
1.00		-1469	212.16	125	4.57	54
1.50		-1475	174.09	113	3.75	62
2.00		-1480	133.70	105	2.88	71
2.50		-1488	90.53	95	1.95	80
Blank	40	-1483	489.13	181	10.63	-
0.80		-1477	285.52	140	6.15	42
1.00		-1468	236.77	128	5.10	52
1.50		-1489	194.99	115	4.20	60
2.00		-1485	148.56	110	3.20	70
2.50		-1488	97.49	98	2.10	80
Blank	45	-1511	687.77	211	14.75	-
0.80		-1490	394.62	143	8.50	41
1.00		-1495	342.62	130	7.38	50
1.50		-1501	287.84	118	6.20	58
2.00		-1507	220.52	111	4.75	68
2.50		-1480	150.88	100	3.25	78
Blank	50	-1497	709.98	171	15.43	-
0.80		-1490	422.48	146	9.10	40
1.00		-1505	369.09	133	7.95	48
1.50		-1511	308.73	121	6.65	57
2.00		-1520	241.41	114	5.20	66
2.50		-1518	162.49	103	3.50	77

Table 3.15: Electrochemical polarization parameters for the corrosion of AZ31 alloy in 0.25 M NaCl solution in the presence of DB at different temperatures.

Inhibitor concentration (mmol dm^{-3})	Temperature (°C)	E_{corr} vs SCE (mV)	i_{corr} (µA cm^{-2})	$-\beta_c$ (mV dec^{-1})	υ_{corr} (mm y^{-1})	η (%)
Blank	30	-1526	520.41	190	11.31	-
0.80		-1480	297.13	146	6.40	43
1.00		-1508	241.41	137	5.20	54
1.50		-1521	198.70	121	4.28	62
2.00		-1508	150.88	111	3.25	71
2.50		-1500	131.38	100	2.83	75
Blank	35	-1515	553.44	192	12.03	-
0.80		-1524	323.59	148	6.97	42
1.00		-1509	271.59	139	5.85	51
1.50		-1534	223.31	124	4.81	60
2.00		-1540	175.95	114	3.79	68
2.50		-1521	143.92	103	3.10	74
Blank	40	-1488	577.18	188	12.54	-
0.80		-1479	348.19	151	7.50	40
1.00		-1470	290.16	140	6.25	50
1.50		-1490	244.66	126	5.27	58
2.00		-1495	197.77	116	4.26	66
2.50		-1489	161.10	105	3.47	72
Blank	45	-1510	706.61	209	15.22	-
0.80		-1523	417.37	153	8.99	39
1.00		-1516	364.44	142	7.85	48
1.50		-1510	297.13	128	6.40	57
2.00		-1522	255.34	118	5.50	64
2.50		-1508	210.31	107	4.53	70
Blank	50	-1494	792.81	186	17.23	-
0.80		-1490	510.69	155	11.00	36
1.00		-1488	428.51	144	9.23	46
1.50		-1512	366.77	130	7.90	54
2.00		-1509	312.91	120	6.74	61
2.50		-1499	279.02	111	6.01	65

Table 3.16: Electrochemical polarization parameters for the corrosion of AZ31 alloy in 0.05 M Na_2SO_4 solution in the presence of DB at different temperatures.

Inhibitor concentration (mmol dm^{-3})	Temperature (°C)	E_{corr} vs SCE (mV)	i_{corr} (μA cm^{-2})	$-\beta_c$ (mV dec^{-1})	v_{corr} (mm y^{-1})	η (%)
Blank	30	-1483	63.33	93	1.37	-
0.80		-1475	20.89	84	0.60	67
1.00		-1465	14.08	73	0.30	78
1.50		-1482	12.51	73	0.27	80
2.00		-1486	6.67	60	0.13	90
2.50		-1495	3.71	60	0.08	94
Blank	35	-1470	110.24	110	2.39	-
0.80		-1523	25.03	96	0.97	59
1.00		-1508	30.65	95	0.66	72
1.50		-1482	25.98	85	0.56	76
2.00		-1492	20.42	74	0.44	81
2.50		-1473	12.53	72	0.27	90
Blank	40	-1502	164.74	125	3.58	-
0.80		-1487	64.95	117	1.40	60
1.00		-1486	51.88	106	1.13	68
1.50		-1497	39.15	95	0.85	76
2.00		-1491	39.00	84	0.84	76
2.50		-1493	26.46	82	0.57	84
Blank	45	-1465	179.03	154	3.89	-
0.80		-1507	73.88	126	1.61	58
1.00		-1494	64.54	115	1.39	64
1.50		-1487	48.23	105	1.04	73
2.00		-1477	42.68	94	0.93	76
2.50		-1496	29.71	83	0.64	83
Blank	50	-1481	190.03	144	4.13	-
0.80		-1551	79.97	127	1.72	58
1.00		-1521	70.56	117	1.52	63
1.50		-1518	55.98	106	1.22	70
2.00		-1524	48.67	95	1.06	74
2.50		-1530	34.35	95	0.74	82

Table 3.17: Electrochemical polarization parameters for the corrosion of AZ31 alloy in 0.10 M Na_2SO_4 solution in the presence of DB at different temperatures.

Inhibitor concentration (mmol dm^{-3})	Temperature (°C)	E_{corr} vs SCE (mV)	i_{corr} (µA cm^{-2})	$-\beta_c$ (mV dec^{-1})	v_{corr} (mm y^{-1})	η (%)
Blank	30	-1522	71.21	117	1.54	-
0.80		-1476	25.53	104	0.55	64
1.00		-1477	21.02	92	0.45	70
1.50		-1469	17.64	82	0.38	75
2.00		-1463	14.39	81	0.31	79
2.50		-1490	12.99	71	0.28	81
Blank	35	-1528	157.60	134	3.42	-
0.80		-1481	62.21	115	1.34	60
1.00		-1477	54.31	105	1.17	65
1.50		-1463	37.93	94	0.86	74
2.00		-1446	37.60	84	0.81	76
2.50		-1475	32.96	82	0.71	79
Blank	40	-1485	191.24	140	4.15	-
0.80		-1505	79.38	125	1.71	58
1.00		-1503	72.42	114	1.56	62
1.50		-1494	60.81	104	1.31	68
2.00		-1482	48.74	93	1.05	74
2.50		-1494	43.64	92	0.94	77
Blank	45	-1481	202.71	150	4.40	-
0.80		-1504	186.35	121	1.86	57
1.00		-1492	101.71	119	1.81	58
1.50		-1509	68.24	105	1.48	66
2.00		-1486	54.78	93	1.18	73
2.50		-1490	50.60	93	1.09	75
Blank	50	-1456	208.41	157	4.53	-
0.80		-1492	95.83	121	2.08	54
1.00		-1530	89.13	113	1.92	57
1.50		-1552	75.67	111	1.63	64
2.00		-1516	60.35	103	1.30	71
2.50		-1499	51.06	93	1.10	74

Table 3.18: Electrochemical polarization parameters for the corrosion of AZ31 in 0.15 M Na_2SO_4 solution in the presence of DB at different temperatures.

Inhibitor concentration (mmol dm^{-3})	Temperature (°C)	E_{corr} vs SCE (mV)	i_{corr} (µA cm^{-2})	$-\beta_c$ (mV dec^{-1})	v_{corr} (mm y^{-1})	η (%)
Blank	30	-1457	218.14	138	4.74	-
0.80		-1505	82.63	124	1.78	62
1.00		-1469	68.24	105	1.47	69
1.50		-1489	57.10	95	1.23	74
2.00		-1487	51.06	89	1.10	77
2.50		-1505	44.10	79	0.95	80
Blank	35	-1457	322.28	142	7.00	-
0.80		-1553	134.63	122	2.90	58
1.00		-1528	109.10	108	2.35	66
1.50		-1523	88.21	99	1.90	73
2.00		-1487	74.28	87	1.60	77
2.50		-1487	69.63	78	1.50	79
Blank	40	-1469	445.19	151	9.67	-
0.80		-1561	198.70	133	4.28	56
1.00		-1517	165.74	125	3.57	63
1.50		-1495	134.63	114	2.90	70
2.00		-1485	113.28	104	2.44	75
2.50		-1483	110.03	83	2.37	76
Blank	45	-1446	461.63	158	10.03	-
0.80		-1517	206.13	137	4.44	56
1.00		-1523	175.49	126	3.78	62
1.50		-1512	155.52	118	3.35	67
2.00		-1512	129.06	99	2.78	72
2.50		-1493	113.28	82	2.44	76
Blank	50	-1448	546.62	170	11.88	-
0.80		-1562	249.77	142	5.38	55
1.00		-1520	220.06	125	4.74	60
1.50		-1517	198.70	118	4.28	64
2.00		-1509	166.20	105	3.58	70
2.50		-1501	136.03	94	2.93	75

Table 3.19: Electrochemical polarization parameters for the corrosion of AZ31 alloy in 0.20 M Na_2SO_4 solution in the presence of DB at different temperatures.

Inhibitor concentration (mmol dm^{-3})	Temperature (°C)	E_{corr} vs SCE (mV)	i_{corr} (µA cm^{-2})	$-\beta_c$ (mV dec^{-1})	v_{corr} (mm y^{-1})	η (%)
Blank	30	-1505	235.63	152	5.12	-
0.80		-1443	98.31	125	2.15	58
1.00		-1441	77.92	106	1.68	67
1.50		-1458	57.56	99	1.24	75
2.00		-1461	53.39	98	1.15	77
2.50		-1453	49.02	82	1.06	79
Blank	35	-1493	354.34	158	7.70	-
0.80		-1485	151.35	122	3.26	57
1.00		-1505	124.42	114	2.68	65
1.50		-1456	95.37	109	1.94	73
2.00		-1452	82.08	98	1.78	76
2.50		-1454	77.53	86	1.67	78
Blank	40	-1489	470.87	164	10.23	-
0.80		-1513	197.31	125	4.25	58
1.00		-1493	168.06	114	3.62	64
1.50		-1493	136.96	103	2.95	71
2.00		-1528	112.81	100	2.43	75
2.50		-1503	104.92	95	2.26	77
Blank	45	-1472	542.13	172	11.78	-
0.80		-1507	227.45	124	4.77	57
1.00		-1505	188.02	113	4.05	63
1.50		-1506	158.77	114	3.42	69
2.00		-1501	149.95	105	3.23	71
2.50		-1514	123.03	97	2.65	76
Blank	50	-1480	672.86	197	14.62	-
0.80		-1506	307.34	133	6.62	56
1.00		-1508	268.81	126	5.79	60
1.50		-1490	242.81	114	5.23	64
2.00		-1508	215.41	103	4.64	68
2.50		-1484	168.06	100	3.62	75

Table 3.20: Electrochemical polarization parameters for the corrosion of AZ31 alloy in 0.25 M Na_2SO_4 solution in the presence of DB at different temperatures.

Inhibitor concentration (mmol dm^{-3})	Temperature (°C)	E_{corr} vs SCE (mV)	i_{corr} (µA cm-^{2})	-β_c (mV dec^{-1})	v_{corr} (mm y^{-1})	η (%)
Blank	30	-1451	372.80	147	8.10	-
0.80		-1505	173.17	120	3.73	54
1.00		-1482	137.42	110	2.96	63
1.50		-1460	105.85	102	2.28	72
2.00		-1497	92.85	98	2.00	75
2.50		-1478	87.28	89	1.86	77
Blank	35	-1411	497.12	158	10.80	-
0.80		-1469	220.52	130	4.75	56
1.00		-1404	196.38	119	4.23	61
1.50		-1467	149.95	112	3.23	70
2.00		-1444	135.10	95	2.91	73
2.50		-1469	118.38	89	2.55	76
Blank	40	-1438	516.71	170	11.23	-
0.80		-1418	248.84	132	5.36	52
1.00		-1479	222.84	129	4.80	57
1.50		-1481	197.31	115	4.25	62
2.00		-1441	168.99	107	3.64	68
2.50		-1520	146.24	96	3.15	72
Blank	45	-1486	583.03	190	12.67	-
0.80		-1520	294.80	138	6.35	49
1.00		-1510	269.27	123	5.80	54
1.50		-1510	248.38	119	5.35	58
2.00		-1498	203.34	106	4.38	65
2.50		-1495	186.63	103	4.02	68
Blank	50	-1463	727.89	201	15.82	-
0.80		-1520	394.62	147	8.50	46
1.00		-1514	364.44	133	7.85	50
1.50		-1500	324.05	120	6.98	56
2.00		-1505	280.88	115	6.05	62
2.50		-1484	255.34	106	5.50	65

Table 3.21: Electrochemical impedance parameters for the corrosion of AZ31 alloy in 0.05 M NaCl solution in the presence of DB at different temperatures.

Inhibitor Concentration (mmol dm^{-3})	Temperature (°C)	R_{hf} (Ω cm^2)	R_f (Ω cm^2)	R_{dif} (Ω cm^2)	C_{dl} (μF cm^{-2})	C_f (μF cm^{-2})	η (%)
Blank	30	580	296	225	138	177	-
0.80		2639	1590	705	70	90	78
1.00		3582	1606	753	67	66	83
1.50		3752	2898	847	60	67	85
2.00		3946	2871	898	55	60	85
2.50		4635	2900	918	52	64	87
Blank	35	550	255	207	153	181	-
0.80		1528	1312	638	68	66	64
1.00		2070	1542	679	63	65	73
1.50		2437	1687	744	53	60	77
2.00		2730	1764	791	55	56	79
2.50		3956	2973	887	50	68	86
Blank	40	422	231	184	161	188	-
0.80		1312	1105	571	73	68	67
1.00		1543	1222	644	64	69	72
1.50		1843	1576	695	66	60	77
2.00		1978	1705	767	60	64	78
2.50		3195	2104	878	56	60	86
Blank	45	340	191	150	170	192	-
0.80		903	789	425	70	68	62
1.00		1133	972	451	60	67	69
1.50		1628	1250	511	61	67	79
2.00		1661	1322	670	64	69	80
2.50		1956	1613	745	61	60	82
Blank	50	318	160	131	171	198	-
0.80		791	582	401	72	62	59
1.00		1016	900	438	68	63	68
1.50		1304	1119	535	67	60	75
2.00		1392	1180	648	57	64	77
2.50		1635	1274	722	56	55	80

Table 3.22: Electrochemical impedance parameters for the corrosion of AZ31 alloy in 0.10 M NaCl solution in the presence of DB at different temperatures.

Inhibitor Concentration (mmol dm^{-3})	Temperature (°C)	R_{hf} (Ω cm^2)	R_f (Ω cm^2)	R_{dif} (Ω cm^2)	C_{dl} (μF cm^{-2})	C_f (μF cm^{-2})	η (%)
Blank	30	507	232	209	166	172	-
0.80		968	634	311	181	83	47
1.00		1209	1012	488	160	52	58
1.50		1465	1034	541	153	40	65
2.00		1997	1479	698	142	30	74
2.50		3650	2691	985	127	23	86
Blank	35	380	192	168	181	179	-
0.80		714	554	246	184	61	46
1.00		894	597	288	169	50	57
1.50		1260	1006	491	150	47	69
2.00		1587	1246	604	135	29	76
2.50		2503	1804	883	128	27	85
Blank	40	366	173	142	191	183	-
0.80		653	546	218	193	74	43
1.00		815	637	269	161	62	55
1.50		1104	890	480	153	51	66
2.00		1361	1146	623	130	40	73
2.50		1777	1532	841	132	32	80
Blank	45	351	152	115	195	185	-
0.80		623	531	229	196	78	44
1.00		719	576	250	163	63	51
1.50		998	781	387	158	54	65
2.00		1185	930	550	145	46	70
2.50		1608	1436	809	139	38	78
Blank	50	301	139	108	200	191	-
0.80		520	408	192	200	81	42
1.00		620	539	238	183	70	51
1.50		880	600	279	160	62	65
2.00		969	718	370	152	53	68
2.50		1366	1167	699	140	44	78

Table 3.23: Electrochemical impedance parameters for the corrosion of AZ31 alloy in 0.15 M NaCl solution in the presence of DB at different temperatures.

Inhibitor Concentration (mmol dm^{-3})	Temperature (°C)	R_{hf} (Ω cm^2)	R_f (Ω cm^2)	R_{dif} (Ω cm^2)	C_{dl} (µF cm^{-2})	C_f (µF cm^{-2})	*η* (%)
Blank	30	358	170	144	172	115	-
0.80		664	547	220	123	95	46
1.00		811	560	249	109	86	55
1.50		976	675	344	102	82	63
2.00		1381	1143	480	97	80	74
2.50		2069	1678	781	85	75	83
Blank	35	301	161	121	184	128	-
0.80		545	500	187	133	100	45
1.00		683	552	215	111	93	56
1.50		950	676	301	106	88	68
2.00		1243	1115	518	100	83	76
2.50		1600	1378	734	98	79	81
Blank	40	288	150	113	197	133	-
0.80		510	457	170	148	111	44
1.00		600	531	217	130	104	52
1.50		832	676	288	121	95	65
2.00		994	753	466	113	90	71
2.50		1373	1158	705	98	83	79
Blank	45	225	128	100	201	140	-
0.80		401	339	155	162	129	44
1.00		448	421	226	144	119	50
1.50		642	571	259	120	110	65
2.00		737	634	313	102	103	69
2.50		974	755	375	95	98	77
Blank	50	130	88	73	218	147	-
0.80		219	142	95	170	138	40
1.00		260	178	134	161	127	50
1.50		400	317	160	147	115	67
2.00		424	345	181	116	100	69
2.50		680	511	208	103	94	79

Table 3.24: Electrochemical impedance parameters for the corrosion of AZ31 alloy in 0.20 M NaCl solution in the presence of DB at different temperatures.

Inhibitor Concentration (mmol dm^{-3})	Temperature (°C)	R_{hf} (Ω cm^2)	R_f (Ω cm^2)	R_{dif} (Ω cm^2)	C_{dl} (µF cm^{-2})	C_f (µF cm^{-2})	η (%)
Blank	30	170	109	95	193	191	-
0.80		309	234	135	121	99	44
1.00		402	318	200	117	87	57
1.50		480	376	218	106	79	64
2.00		644	547	232	104	74	73
2.50		924	789	289	100	70	81
Blank	35	166	97	79	190	199	-
0.80		300	213	121	135	95	44
1.00		359	276	156	112	82	53
1.50		446	355	170	119	73	62
2.00		603	498	185	109	68	72
2.50		880	634	290	105	67	80
Blank	40	158	90	70	212	210	-
0.80		277	214	110	151	89	42
1.00		334	264	138	130	83	52
1.50		400	301	157	117	74	60
2.00		529	467	169	119	65	70
2.50		842	618	275	112	60	81
Blank	45	125	78	58	220	219	-
0.80		218	177	101	161	87	42
1.00		251	189	127	147	82	50
1.50		300	201	135	126	75	58
2.00		416	312	150	109	71	69
2.50		583	400	253	110	60	78
Blank	50	103	73	52	243	232	-
0.80		174	99	93	174	82	40
1.00		202	138	119	165	70	49
1.50		240	143	130	150	68	57
2.00		298	169	144	120	61	65
2.50		453	317	240	107	57	77

Table 3.25: Electrochemical impedance parameters for the corrosion of AZ31 alloy in 0.25 M NaCl solution in the presence of DB at different temperatures.

Inhibitor Concentration (mmol dm^{-3})	Temperature (°C)	R_{hf} (Ω cm^2)	R_f (Ω cm^2)	R_{dif} (Ω cm^2)	C_{dl} (µF cm^{-2})	C_f (µF cm^{-2})	*η* (%)
Blank	30	201	115	99	205	195	-
0.80		354	254	126	179	110	43
1.00		440	312	140	159	103	54
1.50		533	344	159	150	98	62
2.00		709	610	266	144	92	71
2.50		821	722	280	139	90	75
Blank	35	150	107	85	217	205	-
0.80		261	179	110	193	114	42
1.00		312	201	129	189	108	51
1.50		386	223	135	172	100	61
2.00		476	308	150	150	97	68
2.50		590	376	178	138	93	74
Blank	40	141	98	72	221	222	-
0.80		236	163	99	199	123	40
1.00		283	190	106	160	111	50
1.50		340	214	119	159	102	58
2.00		425	300	131	137	93	66
2.50		496	369	158	128	96	71
Blank	45	105	81	68	230	223	-
0.80		174	118	90	201	140	39
1.00		204	149	96	193	125	48
1.50		251	193	105	179	109	58
2.00		295	201	120	169	98	64
2.50		350	238	137	160	94	70
Blank	50	99	70	55	248	239	-
0.80		157	100	78	221	147	37
1.00		186	111	89	211	122	46
1.50		219	140	95	199	111	55
2.00		257	178	110	170	100	61
2.50		285	202	124	153	95	65

Table 3.26: Electrochemical impedance parameters for the corrosion of AZ31 alloy in 0.05 M Na_2SO_4 solution in the presence of DB at different temperatures.

Inhibitor Concentration (mmol dm^{-3})	Temperature (°C)	R_{hf} (Ω cm^2)	R_f (Ω cm^2)	R_{dif} (Ω cm^2)	C_{dl} (µF cm^{-2})	C_f (µF cm^{-2})	η (%)
Blank	30	609	471	412	159	102	-
0.80		1860	1610	712	24	91	67
1.00		2764	1709	890	22	86	77
1.50		2975	1954	955	31	84	79
2.00		4999	3884	1254	32	43	87
2.50		7091	6014	1888	36	41	91
Blank	35	510	367	303	176	129	-
0.80		1208	962	447	59	105	57
1.00		1779	1623	766	20	80	71
1.50		2143	1676	851	38	66	76
2.00		2660	1754	880	55	45	80
2.50		3980	2003	999	35	59	87
Blank	40	477	333	288	201	146	-
0.80		1200	835	398	75	81	60
1.00		1500	1377	634	70	75	68
1.50		1957	1607	770	63	68	75
2.00		2076	1722	821	51	51	77
2.50		2874	1807	867	49	64	83
Blank	45	450	350	275	225	151	-
0.80		1104	899	402	90	73	59
1.00		1270	987	435	71	61	64
1.50		1586	1308	744	68	58	71
2.00		1896	1715	790	63	49	76
2.50		2536	1760	854	51	46	82
Blank	50	412	354	252	261	168	-
0.80		987	355	139	92	81	58
1.00		1132	619	303	81	71	63
1.50		1376	1130	570	76	64	70
2.00		1563	1319	761	62	55	73
2.50		2194	1749	829	55	49	81

Table 3.27: Electrochemical impedance parameters for the corrosion of AZ31 alloy in 0.10 M Na_2SO_4 solution in the presence of DB at different temperatures.

Inhibitor Concentration (mmol dm^{-3})	Temperature (°C)	R_{hf} (Ω cm^2)	R_f (Ω cm^2)	R_{dif} (Ω cm^2)	C_{dl} (μF cm^{-2})	C_f (μF cm^{-2})	η (%)
Blank	30	460	343	319	201	188	-
0.80		1279	1165	688	150	109	64
1.00		1556	1398	799	148	103	70
1.50		1798	1601	823	145	101	74
2.00		2301	2178	931	144	118	80
2.50		2479	2284	985	144	115	81
Blank	35	432	322	293	224	191	-
0.80		1076	979	472	124	141	59
1.00		1215	1105	579	115	137	64
1.50		1692	1489	766	104	122	74
2.00		1837	1645	886	111	108	76
2.50		2211	2002	998	101	94	80
Blank	40	403	254	227	249	225	-
0.80		1001	889	441	133	201	59
1.00		1074	945	470	115	123	62
1.50		1248	1105	550	118	132	67
2.00		1530	1401	735	103	110	73
2.50		1698	1489	789	95	98	76
Blank	45	387	193	160	269	237	-
0.80		942	783	390	212	212	58
1.00		921	811	421	203	189	57
1.50		1177	1022	505	197	171	67
2.00		1382	1202	607	172	119	71
2.50		1495	1367	686	145	99	74
Blank	50	373	209	161	278	241	-
0.80		820	775	339	223	200	54
1.00		874	800	394	122	183	57
1.50		1089	1011	499	118	152	65
2.00		1310	1102	512	111	143	71
2.50		1421	1209	555	114	112	74

Table 3.28: Electrochemical impedance parameters for the corrosion of AZ31 alloy in 0.15 M Na_2SO_4 solution in the presence of DB at different temperatures.

Inhibitor Concentration (mmol dm^{-3})	Temperature (°C)	R_{hf} (Ω cm^2)	R_f (Ω cm^2)	R_{dif} (Ω cm^2)	C_{dl} (μF cm^{-2})	C_f (μF cm^{-2})	η (%)
Blank	30	434	420	383	244	167	-
0.80		1135	1087	548	231	130	61
1.00		1430	1280	637	191	118	69
1.50		1686	1501	751	134	105	74
2.00		1870	1756	850	113	97	76
2.50		2197	2001	968	101	93	80
Blank	35	463	300	280	278	169	-
0.80		1100	993	478	240	134	57
1.00		1350	1197	600	213	128	65
1.50		1696	1500	742	192	119	72
2.00		1888	1721	829	134	108	75
2.50		2099	1913	955	112	99	78
Blank	40	380	230	201	299	180	-
0.80		878	702	361	244	145	56
1.00		1007	900	441	215	133	62
1.50		1280	1150	559	193	121	70
2.00		1501	1309	671	140	117	74
2.50		1612	1401	790	115	103	76
Blank	45	273	237	200	307	188	-
0.80		634	578	275	250	154	56
1.00		700	592	265	221	120	61
1.50		803	700	338	200	130	66
2.00		965	835	411	152	122	71
2.50		1156	1047	557	121	105	76
Blank	50	245	200	178	321	200	-
0.80		540	490	240	251	155	54
1.00		620	501	258	226	130	60
1.50		703	624	308	203	125	65
2.00		852	760	398	156	124	71
2.50		1022	978	479	125	108	76

Table 3.29: Electrochemical impedance parameters for the corrosion of AZ31 alloy in 0.20 M Na_2SO_4 solution in the presence of DB at different temperatures.

Inhibitor Concentration (mmol dm^{-3})	Temperature (°C)	R_{hf} (Ω cm^2)	R_f (Ω cm^2)	R_{dif} (Ω cm^2)	C_{dl} (µF cm^{-2})	C_f (µF cm^{-2})	η (%)
Blank	30	301	226	171	269	179	-
0.80		720	601	371	249	131	58
1.00		902	794	399	161	97	66
1.50		1206	1103	533	111	95	75
2.00		1334	1211	600	108	90	77
2.50		1423	1298	637	117	85	79
Blank	35	287	224	190	287	186	-
0.80		670	513	298	198	135	57
1.00		825	704	354	146	123	65
1.50		1064	923	457	96	111	73
2.00		1215	1188	621	95	103	76
2.50		1320	1206	652	82	93	78
Blank	40	259	192	163	301	191	-
0.80		625	502	250	214	146	58
1.00		724	604	288	142	113	64
1.50		880	735	362	112	105	70
2.00		1034	911	456	105	100	74
2.50		1145	1007	544	99	95	77
Blank	45	236	203	167	321	201	-
0.80		550	444	227	232	151	57
1.00		650	508	252	146	120	63
1.50		754	658	338	119	111	68
2.00		845	732	361	111	102	72
2.50		985	806	401	105	98	76
Blank	50	218	187	159	333	219	-
0.80		500	395	167	235	160	56
1.00		564	432	214	168	124	61
1.50		614	508	253	117	118	64
2.00		676	545	273	113	106	67
2.50		865	712	359	111	101	74

Table 3.30: Electrochemical impedance parameters for the corrosion of AZ31 alloy in 0.25 M Na_2SO_4 solution in the presence of DB at different temperatures.

Inhibitor Concentration (mmol dm^{-3})	Temperature (°C)	R_{hf} (Ω cm^2)	R_f (Ω cm^2)	R_{dif} (Ω cm^2)	C_{dl} (μF cm^{-2})	C_f (μF cm^{-2})	η (%)
Blank	30	392	301	280	300	240	-
0.80		875	734	366	242	211	55
1.00		1074	903	448	218	201	63
1.50		1385	1201	600	178	180	71
2.00		1565	1399	779	160	163	74
2.50		1703	1623	861	141	133	76
Blank	35	350	250	221	333	259	-
0.80		796	659	328	236	230	56
1.00		894	705	354	203	200	60
1.50		1186	1065	549	169	160	70
2.00		1304	1203	622	150	147	73
2.50		1485	1300	658	132	122	76
Blank	40	201	114	96	345	267	-
0.80		417	299	138	218	233	51
1.00		475	351	147	190	199	57
1.50		530	415	200	150	170	62
2.00		631	570	281	142	155	68
2.50		721	645	393	120	142	72
Blank	45	180	109	80	359	280	-
0.80		363	194	100	225	230	50
1.00		393	232	125	188	202	54
1.50		431	305	157	145	160	58
2.00		514	376	175	121	157	64
2.50		570	414	212	118	140	68
Blank	50	170	100	64	389	308	-
0.80		322	137	87	210	218	47
1.00		345	158	96	175	201	50
1.50		394	287	139	135	161	56
2.00		451	304	147	118	141	62
2.50		501	376	163	111	128	66

Table 3.31: Activation parameters for the corrosion of AZ31 alloy in NaCl solutions containing different concentrations of DB inhibitor.

Concentration of NaCl (M)	Concentration of inhibitor (mmol dm^{-3})	E_a (kJ mol^{-1})	$\Delta H^{\#}$ (kJ mol^{-1})	$\Delta S^{\#}$ (J mol^{-1} K^{-1})
0.05	Blank	34.00	34.66	-128.69
	0.80	56.74	54.14	-73.82
	1.00	60.53	62.39	-49.38
	1.50	64.99	66.25	-65.34
	2.00	71.89	69.29	-30.84
	2.50	89.11	76.52	21.11
0.1	Blank	24.55	20.97	-162.88
	0.80	24.57	21.97	-182.43
	1.00	25.02	22.42	-173.28
	1.50	25.72	23.12	-166.30
	2.00	30.24	27.64	-156.60
	2.50	34.86	32.27	-145.30
0.15	Blank	23.57	18.70	-174.42
	0.80	26.03	25.15	-154.22
	1.00	27.76	28.35	-145.57
	1.50	30.95	31.75	-138.92
	2.00	38.40	35.80	-125.87
	2.50	38.81	36.22	-117.86
0.20	Blank	20.67	18.08	-167.27
	0.80	24.49	21.89	-159.37
	1.00	28.25	26.66	-145.66
	1.50	29.62	27.51	-127.86
	2.00	31.46	28.86	-120.22
	2.50	36.16	31.34	-95.86
0.25	Blank	16.94	15.30	-175.67
	0.80	19.33	16.74	-154.32
	1.00	20.76	18.17	-137.78
	1.50	22.22	19.62	-114.40
	2.00	26.92	24.32	-105.09
	2.50	27.55	24.95	-99.76

Table 3.32: Activation parameters for the corrosion of AZ31 alloy in Na_2SO_4 solutions containing different concentrations of DB inhibitor.

Concentration of Na_2SO_4 (M)	Concentration of inhibitor (mmol dm^{-3})	E_a (kJ mol^{-1})	$\Delta H^{\#}$ (kJ mol^{-1})	$\Delta S^{\#}$ (J mol^{-1} K^{-1})
0.05	Blank	44.17	40.04	-108.74
	0.80	44.37	40.28	-115.72
	1.00	48.86	44.77	-103.38
	1.50	52.08	60.20	-56.86
	2.00	69.47	85.68	21.45
	2.50	84.50	91.14	35.66
0.1	Blank	39.64	33.78	-126.03
	0.80	45.20	39.94	-114.98
	1.00	49.74	44.84	-100.76
	1.50	50.11	52.06	-79.39
	2.00	54.85	52.18	-81.56
	2.50	55.95	58.02	-76.82
0.15	Blank	35.65	28.33	-137.09
	0.80	43.37	40.78	-104.50
	1.00	46.23	42.52	-96.77
	1.50	50.12	43.64	-85.71
	2.00	53.66	45.07	-80.99
	2.50	56.43	47.52	-78.22
0.20	Blank	35.21	23.87	-149.98
	0.80	36.19	41.90	-99.76
	1.00	38.95	46.11	-87.79
	1.50	45.57	48.84	-80.89
	2.00	53.10	51.02	-75.40
	2.50	50.63	54.05	-69.67
0.25	Blank	24.39	18.81	-164.69
	0.80	31.18	28.59	-117.75
	1.00	36.57	33.97	-111.90
	1.50	44.58	39.84	-97.86
	2.00	48.49	39.89	-85.54
	2.50	50.44	41.99	-77.72

Table 3.33: Thermodynamic parameters for the adsorption of DB on AZ31 alloy in NaCl solution.

Concentration of NaCl (M)	Temperature (°C)	ΔG^0_{ads} (kJ mol^{-1})	ΔH^0_{ads} (kJ mol^{-1})	ΔS^0_{ads} (J mol^{-1} K^{-1})
0.05	30	-29.25	-53.0	-78.6
	35	-28.78		
	40	-28.35		
	45	-28.25		
	50	-27.63		
0.1	30	-27.55	-49.9	-73.8
	35	-27.28		
	40	-26.15		
	45	-26.39		
	50	-26.06		
0.15	30	-27.32	-47.5	-66.8
	35	-26.95		
	40	-26.57		
	45	-26.35		
	50	-25.99		
0.20	30	-27.23	-45.7	-61.0
	35	-26.91		
	40	-26.60		
	45	-26.30		
	50	-25.99		
0.25	30	-24.46	-43.8	-63.8
	35	-24.16		
	40	-23.97		
	45	-23.53		
	50	-23.15		

Table 3.34: Thermodynamic parameters for the adsorption of DB on AZ31 alloy in Na_2SO_4 solution.

Concentration of Na_2SO_4 (M)	Temperature (°C)	ΔG^0_{ads} (kJ mol^{-1})	ΔH^0_{ads} (kJ mol^{-1})	ΔS^0_{ads} (J mol^{-1} K^{-1})
0.05	30	-29.46	-50.5	-69.20
	35	-29.18		
	40	-28.84		
	45	-28.49		
	50	-28.14		
0.10	30	-28.07	-35.4	-24.20
	35	-27.92		
	40	-27.82		
	45	-27.70		
	50	-27.58		
0.15	30	-27.22	-33.4	-20.40
	35	-27.11		
	40	-27.01		
	45	-26.91		
	50	-26.81		
0.20	30	-26.52	-32.1	-18.40
	35	-26.43		
	40	-26.34		
	45	-26.24		
	50	-26.15		
0.25	30	-26.36	-30.7	-14.40
	35	-26.27		
	40	-26.19		
	45	-26.12		
	50	-26.04		

Table 3.35: Calculated DFT parameters for DB inhibitor.

Parameters	Value
Total energy (KeV)	-16.87
Energy gap (eV)	3.88
E_{HOMO} (eV)	-1.04
E_{LUMO} (eV)	-4.93
Dipole moment (Debye)	15.01
Electronegativity (eV)	2.98
Chemical hardness (eV)	1.94
Electron affinity (eV)	4.93
Ionization potential (eV)	1.04
Softness (eV^{-1})	0.51

3.4 SODIUM 2,2'-(7,16-DIHEXYL-8,15-DIOXO-7,10,13,16-TETRAAZADOCOSANE-10,13-DIYL)DIACETATE (DH) AS CORROSION INHIBITOR ON AZ31 MAGNESIUM ALLOY IN SODIUM CHLORIDE AND SODIUM SULFATE SOLUTIONS

3.4.1 Potentiodynamic polarization measurements

The potentiodynamic polarization plots for the corrosion of AZ31 magnesium alloy in 0.1 M sodium chloride solution and 0.1 M sodium sulfate solution in the presence of different concentrations of DH, at 50 °C are shown in Fig. 3.35. Similar plots were obtained at other temperatures and also in the other five concentrations each of sodium chloride and sodium sulfate at the different temperatures studied. The potentiodynamic polarization parameters such as corrosion potential (E_{corr}), corrosion current density (i_{corr}), cathodic Tafel slopes (β_c) were calculated from the Tafel plots in the presence of different concentrations of DH at different temperatures and media concentrations are summarized in Tables 3.36 to 3.45. As seen from the data, the presence of inhibitor brings down the corrosion rate considerably. Polarization curves are shifted to a lower current density region indicating a decrease in corrosion rate (Pebere et al. 1990). Inhibition efficiency increases with the increase in the concentration of DH in the corrosion medium.

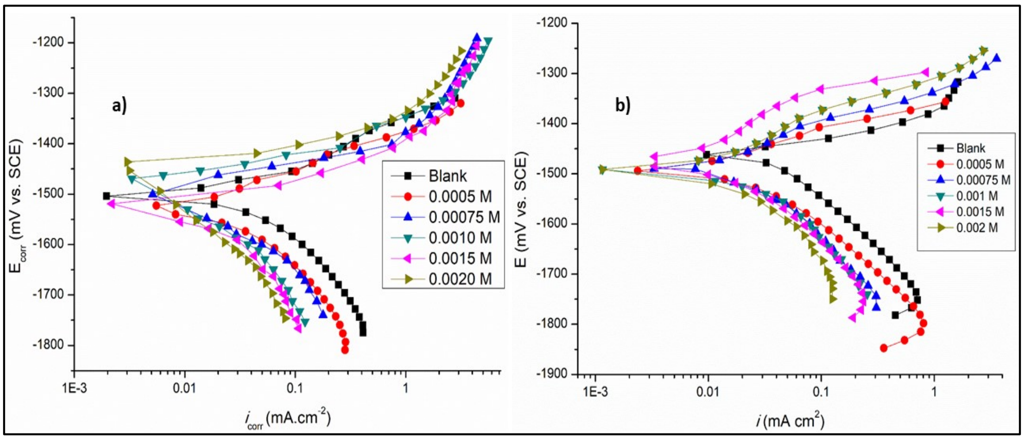

Fig. 3.35: Potentiodynamic polarization curves for the corrosion of AZ31 alloy in the presence of different concentrations of DH in a) 0.1 M NaCl solution and b) 0.1 M Na_2SO_4 solution at 50 °C.

No definite trend is observed in the shift of E_{corr} values; both anodic and cathodic polarization profiles are influenced simultaneously, almost to the same extent, which indicates the influence of DH compound on both the anodic and the cathodic reactions; metal dissolution and hydrogen evolution, respectively. The formation of magnesium salt precipitate on the surface, results in the formation of a film on the alloy surface, blocking both anodic and cathodic sites from the corrosive, rendering the inhibition effect on the corrosion of the alloy (Fuchs-Godec 2009). The data in Tables from 3.36 to 3.45 show that there is no significant change in the values of cathodic Tafel slope β_c with the increase in the concentration of the inhibitor. This suggests that the reduction mechanism at the cathode and the oxidation mechanism at the anode are not affected by the presence of inhibitor and hence the corrosion reaction is slowed down by the surface-blocking effect of the inhibitor (Liu et al. 2019). Thus, the inhibitor, DH, can be regarded as a mixed-type inhibitor.

3.4.2 Electrochemical impedance spectroscopy

Nyquist plots for the corrosion of AZ31 magnesium alloy in 0.1 M NaCl solution and 0.1 M Na_2SO_4 solution in the presence of different concentrations of DH are shown in Fig. 3.36. Similar plots were obtained in other concentrations and also at other temperatures.

The shape of the impedance plots for the alloy in the presence of the inhibitor is quite similar to that in the absence of the inhibitor (Montemor and Ferreira 2007). The presence of the inhibitor only increases the impedance without changing other aspects of the behavior. These results are in agreement with the results of polarization measurements that the inhibitor does not alter the mechanism of electrochemical reactions responsible for corrosion. The Nyquist plots display two capacitive semicircles at higher and medium frequencies, former being much similar to the one explained in section 3.3.2. The electrical equivalent circuit presented in Fig. 3.3 was filled into the impedance data and the electrochemical impedance parameters were calculated. The experimental results of EIS measurements are summarized in Tables 3.46 to 3.55.

The Bode plots of phase angle and amplitude for the corrosion of the AZ31 alloy immersed in 0.1 M NaCl solution and Na_2SO_4 solution at 50 °C in the presence of varying amounts of DH, are shown in Fig. 3.37 and Fig. 3.38, respectively. As seen from the Bode plots, both the impedance modulus (Z_{mod}) at low frequency and the phase maximum (θ_{max}) at intermediate frequency increase with the increase in DH concentration, which collectively indicates that the presence of highly protective surface film protecting the alloy surface.

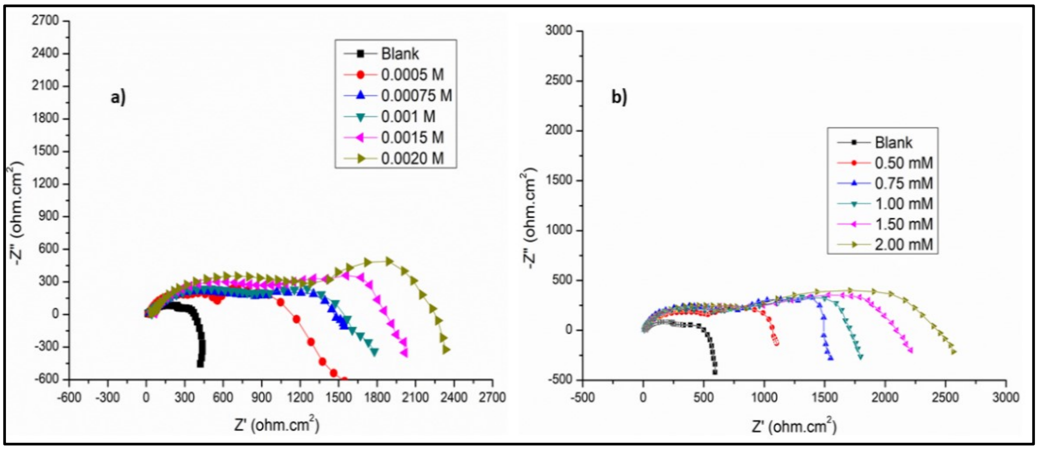

Fig. 3.36: Nyquist plots for the corrosion of AZ31 alloy in the presence of different concentrations of DH in a) 0.1 M NaCl and b) 0.1 M Na_2SO_4 at 50 °C.

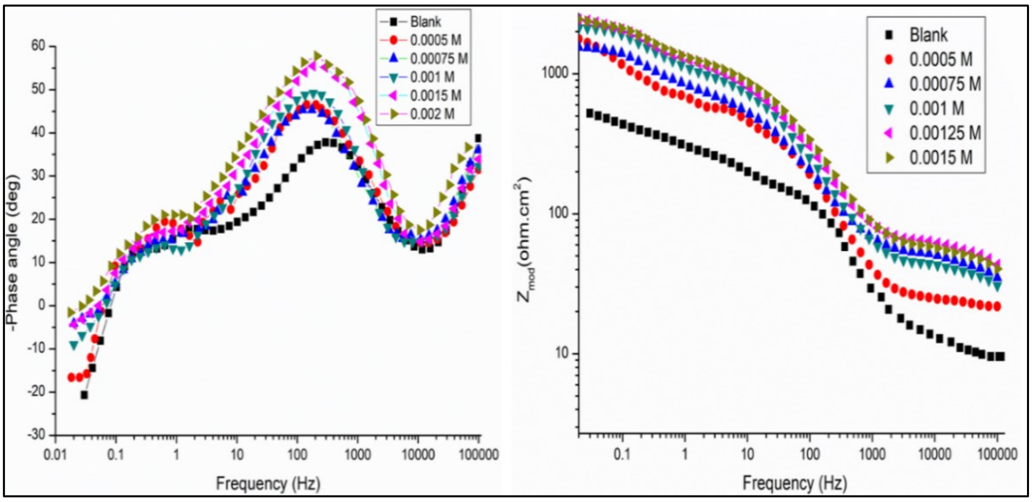

Fig. 3.37: Bode phase angle and amplitude plots for the corrosion of AZ31 alloy in 0.1 M NaCl medium containing different concentrations of DH at 50 °C.

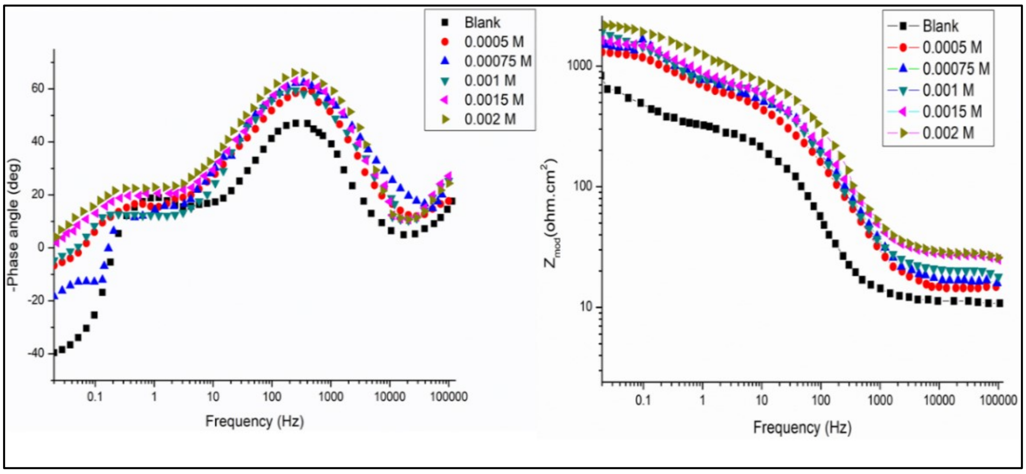

Fig. 3.38: Bode phase angle and amplitude plots for the corrosion of the AZ31 alloy in 0.1 M Na_2SO_4 medium containing different concentrations of DH at 50 °C.

3.4.3 Effect of temperature

The results in Tables 3.36 and 3.45 show that corrosion rate increases and the inhibition efficiency of DH decrease with the increase in temperature. The decrease in inhibition efficiency with the increase in temperature indicates desorption of the inhibitor molecules from the metal surface on increasing the temperature. This fact is also suggestive of physisorption of the inhibitor molecules on the metal surface.

The Arrhenius plots for the corrosion of AZ31 magnesium alloy in the presence of different concentrations of DH in 0.1 M NaCl solution and Na_2SO_4 solution are shown in Fig. 3.39. The plots of $\ln(\upsilon_{corr}/T)$ versus $1/T$ in 0.1 M NaCl solution and Na_2SO_4 solution in the presence of various concentrations of DH are shown in Fig. 3.40. The calculated values of E_a, $\Delta H^{\#}$, and $\Delta S^{\#}$ are given in Tables 3.56 and 3.57. The proportionate increase in the activation energy on the addition of DH can be attributed to the adsorption of DH providing a barrier on the alloy surface.

The values of entropy of activation indicate that the activated complex in the rate-determining step represents an association rather than dissociation, resulting in a decrease in randomness on going from the reactants to the activated complex.

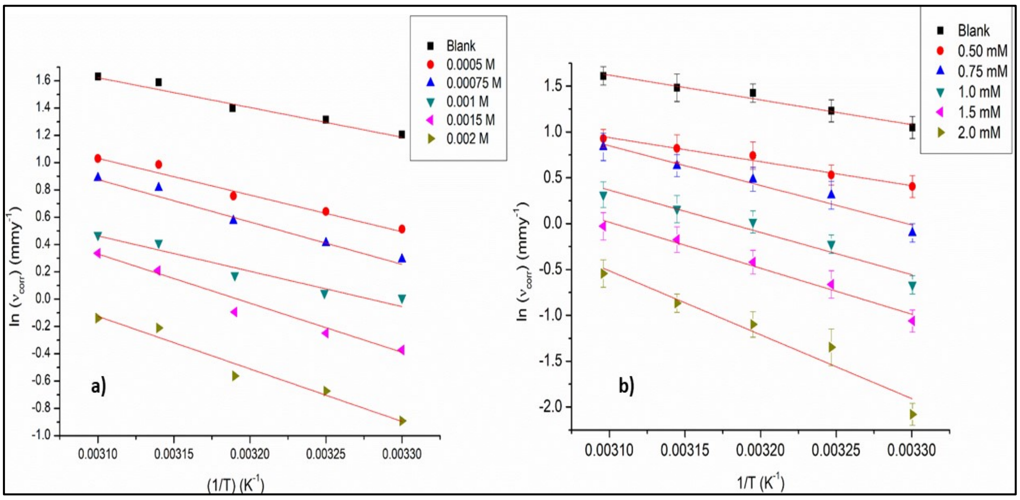

Fig. 3.39: Arrhenius plots for the corrosion of AZ31 magnesium alloy in a) 0.1 M NaCl and b) 0.1 M Na_2SO_4 in the presence of different concentrations of DH.

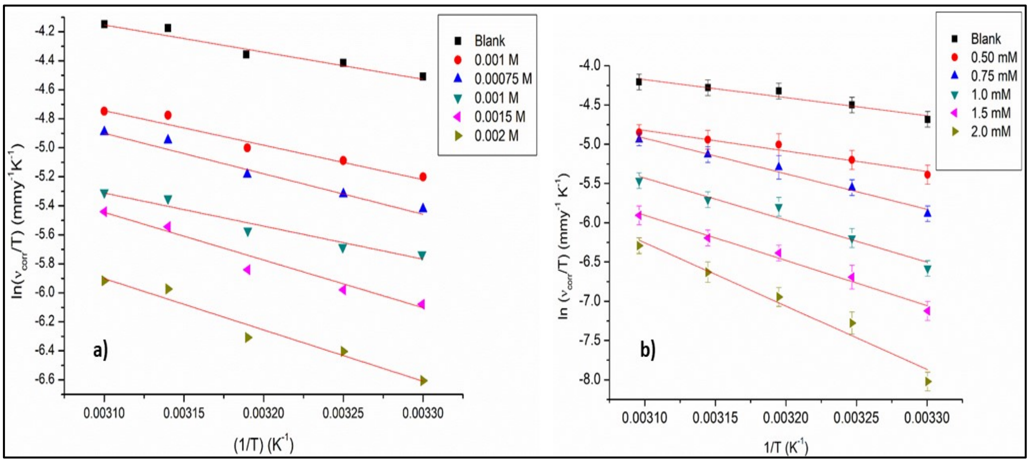

Fig. 3.40: The plots of ln(υ_{corr} /T) versus 1/T for the corrosion of AZ31 magnesium alloy in a) 0.1 M NaCl and b) 0.1 M Na_2SO_4 in the presence of different concentrations of DH.

3.4.4 Adsorption isotherms

The adsorption of DH on the surface of AZ31 magnesium alloy was found to obey Langmuir adsorption isotherm. The Langmuir adsorption isotherms for the adsorption of DH on AZ31 magnesium alloy in 0.1 M NaCl solution and Na_2SO_4 solution are shown in Fig. 3.41.

The thermodynamic data obtained for the adsorption of DH on AZ31 magnesium alloy are tabulated in Tables 3.58 and 3.59. The linear regression coefficients are close to unity and the slopes of the straight lines are nearly unity, suggesting that the adsorption of DH obeys Langmuir's adsorption isotherm with negligible interaction between the adsorbed molecules. The free energy values suggest that the DH undergoes both physisorption and chemisorption. η (%) reduces with the increase in temperature, which is characteristic of physisorbed inhibitors. Both these results hint at the predominance of physisorption over chemisorption.

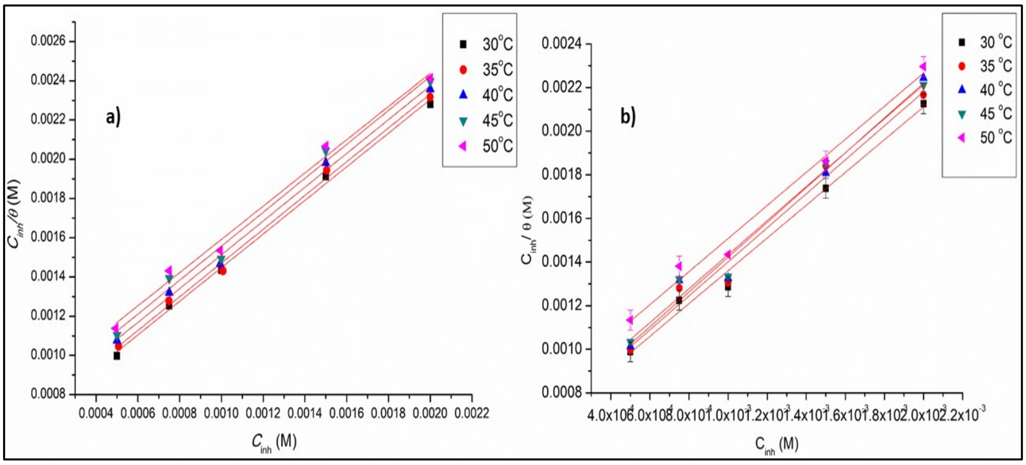

Fig. 3.41: Langmuir's adsorption isotherms for the adsorption of DH on AZ31 magnesium alloy in a) 0.1 M NaCl medium and b) 0.1 M Na_2SO_4 medium.

3.4.5 Mechanism of corrosion inhibition

The corrosion inhibition mechanism of DH in sodium sulfate solution can be explained in the same lines as that of DB in the previous section. The inhibitor DH protects the alloy surface through the predominant physisorption mode in which the DH gets adsorbed on the alloy surface through electrostatic attraction.

3.4.6 SEM

Fig. 3.42 presents the SEM image and EDX spectrum of the AZ31 magnesium alloy surface after the immersion in 0.2 M NaCl in the presence of DH for 3 h at 30 °C. Figure 3.43 presents the SEM image and EDX spectrum of AZ31 magnesium alloy surface after the immersion in 0.2 M Na_2SO_4 in the presence of DH for 3 h at 30 °C. It is noted that the deterioration of the alloy substrate is suppressed in the presence of DH in the NaCl and Na_2SO_4 media as compared with the SEM image of alloy samples immersed in the corrosion media in the absence of the inhibitor presented in Fig. 3.10 and Fig. 3.12. The SEM image in Fig. 3.42 and Fig. 3.43 show a more compact surface and contain fewer cracks in it. The elements present on the surface of the alloy were ascertained by using the EDX spectra of the alloy sample.

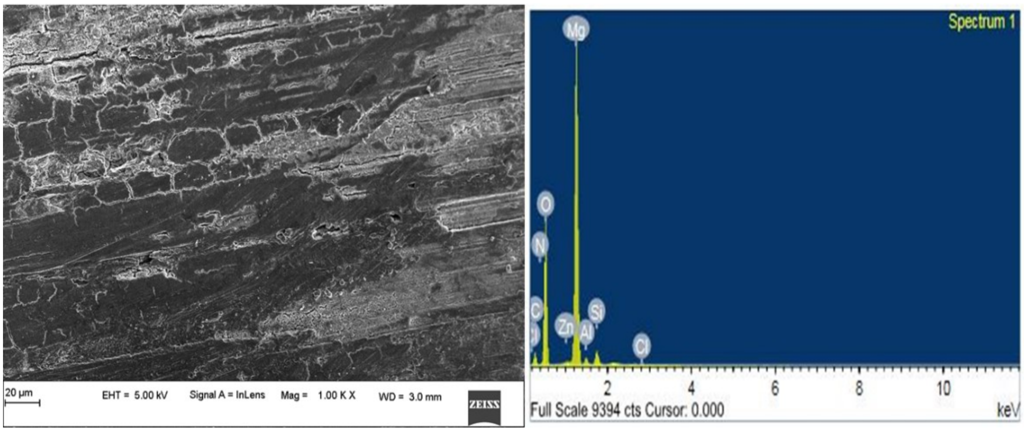

Fig. 3.42: SEM image and EDX spectra of the AZ31 magnesium alloy surface after the immersion in 0.2 M NaCl in the presence of DH for 3 h at 30 °C.

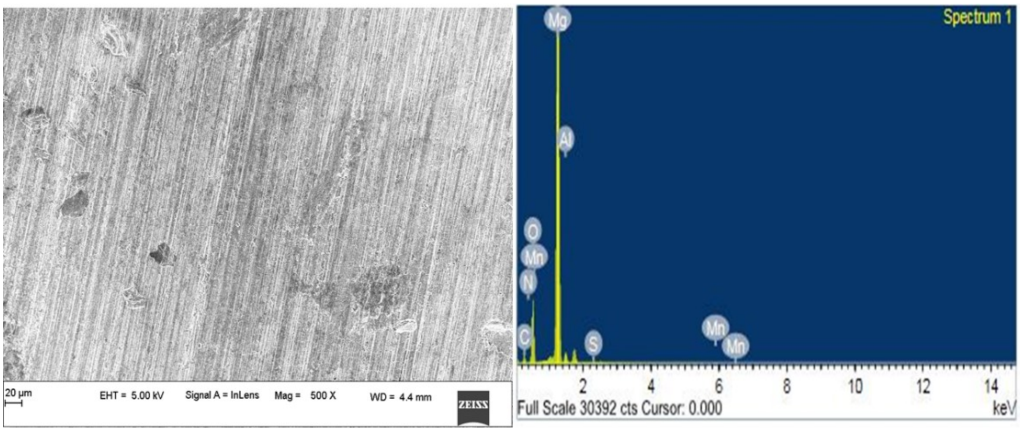

Fig. 3.43: SEM image and EDX spectra of the AZ31 magnesium alloy surface after the immersion in 0.2 M Na_2SO_4 in the presence of DH for 3 h at 30 °C.

3.4.7 XPS

Fig. 3.44 and Fig. 3.45 present the XPS survey spectra of the corroded AZ31 magnesium alloy in the corrosion medium of 0.2 M NaCl and 0.2 M Na_2SO_4 containing 0.001 M DH inhibitor. Fig. 3.46 and Fig. 3.47 show the corresponding individual XPS spectra of Mg (2s), Al (2p), C (1s), O (1s) and, N (1s) in NaCl and Na_2SO_4. The Mg (2s) peak was deconvoluted to three peaks corresponding to $Mg(OH)_2$, $MgCO_3$, and MgO at 88 eV, 88.9 eV, and 89.4 eV, respectively. The C (1s) peak was deconvoluted into three peaks at 284 eV, 286 eV, and 288 eV corresponding to C-C/ C-H bonds, C-N bonds, and COO^- group, respectively (Gece 2008). The O (1s) peak was deconvoluted into two peaks at 532 eV and 534 eV, corresponding to O of C=O, MgO, and $Mg(OH)_2$, respectively (Gao and Liang 2007). The N (1s) peak shows only one peak corresponding to the presence of N as $N\text{-}CH_2$ at ~399 eV. The Al (2p) peak indicates the presence of Al as $MgAl_2O_4$. The above facts indicate the surfactant molecules to be present on the alloy surface and support the proposal that the alloy surface is protected from corrosion through the formation of a protective film by the DH molecules.

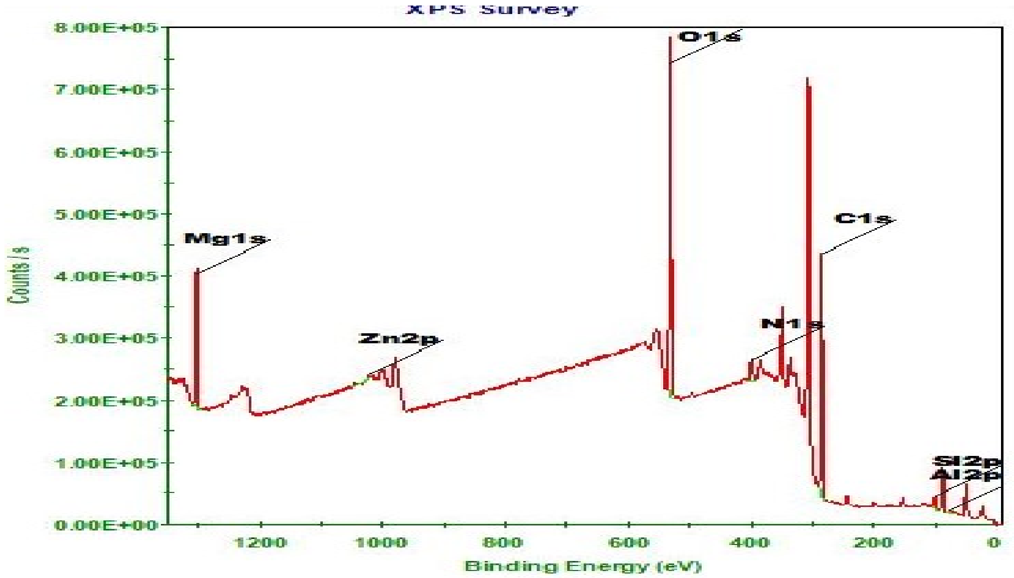

Fig. 3.44: The XPS survey spectra of the corroded AZ31 magnesium alloy immersed in the corrosion medium of 0.2 M NaCl containing 0.001 M of DH for 3 h at 30 °C.

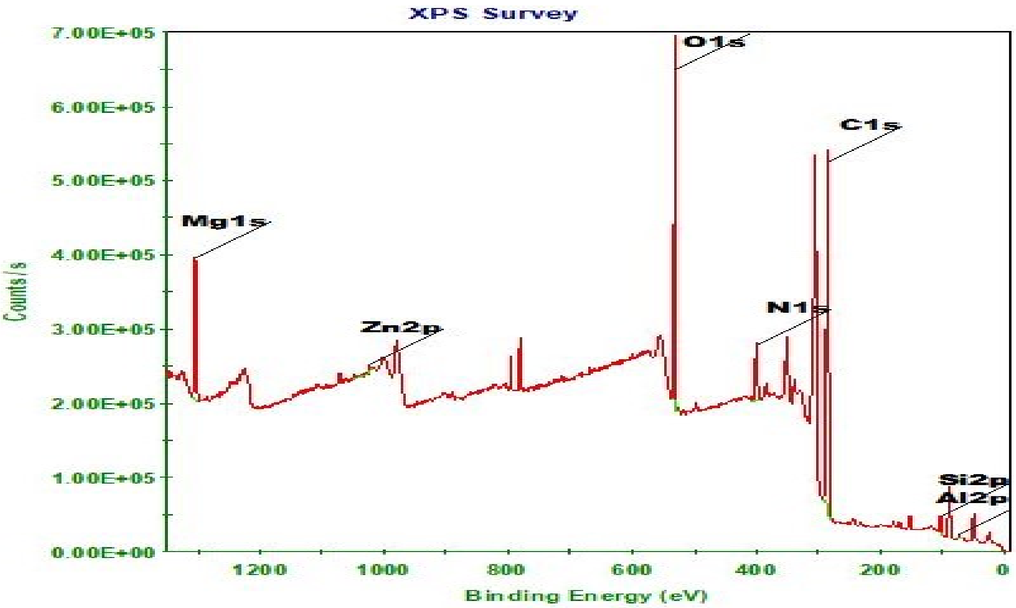

Fig. 3.45: The XPS survey spectra of the corroded AZ31 magnesium alloy immersed in the corrosion medium of 0.2 M Na_2SO_4 containing 0.001 M of DH for 3 h at 30 °C.

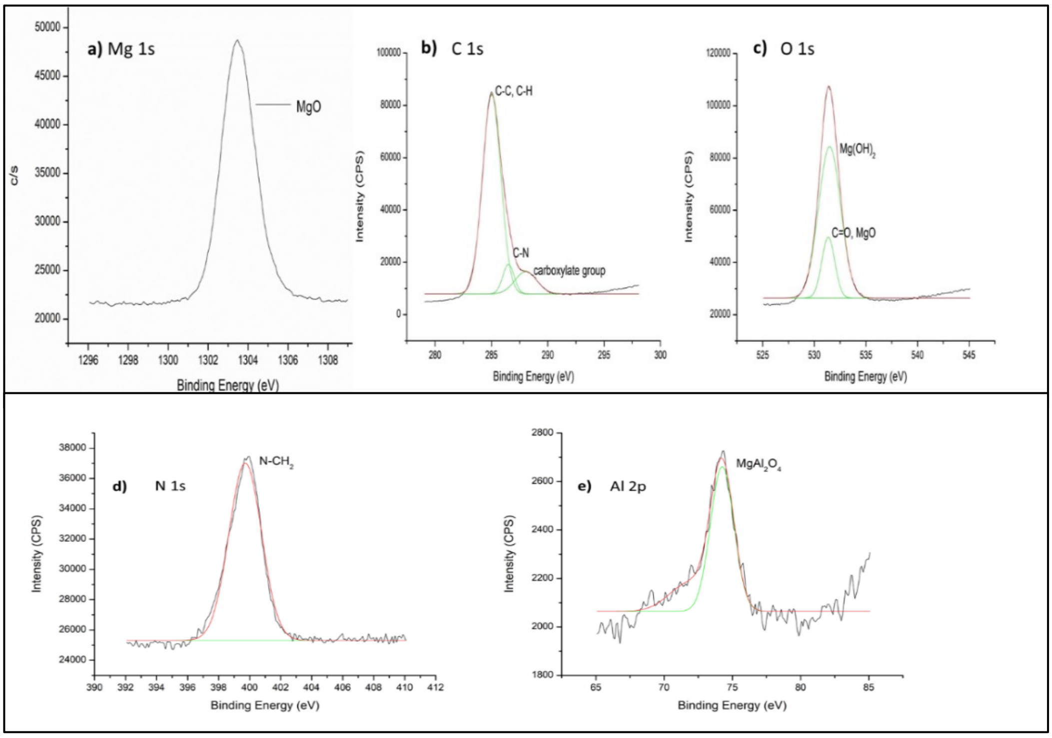

Fig. 3.46: XPS spectra (Mg 1s, Al 2p, C 1s, O 1s and, N 1s) of AZ31 Mg alloy immersed in 0.2 M NaCl medium in the presence of 0.001 M DH for 3 h at 30 °C.

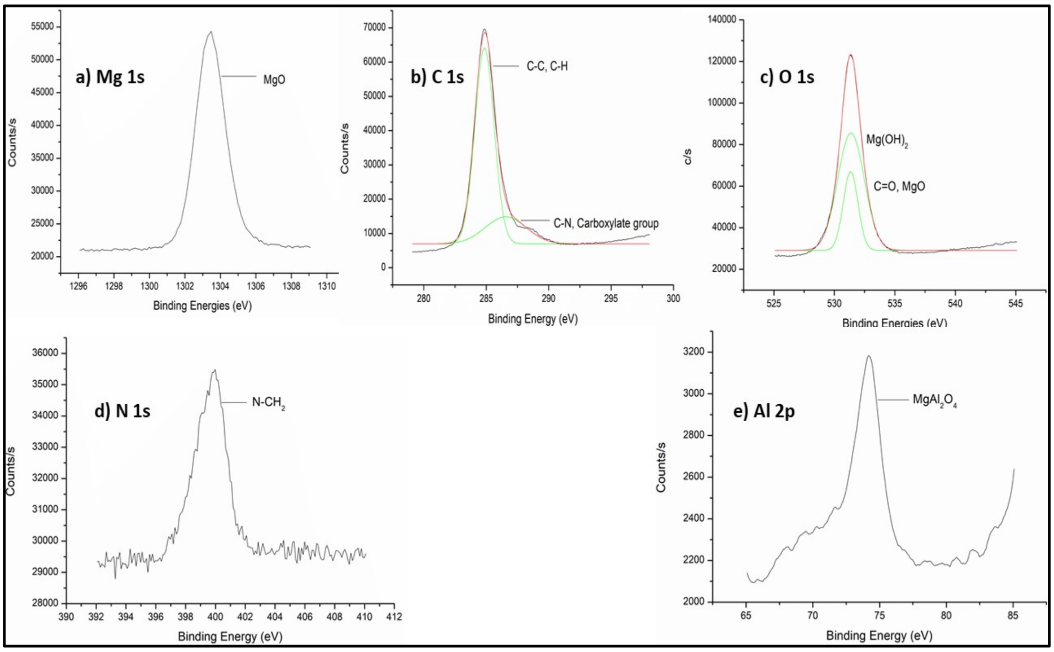

Fig. 3.47: XPS spectra (Mg 1s, Al 2p, C 1s, O 1s and, N 1s) of AZ31 Mg alloy immersed in 0.2 M Na_2SO_4 medium in the presence of 0.001 M DH for 3 hours at 30 °C.

3.4.8 DFT

The optimized structure for the inhibitor, DH, was obtained using DFT calculations at the B3LYP hybrid functional model with def-TZVP basis set and presented in Figure 3.48. The energy of the highest occupied molecular orbital (E_{HOMO}), the energy of the lowest unoccupied molecular orbital (E_{LUMO}), energy gap (ΔE), hardness (η), softness (σ), ionization potential (Ip), electron affinity (EA), electronegativity (χ), and dipole moment (μ) associated with the corrosion-inhibiting ability of DH have been evaluated using DFT. The above-mentioned parameters are presented in Table 3.60.

The structure of the molecule was optimized and a negative value of the total energy (-2.32 keV) indicates a thermodynamically stable molecule. E_{HOMO} value of -1.01 eV for the inhibitor DH, indicates the physical adsorption. The donation of electrons results in chemical adsorption, the negative value of E_{HOMO} indicates physisorption rather than chemisorption (Vengatesh and Sundaravadivelu 2019). The low bandgap energy suggests a higher reactivity of the inhibitor molecules, leading to their ready adsorption on the AZ31 alloy surface. The dipole moment value is the measure of the extent of interaction between charged DH molecules and the charged metal surface. The high value of the dipole moment implies a stronger interaction between DH molecules and the AZ31 alloy surface.

The resistance of the inhibitor to charge transfer and its readiness to receive electrons is indicated by its chemical hardness and softness respectively. The strong tendency of diacetate group to attract electrons from metal shows a higher electronegativity value, which in turn indicates the higher ability of DH to act as a corrosion inhibitor.

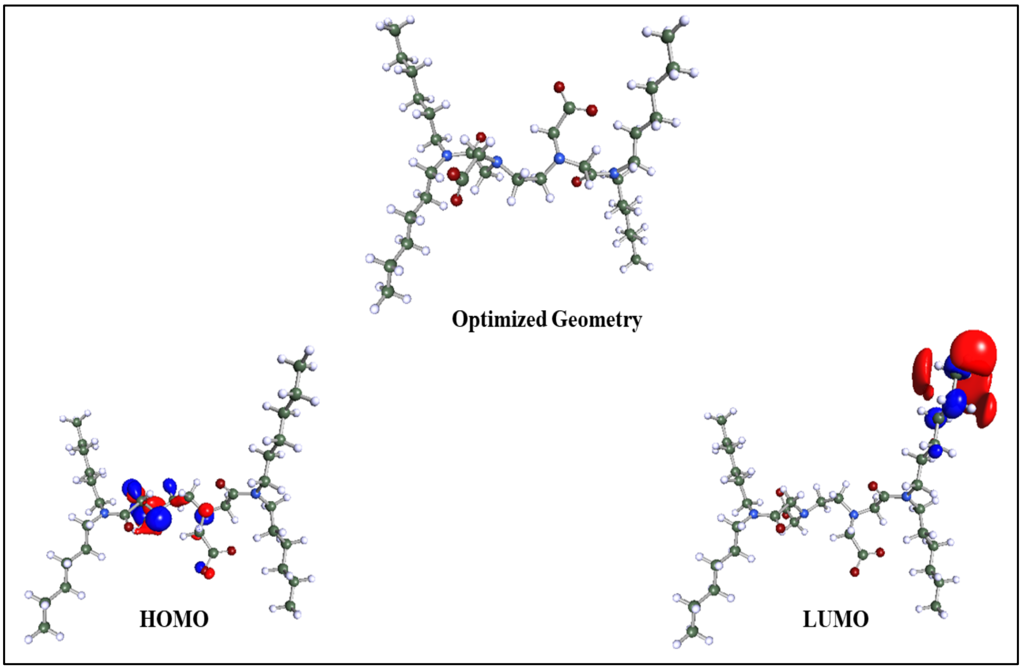

Fig. 3.48: Optimized structure and the frontier molecular orbital density distribution of the DH molecule.

3.4.9 Summary

Anionic Gemini surfactant based on EDTA derivatives, DH, was synthesized and used as corrosion inhibitor on AZ31 Mg alloy in different concentrations of NaCl solution and Na_2SO_4 solution. The surfactant DH acted as a mixed type of inhibitor and the inhibitor efficiency increased with the increase in the concentration of DH and decreased with the rise in temperature and the increase in the concentration of NaCl and Na_2SO_4 in the medium. The surfactant was adsorbed predominantly through physisorption and obeyed Langmuir adsorption isotherm. The quantum chemical calculations supported the experimental observations.

Table 3.36: Electrochemical polarization parameters for the corrosion of AZ31 alloy in 0.05 M NaCl solution in the presence of DH at different temperatures.

Inhibitor concentration (mmol dm^{-3})	Temperature (°C)	E_{corr} vs SCE (mV)	i_{corr} (µA cm^{-2})	$-\beta_c$ (mV dec^{-1})	v_{corr} (mm y^{-1})	η (%)
Blank	30	-1514	70.10	99	1.51	-
0.50		-1544	11.14	107	0.24	84
0.75		-1533	8.35	97	0.18	88
1.00		-1498	6.49	110	0.14	90
1.50		-1494	4.17	92	0.09	94
2.00		-1497	2.78	94	0.06	96
Blank	35	-1490	112.81	122	2.43	-
0.50		-1531	25.53	113	0.55	77
0.75		-1561	19.96	114	0.43	82
1.00		-1538	16.71	112	0.36	85
1.50		-1524	12.53	112	0.27	88
2.00		-1478	7.89	114	0.17	93
Blank	40	-1500	168.06	129	3.62	-
0.50		-1536	40.85	118	0.88	75
0.75		-1564	33.42	116	0.72	80
1.00		-1566	28.78	113	0.62	82
1.50		-1514	30.10	118	0.65	82
2.00		-1479	19.49	110	0.42	88
Blank	45	-1503	183.38	134	3.95	-
0.50		-1545	47.35	119	1.02	74
0.75		-1557	36.67	104	0.79	80
1.00		-1513	33.10	109	0.72	81
1.50		-1529	34.35	106	0.74	81
2.00		-1542	26.92	113	0.58	85
Blank	50	-1493	197.77	140	4.26	-
0.50		-1553	72.42	119	1.56	63
0.75		-1561	62.67	128	1.35	68
1.00		-1538	50.14	117	1.08	74
1.50		-1526	33.42	123	0.72	78
2.00		-1500	23.21	126	0.64	84

Table 3.37: Electrochemical polarization parameters for the corrosion of AZ31 in 0.10 M NaCl solution in the presence of DH at different temperatures.

Inhibitor concentration (mmol dm^{-3})	Temperature (°C)	E_{corr} vs SCE (mV)	i_{corr} (μA cm^{-2})	$-\beta_c$ (mV dec^{-1})	v_{corr} (mm y^{-1})	η (%)
Blank	30	-1483	154.03	135	3.34	-
0.50		-1529	77.53	132	1.67	50
0.75		-1470	62.21	129	1.34	59
1.00		-1460	46.89	125	1.01	69
1.50		-1428	33.42	121	0.72	78
2.00		-1442	40.39	120	0.41	87
Blank	35	-1489	171.58	141	3.73	-
0.50		-1528	88.21	137	1.90	49
0.75		-1486	70.10	134	1.51	59
1.00		-1482	46.89	129	1.01	72
1.50		-1448	36.21	127	0.78	79
2.00		-1484	23.67	127	0.51	86
Blank	40	-1502	210.77	165	4.54	-
0.50		-1498	93.31	153	2.01	46
0.75		-1515	84.49	150	1.62	56
1.00		-1495	55.24	146	1.19	70
1.50		-1518	42.24	142	0.91	75
2.00		-1495	39.36	140	0.57	84
Blank	45	-1516	225.52	162	4.90	-
0.50		-1543	124.42	159	2.68	45
0.75		-1513	104.92	155	2.26	53
1.00		-1510	70.10	152	1.51	69
1.50		-1488	60.35	150	1.30	73
2.00		-1495	37.60	147	0.81	83
Blank	50	-1490	235.47	173	5.11	-
0.50		-1531	129.99	170	2.80	45
0.75		-1488	112.81	168	2.43	52
1.00		-1487	74.28	164	1.60	68
1.50		-1492	64.99	160	1.40	72
2.00		-1497	40.39	158	0.87	82

Table 3.38: Electrochemical polarization parameters for the corrosion of AZ31 alloy in 0.15 M NaCl solution in the presence of DH at different temperatures.

Inhibitor concentration (mmol dm^{-3})	Temperature (°C)	E_{corr} vs SCE (mV)	i_{corr} (μA cm^{-2})	$-\beta_c$ (mV dec^{-1})	v_{corr} (mm y^{-1})	η (%)
Blank	30	-1537	233.52	150	5.03	-
0.50		-1480	119.78	116	2.58	48
0.75		-1560	98.42	120	2.12	58
1.00		-1563	76.60	107	1.65	67
1.50		-1494	53.39	112	1.15	77
2.00		-1569	31.57	130	0.68	86
Blank	35	-1500	333.34	155	7.18	-
0.50		-1490	177.81	124	3.83	46
0.75		-1473	140.20	132	3.02	57
1.00		-1445	98.42	125	2.12	70
1.50		-1524	77.99	122	1.68	76
2.00		-1538	83.56	138	1.08	84
Blank	40	-1515	455.90	168	9.82	-
0.50		-1487	255.34	107	5.50	44
0.75		-1520	204.27	119	4.40	55
1.00		-1554	143.92	123	3.10	68
1.50		-1514	116.53	128	2.51	74
2.00		-1545	75.21	140	1.62	83
Blank	45	-1491	478.65	170	10.31	-
0.50		-1488	267.41	135	5.76	43
0.75		-1527	220.99	108	4.76	53
1.00		-1529	157.85	129	3.40	67
1.50		-1529	129.99	120	2.80	72
2.00		-1475	90.53	146	1.95	81
Blank	50	-1475	567.33	194	12.22	-
0.50		-1496	331.95	115	7.15	41
0.75		-1548	279.48	159	6.02	50
1.00		-1546	189.42	122	4.08	66
1.50		-1526	162.49	123	3.50	71
2.00		-1508	125.35	141	2.70	78

Table 3.39: Electrochemical polarization parameters for the corrosion of AZ31 alloy in 0.20 M NaCl solution in the presence of DH at different temperatures.

Inhibitor concentration (mmol dm^{-3})	Temperature (°C)	E_{corr} vs SCE (mV)	i_{corr} (µA cm^{-2})	$-\beta_c$ (mV dec^{-1})	v_{corr} (mm y^{-1})	η (%)
Blank	30	-1500	432.55	189	9.40	-
0.50		-1476	248.38	182	5.35	43
0.75		-1555	113.28	158	2.44	74
1.00		-1542	99.81	122	2.15	77
1.50		-1456	87.28	122	1.88	80
2.00		-1476	48.28	110	1.04	89
Blank	35	-1485	457.04	214	9.93	-
0.50		-1499	266.95	154	5.75	42
0.75		-1529	129.99	116	2.80	72
1.00		-1538	110.03	126	2.37	76
1.50		-1464	95.17	111	2.05	79
2.00		-1484	60.35	107	1.30	87
Blank	40	-1483	489.13	181	10.63	-
0.50		-1479	290.16	160	6.25	41
0.75		-1532	140.20	146	3.02	71
1.00		-1550	113.28	124	2.44	77
1.50		-1530	97.49	123	2.10	80
2.00		-1495	78.92	112	1.70	84
Blank	45	-1511	687.77	211	14.75	-
0.50		-1496	408.55	171	8.80	40
0.75		-1548	204.27	147	4.40	70
1.00		-1547	175.95	126	3.79	74
1.50		-1539	162.49	103	3.50	76
2.00		-1479	121.17	101	2.61	82
Blank	50	-1526	709.98	171	15.43	-
0.50		-1482	441.05	151	9.50	38
0.75		-1535	236.77	132	5.10	67
1.00		-1551	198.24	122	4.27	72
1.50		-1518	178.74	114	3.85	75
2.00		-1515	141.60	102	3.05	80

Table 3.40: Electrochemical polarization parameters for the corrosion of AZ31 alloy in 0.25 M NaCl solution in the presence of DH at different temperatures.

Inhibitor concentration (mmol dm^{-3})	Temperature (°C)	E_{corr} vs SCE (mV)	i_{corr} (μA cm^{-2})	$-\beta_c$ (mV dec^{-1})	υ_{corr} (mm y^{-1})	η (%)
Blank	30	-1526	520.41	190	11.31	-
0.50		-1489	304.09	125	6.55	42
0.75		-1516	146.24	140	3.15	72
1.00		-1551	131.85	120	2.84	75
1.50		-1499	118.38	171	2.55	77
2.00		-1541	73.35	145	1.58	86
Blank	35	-1515	553.00	192	12.03	-
0.50		-1504	334.27	168	7.20	40
0.75		-1517	167.13	165	3.60	70
1.00		-1528	138.81	108	2.99	75
1.50		-1522	120.70	156	2.60	78
2.00		-1526	83.56	173	1.80	85
Blank	40	-1488	577.18	188	12.54	-
0.50		-1498	348.19	122	7.50	40
0.75		-1514	185.70	125	4.00	68
1.00		-1528	149.95	121	3.23	74
1.50		-1539	127.67	160	2.75	78
2.00		-1523	92.85	162	2.00	84
Blank	45	-1510	706.61	209	15.22	-
0.50		-1519	432.69	174	9.32	38
0.75		-1528	239.09	150	5.15	66
1.00		-1515	192.20	121	4.14	72
1.50		-1527	176.42	171	3.80	75
2.00		-1523	126.74	137	2.73	82
Blank	50	-1494	792.81	186	17.23	-
0.50		-1518	500.47	169	10.78	37
0.75		-1479	287.84	164	6.20	64
1.00		-1561	236.77	178	5.10	70
1.50		-1481	216.81	165	4.67	73
2.00		-1518	168.06	150	3.62	79

Table 3.41: Electrochemical polarization parameters for the corrosion of AZ31 alloy in 0.05 M Na_2SO_4 solution in the presence of DH at different temperatures.

Inhibitor concentration (mmol dm^{-3})	Temperature (°C)	E_{corr} vs SCE (mV)	i_{corr} (μA cm^{-2})	$-\beta_c$ (mV dec^{-1})	v_{corr} (mm y^{-1})	η (%)
Blank	30	-1483	63.33	93	1.37	-
0.50		-1468	15.40	91	0.33	75
0.75		-1503	10.60	87	0.23	83
1.00		-1471	9.13	81	0.19	86
1.50		-1469	3.84	77	0.08	94
2.00		-1507	1.82	75	0.03	97
Blank	35	-1470	110.24	110	2.39	-
0.50		-1456	28.60	99	0.61	74
0.75		-1472	19.16	93	0.41	82
1.00		-1498	16.24	93	0.34	85
1.50		-1492	10.22	88	0.22	90
2.00		-1475	5.2	80	0.11	95
Blank	40	-1502	164.74	125	3.58	-
0.50		-1542	58.00	116	1.27	64
0.75		-1475	44.70	104	0.97	72
1.00		-1447	37.1	92	0.80	77
1.50		-1512	20.0	97	0.43	87
2.00		-1479	9.20	95	0.19	94
Blank	45	-1465	179.03	154	3.89	-
0.50		-1471	72.50	130	1.58	59
0.75		-1522	50.18	131	1.08	72
1.00		-1537	39.37	131	0.84	78
1.50		-1500	25.97	124	0.55	85
2.00		-1523	15.50	118	0.33	91
Blank	50	-1481	190.03	144	4.13	-
0.50		-1527	103.06	126	2.22	46
0.75		-1476	66.66	116	1.45	64
1.00		-1463	40.74	103	0.88	78
1.50		-1536	35.33	104	0.77	81
2.00		-1482	20.2	92	0.43	89

Table 3.42: Electrochemical polarization parameters for the corrosion of AZ31 alloy in 0.10 M Na_2SO_4 solution in the presence of DH at different temperatures.

Inhibitor concentration (mmol dm^{-3})	Temperature (°C)	E_{corr} vs SCE (mV)	i_{corr} (μA cm^{-2})	-β_c (mV dec^{-1})	v_{corr} (mm y^{-1})	η (%)
Blank	30	-1482.0	71.21	117	1.54	-
0.50		-1491.3	35.30	116	0.76	50
0.75		-1496.3	32.10	119	0.69	56
1.00		-1490.5	19.40	102	0.42	72
1.50		-1493.1	10.00	106	0.21	86
2.00		-1579.7	4.30	102	0.09	94
Blank	35	-1528	157.60	134	3.42	-
0.50		-1464.8	79.30	126	1.70	50
0.75		-1471.9	64.90	132	1.39	59
1.00		-1466.8	37.48	135	0.80	76
1.50		-1509.6	29.38	123	0.63	81
2.00		-1509.5	12.40	123	0.26	92
Blank	40	-1485.0	191.24	140	4.15	-
0.50		-1484.8	97.80	115	2.10	49
0.75		-1466.3	88.70	104	1.92	53
1.00		-1518.2	47.60	117	1.02	75
1.50		-1456.7	40.60	117	0.87	79
2.00		-1492.4	21.11	113	0.45	89
Blank	45	-1481	202.71	150	4.40	-
0.50		-1466.5	105.0	117	2.27	48
0.75		-1513.8	87.5	116	1.88	57
1.00		-1508.7	49.4	129	1.06	75
1.50		-1459.3	39.9	117	0.84	80
2.00		-1477.5	19.80	112	0.42	90
Blank	50	-1456	208.41	157	4.53	-
0.50		-1460.6	116.2	122	2.53	44
0.75		-1483.2	106.3	122	2.31	49
1.00		-1516.4	62.80	124	1.37	69
1.50		-1446.5	40.6	118	0.88	80
2.00		-1518.3	26.99	104	0.58	87

Table 3.43: Electrochemical polarization parameters for the corrosion of AZ31 alloy in 0.15 M Na_2SO_4 solution in the presence of DH at different temperatures.

Inhibitor concentration (mmol dm^{-3})	Temperature (°C)	E_{corr} vs SCE (mV)	i_{corr} (µA cm^{-2})	$-\beta_c$ (mV dec^{-1})	v_{corr} (mm y^{-1})	η (%)
Blank	30	-1457	218.14	138	4.74	-
0.50		-1505	116.06	117	2.50	47
0.75		-1508	105.85	105	2.28	52
1.00		-1536	71.49	98	1.54	68
1.50		-1495	41.78	91	0.90	81
2.00		-1469	17.64	82	0.38	92
Blank	35	-1457	322.28	142	7.00	-
0.50		-1510	162.49	116	3.50	50
0.75		-1527	140.20	111	3.02	57
1.00		-1529	91.46	103	1.97	72
1.50		-1479	65.46	94	1.41	80
2.00		-1463	32.49	81	0.70	90
Blank	40	-1469	445.19	151	9.67	-
0.50		-1516	236.77	114	5.10	47
0.75		-1512	219.59	105	4.73	51
1.00		-1521	113.74	91	2.45	74
1.50		-1476	99.81	96	2.15	77
2.00		-1465	56.17	98	1.21	87
Blank	45	-1446	461.63	158	10.03	-
0.50		-1486	253.95	120	5.47	45
0.75		-1514	233.06	114	5.02	50
1.00		-1520	136.03	108	2.93	71
1.50		-1459	118.38	96	2.55	75
2.00		-1462	70.10	96	1.51	85
Blank	50	-1448	546.62	170	11.88	-
0.50		-1492	318.02	137	6.85	42
0.75		-1536	288.30	120	6.21	48
1.00		-1507	184.77	110	3.98	66
1.50		-1491	149.49	104	3.22	73
2.00		-1464	91.92	95	1.98	83

Table 3.44: Electrochemical polarization parameters for the corrosion of AZ31 alloy in 0.2 M Na_2SO_4 solution in the presence of DH at different temperatures.

Inhibitor concentration (mmol dm^{-3})	Temperature (°C)	E_{corr} vs SCE (mV)	i_{corr} (µA cm^{-2})	$-\beta_c$ (mV dec^{-1})	υ_{corr} (mm y^{-1})	η (%)
Blank	30	-1505	235.63	152	5.12	-
0.50		-1566	126.7	121	2.83	44
0.75		-1497	54.70	116	1.19	76
1.00		-1526	47.70	125	1.04	79
1.50		-1537	44.36	118	0.96	80
2.00		-1500	17.3	127	0.37	91
Blank	35	-1493	354.34	158	7.70	-
0.50		-1516	204.5	149	4.40	42
0.75		-1457	91.9	125	1.98	74
1.00		-1519	72.88	133	1.57	79
1.50		-1485	62.67	125	1.35	82
2.00		-1508	41.1	130	0.89	88
Blank	40	-1489	470.87	164	10.23	-
0.50		-1459	267.9	157	5.81	43
0.75		-1486	118.8	155	2.56	74
1.00		-1503	97.5	126	2.10	79
1.50		-1505	89.13	128	1.92	81
2.00		-1486	68.24	127	1.47	85
Blank	45	-1472	542.13	172	11.23	-
0.50		-1484	304.55	167	6.56	41
0.75		-1517	139.27	159	3.00	73
1.00		-1498	129.99	148	2.80	75
1.50		-1522	115.6	122	2.49	77
2.00		-1514	98.42	126	2.12	81
Blank	50	-1480	672.86	197	14.62	-
0.50		-1539	394.6	189	8.5	41
0.75		-1535	203.3	188	4.38	70
1.00		-1489	171.77	175	3.7	74
1.50		-1521	166.20	164	3.58	75
2.00		-1458	131.85	158	2.84	80

Table 3.45: Electrochemical polarization parameters for the corrosion of AZ31 in 0.25 M Na_2SO_4 solution in the presence of DH at different temperatures.

Inhibitor concentration (mmol dm^{-3})	Temperature (°C)	E_{corr} vs SCE (mV)	i_{corr} (μA cm^{-2})	$-\beta_c$ (mV dec^{-1})	v_{corr} (mm y^{-1})	η (%)
Blank	30	-1451	372.80	147	8.10	-
0.50		-1499	218.20	121	4.70	42
0.75		-1514	96.56	123	2.08	74
1.00		-1441	86.81	119	1.87	77
1.50		-1483	77.99	117	1.68	79
2.00		-1530	44.10	114	0.95	88
Blank	35	-1411	497.12	158	10.80	-
0.50		-1522	301.77	122	6.50	40
0.75		-1525	146.24	123	3.15	71
1.00		-1439	118.38	100	2.55	76
1.50		-1449	116.06	118	2.50	77
2.00		-1470	75.67	117	1.63	85
Blank	40	-1438	516.71	170	11.23	-
0.50		-1502	315.70	138	6.80	39
0.75		-1524	155.06	126	3.34	70
1.00		-1507	135.56	114	2.92	74
1.50		-1463	129.06	117	2.78	75
2.00		-1466	89.13	119	1.92	83
Blank	45	-1486	583.03	190	12.67	-
0.50		-1491	368.62	151	7.94	37
0.75		-1535	188.02	119	4.05	68
1.00		-1502	162.49	121	3.50	72
1.50		-1478	154.60	115	3.33	74
2.00		-1496	113.74	118	2.45	81
Blank	50	-1463	727.89	201	15.82	-
0.50		-1497	486.08	185	10.47	34
0.75		-1511	258.59	195	5.57	65
1.00		-1487	220.52	156	4.75	70
1.50		-1476	206.13	115	4.44	72
2.00		-1491	155.52	138	3.35	79

Table 3.46: Electrochemical impedance parameters for the corrosion of AZ31 alloy in 0.05 M NaCl solution in the presence of DH at different temperatures.

Inhibitor Concentration (mmol dm^{-3})	Temperature (°C)	R_{hf} (Ω cm^2)	R_f (Ω cm^2)	R_{dif} (Ω cm^2)	C_{dl} (μF cm^{-2})	C_f (μF cm^{-2})	η (%)
Blank	30	580	296	225	138	177	-
0.50		3589	3345	1423	123	111	84
0.75		4967	4785	1899	113	104	88
1.00		5300	5203	2210	102	98	89
1.50		6934	6788	2892	95	91	91
2.00		8842	8689	3856	91	88	93
Blank	35	550	255	207	153	181	-
0.50		2600	2476	1214	137	115	78
0.75		3120	3065	1423	124	108	82
1.00		3828	3734	1566	112	100	85
1.50		4401	4313	2100	101	96	87
2.00		6280	6189	2788	94	91	91
Blank	40	422	231	184	161	188	-
0.50		1705	1585	792	139	119	75
0.75		2009	1911	955	126	111	78
1.00		2319	2256	1108	115	103	81
1.50		2321	2281	1116	100	97	81
2.00		3412	3302	1521	92	93	87
Blank	45	340	191	150	170	192	-
0.50		1288	1109	588	140	123	73
0.75		1700	1534	782	131	117	80
1.00		1749	1603	856	123	111	80
1.50		1823	1715	879	111	105	81
2.00		2335	2189	1057	103	100	85
Blank	50	318	160	131	171	198	-
0.50		867	700	347	137	126	63
0.75		980	831	422	129	119	67
1.00		1206	1100	552	118	108	73
1.50		1388	1201	601	102	100	77
2.00		1750	1588	833	99	94	82

Table 3.47: Electrochemical impedance parameters for the corrosion of AZ31 alloy in 0.10 M NaCl solution in the presence of DH at different temperatures.

Inhibitor Concentration (mmol dm^{-3})	Temperature (°C)	R_{hf} (Ω cm^2)	R_f (Ω cm^2)	R_{dif} (Ω cm^2)	C_{dl} (µF cm^{-2})	C_f (µF cm^{-2})	η (%)
Blank	30	507	232	209	166	172	-
0.50		1009	954	484	128	114	49
0.75		1288	1168	645	114	106	60
1.00		1709	1560	787	105	98	70
1.50		2300	2202	1133	98	93	77
2.00		3706	3613	1582	94	87	86
Blank	35	380	192	168	181	179	-
0.50		760	600	288	134	117	50
0.75		941	779	335	121	110	59
1.00		1330	1269	628	110	104	71
1.50		1823	1700	935	99	99	79
2.00		2805	2731	1100	95	90	86
Blank	40	366	173	142	191	183	-
0.50		679	510	201	135	121	46
0.75		821	702	346	124	116	55
1.00		1209	1104	521	114	108	69
1.50		1500	1394	646	103	100	75
2.00		2280	2197	1088	98	93	84
Blank	45	351	152	115	195	185	-
0.50		639	520	263	137	125	45
0.75		766	681	320	127	117	54
1.00		1134	1085	489	118	104	69
1.50		1304	1200	592	105	97	73
2.00		1899	1790	781	100	94	81
Blank	50	301	139	108	200	191	-
0.50		553	478	238	140	128	45
0.75		643	591	303	136	118	53
1.00		949	813	407	129	107	68
1.50		1057	943	461	120	101	71
2.00		1690	1600	811	112	98	82

Table 3.48: Electrochemical impedance parameters for the corrosion of AZ31 alloy in 0.15 M NaCl solution in the presence of DH at different temperatures.

Inhibitor Concentration (mmol dm^{-3})	Temperature (°C)	R_{hf} (Ω cm^2)	R_f (Ω cm^2)	R_{dif} (Ω cm^2)	C_{dl} (µF cm^{-2})	C_f (µF cm^{-2})	η (%)
Blank	30	358	170	144	172	115	-
0.50		700	604	303	131	112	48
0.75		867	786	375	127	103	58
1.00		1101	1075	534	119	98	67
1.50		1553	1409	756	103	93	76
2.00		2494	2400	1211	99	86	85
Blank	35	301	161	121	184	128	-
0.50		561	400	191	140	113	46
0.75		714	602	299	132	104	57
1.00		1030	923	439	121	97	70
1.50		1282	1179	611	113	94	76
2.00		1794	1589	844	104	88	83
Blank	40	288	150	113	197	133	-
0.50		530	401	191	142	126	45
0.75		642	539	270	135	120	55
1.00		921	804	394	126	111	68
1.50		1111	992	451	114	103	74
2.00		1591	1403	753	103	97	81
Blank	45	225	128	100	201	140	-
0.50		404	342	139	145	127	44
0.75		478	389	206	136	120	52
1.00		679	588	248	124	113	66
1.50		808	709	344	115	105	72
2.00		1200	1103	519	107	100	81
Blank	50	130	88	73	218	147	-
0.50		221	207	100	142	135	41
0.75		260	177	113	137	124	50
1.00		387	260	121	126	116	66
1.50		453	350	155	115	108	71
2.00		603	502	247	105	100	78

Table 3.49: Electrochemical impedance parameters for the corrosion of AZ31 alloy in 0.2 M NaCl solution in the presence of DH at different temperatures.

Inhibitor Concentration (mmol dm^{-3})	Temperature (°C)	R_{hf} (Ω cm^2)	R_f (Ω cm^2)	R_{dif} (Ω cm^2)	C_{dl} (μF cm^{-2})	C_f (μF cm^{-2})	η (%)
Blank	30	170	109	95	193	191	-
0.50		301	200	106	147	134	43
0.75		700	596	273	132	128	74
1.00		780	649	326	125	111	77
1.50		869	701	350	118	101	80
2.00		1496	1399	737	104	96	89
Blank	35	166	97	79	190	199	-
0.50		289	169	88	152	137	42
0.75		583	500	248	134	128	72
1.00		696	580	285	125	114	76
1.50		979	877	479	119	105	779
2.00		1254	1106	631	105	99	87
Blank	40	158	90	70	212	210	-
0.50		275	150	82	154	142	41
0.75		562	434	216	137	130	71
1.00		701	600	300	126	119	77
1.50		800	704	341	116	112	80
2.00		977	885	438	109	100	84
Blank	45	125	78	58	220	219	-
0.50		208	145	76	157	143	40
0.75		438	351	178	139	133	70
1.00		500	410	222	122	122	74
1.50		549	478	245	114	113	76
2.00		701	628	315	111	102	82
Blank	50	103	73	52	243	232	-
0.50		169	98	72	155	146	38
0.75		315	287	136	140	135	67
1.00		382	242	125	129	123	72
1.50		423	310	151	115	115	75
2.00		513	401	212	110	105	80

Table 3.50: Electrochemical impedance parameters for the corrosion of AZ31 in 0.25 M NaCl solution in the presence of DH at different temperatures.

Inhibitor Concentration (mmol dm^{-3})	Temperature (°C)	R_{hf} (Ω cm^2)	R_f (Ω cm^2)	R_{dif} (Ω cm^2)	C_{dl} (µF cm^{-2})	C_f (µF cm^{-2})	η (%)
Blank	30	201	201	99	205	195	-
0.50		649	503	267	153	140	42
0.75		774	666	331	146	126	71
1.00		809	730	361	132	119	75
1.50		895	798	395	126	104	77
2.00		1019	995	501	111	95	85
Blank	35	150	150	85	217	205	-
0.50		642	549	287	148	143	40
0.75		768	658	314	143	128	70
1.00		800	711	325	135	121	75
1.50		875	757	364	127	107	78
2.00		1001	900	450	113	97	85
Blank	40	141	141	72	221	222	-
0.50		637	505	240	150	145	41
0.75		761	650	328	144	131	69
1.00		788	691	346	137	125	75
1.50		864	746	362	124	111	79
2.00		991	886	441	115	103	85
Blank	45	105	105	68	230	223	-
0.50		629	563	254	147	147	38
0.75		757	623	311	145	134	65
1.00		779	680	341	135	127	72
1.50		857	699	354	127	113	75
2.00		982	800	400	116	105	82
Blank	50	99	99	55	248	239	-
0.50		621	501	246	153	150	40
0.75		748	625	301	145	137	64
1.00		768	684	341	138	130	70
1.50		845	700	348	128	121	72
2.00		977	793	366	118	108	78

Table 3.51: Electrochemical impedance parameters for the corrosion of AZ31 alloy in 0.05 M Na_2SO_4 solution in the presence of DH at different temperatures.

Inhibitor Concentration (mmol dm^{-3})	Temperature (°C)	R_{hf} (Ω cm^2)	R_f (Ω cm^2)	R_{dif} (Ω cm^2)	C_{dl} (µF cm^{-2})	C_f (µF cm^{-2})	η (%)
Blank	30	609	471	412	159	102	-
0.50		2420	2377	1190	44	68	74
0.75		3500	3403	1566	32	62	82
1.00		4388	4276	2123	28	55	86
1.50		7592	7460	3111	22	44	92
2.00		9988	9801	4161	15	31	94
Blank	35	510	367	303	176	129	-
0.50		1950	1756	876	40	81	74
0.75		2790	2640	1216	36	70	81
1.00		3340	3259	1615	24	58	84
1.50		4967	4756	1965	20	47	89
2.00		7699	7500	3101	12	40	93
Blank	40	477	333	288	201	146	-
0.50		1330	1201	610	36	74	64
0.75		1690	1500	735	36	68	72
1.00		2113	2001	967	32	56	77
1.50		3558	3408	1511	27	55	87
2.00		4912	4790	2021	14	47	90
Blank	45	450	350	275	225	151	-
0.50		1108	981	463	41	72	59
0.75		1628	1501	733	40	66	72
1.00		2108	1988	965	33	66	79
1.50		2966	2804	1107	32	64	85
2.00		4199	4002	2034	26	44	89
Blank	50	412	354	252	261	168	-
0.50		763	600	287	50	62	46
0.75		1189	1003	500	39	61	65
1.00		1900	1782	647	38	47	78
1.50		2201	2075	1032	25	44	81
2.00		3541	3402	1523	24	43	88

Table 3.52: Electrochemical impedance parameters for the corrosion of AZ31 alloy in 0.10 M Na_2SO_4 solution in the presence of DH at different temperatures.

Inhibitor Concentration (mmol dm^{-3})	Temperature (°C)	R_{hf} (Ω cm^2)	R_f (Ω cm^2)	R_{dif} (Ω cm^2)	C_{dl} (μF cm^{-2})	C_f (μF cm^{-2})	η (%)
Blank	30	460	343	319	201	188	-
0.50		930	800	400	30	77	50
0.75		1047	901	453	30	76	56
1.00		1595	1477	844	22	71	71
1.50		3341	3201	1522	20	70	86
2.00		5730	5611	2511	15	53	92
Blank	35	432	322	293	224	191	-
0.50		876	703	353	54	79	50
0.75		1104	945	444	44	75	61
1.00		1791	1688	848	38	74	75
1.50		2282	2197	1213	29	74	81
2.00		4450	4385	2101	22	59	90
Blank	40	403	254	227	249	225	-
0.50		795	680	319	57	85	49
0.75		865	790	371	46	77	53
1.00		1590	1500	844	38	75	74
1.50		1904	1813	988	29	74	79
2.00		3477	3343	1522	23	65	88
Blank	45	387	193	160	269	237	-
0.50		760	621	316	58	90	49
0.75		895	783	370	40	83	45
1.00		1545	1430	746	39	80	75
1.50		1934	1711	911	27	73	80
2.00		3190	3056	1419	25	70	88
Blank	50	373	209	161	278	241	-
0.50		680	534	256	60	100	45
0.75		723	627	310	52	83	48
1.00		1224	1104	654	44	81	69
1.50		1852	1531	838	28	76	80
2.00		2550	1850	893	27	80	86

Table 3.53: Electrochemical impedance parameters for the corrosion of AZ31 alloy in 0.15 M Na_2SO_4 solution in the presence of DH at different temperatures.

Inhibitor Concentration (mmol dm^{-3})	Temperature (°C)	R_{hf} (Ω cm^2)	R_f (Ω cm^2)	R_{dif} (Ω cm^2)	C_{dl} (μF cm^{-2})	C_f (μF cm^{-2})	η (%)
Blank	30	434	420	383	244	167	-
0.50		813	702	410	80	99	46
0.75		900	811	422	78	84	52
1.00		1343	1286	678	75	66	68
1.50		2283	2198	1000	71	60	80
2.00		3965	3901	1855	67	55	89
Blank	35	463	300	280	278	169	-
0.50		950	886	448	84	114	51
0.75		1100	945	463	81	108	58
1.00		1672	1589	822	77	95	72
1.50		2483	2400	1178	74	90	81
2.00		3975	3834	1834	70	83	88
Blank	40	380	230	201	299	180	-
0.50		723	602	294	90	123	47
0.75		796	688	343	87	106	52
1.00		1484	1320	766	82	99	74
1.50		1623	1501	811	78	92	77
2.00		2872	2714	1310	72	87	87
Blank	45	273	237	200	307	188	-
0.50		493	388	216	96	126	45
0.75		553	418	230	91	117	51
1.00		909	821	417	85	108	70
1.50		1078	974	463	80	99	75
2.00		1840	1623	810	77	91	85
Blank	50	245	200	178	321	200	-
0.50		425	310	199	102	130	42
0.75		471	334	210	95	121	48
1.00		723	600	300	89	111	66
1.50		895	706	351	84	101	73
2.00		1430	1321	744	78	93	83

Table 3.54: Electrochemical impedance parameters for the corrosion of AZ31 alloy in 0.20 M Na_2SO_4 solution in the presence of DH at different temperatures.

Inhibitor Concentration (mmol dm^{-3})	Temperature (°C)	R_{hf} (Ω cm^2)	R_f (Ω cm^2)	R_{dif} (Ω cm^2)	C_{dl} (µF cm^{-2})	C_f (µF cm^{-2})	η (%)
Blank	30	301	226	171	269	179	-
0.50		550	461	223	41	98	45
0.75		1280	1171	625	29	82	76
1.00		1397	1300	661	25	67	78
1.50		1450	1323	672	19	60	79
2.00		2994	2895	1445	18	56	90
Blank	35	287	224	190	287	186	-
0.50		500	401	213	48	110	42
0.75		1090	1001	515	42	104	73
1.00		1390	1275	688	35	85	79
1.50		1523	1401	743	25	68	81
2.00		2590	2389	1350	20	61	89
Blank	40	259	192	163	301	191	-
0.50		462	330	171	65	120	44
0.75		987	904	448	58	117	74
1.00		1193	1023	510	32	89	78
1.50		1352	1202	621	25	75	81
2.00		1672	1488	728	22	69	84
Blank	45	236	203	167	321	201	-
0.50		400	331	186	66	131	41
0.75		893	789	375	56	123	74
1.00		950	840	419	50	92	75
1.50		1066	945	471	45	89	78
2.00		1230	1114	545	27	71	81
Blank	50	218	187	159	333	219	-
0.50		376	245	126	72	143	42
0.75		762	664	331	61	125	71
1.00		831	718	358	53	95	73
1.50		865	723	361	48	84	75
2.00		1076	945	463	35	79	80

Table 3.55: Electrochemical impedance parameters for the corrosion of AZ31 alloy in 0.25 M Na_2SO_4 solution in the presence of DH at different temperatures.

Inhibitor Concentration (mmol dm^{-3})	Temperature (°C)	R_{hf} (Ω cm^2)	R_f (Ω cm^2)	R_{dif} (Ω cm^2)	C_{dl} (µF cm^{-2})	C_f (µF cm^{-2})	η (%)
Blank	30	492	301	280	320	240	-
0.50		680	578	214	134	113	42
0.75		1545	1460	745	121	107	74
1.00		1699	1509	756	117	100	76
1.50		1858	1723	867	105	97	78
2.00		2990	2845	1422	97	86	87
Blank	35	350	250	221	333	259	-
0.50		588	479	223	137	118	40
0.75		1204	1101	542	128	110	71
1.00		1468	1334	735	116	99	76
1.50		1605	1510	801	105	95	78
2.00		2200	2099	1034	99	91	84
Blank	40	201	114	96	345	267	-
0.50		330	222	120	145	123	39
0.75		650	540	251	131	119	69
1.00		745	678	348	122	113	73
1.50		793	700	352	104	105	74
2.00		1187	1033	529	97	93	83
Blank	45	180	109	80	359	280	-
0.50		284	159	89	153	130	37
0.75		589	300	150	128	123	69
1.00		650	521	254	121	116	72
1.50		708	602	311	113	103	74
2.00		943	851	479	95	96	80
Blank	50	170	100	64	389	308	-
0.50		264	111	75	157	134	36
0.75		501	395	165	139	126	66
1.00		579	488	234	121	114	70
1.50		612	500	250	116	101	72
2.00		856	711	353	101	95	80

Table 3.56: Activation parameters for the corrosion of AZ31 alloy in NaCl solutions containing different concentrations of DH inhibitor.

Concentration of NaCl (M)	Concentration of inhibitor (mmol dm^{-3})	E_a (kJ mol^{-1})	$\Delta H^{\#}$ (kJ mol^{-1})	$\Delta S^{\#}$ (J mol^{-1} K^{-1})
0.05	Blank	34.00	34.66	-128.69
	0.50	59.96	57.37	-65.93
	0.75	65.43	62.83	-50.21
	1.00	70.11	67.51	-36.58
	1.50	79.18	76.58	-2.57
	2.00	82.50	79.91	32.08
0.1	Blank	18.14	15.55	-183.86
	0.50	22.35	18.94	-182.93
	0.75	22.35	19.76	-175.71
	1.00	25.81	23.21	-166.30
	1.50	27.32	27.32	-158.09
	2.00	29.40	29.40	-155.46
0.15	Blank	23.57	18.70	-174.42
	0.50	28.67	26.08	-151.73
	0.75	30.46	27.86	-147.40
	1.00	26.70	32.42	-137.34
	1.50	41.35	38.27	-117.89
	2.00	43.87	38.75	-122.13
0.20	Blank	20.67	18.08	-167.27
	0.50	25.46	22.87	-156.30
	0.75	31.07	27.03	-143.99
	1.00	34.63	28.48	-133.35
	1.50	35.71	29.10	-127.78
	2.00	46.37	43.78	-100.51
0.25	Blank	16.94	15.30	-175.67
	0.50	18.08	15.43	-165.53
	0.75	25.20	19.51	-161.37
	1.00	30.42	20.35	-130.94
	1.50	31.26	22.53	-120.96
	2.00	32.53	27.94	-116.22

Table 3.57: Activation parameters for the corrosion of AZ31 alloy in Na_2SO_4 solutions containing different concentrations of DH inhibitor.

Concentration of medium (M)	Concentration of inhibitor (mmol dm^{-3})	E_a (kJ mol^{-1})	$\Delta H^{\#}$ (kJ mol^{-1})	$\Delta S^{\#}$ (J mol^{-1} K^{-1})
0.05	Blank	44.17	40.04	-108.74
	0.50	72.18	71.88	-21.19
	0.75	77.79	73.20	-15.21
	1.00	83.32	82.61	4.24
	1.50	88.44	86.44	31.51
	2.00	90.17	91.14	36.08
0.10	Blank	39.64	33.78	-126.03
	0.50	50.78	40.36	-102.84
	0.75	55.01	48.18	-85.38
	1.00	55.19	48.91	-80.80
	1.50	56.82	49.99	-80.72
	2.00	74.56	70.05	-20.94
0.15	Blank	35.65	28.33	-137.09
	0.50	40.33	37.73	-127.45
	0.75	41.24	38.65	-110.24
	1.00	45.44	34.53	-83.88
	1.50	51.45	48.86	-40.32
	2.00	66.73	64.14	-24.31
0.20	Blank	35.21	23.87	-149.98
	0.50	23.45	21.80	-170.10
	0.75	36.27	37.66	-121.71
	1.00	38.34	44.54	-104.61
	1.50	41.67	47.82	-98.43
	2.00	74.56	67.02	-41.81
0.25	Blank	24.39	18.81	-164.69
	0.50	28.93	26.35	-145.07
	0.75	35.74	32.58	-132.10
	1.00	36.00	33.14	-129.03
	1.50	47.45	33.42	-96.60
	2.00	49.05	44.86	-76.73

Table 3.58: Thermodynamic parameters for the adsorption of DH inhibitor on AZ31 alloy in NaCl solutions.

Concentration of NaCl (M)	Temperature (°C)	ΔG^0_{ads} (kJ mol^{-1})	ΔH^0_{ads} (kJ mol^{-1})	ΔS^0_{ads} (J mol^{-1} K^{-1})
0.05	30	-34.19	-57.7	-77.6
	35	-33.80		
	40	-33.42		
	45	-33.04		
	50	-32.65		
0.1	30	-32.84	-50.8	-59.6
	35	-32.53		
	40	-32.22		
	45	-31.92		
	50	-31.62		
0.15	30	-28.65	-48.6	-66.2
	35	-28.24		
	40	-27.90		
	45	-27.55		
	50	-27.25		
0.20	30	-27.17	-43.6	-54.2
	35	-26.90		
	40	-26.63		
	45	-26.36		
	50	-26.09		
0.25	30	-26.39	-37.0	-35.0
	35	-26.24		
	40	-26.08		
	45	-25.87		
	50	-25.69		

Table 3.59: Thermodynamic parameters for the adsorption of DH on AZ31 alloy in Na_2SO_4 solutions.

Concentration of NaCl (M)	Temperature (°C)	ΔG^0_{ads} (kJ mol^{-1})	ΔH^0_{ads} (kJ mol^{-1})	ΔS^0_{ads} (J mol^{-1} K^{-1})
0.05	30	-28.38	-40.2	-39.0
	35	-28.18		
	40	-27.99		
	45	-27.79		
	50	-27.60		
0.10	30	-30.52	-38.1	-25.0
	35	-30.40		
	40	-30.27		
	45	-30.15		
	50	-30.02		
0.15	30	-27.97	-34.0	-20.0
	35	-27.84		
	40	-27.76		
	45	-27.64		
	50	-29.54		
0.20	30	-28.62	-32.0	-11.0
	35	-28.61		
	40	-28.55		
	45	-28.50		
	50	-28.44		
0.25	30	-27.55	-31.2	-12.0
	35	-27.50		
	40	-27.44		
	45	-27.38		
	50	-27.32		

Table 3.60: Calculated parameters for DH inhibitor.

Parameters	Value
Total Energy (KeV)	-2.32
Energy gap (eV)	3.19
E_{HOMO} (eV)	-1.01
E_{LUMO} (eV)	-4.21
Dipole moment (Debye)	12.98
Electronegativity (eV)	2.61
Chemical hardness (eV)	1.60
Electron affinity (eV)	4.21
Ionization potential (eV)	1.01
Softness (eV^{-1})	0.62

3.5 SODIUM 2,2'-(9,18-DIOCTYL-10,17-DIOXO-9,12,15,18-TETRAAZAHEXACOSANE-12,15-DIYL)DIACETATE (DO) AS CORROSION INHIBITOR ON AZ31 ALLOY IN SODIUM CHLORIDE AND SODIUM SULFATE SOLUTIONS

3.5.1 Potentiodynamic polarization measurements

Potentiodynamic polarization plots for the corrosion of AZ31 Mg alloy in 0.1 M NaCl solution and 0.1 M Na_2SO_4 solution in the presence of varying concentrations of DO compound at 50 °C is shown in Fig**.** 3.49. Similar plots were obtained at other temperatures also. The corrosion current density (i_{corr}) values were obtained by the extrapolation of cathodic branches of the polarization plots. The polarization curves are shifted to a lower current density region as the concentration of DO increases, which reflects the corrosion inhibition produced by DO. But there is no significant change in the shape of the Tafel branches, indicating that DO did not alter the corrosion mechanism. DO might have played an important role by blocking the active sites of reaction on the metal surface, likely to be by adsorption.

Tables 3.61 to 3.70 summarize the potentiodynamic polarization parameters like corrosion potential (E_{corr}), corrosion current density (i_{corr}), and cathodic slope (β_c), corrosion rate (υ_{corr}), and inhibition efficiency (η) in NaCl and Na_2SO_4 media.

From Tables 3.61 to 3.70 it is observed that the inhibition efficiency increases with the increase in the concentration of DO up to an optimum concentration of 1.5 mmol dm^{-3}, and above which the increase in inhibition is negligible. Efficient surface coverage could be credited to the increase in inhibition efficiency. Thus, 1.5 mmol dm^{-3} of DO could be attributed as the most optimum and economic concentration of the surfactant for inhibiting AZ31 Mg alloy, at the presented conditions. The results show that there are no significant changes in the E_{corr} values on the addition of the surfactant, indicating that DO inhibits both the anodic and cathodic reactions as a mixed inhibitor, presumably by covering both the anodic and cathodic sites on the alloy surface.

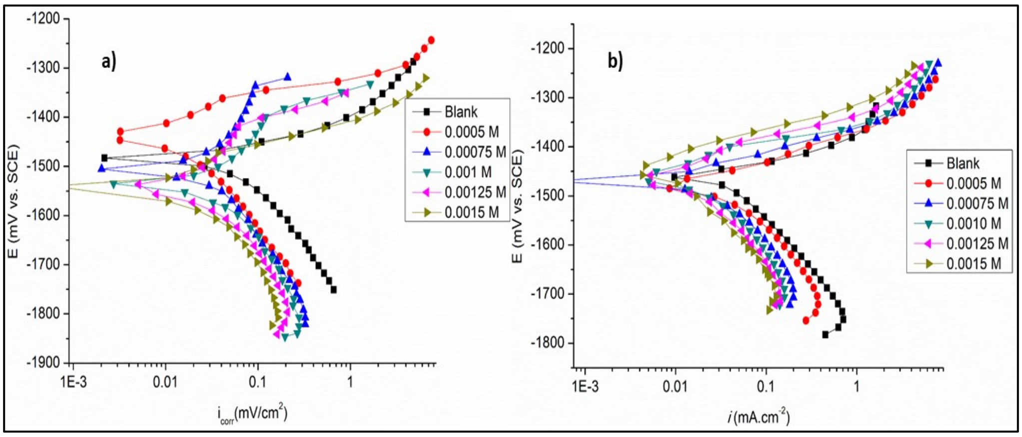

Fig. 3.49: Potentiodynamic polarization curves for the corrosion of AZ31 alloy in the presence of different concentrations of DO in a) 0.1 M NaCl solution and b) 0.1 M Na_2SO_4 solution at 50 °C.

3.5.2 Electrochemical impedance spectroscopy

The Nyquist plots for the corrosion of alloy in 0.1 M NaCl medium and 0.1 M Na_2SO_4 medium at 50 °C with varying concentrations of DO are presented in Fig. 3.50. The Nyquist plots are similar to the ones in the previous sections. As shown in Fig. 3.50, there is an increase in the size of the capacitance loop with the increase in the concentration of DO with no change in its shape compared with the blank solution, which implies that DO consistently reduces the corrosion rate without changing the corrosion mechanism.

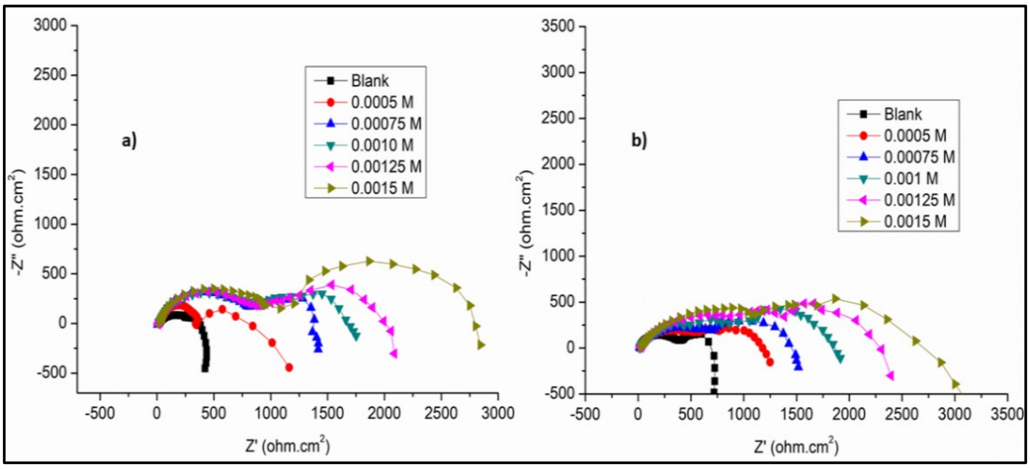

Fig. 3.50: Nyquist plots for the corrosion of AZ31 alloy in the presence of different concentrations of DO in a) 0.1 M NaCl solution and b) 0.1 M Na_2SO_4 solution at 50 °C.

The impedance parameters (R_{hf}, C_{dl}, R_f, R_{dif}, C_f) deduced from impedance measurements are tabulated in Tables 3.71 to 3.80 in NaCl and Na_2SO_4 solutions of different concentrations, in the presence of different concentrations of DO at different temperatures.

The Bode plots of phase angle and amplitude for the corrosion of the AZ31 Mg alloy immersed in 0.1 M NaCl solution and 0.1 M Na_2SO_4 solution at 50 °C, respectively, are shown in Fig. 3.51 and Fig. 3.52. As seen from the Bode plots, both the impedance modulus (Z_{mod}) at low frequency and the phase maximum (θ_{max}) at intermediate frequency increase with the increase in DO concentration, which collectively indicates the progressive formation of protective surface film by the inhibitor, protecting the alloy surface.

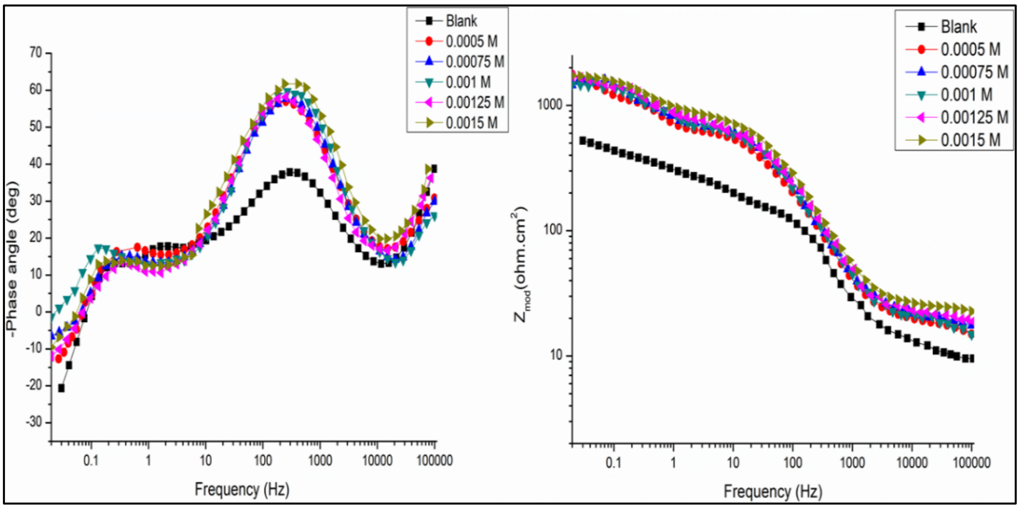

Fig. 3.51: Bode phase angle and amplitude plots for the corrosion of the AZ31 alloy in 0.1 M NaCl medium containing different concentrations of DO at 50 °C.

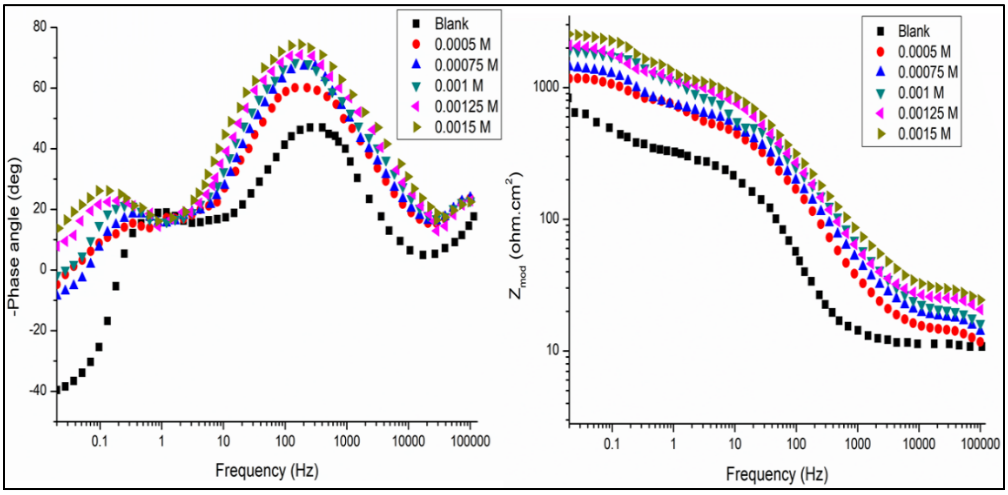

Fig. 3.52: Bode phase angle and amplitude plots for the corrosion of the AZ31 alloy in 0.1 M Na_2SO_4 medium containing different concentrations of DO at 50 °C.

3.5.3 Effect of temperature

The data presented in the previously mentioned tables show a steady decrease in the inhibition efficiency as the temperature increases, indicating the possible physisorption of the inhibitor molecules on the alloy surface. Fig. 3.53 shows the Arrhenius plots for the corrosion of AZ31 Mg alloy in 0.1 M NaCl and 0.1 M Na_2SO_4 containing different concentrations of DO. The average linear regression coefficient (R^2) of 0.95 was obtained.

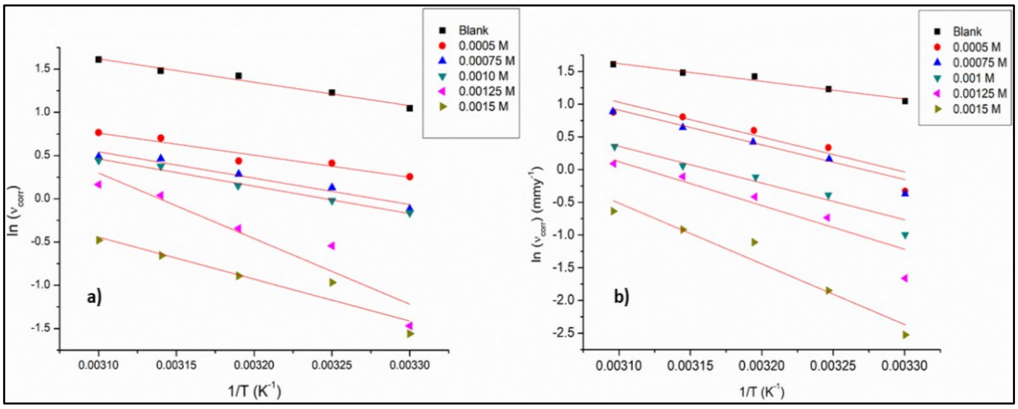

Fig. 3.53: Arrhenius plots for the corrosion of AZ31 magnesium alloy in a) 0.1 M NaCl and b) 0.1 M Na_2SO_4 media in the presence of different concentrations of DO.

Fig. 3.54 represents the plots of ln (v_{corr}/T) versus ($1/T$) for the corrosion of AZ31 Mg alloy in 0.1 M NaCl and Na_2SO_4 containing varying concentrations of DO inhibitor. Calculated data of $\Delta H^{\#}$, $\Delta S^{\#}$, E_a, are tabulated in Tables 3.81 and 3.82. As observed from the data in Tables 3.81 and 3.82, E_a values increase with the increase in the concentration of inhibitor, which indicates the increased energy barrier for the occurrence of corrosion, because of the increase in surface coverage brought by the inhibitor (Lamaka et al. 2007). $\Delta S^{\#}$ in both blank and DO containing systems show large negative values which show that the activated complex in the rate-determining step represents association rather than dissociation. This indicates that there is a decrease in randomness when the activated complex is formed from the reactants of corrosion reaction (Heakal et al. 2012, Frignani et al. 2012).

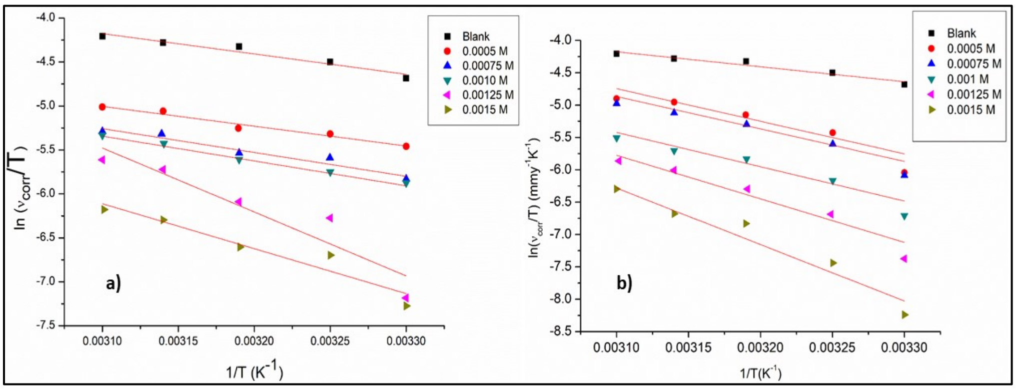

Fig. 3.54: The plots of ln(v_{corr} /T) versus 1/T for the corrosion of AZ31 magnesium alloy in a) 0.1 M NaCl and b) 0.1 M Na_2SO_4 in the presence of different concentrations of DO.

3.5.4 Adsorption isotherms

The Langmuir adsorption isotherms for the adsorption of DO compound on AZ31 Mg alloy surface at different temperatures in 0.1 M NaCl and 0.1 M Na_2SO_4 are presented in Fig. 3.55. The graph exhibited linear behavior, but the slopes are not equal to one. The average linear regression coefficient (R^2) of 0.95 was obtained. This deviation from ideal Langmuir behavior can be attributed to interactions among the adsorbed species (Frignani et al. 2012).

The thermodynamic parameters for the adsorption of DO on the AZ31 Mg alloy surface in NaCl and Na_2SO_4 media are tabulated in Tables 3.83 and 3.84. The negative values of ΔG^{o}_{ads} indicate that the process of adsorption of DO is spontaneous and an adsorbed film on the alloy surface is stable. The free energy values suggest that the DO undergoes both physisorption and chemisorption. The fact that both $\Delta G°_{ads}$ and inhibition efficiency decrease with the increase in temperature indicates that the adsorption of the inhibitor on the AZ31 alloy surface in NaCl and Na_2SO_4 media is not favored at high temperature and hence can be considered to be predominantly physisorption. The standard entropy of adsorption value is negative; indicating that a decrease in disordering takes place when the inhibitor species gets adsorbed on the alloy surface.

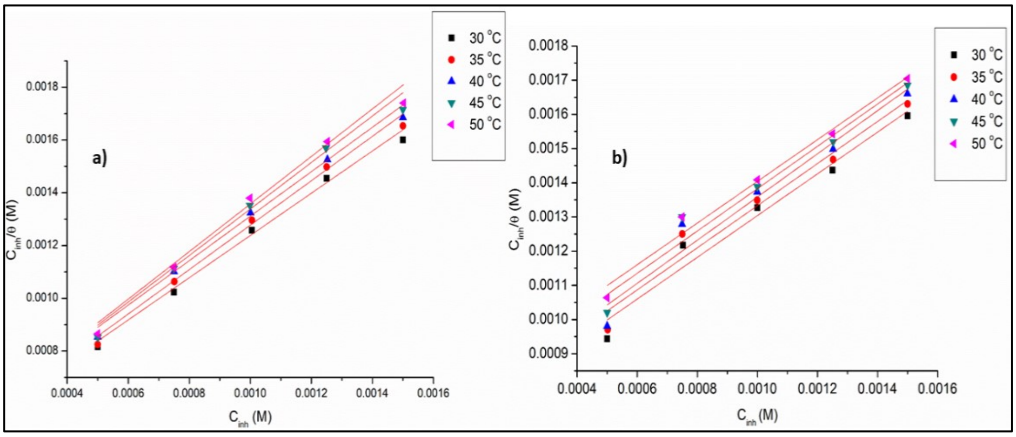

Fig. 3.55: Langmuir adsorption isotherm for the adsorption of DO on AZ31 magnesium alloy in a) 0.1 M NaCl medium and b) 0.1 M Na_2SO_4 medium.

3.5.5 SEM

Fig. 3.56 and Fig. 3.57 present the SEM images and EDX spectra of the alloy surface immersed in 0.1 M NaCl solution and 0.1 M Na_2SO_4 solution, respectively. It can be seen from SEM images in Fig. 3.8 (section 3.1), Fig. 3.56, and Fig. 3.57 that the surface of the AZ31 alloy is less deteriorated in the presence of the inhibitor. EDX spectra in the presence of inhibitor show that the surface contains intense peaks of carbon, nitrogen, and oxygen along with Mg, Al, and other alloying elements, indicating the DO surfactant on the surface of the alloy.

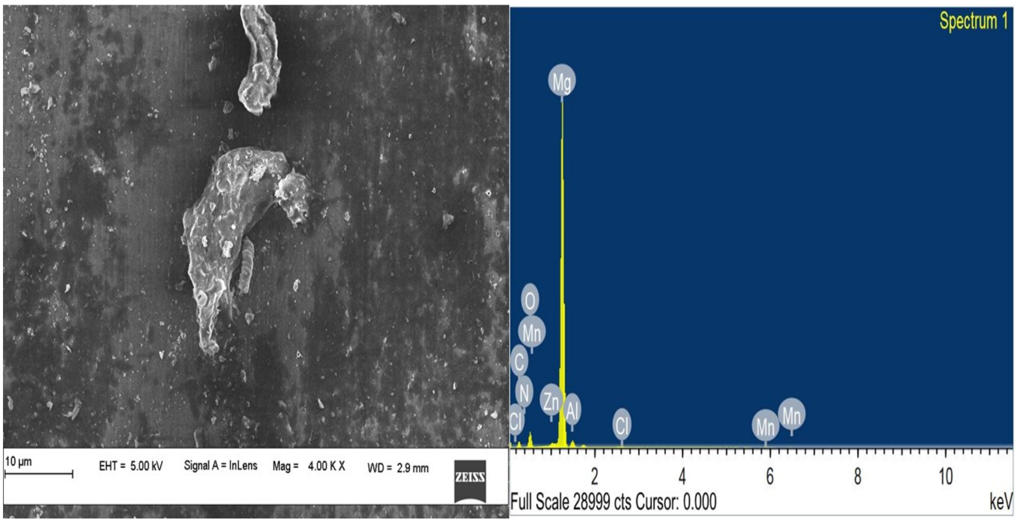

Fig. 3.56: SEM image and EDX spectrum of the AZ31 magnesium alloy surface after immersion in 0.1 M NaCl in the presence of DO for 3 h at 30 °C.

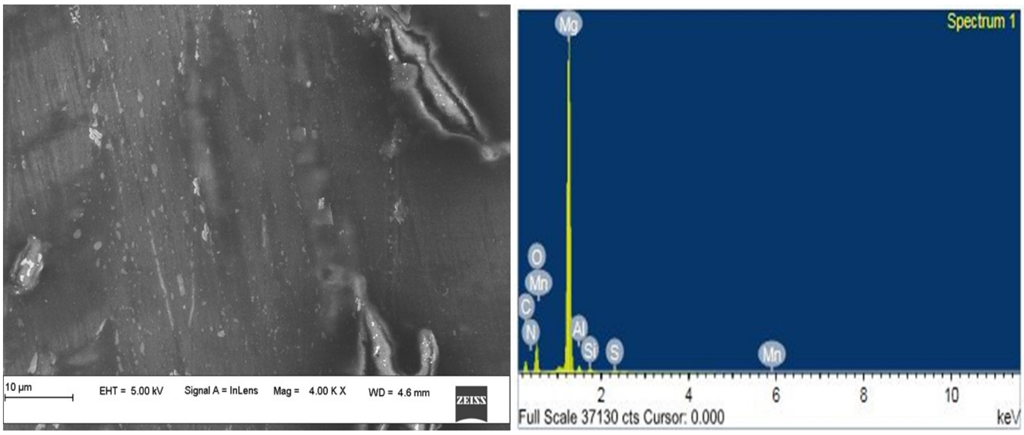

Fig. 3.57: SEM image and EDX spectrum of the AZ31 magnesium alloy surface after immersion in 0.1 M Na_2SO_4 in the presence of DO for 3 h at 30 °C.

3.5.6 XPS

Fig. 3.58 and Fig. 3.59 show the XPS survey spectra and individual spectra of elements of AZ31 magnesium alloy immersed in 0.1 M NaCl and 0.1 M Na_2SO_4, respectively. The high-resolution Mg 2s spectrum for magnesium alloys in the absence of inhibitor displays three peaks at 88.8 eV, 87.3 eV, and 89.2 eV. It is attributed to MgO, $Mg(OH)_2$, and Mg, respectively (Gece 2008). The MgO and $Mg(OH)_2$ are the main components of the alloy with the larger peak area indicating the corrosion. The Mg 1s spectrum for Mg AZ31 alloy immersed in anionic Gemini surfactant also has three peaks corresponding to the same products, MgO, $Mg(OH)_2$, and Mg, except that the peak area is varied. The corrosion is retarded since the peak area of Mg is larger than that of other corrosion products.

In the presence of inhibitors, O 1s gave a peak of $Mg(OH)_2$ /MgO is kept at 531.1 eV [47 Zhang 2020]. The appearance of C 1s deconvoluted peak at 284.8 eV of -C-O and -C=O should be related to the presence of DO, which consists of carboxylate groups on the surface of the alloy. The N 1s spectrum shows a peak at 399.2 eV, which shows the presence of CH_2-N-C=O bond. The XPS results evidently show that the inhibitor is adsorbed on the surface to repel the water molecules and corrosive species.

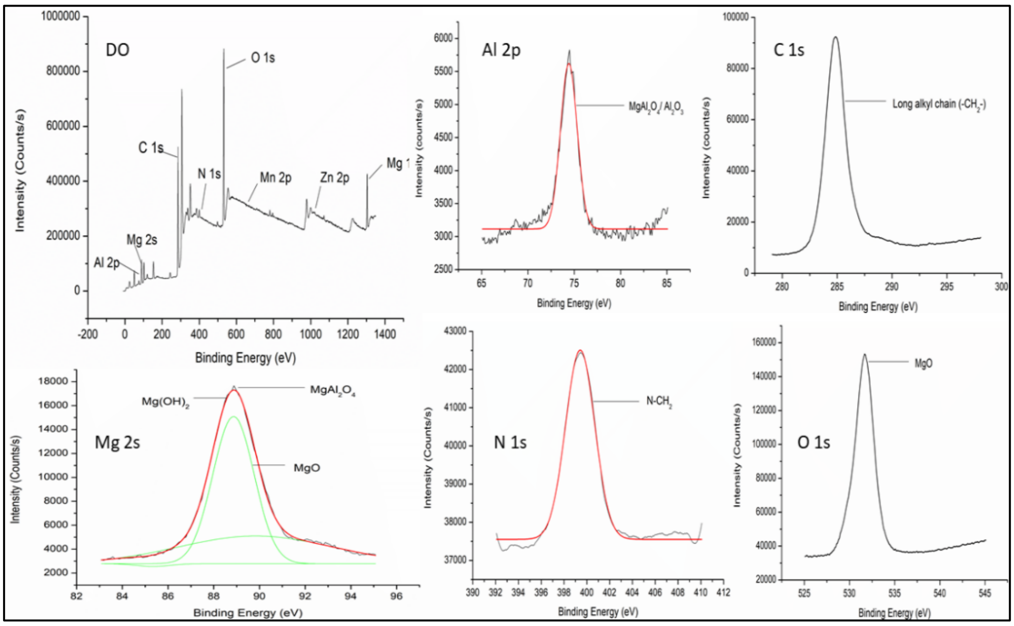

Fig. 3.58: XPS survey spectra and individual spectra of elements (Mg 1s, Al 2p, C 1s, O 1s and, N 1s) of AZ31 Mg alloy immersed in 0.1 M NaCl medium in the presence of 0.001 M DO for 3 h at 30 °C.

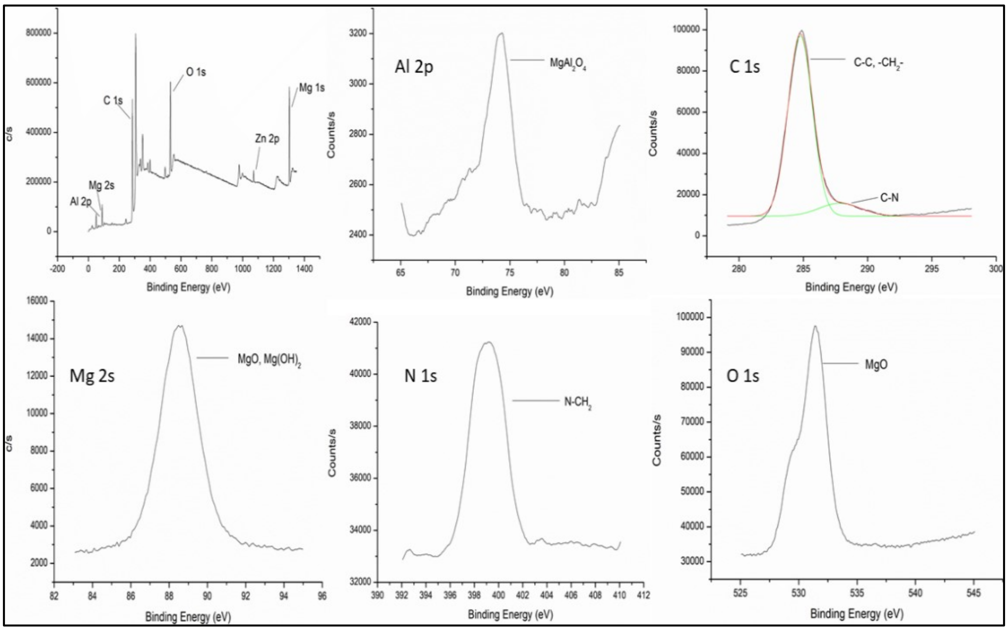

Fig. 3.59: XPS survey spectra and individual spectra of elements (Mg 1s, Al 2p, C 1s, O 1s and, N 1s) of AZ31 Mg alloy immersed in 0.1 M Na_2SO_4 medium in the presence of 0.001 M DO for 3 h at 30 °C.

3.5.7 DFT

The optimized structure for the inhibitor, DO, was obtained using DFT calculations at the B3LYP hybrid functional model with def-TZVP basis set and presented in Fig. 3.60. The calculated parameters are presented in Table 3.85.

The structure of the molecule is optimized and the negative value of the total energy (-2.315 KeV) indicates a thermodynamically stable molecule. E_{HOMO} value indicates the physical adsorption as the basis for the corrosion inhibition action. The low bandgap energy suggests a higher reactivity of the inhibitor molecules, leading to their ready adsorption on AZ31 alloy surface (H. A. Videla; M. F. L. de Mele; G.Brankevich 1988)(Williams et al. 2013)(Liu et al. 2018). The high value of the dipole moment implies a stronger interaction of DO molecules with the AZ31 alloy surface.

The strong tendency of DO to attract electrons from metal shows a higher electronegativity value, which in turn indicates the higher ability of DO to act as a corrosion inhibitor.

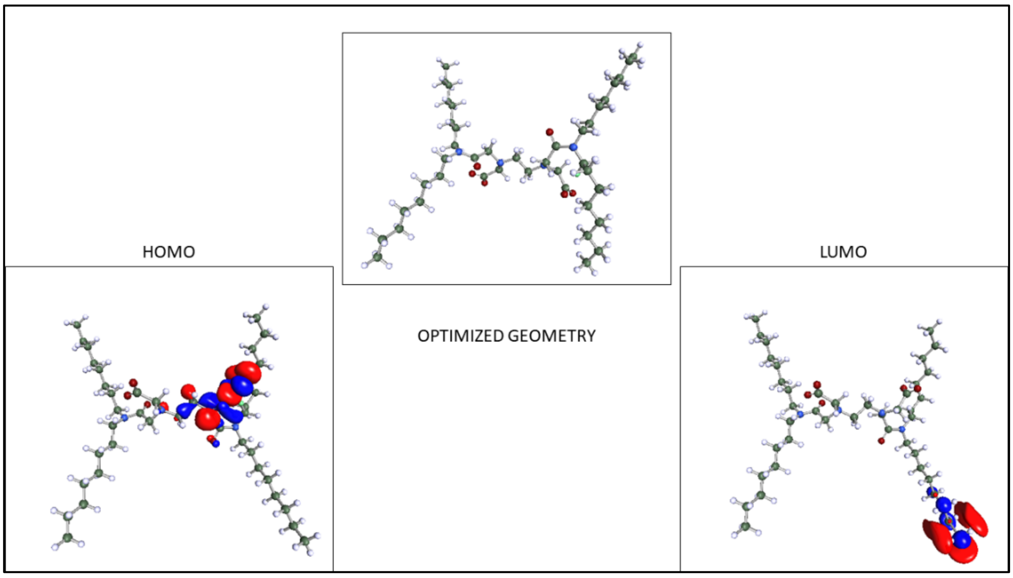

Fig. 3.60: Optimized structure and the frontier molecular orbital density distribution of the DO molecule.

3.5.8 Summary

Anionic Gemini surfactant, DO, was synthesized and used as a corrosion inhibitor on AZ31 Mg alloy in different concentrations of NaCl solution and Na_2SO_4 solution. The inhibitor surfactant acted as a mixed type of inhibitor and the inhibitor efficiency increased with the increase in the concentration of DO and decreased with the increase in temperature and the increase in the concentration of NaCl and Na_2SO_4 media. The surfactant was adsorbed predominantly through physisorption and obeyed Langmuir adsorption isotherm. The quantum chemical calculations supported the experimental observations.

Table 3.61: Electrochemical polarization parameters for the corrosion of AZ31 in 0.05 M NaCl in the presence of DO at different temperatures.

Inhibitor concentration (mmol dm^{-3})	Temperature (°C)	E_{corr} vs SCE (mV)	i_{corr} ($\mu A\ cm^{-2}$)	$-\beta_c$ (mV dec^{-1})	v_{corr} (mm y^{-1})	η (%)
Blank	30	-1514	70.10	99	1.51	-
0.50		-1520	12.99	45	0.28	81
0.75		-1524	9.28	41	0.20	86
1.00		-1510	7.42	37	0.16	89
1.25		-1531	4.64	33	0.10	93
1.50		-1511	2.78	25	0.06	96
Blank	35	-1490	112.81	122	2.43	-
0.50		-1495	37.60	48	0.81	66
0.75		-1500	27.85	44	0.60	75
1.00		-1511	22.28	38	0.48	80
1.25		-1508	10.21	35	0.22	91
1.50		-1512	5.57	27	0.12	95
Blank	40	-1500	168.06	129	3.62	-
0.50		-1541	62.67	53	1.35	63
0.75		-1499	46.42	49	1.00	72
1.00		-1487	38.06	44	0.82	77
1.25		-1490	18.57	39	0.40	88
1.50		-1498	11.14	31	0.24	93
Blank	45	-1503	183.38	134	3.95	-
0.50		-1514	70.56	55	1.52	61
0.75		-1522	53.39	52	1.15	70
1.00		-1528	45.03	47	0.97	75
1.25		-1510	27.85	41	0.60	85
1.50		-1501	16.24	36	0.35	91
Blank	50	-1493	197.77	140	4.26	-
0.50		-1480	78.92	56	1.70	60
0.75		-1499	62.21	53	1.34	68
1.00		-1504	53.39	49	1.15	73
1.25		-1515	33.89	44	0.73	83
1.50		-1520	20.89	40	0.45	89

Table 3.62: Electrochemical polarization parameters for the corrosion of AZ31 in 0.1 M NaCl in the presence of DO at different temperatures.

Inhibitor concentration (mmol.dm^{-3})	Temperature (°C)	E_{corr} vs SCE (mV)	i_{corr} (μA cm^{-2})	$-\beta_c$ (mV dec^{-1})	v_{corr} (mm y^{-1})	η (%)
Blank	30	-1483	154.03	135	3.34	-
0.50		-1436	59.49	39	1.29	61
0.75		-1507	41.17	36	0.89	73
1.00		-1537	39.23	28	0.85	74
1.25		-1543	10.56	22	0.23	93
1.50		-1540	10.05	18	0.21	93
Blank	35	-1489	171.58	141	3.73	-
0.50		-1502	70.38	50	1.51	60
0.75		-1507	52.53	38	1.14	69
1.00		-1527	45.07	39	0.98	73
1.25		-1543	26.75	21	0.58	84
1.50		-1519	17.50	21	0.38	89
Blank	40	-1502	210.77	165	4.54	-
0.50		-1493	71.39	59	1.55	58
0.75		-1496	55.53	48	1.19	68
1.00		-1516	47.23	38	1.02	72
1.25		-1539	32.61	28	0.71	81
1.50		-1523	19.05	23	0.41	89
Blank	45	-1516	225.52	162	4.90	-
0.50		-1487	92.85	44	2.02	58
0.75		-1502	74.0	30	1.59	67
1.00		-1520	67.16	27	1.46	70
1.25		-1517	48.01	24	1.04	78
1.50		-1555	31.39	19	0.68	86
Blank	50	-1490	235.47	173	5.11	-
0.50		-1481	100.05	48	2.15	57
0.75		-1512	77.98	37	1.63	67
1.00		-1517	72.50	27	1.56	69
1.25		-1505	54.45	19	1.18	76
1.50		-1556	28.75	18	0.62	87

Table 3.63: Electrochemical polarization parameters for the corrosion of AZ31 in 0.15 M NaCl in the presence of DO at different temperatures.

Inhibitor concentration ($mmol.dm^{-3}$)	Temperature (°C)	E_{corr} vs SCE (mV)	i_{corr} ($\mu A\ cm^{-2}$)	$-\beta_c$ ($mV\ dec^{-1}$)	v_{corr} ($mm\ y^{-1}$)	η (%)
Blank	30	-1537	233.52	150	5.03	-
0.50		-1525	91.92	124	1.98	59
0.75		-1510	66.39	112	1.43	71
1.00		-1500	60.35	104	1.30	74
1.25		-1542	24.60	85	0.53	89
1.50		-1528	20.42	68	0.44	91
Blank	35	-1500	333.34	155	7.18	-
0.50		-1510	139.27	127	3.00	58
0.75		-1501	110.49	120	2.38	67
1.00		-1489	95.17	111	2.05	71
1.25		-1494	60.35	90	1.30	82
1.50		-1531	37.14	75	0.80	88
Blank	40	-1515	455.90	168	9.82	-
0.50		-1502	196.84	134	4.24	56
0.75		-1523	155.52	121	3.35	66
1.00		-1509	134.63	113	2.90	70
1.25		-1520	90.53	94	1.95	80
1.50		-1525	60.35	78	1.30	86
Blank	45	-1491	478.65	170	10.31	-
0.50		-1485	215.88	136	4.65	54
0.75		-1496	169.45	124	3.65	64
1.00		-1512	144.85	115	3.12	69
1.25		-1522	107.70	96	2.32	77
1.50		-1545	73.35	80	1.58	84
Blank	50	-1475	567.33	194	12.22	-
0.50		-1493	262.31	140	5.65	53
0.75		-1499	200.56	127	4.32	64
1.00		-1500	178.74	116	3.85	68
1.25		-1505	133.24	99	2.87	76
1.50		-1520	67.31	83	2.10	82

Table 3.64: Electrochemical polarization parameters for the corrosion of AZ31 in 0.20 M NaCl in the presence of DO at different temperatures.

Inhibitor concentration ($mmol.dm^{-3}$)	Temperature (°C)	E_{corr} vs SCE (mV)	i_{corr} ($\mu A\ cm^{-2}$)	$-\beta_c$ ($mV\ dec^{-1}$)	v_{corr} ($mm\ y^{-1}$)	η (%)
Blank	30	-1500	432.55	189	9.40	-
0.50		-1535	186.17	130	4.01	57
0.75		-1498	131.85	116	2.84	70
1.00		-1523	121.63	101	2.62	72
1.25		-1538	51.99	88	1.12	88
1.50		-1512	42.71	67	0.92	90
Blank	35	-1485	457.04	214	9.93	-
0.50		-1480	201.95	133	4.35	56
0.75		-1488	147.63	118	3.18	68
1.00		-1520	125.35	104	2.70	73
1.25		-1494	69.63	92	1.50	85
1.50		-1499	54.31	70	1.17	88
Blank	40	-1483	489.13	181	10.63	-
0.50		-1488	225.16	136	4.85	54
0.75		-1493	167.13	121	3.60	66
1.00		-1500	141.60	107	3.05	71
1.25		-1510	83.56	95	1.80	83
1.50		-1498	68.24	74	1.47	86
Blank	45	-1511	687.77	211	14.75	-
0.50		-1512	327.30	140	7.05	52
0.75		-1490	244.66	124	5.27	64
1.00		-1540	204.27	110	4.40	70
1.25		-1525	130.92	98	2.82	81
1.50		-1528	109.10	78	2.35	84
Blank	50	-1497	709.98	171	15.43	-
0.50		-1484	348.19	143	7.50	51
0.75		-1475	271.59	126	5.85	62
1.00		-1506	227.49	114	4.90	68
1.25		-1525	155.99	100	3.36	78
1.50		-1520	127.67	81	2.75	82

Table 3.65: Electrochemical polarization parameters for the corrosion of AZ31 in 0.25 M NaCl in the presence of DO at different temperatures.

Inhibitor concentration (mmol.dm^{-3})	Temperature (°C)	E_{corr} vs SCE (mV)	i_{corr} (μA cm^{-2})	$-\beta_c$ (mV dec^{-1})	v_{corr} (mm y^{-1})	η (%)
Blank	30	-1526	520.41	190	11.31	-
0.50		-1490	235.38	140	5.07	55
0.75		-1495	167.13	121	3.60	68
1.00		-1512	150.88	111	3.25	71
1.25		-1515	71.49	95	1.54	86
1.50		-1520	62.67	72	1.35	88
Blank	35	-1515	553.44	192	12.03	-
0.50		-1526	255.34	144	5.50	54
0.75		-1533	187.56	125	4.04	66
1.00		-1537	167.13	114	3.60	70
1.25		-1540	95.17	96	2.05	83
1.50		-1499	76.60	75	1.65	86
Blank	40	-1488	577.18	188	12.54	-
0.50		-1532	278.55	147	6.00	52
0.75		-1538	208.91	127	4.50	64
1.00		-1542	190.34	116	4.10	67
1.25		-1490	104.45	98	2.25	82
1.50		-1505	92.85	78	2.00	84
Blank	45	-1510	706.61	209	15.22	-
0.50		-1523	348.19	150	7.50	50
0.75		-1528	276.23	131	5.95	61
1.00		-1535	253.95	117	5.47	64
1.25		-1540	139.27	100	3.00	80
1.50		-1524	735.21	81	2.77	81
Blank	50	-1494	792.81	186	17.23	-
0.50		-1489	422.48	153	9.10	47
0.75		-1480	337.98	133	7.28	58
1.00		-1495	311.05	121	6.70	61
1.25		-1502	199.63	102	4.30	75
1.50		-1511	174.09	84	3.75	78

Table 3.66: Electrochemical polarization parameters for the corrosion of AZ31 alloy in 0.05 M Na_2SO_4 in the presence of DO at different temperatures.

Inhibitor concentration (mmol dm^{-3})	Temperature (°C)	E_{corr} vs SCE (mV)	i_{corr} (µA cm^{-2})	$-\beta_c$ (mV dec^{-1})	v_{corr} (mm y^{-1})	η (%)
Blank	30	-1483	63.33	93	1.37	-
0.50		-1520	34.35	68	0.74	46
0.75		-1478	28.54	61	0.62	55
1.00		-1461	17.75	83	0.38	72
1.25		-1465	7.80	53	0.17	88
1.50		-1432	3.40	63	0.07	95
Blank	35	-1470	110.24	110	2.39	-
0.50		-1500	59.87	103	1.30	45
0.75		-1508	46.29	108	1.00	58
1.00		-1493	34.31	105	0.74	69
1.25		-1449	22.50	95	0.49	80
1.50		-1520	13.92	109	0.30	87
Blank	40	-1502	164.74	125	3.58	-
0.50		-1535	60.24	108	1.31	63
0.75		-1523	59.77	116	1.30	63
1.00		-1527	47.27	118	1.03	71
1.25		-1520	45.70	124	0.99	72
1.50		-1517	25.07	113	0.54	85
Blank	45	-1465	179.03	154	3.89	-
0.50		-1523	54.47	123	1.18	69
0.75		-1517	49.39	148	1.07	72
1.00		-1523	45.79	145	0.99	75
1.25		-1507	36.28	136	0.79	80
1.50		-1501	25.99	125	0.56	86
Blank	50	-1481	190.03	144	4.13	-
0.50		-1521	77.03	123	1.67	60
0.75		-1511	62.95	132	1.37	67
1.00		-1492	55.43	114	1.20	71
1.25		-1502	43.85	127	0.95	77
1.50		-1492	29.71	140	0.64	85

Table 3.67: Electrochemical polarization parameters for the corrosion of AZ31 alloy in 0.10 M Na_2SO_4 in the presence of DO at different temperatures.

Inhibitor concentration ($mmol.dm^{-3}$)	Temperature (°C)	E_{corr} vs SCE (mV)	i_{corr} ($\mu A\ cm^{-2}$)	$-\beta_c$ ($mV\ dec^{-1}$)	υ_{corr} ($mm\ y^{-1}$)	η (%)
Blank	30	-1482	71.21	117	1.54	-
0.50		-1475	33.42	113	0.72	53
0.75		-1466	32.12	110	0.69	56
1.00		-1465	17.17	112	0.37	75
1.25		-1458	8.82	103	0.19	87
1.50		-1443	3.71	104	0.08	94
Blank	35	-1528	157.60	134	3.42	-
0.50		-1550	77.90	125	1.68	50
0.75		-1532	62.67	122	1.35	60
1.00		-1518	35.74	118	0.77	77
1.25		-1511	27.85	112	0.60	82
1.50		-1507	11.14	119	0.24	92
Blank	40	-1485	191.24	140	4.15	-
0.50		-1515	94.24	117	2.03	51
0.75		-1514	85.88	113	1.85	55
1.00		-1513	46.42	115	1.00	75
1.25		-1510	38.99	102	0.84	79
1.50		-1479	19.96	105	0.43	89
Blank	45	-1481	202.71	150	4.40	-
0.50		-1482	103.99	132	2.24	49
0.75		-1476	88.21	131	1.90	56
1.00		-1483	49.4	121	1.06	75
1.25		-1488	41.78	122	0.90	79
1.50		-1492	18.57	112	0.40	89
Blank	50	-1456	208.41	157	4.53	-
0.50		-1495	111.42	137	2.40	47
0.75		-1491	103.53	124	2.23	50
1.00		-1488	60.81	110	1.31	71
1.25		-1484	38.99	108	0.84	81
1.50		-1490	24.60	104	0.53	88

Table 3.68: Electrochemical polarization parameters for the corrosion of AZ31 alloy in 0.15 M Na_2SO_4 in the presence of DO at different temperatures.

Inhibitor concentration (mmol dm^{-3})	Temperature (°C)	E_{corr} vs SCE (mV)	i_{corr} (µA cm^{-2})	$-\beta_c$ (mV dec^{-1})	v_{corr} (mm y^{-1})	η (%)
Blank	30	-1457	218.14	138	4.74	-
0.50		-1517	105.38	126	2.27	52
0.75		-1494	98.42	124	2.12	55
1.00		-1483	59.42	125	1.28	73
1.25		-1503	32.49	142	0.70	85
1.50		-1443	17.64	134	0.38	92
Blank	35	-1457	322.28	142	7.00	-
0.50		-1509	158.77	125	3.42	51
0.75		-1491	135.56	120	2.92	58
1.00		-1497	81.24	120	1.75	75
1.25		-1479	54.78	123	1.18	83
1.50		-1476	32.49	127	0.70	90
Blank	40	-1469	445.19	151	9.67	-
0.50		-1543	222.84	117	4.80	50
0.75		-1482	192.67	122	4.15	57
1.00		-1487	120.70	122	2.60	73
1.25		-1492	85.88	120	1.85	81
1.50		-1496	53.39	145	1.15	88
Blank	45	-1446	461.63	158	10.03	-
0.50		-1565	241.41	141	5.20	48
0.75		-1493	208.91	120	4.50	55
1.00		-1524	120.70	123	2.60	74
1.25		-1502	92.85	144	2.00	80
1.50		-1510	64.99	142	1.40	86
Blank	50	-1448	546.62	170	11.88	-
0.50		-1538	297.13	149	6.40	46
0.75		-1518	253.02	137	5.45	54
1.00		-1514	154.13	146	3.32	72
1.25		-1506	120.70	131	2.60	78
1.50		-1509	88.21	134	1.90	84

Table 3.69: Electrochemical polarization parameters for the corrosion of AZ31 alloy in 0.20 M Na_2SO_4 in the presence of DO at different temperatures.

Inhibitor concentration (mmol dm^{-3})	Temperature (°C)	E_{corr} vs SCE (mV)	i_{corr} (µA cm^{-2})	$-\beta_c$ (mV dec^{-1})	υ_{corr} (mm y^{-1})	η (%)
Blank	30	-1505	235.63	152	5.12	-
0.50		-1437	116.06	137	2.50	51
0.75		-1482	111.42	124	2.40	53
1.00		-1506	66.39	116	1.43	72
1.25		-1489	39.92	136	0.86	83
1.50		-1469	23.21	142	0.50	90
Blank	35	-1493	354.34	158	7.70	-
0.50		-1520	177.81	120	3.83	50
0.75		-1501	171.77	151	3.70	52
1.00		-1503	106.78	129	2.30	70
1.25		-1494	67.31	140	1.45	81
1.50		-1521	42.71	122	0.92	88
Blank	40	-1489	470.87	164	10.23	-
0.50		-1498	246.06	116	5.30	48
0.75		-1522	232.13	109	5.00	51
1.00		-1494	152.27	125	3.28	68
1.25		-1494	94.71	135	2.04	80
1.50		-1504	64.99	123	1.40	86
Blank	45	-1472	542.13	172	11.23	-
0.50		-1483	276.70	143	5.96	47
0.75		-1508	259.98	150	5.60	50
1.00		-1495	176.42	141	3.80	66
1.25		-1505	113.74	150	2.45	78
1.50		-1487	82.63	151	1.78	84
Blank	50	-1480	672.86	197	14.62	-
0.50		-1490	364.44	141	7.85	46
0.75		-1498	352.84	130	7.60	48
1.00		-1486	242.34	134	5.22	64
1.25		-1492	162.49	146	3.50	76
1.50		-1483	113.74	139	2.45	82

Table 3.70: Electrochemical polarization parameters for the corrosion of AZ31 alloy in 0.25 M Na_2SO_4 in the presence of DO at different temperatures.

Inhibitor concentration (mmol dm^{-3})	Temperature (°C)	E_{corr} vs SCE (mV)	i_{corr} (µA cm^{-2})	$-\beta_c$ (mV dec^{-1})	v_{corr} (mm y^{-1})	η (%)
Blank	30	-1451	372.80	147	8.10	-
0.50		-1507	188.02	136	4.05	50
0.75		-1499	180.13	108	3.88	52
1.00		-1490	111.42	127	2.40	70
1.25		-1472	67.31	125	1.45	82
1.50		-1472	44.10	125	0.95	88
Blank	35	-1411	497.12	158	10.80	-
0.50		-1510	255.34	118	5.50	49
0.75		-1481	250.70	146	5.40	50
1.00		-1510	155.52	147	3.35	69
1.25		-1522	95.63	120	2.06	81
1.50		-1535	69.63	113	1.50	86
Blank	40	-1438	516.71	170	11.23	-
0.50		-1528	276.23	145	5.95	47
0.75		-1498	265.56	128	5.72	49
1.00		-1507	171.77	139	3.70	67
1.25		-1500	114.67	147	2.47	78
1.50		-1501	82.63	150	1.78	84
Blank	45	-1486	583.03	190	12.67	-
0.50		-1513	322.66	180	6.95	45
0.75		-1511	311.05	140	6.70	47
1.00		-1500	199.63	151	4.30	66
1.25		-1505	140.20	147	3.02	76
1.50		-1494	104.45	154	2.25	82
Blank	50	-1463	727.89	201	15.82	-
0.50		-1514	408.55	168	8.80	44
0.75		-1523	403.91	143	8.70	45
1.00		-1544	262.31	171	5.65	64
1.25		-1521	190.81	157	4.11	74
1.50		-1502	144.85	166	3.12	80

Table 3.71: Electrochemical impedance parameters for the corrosion of AZ31 alloy in 0.05 M NaCl solution in the presence of DO at different temperatures.

Inhibitor Concentration (mmol dm^{-3})	Temperature (°C)	R_{hf} (Ω cm^2)	R_f (Ω cm^2)	R_{dif} (Ω cm^2)	C_{dl} (μF cm^{-2})	C_f (μF cm^{-2})	η (%)
Blank	30	580	296	225	138	177	-
0.50		2888	2702	1355	120	110	80
0.75		3995	3833	1542	116	104	85
1.00		4967	4888	2231	110	98	88
1.25		6324	6251	3210	106	94	91
1.50		8321	8210	3786	93	86	93
Blank	35	550	255	207	153	181	-
0.50		1621	1503	756	127	115	66
0.75		2210	2187	1076	120	109	75
1.00		2806	2700	1310	114	100	80
1.25		4910	4799	2377	108	95	89
1.50		6911	6834	3212	95	89	92
Blank	40	422	231	184	161	188	-
0.50		1194	1098	553	131	119	64
0.75		1499	1354	624	124	112	71
1.00		1855	1702	886	117	104	77
1.25		3254	3177	1541	110	99	87
1.50		4812	4703	2411	98	92	91
Blank	45	340	191	150	170	192	-
0.50		890	794	358	136	123	62
0.75		1149	1005	533	127	115	70
1.00		1359	1288	676	119	107	75
1.25		2251	2140	1107	111	100	85
1.50		3318	3209	1589	101	94	90
Blank	50	318	160	131	171	198	-
0.50		805	700	298	140	126	60
0.75		998	896	439	130	117	68
1.00		1220	1104	515	122	109	74
1.25		1850	1705	868	115	103	83
1.50		2841	2700	1605	103	97	89

Table 3.72: Electrochemical impedance parameters for the corrosion of AZ31 alloy in 0.10 M NaCl solution in the presence of DO at different temperatures.

Inhibitor Concentration (mmol dm^{-3})	Temperature (°C)	R_{hf} (Ω cm^2)	R_f (Ω cm^2)	R_{dif} (Ω cm^2)	C_{dl} (μF cm^{-2})	C_f (μF cm^{-2})	η (%)
Blank	30	507	232	209	166	172	-
0.50		1307	1185	512	119	72	61
0.75		1788	1600	823	55	61	72
1.00		2010	1933	959	27	27	75
1.25		4961	4785	2310	21	19	89
1.50		5077	4992	2475	17	18	90
Blank	35	380	192	168	181	179	-
0.50		960	803	396	137	81	60
0.75		1212	1167	573	71	69	68
1.00		1412	1309	678	54	59	73
1.25		2372	2220	1107	41	52	84
1.50		3116	3003	1519	29	39	88
Blank	40	366	173	142	191	183	-
0.50		869	744	362	151	87	58
0.75		1193	1088	546	89	79	69
1.00		1295	1169	615	68	63	71
1.25		1989	1893	993	57	51	81
1.50		3195	3056	1503	41	46	88
Blank	45	351	152	115	195	185	-
0.50		845	765	354	167	99	58
0.75		1062	982	501	101	81	66
1.00		1181	1012	522	79	76	70
1.25		1593	1406	768	63	69	78
1.50		2456	2384	1192	58	55	85
Blank	50	301	139	108	200	191	-
0.50		703	655	308	173	113	57
0.75		922	854	425	111	97	67
1.00		1007	963	507	87	88	70
1.25		1251	1114	573	72	78	75
1.50		2244	2159	1180	65	61	86

Table 3.73: Electrochemical impedance parameters for the corrosion of AZ31 alloy in 0.15 M NaCl solution in the presence of DO at different temperatures.

Inhibitor Concentration (mmol dm^{-3})	Temperature (°C)	R_{hf} (Ω cm^2)	R_f (Ω cm^2)	R_{dif} (Ω cm^2)	C_{dl} (μF cm^{-2})	C_f (μF cm^{-2})	η (%)
Blank	30	358	170	144	172	115	-
0.50		867	774	320	121	98	59
0.75		1245	1138	603	116	94	71
1.00		1400	1278	628	104	90	74
1.25		2980	2786	1367	100	86	89
1.50		3507	3367	1578	93	81	91
Blank	35	301	161	121	184	128	-
0.50		735	642	321	130	101	57
0.75		908	804	400	123	95	66
1.00		1041	975	452	111	90	72
1.25		1673	1562	758	101	87	82
1.50		2526	2413	1131	94	84	87
Blank	40	288	150	113	197	133	-
0.50		653	565	247	135	104	56
0.75		851	743	351	125	97	66
1.00		932	814	407	114	90	70
1.25		1426	1305	734	104	91	80
1.50		1992	1780	880	97	85	85
Blank	45	225	128	100	201	140	-
0.50		503	404	200	140	108	54
0.75		642	523	260	129	100	63
1.00		723	605	300	121	95	68
1.25		1002	903	451	109	92	77
1.50		1373	1032	524	100	89	84
Blank	50	130	123	73	218	147	-
0.50		279	177	90	143	113	53
0.75		368	198	97	131	103	62
1.00		406	231	145	127	97	67
1.25		549	401	208	114	95	76
1.50		750	602	315	102	90	82

Table 3.74: Electrochemical impedance parameters for the corrosion of AZ31 alloy in 0.20 M NaCl solution in the presence of DO at different temperatures.

Inhibitor Concentration (mmol dm^{-3})	Temperature (°C)	R_{hf} (Ω cm^2)	R_f (Ω cm^2)	R_{dif} (Ω cm^2)	C_{dl} (µF cm^{-2})	C_f (µF cm^{-2})	η (%)
Blank	30	170	109	95	193	191	-
0.50		400	311	154	130	102	57
0.75		580	457	228	124	97	69
1.00		604	502	250	119	94	71
1.25		1393	1300	756	108	89	88
1.50		1910	1792	932	99	85	89
Blank	35	166	97	79	190	199	-
0.50		377	256	129	133	105	55
0.75		525	410	203	128	99	68
1.00		632	541	250	120	96	72
1.25		1120	1009	522	111	90	85
1.50		1388	1269	664	103	87	88
Blank	40	158	90	70	212	210	-
0.50		352	240	101	138	108	54
0.75		471	362	154	130	100	66
1.00		553	450	227	125	99	72
1.25		922	820	411	112	94	83
1.50		1140	1055	531	102	90	85
Blank	45	125	78	58	220	219	-
0.50		262	138	81	142	111	52
0.75		344	231	109	134	103	63
1.00		420	302	145	128	100	71
1.25		679	548	254	114	97	82
1.50		777	618	309	103	92	84
Blank	50	103	73	52	243	232	-
0.50		230	132	84	150	114	51
0.75		270	182	105	142	106	62
1.00		323	200	114	137	100	67
1.25		470	323	173	120	99	76
1.50		586	429	220	111	95	82

Table 3.75: Electrochemical impedance parameters for the corrosion of AZ31 alloy in 0.25 M NaCl solution in the presence of DO at different temperatures.

Inhibitor Concentration (mmol dm^{-3})	**Temperature (°C)**	$\boldsymbol{R_{hf}}$ **(Ω cm^2)**	$\boldsymbol{R_f}$ **(Ω cm^2)**	$\boldsymbol{R_{dif}}$ **(Ω cm^2)**	$\boldsymbol{C_{dl}}$ **(µF cm^{-2})**	$\boldsymbol{C_f}$ **(µF cm^{-2})**	$\boldsymbol{\eta}$ **(%)**
Blank	30	201	115	99	205	195	-
0.50		450	334	115	138	119	55
0.75		627	506	248	131	107	67
1.00		702	613	310	120	99	71
1.25		1398	1300	750	113	93	86
1.50		1669	1538	876	102	87	88
Blank	35	150	107	85	217	205	-
0.50		334	216	108	142	123	55
0.75		450	328	170	133	109	66
1.00		512	434	217	124	100	70
1.25		858	751	356	114	95	82
1.50		1100	1003	513	104	92	86
Blank	40	141	98	72	221	222	-
0.50		297	166	90	143	125	52
0.75		406	296	150	132	112	65
1.00		445	326	163	126	104	68
1.25		826	694	340	115	98	82
1.50		879	760	372	105	96	83
Blank	45	105	81	68	230	223	-
0.50		210	113	85	146	128	50
0.75		269	174	93	135	114	61
1.00		298	190	100	127	105	64
1.25		552	388	174	118	100	80
1.50		555	402	203	106	96	81
Blank	50	99	70	55	248	239	-
0.50		186	108	79	150	130	46
0.75		242	162	85	148	121	59
1.00		253	189	100	136	116	60
1.25		394	221	115	128	110	74
1.50		458	363	152	112	105	78

Table 3.76: Electrochemical impedance parameters for the corrosion of AZ31 alloy in 0.05 M Na_2SO_4 solution in the presence of DO at different temperatures.

Inhibitor Concentration (mmol dm^{-3})	Temperature (°C)	R_{hf} (Ω cm^2)	R_f (Ω cm^2)	R_{dif} (Ω cm^2)	C_{dl} (μF cm^{-2})	C_f (μF cm^{-2})	η (%)
Blank	30	609	471	412	159	102	-
0.50		1139	1057	520	35	75	46
0.75		1358	1287	634	33	73	55
1.00		2183	2015	1009	25	70	72
1.25		4934	4802	2439	19	66	87
1.50		9312	9202	3890	17	50	93
Blank	35	510	367	303	176	129	-
0.50		923	802	400	57	82	45
0.75		1232	1115	548	40	76	58
1.00		1720	1603	811	35	72	70
1.25		2532	2350	1189	30	59	79
1.50		3923	3756	1505	28	57	86
Blank	40	477	333	288	201	146	-
0.50		1300	1201	665	65	84	63
0.75		1314	1212	684	58	77	63
1.00		1599	1480	729	46	63	71
1.25		1696	1503	751	43	60	71
1.50		2945	2812	1399	39	56	84
Blank	45	450	350	275	225	151	-
0.50		1512	1403	725	69	85	70
0.75		1603	1499	758	61	79	71
1.00		1805	1710	861	56	66	75
1.25		2278	2200	1094	50	62	80
1.50		2994	2845	1405	44	58	85
Blank	50	412	354	252	261	168	-
0.50		1054	967	508	71	88	60
0.75		1284	1193	645	64	81	68
1.00		1435	1362	723	60	69	71
1.25		1830	1688	895	57	63	77
1.50		2705	2585	1173	48	59	85

Table 3.77: Electrochemical impedance parameters for the corrosion of AZ31 alloy in 0.10 M Na_2SO_4 solution in the presence of DO at different temperatures.

Inhibitor Concentration (mmol dm^{-3})	Temperature (°C)	R_{hf} (Ω cm^2)	R_f (Ω cm^2)	R_{dif} (Ω cm^2)	C_{dl} (µF cm^{-2})	C_f (µF cm^{-2})	η (%)
Blank	30	460	343	319	201	188	-
0.50		985	856	427	37	79	53
0.75		1048	952	450	33	76	566
1.00		1832	1702	886	27	70	74
1.25		3429	3308	1834	20	68	86
1.50		6532	6411	3102	16	52	92
Blank	35	432	322	293	224	191	-
0.50		860	775	348	60	83	49
0.75		1100	1001	500	42	77	60
1.00		1852	1701	853	36	72	76
1.25		2339	2200	1089	31	60	81
1.50		4170	4034	2005	23	58	89
Blank	40	403	254	227	249	225	-
0.50		840	718	358	63	81	52
0.75		892	801	410	59	78	54
1.00		1649	1502	843	44	72	75
1.25		1832	1711	869	41	71	78
1.50		3359	3208	1734	38	66	88
Blank	45	387	193	160	269	237	-
0.50		779	681	340	60	94	50
0.75		886	812	403	57	81	56
1.00		1558	1429	741	40	81	75
1.25		1856	1702	800	38	71	79
1.50		3291	3105	1501	22	68	88
Blank	50	373	209	161	278	241	-
0.50		725	599	248	65	103	48
0.75		760	641	326	57	87	50
1.00		1300	1204	600	48	82	71
1.25		1935	1799	918	39	79	80
1.50		2988	2819	1425	30	75	87

Table 3.78: Electrochemical impedance parameters for the corrosion of AZ31 alloy in 0.15 M Na_2SO_4 solution in the presence of DO at different temperatures.

Inhibitor Concentration (mmol dm^{-3})	Temperature (°C)	R_{hf} (Ω cm^2)	R_f (Ω cm^2)	R_{dif} (Ω cm^2)	C_{dl} (μF cm^{-2})	C_f (μF cm^{-2})	η (%)
Blank	30	434	420	383	244	167	-
0.50		904	819	402	44	83	51
0.75		968	823	414	41	80	55
1.00		1630	1541	822	38	76	73
1.25		2784	2599	1245	34	71	84
1.50		3954	3812	1584	31	66	89
Blank	35	463	300	280	278	169	-
0.50		940	845	421	47	85	50
0.75		1096	989	470	44	81	58
1.00		1897	1800	943	40	79	75
1.25		2801	2704	1308	36	73	83
1.50		3999	3859	1756	33	69	88
Blank	40	380	230	201	299	180	-
0.50		764	658	325	49	88	50
0.75		903	834	415	45	82	57
1.00		1402	1320	806	41	77	72
1.25		1981	1834	920	40	75	80
1.50		3182	3076	1529	35	71	88
Blank	45	273	237	200	307	188	-
0.50		549	430	217	52	91	50
0.75		617	500	246	48	83	55
1.00		1043	950	474	43	78	74
1.25		1375	1205	600	42	76	80
1.50		1891	1766	895	38	73	86
Blank	50	245	200	178	321	200	-
0.50		454	371	157	55	92	46
0.75		544	488	239	51	85	55
1.00		881	760	354	47	80	72
1.25		1135	1022	511	45	78	78
1.50		1502	1416	751	42	76	84

Table 3.79: Electrochemical impedance parameters for the corrosion of AZ31 alloy in 0.20 M Na_2SO_4 solution in the presence of DO at different temperatures.

Inhibitor Concentration (mmol dm^{-3})	Temperature (°C)	R_{hf} (Ω cm^2)	R_f (Ω cm^2)	R_{dif} (Ω cm^2)	C_{dl} (µF cm^{-2})	C_f (µF cm^{-2})	η (%)
Blank	30	301	226	171	269	179	-
0.50		615	521	273	43	85	51
0.75		644	540	222	40	83	53
1.00		1074	967	475	38	80	71
1.25		1810	1711	877	35	77	83
1.50		2831	2710	1301	32	76	89
Blank	35	287	224	190	287	186	-
0.50		578	470	234	44	87	50
0.75		602	511	202	41	84	52
1.00		970	805	397	39	82	70
1.25		1605	1502	794	38	78	82
1.50		2293	2189	1044	33	78	87
Blank	40	259	192	163	301	191	-
0.50		509	403	195	47	90	49
0.75		525	412	210	42	85	50
1.00		828	721	353	40	84	68
1.25		1334	1229	601	39	80	80
1.50		1923	1812	887	35	81	86
Blank	45	236	203	167	321	201	-
0.50		459	388	179	50	91	49
0.75		502	487	241	44	87	53
1.00		702	681	339	41	85	66
1.25		1101	997	486	40	82	78
1.50		1457	1321	677	36	80	83
Blank	50	218	187	159	333	219	-
0.50		405	312	151	52	94	46
0.75		422	317	164	45	90	48
1.00		613	500	248	42	86	64
1.25		928	796	400	41	82	76
1.50		1220	1185	578	38	81	82

Table 3.80: Electrochemical impedance parameters for the corrosion of AZ31 alloy in 0.25 M Na_2SO_4 solution in the presence of DO at different temperatures.

Inhibitor Concentration (mmol dm^{-3})	Temperature (°C)	R_{hf} (Ω cm^2)	R_f (Ω cm^2)	R_{dif} (Ω cm^2)	C_{dl} (µF cm^{-2})	C_f (µF cm^{-2})	η (%)
Blank	30	392	301	280	320	240	-
0.50		789	672	336	46	89	50
0.75		816	759	378	44	84	52
1.00		1311	1201	589	41	79	70
1.25		2199	2015	1004	38	75	82
1.50		3226	3118	1538	35	68	87
Blank	35	350	250	221	333	259	-
0.50		705	614	303	49	92	50
0.75		711	630	311	46	86	51
1.00		1124	1059	556	41	81	69
1.25		1901	1800	926	39	76	81
1.50		2601	2512	1307	37	70	86
Blank	40	201	114	96	345	267	-
0.50		380	189	99	52	94	47
0.75		402	311	154	47	90	50
1.00		621	501	254	43	89	67
1.25		899	791	403	41	77	77
1.50		1290	1163	656	37	69	84
Blank	45	180	109	80	359	280	-
0.50		334	218	110	54	95	46
0.75		340	222	116	48	91	47
1.00		533	410	209	46	88	66
1.25		762	655	329	43	79	76
1.50		1028	978	438	40	71	82
Blank	50	170	100	64	389	308	-
0.50		301	229	115	57	97	43
0.75		320	238	106	53	93	46
1.00		472	302	155	50	90	64
1.25		662	511	249	47	83	74
1.50		901	800	397	43	75	81

Table 3.81: Activation parameters for the corrosion of AZ31 alloy in NaCl solutions containing different concentrations of DO inhibitor.

Concentration of NaCl (M)	Concentration of inhibitor (mmol dm^{-3})	E_a (kJ mol^{-1})	$\Delta H^{\#}$ (kJ mol^{-1})	$\Delta S^{\#}$ (J mol^{-1} K^{-1})
0.05	Blank	34.00	34.66	-128.69
	0.50	56.72	54.13	-75.07
	0.75	61.30	58.71	-62.77
	1.00	63.78	61.19	-56.53
	1.25	85.20	82.60	6.23
	1.50	95.10	92.50	33.42
0.1	Blank	24.55	20.97	-162.88
	0.50	25.24	21.74	-181.02
	0.75	25.34	22.53	-171.38
	1.00	26.34	23.58	-169.09
	1.25	40.34	42.51	-116.55
	1.50	63.11	60.52	-55.53
0.15	Blank	23.57	18.70	-174.42
	0.50	29.39	26.80	-151.06
	0.75	31.60	29.49	-144.66
	1.00	32.37	30.27	-140.00
	1.25	53.50	49.01	-90.04
	1.50	54.61	50.91	-81.22
0.20	Blank	20.67	18.08	-167.27
	0.50	28.15	25.55	-149.56
	0.75	31.60	25.54	-141.08
	1.00	38.14	29.00	-136.76
	1.25	45.90	43.31	-101.26
	1.50	46.93	44.33	-99.68
0.25	Blank	16.94	15.30	-175.67
	0.50	21.40	18.81	-169.77
	0.75	26.16	23.57	-156.96
	1.00	27.55	24.95	-129.61
	1.25	36.51	33.92	-121.13
	1.50	39.49	36.90	-96.54

Table 3.82: Activation parameters for the corrosion of AZ31 alloy in Na_2SO_4 solutions containing different concentrations of DO inhibitor.

Concentration of Na_2SO_4 (M)	Concentration of inhibitor (mmol dm^{-3})	E_a (kJ mol^{-1})	$\Delta H^\#$ (kJ mol^{-1})	$\Delta S^\#$ (J mol^{-1} K^{-1})
0.05	Blank	44.17	40.04	-108.74
	0.50	44.77	22.00	-90.29
	0.75	45.46	32.86	-83.38
	1.00	47.63	40.56	-69.17
	1.25	65.12	62.52	-50.05
	1.50	83.57	80.97	-4.40
0.1	Blank	39.64	33.78	-126.03
	0.50	44.07	41.84	-107.29
	0.75	44.29	41.65	-108.88
	1.00	46.66	44.09	-105.90
	1.25	55.67	55.96	-72.07
	1.50	77.11	72.57	-24.77
0.15	Blank	35.65	28.33	-137.09
	0.50	38.04	35.45	-121.21
	0.75	38.00	38.23	-118.14
	1.00	40.83	38.77	-84.88
	1.25	51.68	49.09	-49.21
	1.50	64.02	61.44	-35.00
0.20	Blank	35.21	23.87	-149.98
	0.50	44.54	41.68	-98.27
	0.75	44.82	41.95	-91.20
	1.00	50.39	47.80	-83.55
	1.25	54.21	51.62	-75.15
	1.50	62.67	60.08	-51.54
0.25	Blank	24.39	18.81	−164.69
	0.50	28.80	26.21	-146.49
	0.75	29.46	26.87	-144.66
	1.00	39.47	29.65	-127.28
	1.25	40.56	36.88	-121.46
	1.50	45.04	42.45	-104.75

Table 3.83: Thermodynamic parameters for the adsorption of DO inhibitor on AZ31 alloy in NaCl solution.

Concentration of NaCl (M)	Temperature (°C)	ΔG^0_{ads} (kJ mol^{-1})	ΔH^0_{ads} (kJ mol^{-1})	ΔS^0_{ads} (J mol^{-1} K^{-1})
0.05	30	-30.04	-50.24	-68.0
	35	-29.41		
	40	-28.94		
	45	-28.61		
	50	-28.24		
0.10	30	-28.41	-42.17	-45.4
	35	-28.18		
	40	-27.95		
	45	-27.73		
	50	-27.50		
0.15	30	-28.45	-33.30	-16.0
	35	-28.31		
	40	-28.29		
	45	-28.21		
	50	-28.13		
0.20	30	-27.39	-32.84	-18.2
	35	-27.29		
	40	-27.20		
	45	-27.16		
	50	-27.02		
0.25	30	-26.79	-31.34	-15.8
	35	-26.72		
	40	-26.45		
	45	-26.37		
	50	-26.30		

Table 3.84: Thermodynamic parameters for the adsorption of DO inhibitor on AZ31 alloy in Na_2SO_4 solution.

Concentration of Na_2SO_4 (M)	Temperature (°C)	ΔG^0_{ads} (kJ mol^{-1})	ΔH^0_{ads} (kJ mol^{-1})	ΔS^0_{ads} (J mol^{-1} K^{-1})
0.05	30	-29.94	-51.0	-69.5
	35	-29.45		
	40	-29.24		
	45	-28.89		
	50	-28.55		
0.1	30	-28.49	-45.4	-55.8
	35	-28.21		
	40	-27.93		
	45	-27.65		
	50	-27.37		
0.15	30	-28.24	-42.2	-46.0
	35	-28.03		
	40	-27.80		
	45	-27.57		
	50	-27.34		
0.20	30	-28.64	-40.1	-37.8
	35	-28.45		
	40	-28.26		
	45	-28.07		
	50	-27.89		
0.25	30	-28.91	-37.4	-28.0
	35	-28.77		
	40	-28.63		
	45	-28.49		
	50	-28.35		

Table 3.85: Calculated DFT parameters for DO inhibitor.

Parameters	Value
Total energy (KeV)	-2.315
Energy gap (eV)	3.149
E_{HOMO} (eV)	-0.756
E_{LUMO} (eV)	-3.904
Dipole moment (Debye)	54.641
Electronegativity (eV)	2.33
Chemical hardness (eV)	1.574
Electron affinity (eV)	3.904
Ionization potential (eV)	0.756
Softness (eV^{-1})	0.635

3.6 SODIUM 2,2'-(11,20-DIDECYL-12,19-DIOXO-11,14,17,20-TETRAAZATRIACONTANE-14,17-DIYL)DIACETATE (DC) AS CORROSION INHIBITOR FOR AZ31 ALLOY IN SODIUM CHLORIDE AND SODIUM SULFATE SOLUTIONS

3.6.1 Potentiodynamic polarization measurements

Potentiodynamic polarization plots for the corrosion of AZ31 Mg alloy in 0.1 M NaCl and 0.1 M Na_2SO_4 at 50 °C in the presence of varying concentrations of DC are shown in Fig. 3.61. Similar plots were obtained at other temperatures also. The polarization curves are shifted to a lower current density region as the concentration of DC increases, which reflects the corrosion inhibition produced by the inhibitor. But there is no significant change in the shape of the Tafel branches, indicating that DC did not alter the corrosion mechanism. DC might have played an important role by blocking the active sites of reaction on the metal surface, likely to be by adsorption.

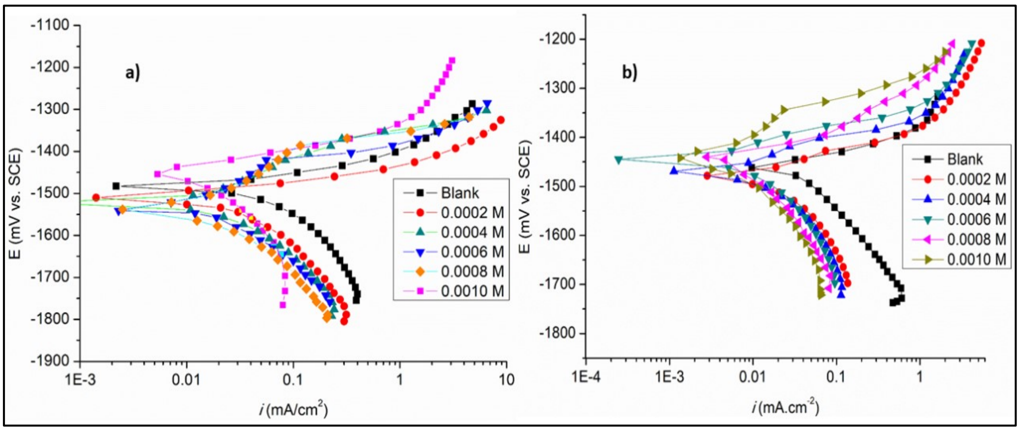

Fig. 3. 61: Potentiodynamic polarization curves for the corrosion of AZ31 alloy in the presence of different concentrations of DC in a) 0.1 M NaCl solution and b) 0.1 M Na_2SO_4 solution at 50 °C.

The electrochemical polarization parameters are summarized in Tables 3.86 to 3.95. From Table 3.86 to 3.95, it is observed that in the presence of DC, i_{corr} (corrosion current density) decreases, which shows that corrosion inhibition is achieved upon the addition of DC. The inhibition efficiency increases with the increase in the concentration of DC up to an optimum concentration of 0.001 M, and above which the increase in inhibition efficiency is negligible. Efficient surface coverage could be credited to the increase in inhibition efficiency. Thus, 0.001 M could be attributed as the most optimum and economic concentration of DC for inhibiting AZ31 Mg alloy, at the presented conditions.

3.6.2 Electrochemical impedance spectroscopy

The Nyquist plots for the corrosion of alloy AZ31 Mg alloy in 0.1 M NaCl and 0.1 M Na_2SO_4 medium at 50 °C in the presence of varying concentrations of DC are represented in Fig. 3.62. The Nyquist plots are similar to the ones discussed in the earlier sections. As shown in Fig. 3.62, there is an increase in the size of capacitance loop with the increase in the concentration of DC with no change in its shape, which implies that DC consistently reduces the corrosion rate without changing the corrosion mechanism. The impedance parameter are summarized in Tables 3.96 to 3.105.

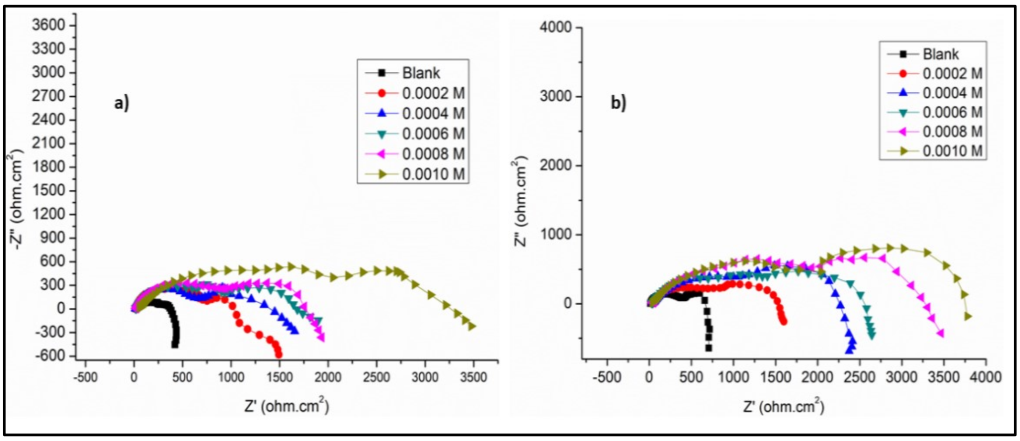

Fig. 3.62: Nyquist plots for the corrosion of AZ31 alloy in a) 0.1 M NaCl and b) 0.1 M Na_2SO_4 in the presence of different concentrations of DC at 50 °C.

It can be seen from Tables 3.96 to 3.105 that the increase in the concentration of DC results in an increase in R_f, and R_{dif} and the decrease in both C_{dl} and C_f, which can be possibly due to the decrease in local dielectric constant or increase in the thickness of surface film. R_f on the other hand is the measure of protective performance of surface film, which increases upon the addition of DC.

The Bode plots of phase angle and amplitude for the corrosion of the AZ31 alloy immersed in 0.1 M NaCl and 0.1 M Na_2SO_4 solutions at 50 °C in the presence of varying amounts of DC, are shown in Fig. 3.63 and Fig. 3.64, respectively. As seen from the Bode plots, both the impedance modulus (Z_{mod}) at low frequency and the phase maximum (θ_{max}) at intermediate frequency increase with the increase in DC concentration, which collectively indicates that the presence of highly protective surface film protects the alloy surface.

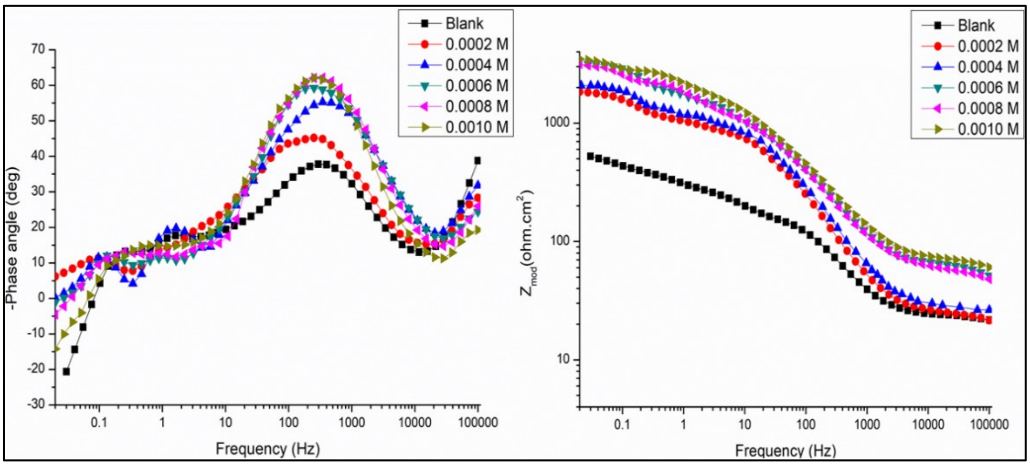

Fig. 3.63: Bode phase angle and amplitude plots for the corrosion of AZ31 alloy in 0.1 M NaCl medium in the presence of different concentrations of DC at 50 °C.

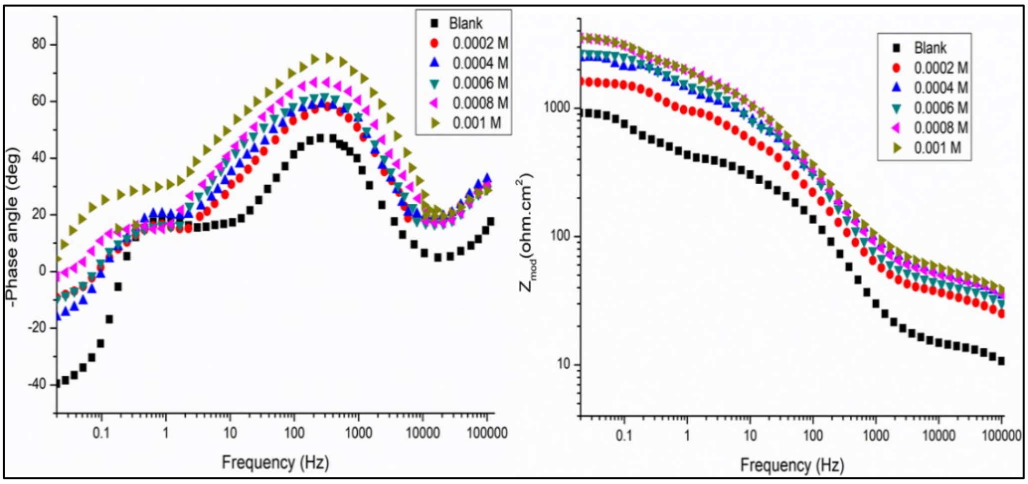

Fig. 3.64: Bode phase angle and amplitude plots for the corrosion of AZ31 alloy in 0.1 M Na_2SO_4 medium in the presence of different concentrations of DC at 50 °C.

3.6.3 Effect of temperature

The values presented in Tables 3.85 and 3.94 show a steady decrease in inhibition efficiency as the temperature increases, indicating the physisorption of the inhibitor molecules on the allot surface. On the other hand, it can also be due to the increased solubility of the magnesium - DC precipitate film, causing desorption of the inhibitor layer from the alloy surface (Wang et al. 2010). The Arrhenius plots for the corrosion of AZ31 alloy in 0.1 M NaCl and 0.1 M Na_2SO_4 containing varying concentrations of DC compound are shown in Fig. 3. 65.

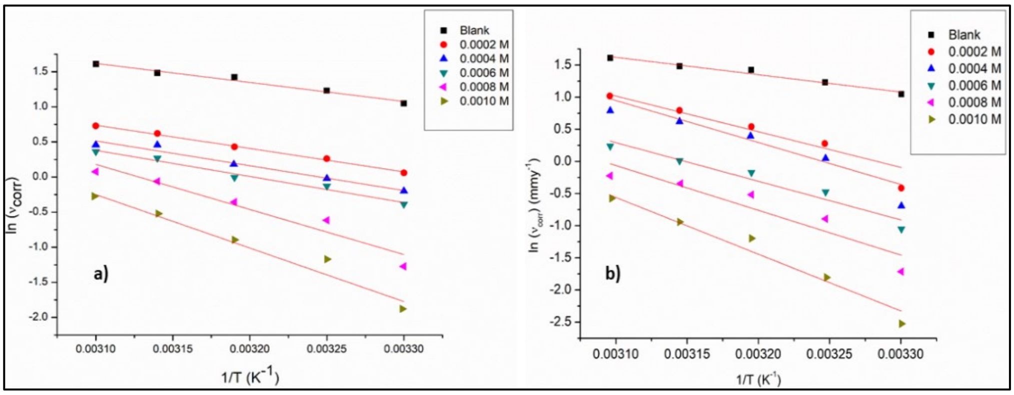

Fig. 3.65: Arrhenius plots for the corrosion of AZ31 magnesium alloy in a) 0.1 M NaCl and b) 0.1 M Na_2SO_4 media in the presence of different concentrations of DC.

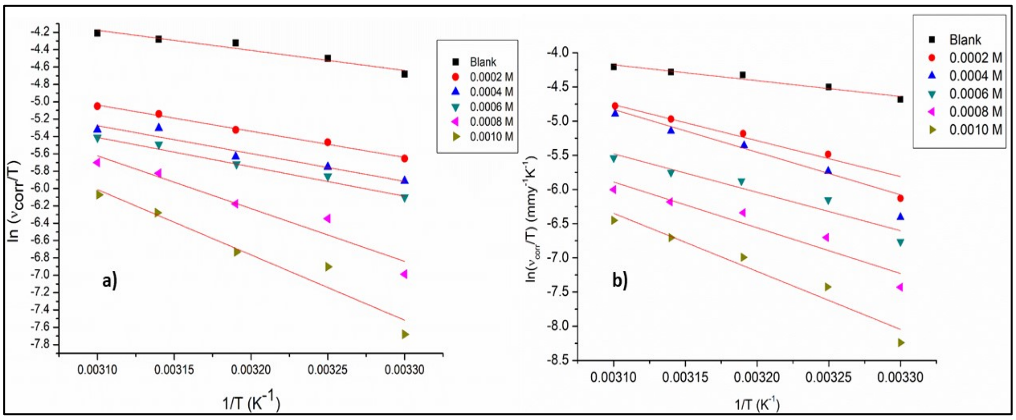

Fig. 3.66: The plots of ln(v_{corr} /T) versus 1/T for the corrosion of AZ31 magnesium alloy in a) 0.1 M NaCl and b) 0.1 M Na_2SO_4 in the presence of different concentrations of DC.

Fig. 3. 66 presents the plots of ln (υ_{corr}/T) versus ($1/T$) for the corrosion of AZ31 Mg alloy in 0.1 M NaCl and 0.1 M Na_2SO_4 containing varying concentrations of DC. Calculated data of $\Delta H^{\#}$, $\Delta S^{\#}$, E_a, are tabulated in Tables 3.106 and 3.107.

As observed from the data in Table 3.106 and 3.107, E_a values increase with the increase in the concentration of DC, which indicates the increased energy barrier for the occurrence of corrosion due to the increase in surface coverage brought by the inhibitor (Ardelean et al. 2008). $\Delta S^{\#}$ in both blank and DC containing systems shows large negative values which show that the activated complex in the rate-determining step represents association rather than dissociation.

3.6.4 Adsorption Behavior

The values of θ at different DC concentrations (C_{inh}) were calculated from the results of polarization studies. The values of θ and C_{inh} were fitted to various adsorption isotherms with an aim to obtain a linear relationship. It was found that Langmuir adsorption isotherm gave best fit results. The Langmuir adsorption isotherms for the adsorption of DC on AZ31 Mg alloy surface in 0.1 M NaCl and 0.1 M Na_2SO_4 at different temperatures are presented in Fig. 3.67. The graph exhibited linear behavior, but the slopes are not equal to one. The average linear regression coefficient (R^2) of 0.95 was obtained. This deviation from ideal Langmuir behavior can be attributed to interactions among the adsorbed species (Baril and Pébère 2001).

The thermodynamic parameters for the adsorption of DC on the AZ31 Mg alloy surface in NaCl and Na_2SO_4 are tabulated in Tables 3.108 and 3.109. The negative values of ΔG°_{ads} indicate that the process of adsorption of DC is spontaneous and an adsorbed film on the alloy surface is stable. The values obtained for ΔG°_{ads} are negative and fall within the range of -28 to -33 kJ mol^{-1}, indicating the adsorption of the inhibitor molecules are by both physical and chemical processes. The fact that both ΔG°_{ads} and inhibition efficiency decrease with the increase in temperature indicates that the adsorption of the inhibitor on the AZ31 alloy surface in NaCl and Na_2SO_4 medium is not favored at high temperature and hence can be considered to be predominantly physisorption. The standard adsorption entropy value is negative; indicating that a decrease in disordering takes place when the inhibitor species gets adsorbed on the alloy surface.

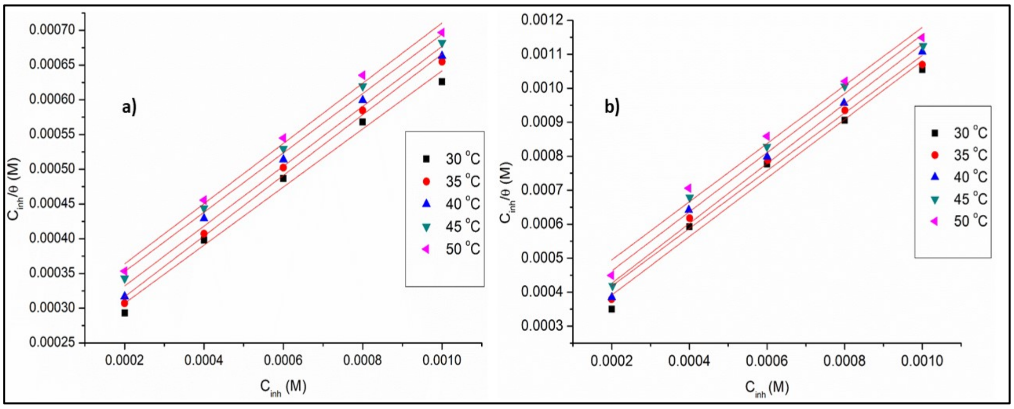

Fig. 3.67: Langmuir's adsorption isotherm for the adsorption of DC on AZ31 magnesium alloy in a) 0.1 M NaCl medium and b) 0.1 M Na_2SO_4 medium.

3.6.5 SEM

Fig. 3.68 depicts the SEM image and EDX spectrum of AZ31 Mg alloy surface immersed in 0.1 M NaCl solution in the presence of 0.001 M DC. Fig. 3.69 presents the SEM image and EDX spectrum of AZ31 Mg alloy surface immersed in 0.1 M Na_2SO_4 solution in the presence of 0.001 M DC. In the EDX spectra apart from the peaks of Mg, Al, Zn, and Cl, additional small peaks for carbon, oxygen, and nitrogen are obtained, which indicate the presence of some organic moieties on the alloy surface, possibly the surface adsorbed DC molecules. It is also observed that the intensity of the Mg peak is reduced.

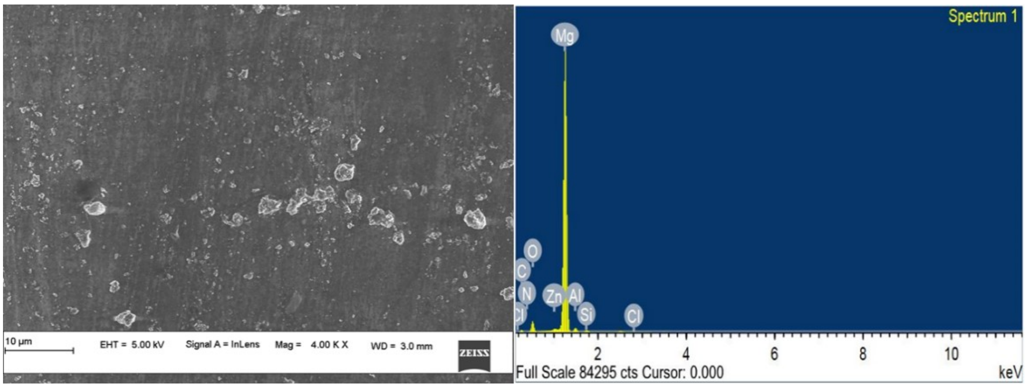

Fig. 3.68: SEM image and EDX spectrum of the AZ31 magnesium alloy surface immersed in 0.1 M NaCl in the presence of DC for 3 h at 30 °C.

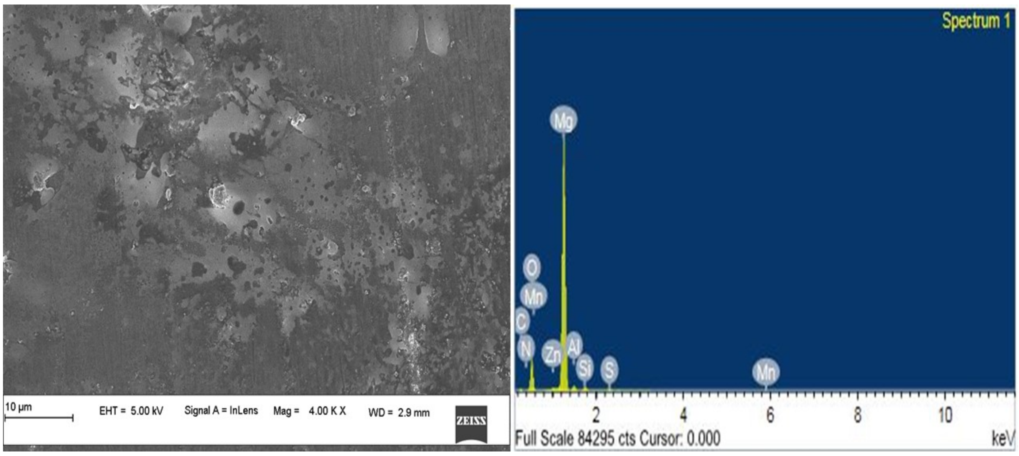

Fig. 3.69: SEM image and EDX spectrum of the AZ31 magnesium alloy surface immersed in 0.1 M Na_2SO_4 in the presence of DC for 3 h at 30 °C.

3.6.6 XPS

Fig. 3.70 and Fig. 3.71 show the XPS survey spectra and individual spectrum corresponding to different elements present on the surface of the AZ31 alloy immersed in 0.1 M NaCl and 0.1 M Na_2SO_4 media for 3 h in the presence of 0.001 M DC at 30 °C. The high-resolution Mg 2s spectrum for magnesium alloys immersed in DC inhibitor has peaks assigned to Mg, MgO, and $Mg(OH)_2$.

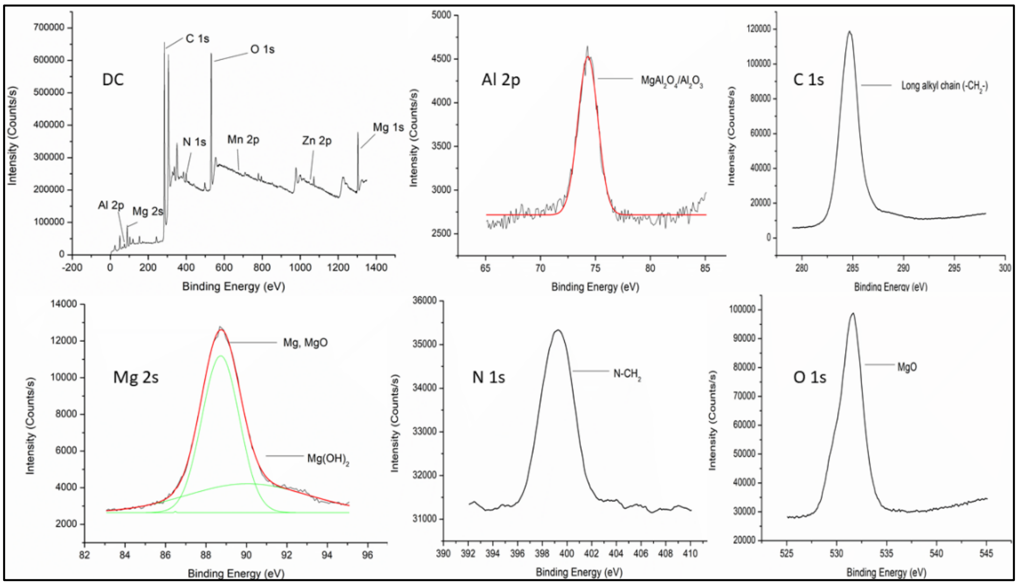

Fig. 3.70: XPS survey spectra and individual spectra of elements (Mg 2s, Al 2p, C 1s, O 1s and, N 1s) of AZ31 Mg alloy immersed in 0.1 M NaCl medium in the presence of 0.001 M DC for 3 h at 30 °C.

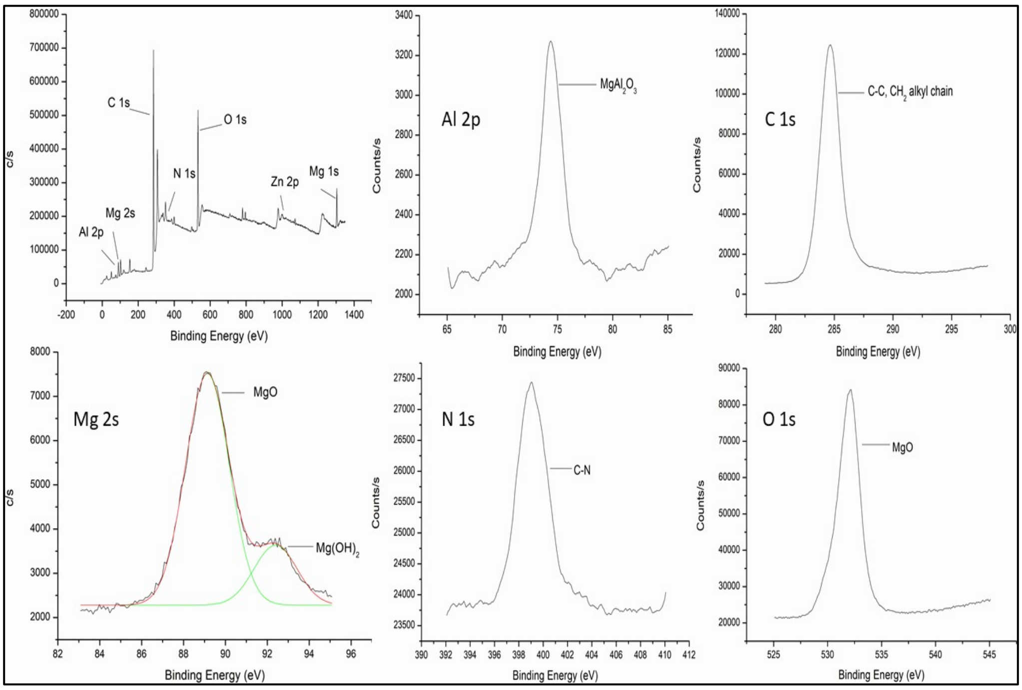

Fig. 3.71: XPS survey spectra and individual spectra of elements (Mg 2s, Al 2p, C 1s, O 1s and, N 1s) of AZ31 Mg alloy immersed in 0.1 M Na_2SO_4 medium in the presence of 0.001 M DC for 3 h at 30 °C.

The corrosion is retarded since the peak area of Mg is larger than $Mg(OH)_2$. For the O 1s spectrum, the peak ~531.2 corresponds to MgO. The Al 2p spectra show a broad peak centered at 74.7 eV which indicates the co-existence of aluminum oxide or aluminum hydroxide. The C 1s spectra can be fitted to the presence of C-C/C-H groups at peak 284.8 eV. N 1s spectrum shows a peak at 399.2 eV, which shows the presence of C-N bond. The XPS results show that the inhibitor not only is adsorbed on the surface to repel the water molecules.

3.6.7 DFT

The optimized structure for the inhibitor, DC, was obtained using theoretical calculations using B3LYP hybrid functional model with def-TZVP basis set and presented in Fig. 3. 72. The structure of the molecule is optimized and the negative value of the total energy (-2.629 KeV) predicts a thermodynamically stable molecule. E_{HOMO} value shows the physical adsorption as the basis for corrosion inhibition action. The low bandgap energy shows higher reactivity of the inhibitor molecules, leading to their ready adsorption on AZ31 Mg alloy surface. The high value of the dipole moment implies a stronger interaction of DC molecules with the AZ31 alloy surface. The strong tendency of DC to attract electrons from metal shows a higher electronegativity value, which in turn indicates the higher ability of DC to act as a corrosion inhibitor. The calculated parameters are presented in Table 3.110.

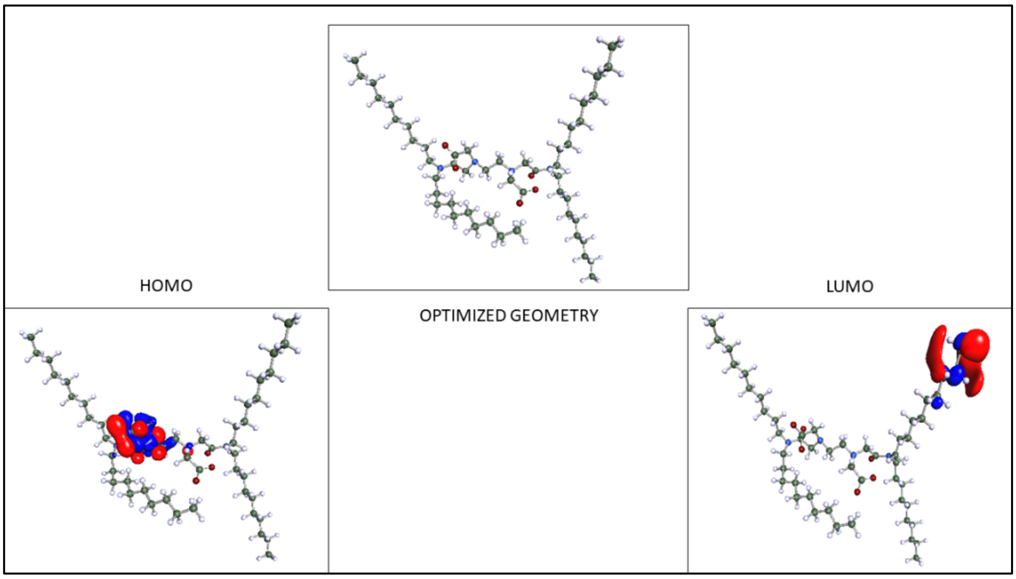

Fig. 3.72: Optimized structure and the frontier molecular orbital density distribution of the DC molecule.

3.6.8 Summary

Anionic Gemini surfactant, DC, was synthesized and used as a corrosion inhibitor on AZ31 Mg alloy in different concentrations of NaCl and Na_2SO_4. The surfactant DC acted as a mixed type of inhibitor and the inhibitor efficiency increased with the increase in the concentration of DC and decreased with the rise in temperature and the increase in the concentration of NaCl and Na_2SO_4 in the medium. The surfactant was adsorbed predominantly through physisorption and obeyed Langmuir adsorption isotherm. The quantum chemical calculation supported the experimental observation.

Table 3.86: Electrochemical polarization parameters for the corrosion of AZ31 alloy in 0.05 M NaCl solution in the presence of DC at different temperatures.

Inhibitor concentration ($mmol.dm^{-3}$)	Temperature (°C)	E_{corr} vs SCE (mV)	i_{corr} ($\mu A\ cm^{-2}$)	$-\beta_c$ ($mV\ dec^{-1}$)	v_{corr} ($mm\ y^{-1}$)	η (%)
Blank	30	-1514	70.10	99	1.51	-
0.2		-1521	20.42	67	0.44	71
0.4		-1534	15.32	50	0.33	78
0.6		-1540	12.99	44	0.28	81
0.8		-1500	4.64	31	0.10	93
1.0		-1505	1.52	18	0.04	97
Blank	35	-1490	112.81	122	2.43	-
0.2		-1499	37.14	73	0.80	67
0.4		-1488	27.85	54	0.60	75
0.6		-1523	22.28	49	0.48	80
0.8		-1515	10.67	35	0.23	90
1.0		-1520	6.96	22	0.15	94
Blank	40	-1500	168.06	129	3.62	-
0.2		-1513	58.03	76	1.25	65
0.4		-1521	44.56	56	0.96	73
0.6		-1500	38.06	51	0.82	77
0.8		-1511	20.89	38	0.45	87
1.0		-1520	14.85	26	0.32	91
Blank	45	-1503	183.38	134	3.95	-
0.2		-1533	65.92	79	1.42	64
0.4		-1505	52.46	59	1.13	71
0.6		-1514	45.03	54	0.97	75
0.8		-1523	27.85	42	0.60	85
1.0		-1490	19.96	29	0.43	89
Blank	50	-1493	197.77	140	4.26	-
0.2		-1507	74.28	82	1.60	62
0.4		-1514	62.67	62	1.35	68
0.6		-1521	52.92	58	1.14	73
0.8		-1525	33.42	46	0.72	83
1.0		-1530	27.39	32	0.59	86

Table 3.87: Electrochemical polarization parameters for the corrosion of AZ31 alloy in 0.10 M NaCl solution in the presence of DC at different temperatures.

Inhibitor concentration ($mmol.dm^{-3}$)	Temperature (°C)	E_{corr} vs SCE (mV)	i_{corr} ($\mu A\ cm^{-2}$)	$-\beta_c$ ($mV\ dec^{-1}$)	v_{corr} ($mm\ y^{-1}$)	η (%)
Blank	30	-1483	154.03	135	3.34	-
0.2		-1436	48.98	38	1.06	68
0.4		-1442	37.74	27	0.82	75
0.6		-1417	31.54	27	0.68	79
0.8		-1507	13.13	19	0.28	91
1.0		-1534	6.42	15	0.14	95
Blank	35	-1489	171.58	141	3.73	-
0.2		-1532	60.38	30	1.30	65
0.4		-1505	45.07	22	0.98	73
0.6		-1518	41.10	27	0.88	76
0.8		-1470	25.10	25	0.54	85
1.0		-1429	14.40	21	0.31	91
Blank	40	-1502	210.77	165	4.54	-
0.2		-1497	64.10	23	1.38	63
0.4		-1501	52.40	28	1.12	69
0.6		-1530	43.40	26	0.93	75
0.8		-1519	30.30	25	0.65	82
1.0		-1426	16.50	22	0.35	90
Blank	45	-1516	225.52	162	4.90	-
0.2		-1517	86.60	29	1.86	61
0.4		-1519	73.50	22	1.58	67
0.6		-1529	60.90	29	1.31	73
0.8		-1505	43.80	24	0.94	80
1.0		-1480	31.20	14	0.67	86
Blank	50	-1490	235.47	173	5.11	-
0.2		-1505	96.40	27	2.07	59
0.4		-1506	75.80	28	1.69	66
0.6		-1497	66.90	20	1.44	71
0.8		-1527	50.30	18	1.08	78
1.0		-1470	32.80	15	0.70	86

Table 3.88: Electrochemical polarization parameters for the corrosion of AZ31 alloy in 0.15 M NaCl solution in the presence of DC at different temperatures.

Inhibitor concentration ($mmol.dm^{-3}$)	Temperature (°C)	E_{corr} vs SCE (mV)	i_{corr} ($\mu A\ cm^{-2}$)	$-\beta_c$ ($mV\ dec^{-1}$)	v_{corr} ($mm\ y^{-1}$)	η (%)
Blank	30	-1537	233.52	150	5.03	-
0.2		-1521	78.92	80	1.70	66
0.4		-1503	60.35	74	1.30	74
0.6		-1540	52.46	61	1.13	77
0.8		-1514	25.53	50	0.55	89
1.0		-1509	12.99	43	0.28	94
Blank	35	-1500	333.34	155	7.18	-
0.2		-1520	118.85	84	2.56	64
0.4		-1502	92.85	77	2.00	72
0.6		-1498	86.35	65	1.86	74
0.8		-1495	55.71	53	1.20	83
1.0		-1512	32.96	47	0.71	90
Blank	40	-1515	455.90	168	9.82	-
0.2		-1509	176.42	88	3.80	61
0.4		-1524	153.20	79	3.30	66
0.6		-1531	126.74	69	2.73	72
0.8		-1539	88.21	56	1.90	80
1.0		-1497	51.99	50	1.12	88
Blank	45	-1491	478.65	170	10.31	-
0.2		-1489	192.67	92	4.15	59
0.4		-1521	171.77	81	3.70	64
0.6		-1526	140.67	71	3.03	70
0.8		-1530	107.24	58	2.31	77
1.0		-1534	64.99	53	1.40	86
Blank	50	-1475	567.33	194	12.22	-
0.2		-1500	241.41	95	5.20	57
0.4		-1512	213.56	85	4.60	62
0.6		-1530	185.70	76	4.00	67
0.8		-1533	139.27	61	3.00	75
1.0		-1496	90.53	56	1.95	84

Table 3.89: Electrochemical polarization parameters for the corrosion of AZ31 alloy in 0.20 M NaCl solution in the presence of DC at different temperatures.

Inhibitor concentration ($mmol.dm^{-3}$)	Temperature (°C)	E_{corr} vs SCE (mV)	i_{corr} ($\mu A\ cm^{-2}$)	$-\beta_c$ ($mV\ dec^{-1}$)	v_{corr} ($mm\ y^{-1}$)	η (%)
Blank	30	-1500	432.55	189	9.40	-
0.2		-1533	155.52	94	3.35	64
0.4		-1540	123.03	85	2.65	72
0.6		-1513	109.10	76	2.35	75
0.8		-1510	57.10	68	1.23	87
1.0		-1542	34.81	56	0.75	92
Blank	35	-1485	457.04	214	9.93	-
0.2		-1496	174.09	96	3.75	62
0.4		-1507	136.95	88	2.95	70
0.6		-1516	123.03	79	2.65	73
0.8		-1509	68.71	71	1.48	85
1.0		-1522	51.06	59	1.10	90
Blank	40	-1483	489.13	181	10.63	-
0.2		-1495	198.24	100	4.27	60
0.4		-1499	162.49	91	3.50	67
0.6		-1505	141.60	82	3.05	71
0.8		-1524	84.49	75	1.82	83
1.0		-1530	59.42	62	1.28	88
Blank	45	-1511	687.77	211	14.75	-
0.2		-1519	287.84	103	6.20	58
0.4		-1523	250.70	95	5.40	63
0.6		-1526	219.59	85	4.73	68
0.8		-1499	162.49	79	3.50	76
1.0		-1508	109.10	65	2.35	84
Blank	50	-1497	709.98	171	15.43	-
0.2		-1537	313.37	107	6.75	56
0.4		-1508	273.91	98	5.90	60
0.6		-1522	248.38	88	5.35	65
0.8		-1528	191.74	83	4.13	73
1.0		-1518	133.24	69	2.87	81

Table 3.90: Electrochemical polarization parameters for the corrosion of AZ31 alloy in 0.25 M NaCl solution in the presence of DC at different temperatures.

Inhibitor concentration ($mmol.dm^{-3}$)	Temperature (°C)	E_{corr} vs SCE (mV)	i_{corr} ($\mu A\ cm^{-2}$)	$-\beta_c$ ($mV\ dec^{-1}$)	υ_{corr} ($mm\ y^{-1}$)	η (%)
Blank	30	-1526	520.41	190	11.31	-
0.2		-1515	194.06	145	4.18	63
0.4		-1509	155.52	129	3.35	70
0.6		-1522	141.60	111	3.05	73
0.8		-1524	71.96	98	1.55	86
1.0		-1541	51.06	88	1.10	90
Blank	35	-1515	553.44	192	12.03	-
0.2		-1544	222.84	146	4.80	60
0.4		-1531	183.38	131	3.95	67
0.6		-1518	161.56	114	3.48	71
0.8		-1522	88.21	102	1.90	84
1.0		-1525	67.31	92	1.45	88
Blank	40	-1488	577.18	188	12.54	-
0.2		-1511	243.73	148	5.25	58
0.4		-1525	208.91	134	4.50	64
0.6		-1530	185.70	116	4.00	68
0.8		-1517	104.45	105	2.25	82
1.0		-1543	81.24	95	1.75	86
Blank	45	-1510	706.61	209	15.22	-
0.2		-1499	315.70	150	6.80	55
0.4		-1487	264.16	136	5.69	62
0.6		-1522	213.56	118	4.60	65
0.8		-1540	139.27	107	3.00	80
1.0		-1528	112.81	98	2.43	84
Blank	50	-1494	792.81	186	17.23	-
0.2		-1480	377.44	152	8.13	53
0.4		-1491	320.34	140	6.90	60
0.6		-1521	293.41	121	6.32	63
0.8		-1516	174.09	110	3.75	78
1.0		-1530	143.92	101	3.10	82

Table 3.91: Electrochemical polarization parameters for the corrosion of AZ31 alloy in 0.05 M Na_2SO_4 solution in the presence of DC at different temperatures.

Inhibitor concentration (mmol dm^{-3})	Temperature (°C)	E_{corr} vs SCE (mV)	i_{corr} (μA cm^{-2})	$-\beta_c$ (mV dec^{-1})	v_{corr} (mm y^{-1})	η (%)
Blank	30	-1483	63.33	93	1.37	-
0.2		-1514	20.42	77	0.44	68
0.4		-1478	14.39	87	0.31	77
0.6		-1462	10.21	51	0.22	84
0.8		-1480	6.49	79	0.14	90
1.0		-1414	3.71	87	0.08	94
Blank	35	-1470	110.24	110	2.39	-
0.2		-1523	41.78	104	0.90	65
0.4		-1516	29.71	105	0.64	73
0.6		-1507	19.96	114	0.43	82
0.8		-1500	14.39	103	0.31	87
1.0		-1512	8.82	104	0.19	92
Blank	40	-1502	164.74	125	3.58	-
0.2		-1518	61.28	113	1.32	63
0.4		-1527	48.28	103	1.04	71
0.6		-1491	32.49	106	0.70	80
0.8		-1491	24.60	105	0.53	85
1.0		-1484	16.24	106	0.35	90
Blank	45	-1465	179.03	154	3.89	-
0.2		-1477	71.96	140	1.55	60
0.4		-1515	57.56	141	1.24	68
0.6		-1490	40.85	146	0.88	77
0.8		-1488	32.49	112	0.70	82
1.0		-1490	23.21	107	0.50	87
Blank	50	-1481	190.03	144	4.13	-
0.2		-1484	80.31	106	1.73	58
0.4		-1490	66.85	135	1.44	65
0.6		-1492	49.67	107	1.07	74
0.8		-1495	38.06	106	0.82	80
1.0		-1483	28.78	102	0.62	85

Table 3.92: Electrochemical polarization parameters for the corrosion of AZ31 alloy in 0.10 M Na_2SO_4 solution in the presence of DC at different temperatures.

Inhibitor concentration (mmol.dm^{-3})	Temperature (°C)	E_{corr} vs SCE (mV)	i_{corr} (µA cm^{-2})	$-\beta_c$ (mV dec^{-1})	v_{corr} (mm y^{-1})	η (%)
Blank	30	-1482.0	71.21	117	1.54	-
0.2		-1483	30.64	115	0.66	57
0.4		-1472	23.21	108	0.50	67
0.6		-1447	16.24	110	0.35	77
0.8		-1437	8.35	104	0.18	88
1.0		-1431	3.71	101	0.08	94
Blank	35	-1528	157.60	134	3.42	-
0.2		-1527	76.03	128	1.65	51
0.4		-1516	61.28	110	1.32	61
0.6		-1507	34.81	114	0.75	78
0.8		-1493	28.32	105	0.61	82
1.0		-1488	10.21	108	0.22	93
Blank	40	-1485	191.24	140	4.15	-
0.2		-1509	92.38	130	1.99	52
0.4		-1508	84.03	124	1.81	56
0.6		-1507	47.81	120	1.03	75
0.8		-1502	36.67	117	0.79	80
1.0		-1490	18.57	119	0.40	90
Blank	45	-1481	202.71	150	4.40	-
0.2		-1505	102.60	133	2.21	49
0.4		-1508	86.35	128	1.86	57
0.6		-1505	46.89	120	1.01	77
0.8		-1503	41.78	127	0.90	79
1.0		-1490	18.10	121	0.39	91
Blank	50	-1456	208.41	157	4.53	-
0.2		-1499	107.70	130	2.32	48
0.4		-1491	102.13	128	2.20	51
0.6		-1486	58.96	120	1.27	71
0.8		-1486	37.14	114	0.80	82
1.0		-1486	23.67	110	0.51	88

Table 3.93: Electrochemical polarization parameters for the corrosion of AZ31 alloy in 0.15 M Na_2SO_4 solution in the presence of DC at different temperatures.

Inhibitor concentration ($mmol.dm^{-3}$)	Temperature (°C)	E_{corr} vs SCE (mV)	i_{corr} ($\mu A\ cm^{-2}$)	$-\beta_c$ ($mV\ dec^{-1}$)	v_{corr} ($mm\ y^{-1}$)	η (%)
Blank	30	-1457	218.14	138	4.74	-
0.2		-1495	96.56	108	2.08	56
0.4		-1471	74.28	120	1.60	66
0.6		-1391	54.78	103	1.18	75
0.8		-1448	30.17	108	0.65	86
1.0		-1527	17.64	124	0.38	92
Blank	35	-1457	322.28	142	7.00	-
0.2		-1461	148.56	120	3.20	54
0.4		-1471	116.06	140	2.50	64
0.6		-1550	87.28	117	1.88	73
0.8		-1468	51.99	116	1.12	84
1.0		-1462	32.49	140	0.70	90
Blank	40	-1469	445.19	151	9.67	-
0.2		-1535	209.84	105	4.52	53
0.4		-1539	170.85	119	3.68	62
0.6		-1521	129.99	150	2.80	71
0.8		-1521	81.24	117	1.75	82
1.0		-1521	48.74	139	1.05	89
Blank	45	-1446	461.63	158	10.03	-
0.2		-1529	227.49	118	4.90	51
0.4		-1557	185.70	102	4.00	60
0.6		-1542	143.92	142	3.10	69
0.8		-1533	92.85	106	2.00	80
1.0		-1500	60.35	106	1.30	87
Blank	50	-1448	546.62	170	11.88	-
0.2		-1555	280.88	139	6.05	49
0.4		-1495	229.34	117	4.94	58
0.6		-1522	181.06	113	3.90	67
0.8		-1488	120.70	137	2.60	78
1.0		-1495	81.24	161	1.75	85

Table 3.94: Electrochemical polarization parameters for the corrosion of AZ31 alloy in 0.20 M Na_2SO_4 solution in the presence of DC at different temperatures.

Inhibitor concentration ($mmol.dm^{-3}$)	Temperature (°C)	E_{corr} vs SCE (mV)	i_{corr} ($\mu A\ cm^{-2}$)	$-\beta_c$ ($mV\ dec^{-1}$)	v_{corr} ($mm\ y^{-1}$)	η (%)
Blank	30	-1505	235.63	152	5.12	-
0.2		-1509	106.78	104	2.30	55
0.4		-1464	84.96	122	1.83	64
0.6		-1492	64.06	137	1.38	73
0.8		-1467	37.14	109	0.80	84
1.0		-1461	23.21	127	0.50	90
Blank	35	-1493	354.34	158	7.70	-
0.2		-1495	167.13	137	3.60	53
0.4		-1500	134.63	135	2.90	62
0.6		-1459	102.13	146	2.20	71
0.8		-1494	63.60	136	1.37	82
1.0		-1485	41.78	130	0.90	88
Blank	40	-1489	470.87	164	10.23	-
0.2		-1530	232.13	153	5.00	51
0.4		-1481	189.42	159	4.08	60
0.6		-1485	141.60	141	3.05	70
0.8		-1491	93.78	141	2.02	80
1.0		-1489	64.99	131	1.40	86
Blank	45	-1472	542.13	172	11.23	-
0.2		-1519	259.98	140	5.60	50
0.4		-1512	218.20	110	4.70	58
0.6		-1511	166.20	114	3.58	68
0.8		-1505	118.38	140	2.55	77
1.0		-1489	82.63	143	1.78	84
Blank	50	-1480	672.86	197	14.62	-
0.2		-1489	358.41	135	7.72	47
0.4		-1487	296.20	122	6.38	56
0.6		-1495	222.84	129	4.80	67
0.8		-1485	169.45	148	3.65	75
1.0		-1484	113.74	140	2.45	83

Table 3.95: Electrochemical polarization parameters for the corrosion of AZ31 alloy in 0.25 M Na_2SO_4 solution in the presence of DC at different temperatures.

Inhibitor concentration ($mmol.dm^{-3}$)	Temperature (°C)	E_{corr} vs SCE (mV)	i_{corr} ($\mu A\ cm^{-2}$)	$-\beta_c$ ($mV\ dec^{-1}$)	v_{corr} ($mm\ y^{-1}$)	η (%)
Blank	30	-1451	372.80	147	8.10	-
0.2		-1429	176.42	122	3.80	53
0.4		-1487	142.52	125	3.07	62
0.6		-1461	105.38	130	2.27	72
0.8		-1542	63.60	110	1.37	83
1.0		-1443	44.10	118	0.95	88
Blank	35	-1411	497.12	158	10.80	-
0.2		-1560	244.66	114	5.27	51
0.4		-1539	199.63	123	4.30	60
0.6		-1550	149.49	117	3.22	70
0.8		-1540	99.81	108	2.15	80
1.0		-1542	69.63	110	1.50	86
Blank	40	-1438	516.71	170	11.23	-
0.2		-1561	259.06	125	5.58	50
0.4		-1545	222.84	110	4.80	57
0.6		-1521	166.20	155	3.58	68
0.8		-1512	113.28	149	2.44	78
1.0		-1522	82.63	105	1.78	84
Blank	45	-1486	583.03	190	12.67	-
0.2		-1533	304.09	119	6.55	48
0.4		-1535	264.63	151	5.70	55
0.6		-1542	199.63	142	4.30	66
0.8		-1543	134.63	114	2.90	77
1.0		-1545	105.38	110	2.27	82
Blank	50	-1463	727.89	201	15.82	-
0.2		-1518	387.19	141	8.34	47
0.4		-1500	336.59	181	7.25	54
0.6		-1522	271.59	113	5.85	63
0.8		-1510	182.45	111	3.93	75
1.0		-1484	146.24	106	3.15	80

Table 3.96: Electrochemical impedance parameters for the corrosion of AZ31 alloy in 0.05 M NaCl in the presence of DC at different temperatures.

Inhibitor Concentration (mmol dm^{-3})	Temperature (°C)	R_{hf} (Ω cm^2)	R_f (Ω cm^2)	R_{dif} (Ω cm^2)	C_{dl} (µF cm^{-2})	C_f (µF cm^{-2})	η (%)
Blank	30	580	296	225	138	177	-
0.2		1990	1843	993	99	79	70
0.4		2593	2426	1210	73	71	77
0.6		3100	2955	1455	69	66	81
0.8		6542	6400	2989	60	57	91
1.0		9834	9743	3777	57	43	94
Blank	35	550	255	207	153	181	-
0.2		1662	1502	745	106	83	67
0.4		2206	2088	1022	89	76	75
0.6		2825	2691	1288	80	70	80
0.8		4166	4030	2001	72	65	87
1.0		4231	4067	2177	60	53	92
Blank	40	422	231	184	161	188	-
0.2		1210	1012	503	111	88	65
0.4		1577	1400	701	94	81	73
0.6		1865	1711	895	89	75	77
0.8		3190	3002	1588	75	69	87
1.0		3992	3817	1595	68	58	89
Blank	45	340	191	150	170	192	-
0.2		963	850	424	114	97	65
0.4		1154	1031	544	100	89	71
0.6		1372	1202	600	95	82	75
0.8		2255	2101	1013	80	73	85
1.0		2891	2782	1133	73	64	88
Blank	50	318	160	131	171	198	-
0.2		833	717	333	117	104	62
0.4		991	835	411	104	90	68
0.6		1185	1021	530	97	80	73
0.8		1855	1702	869	86	77	83
1.0		2194	2020	1003	76	69	86

Table 3.97: Electrochemical impedance parameters for the corrosion of AZ31 alloy in 0.10 M NaCl in the presence of DC at different temperatures.

Inhibitor Concentration (mmol dm^{-3})	Temperature (°C)	R_{hf} (Ω cm^2)	R_f (Ω cm^2)	R_{dif} (Ω cm^2)	C_{dl} (µF cm^{-2})	C_f (µF cm^{-2})	η (%)
Blank	30	507	232	209	166	172	-
0.2		1590	1411	703	107	70	68
0.4		2017	1903	933	50	49	75
0.6		2411	2306	1107	31	41	79
0.8		4910	4802	2200	20	31	90
1.0		7945	7803	3386	15	19	94
Blank	35	380	192	168	181	179	-
0.2		1107	994	465	119	88	65
0.4		1423	1306	700	62	66	73
0.6		1579	1422	713	44	58	76
0.8		2495	2334	1155	33	47	85
1.0		3991	3877	1539	27	28	90
Blank	40	366	173	142	191	183	-
0.2		1007	931	465	131	93	64
0.4		1223	1119	523	78	74	70
0.6		1476	1301	655	62	67	75
0.8		1989	1855	924	54	51	81
1.0		3292	3100	1500	41	35	89
Blank	45	351	152	115	195	185	-
0.2		911	775	325	147	104	61
0.4		1078	957	451	98	82	67
0.6		1299	1105	548	69	71	72
0.8		1799	1673	834	60	60	80
1.0		2428	2304	1147	55	48	86
Blank	50	301	139	108	200	191	-
0.2		738	600	300	162	113	59
0.4		880	704	343	103	92	66
0.6		1054	985	449	73	82	71
0.8		1388	1244	569	68	71	78
1.0		2195	1968	1019	59	57	86

Table 3.98: Electrochemical impedance parameters for the corrosion of AZ31 alloy in 0.15 M NaCl in the presence of DC at different temperatures.

Inhibitor Concentration (mmol dm^{-3})	Temperature (°C)	R_{hf} (Ω cm^2)	R_f (Ω cm^2)	R_{dif} (Ω cm^2)	C_{dl} (µF cm^{-2})	C_f (µF cm^{-2})	η (%)
Blank	30	358	170	144	172	115	-
0.2		1056	902	449	112	79	66
0.4		1400	1289	645	99	70	74
0.6		1602	1495	754	87	67	78
0.8		3298	3144	1600	80	61	89
1.0		4694	4503	2146	71	57	92
Blank	35	301	161	121	184	128	-
0.2		841	702	350	115	92	64
0.4		1080	933	457	106	78	72
0.6		1183	1012	505	93	70	75
0.8		1766	1560	896	88	66	83
1.0		3111	3010	1501	75	60	90
Blank	40	288	150	113	197	133	-
0.2		744	600	296	119	95	61
0.4		859	722	353	108	83	66
0.6		1048	977	454	96	78	73
0.8		1401	1276	617	90	69	79
1.0		2284	2105	1009	81	65	87
Blank	45	225	128	100	201	140	-
0.2		550	400	199	122	101	59
0.4		626	517	249	111	86	64
0.6		749	616	300	100	80	69
0.8		1027	908	451	96	73	78
1.0		1611	1487	775	88	71	86
Blank	50	130	88	73	218	147	-
0.2		303	221	103	125	105	57
0.4		343	239	117	114	93	62
0.6		395	251	127	103	85	67
0.8		525	319	159	99	78	75
1.0		862	700	354	93	74	84

Table 3.99: Electrochemical impedance parameters for the corrosion of AZ31 alloy in 0.20 M NaCl in the presence of DC at different temperatures.

Inhibitor Concentration (mmol dm^{-3})	Temperature (°C)	R_{hf} (Ω cm^2)	R_f (Ω cm^2)	R_{dif} (Ω cm^2)	C_{dl} (μF cm^{-2})	C_f (μF cm^{-2})	η (%)
Blank	30	170	109	95	193	191	-
0.2		473	302	151	116	82	64
0.4		602	489	246	102	77	72
0.6		683	515	255	90	71	75
0.8		1300	1188	653	86	68	86
1.0		1899	1700	921	78	62	91
Blank	35	166	97	79	190	199	-
0.2		442	203	101	122	84	62
0.4		560	400	200	106	79	70
0.6		1043	941	372	95	75	84
0.8		1132	1005	521	88	70	85
1.0		1733	1576	784	81	65	90
Blank	40	158	90	70	212	210	-
0.2		399	251	123	125	87	60
0.4		477	361	156	110	80	69
0.6		551	376	167	101	78	71
0.8		967	804	401	94	74	84
1.0		1288	1099	526	89	70	87
Blank	45	125	78	58	220	219	-
0.2		297	160	80	130	92	58
0.4		339	169	85	115	84	63
0.6		401	289	138	107	79	69
0.8		533	400	200	98	75	77
1.0		818	702	338	92	70	85
Blank	50	103	73	52	243	232	-
0.2		236	118	71	136	95	56
0.4		255	132	82	119	88	60
0.6		301	201	103	109	81	66
0.8		383	235	144	102	79	73
1.0		549	302	155	95	74	81

Table 3.100: Electrochemical impedance parameters for the corrosion of AZ31 alloy in 0.25 M NaCl in the presence of DC at different temperatures.

Inhibitor Concentration (mmol dm^{-3})	Temperature (°C)	R_{hf} (Ω cm^2)	R_f (Ω cm^2)	R_{dif} (Ω cm^2)	C_{dl} (μF cm^{-2})	C_f (μF cm^{-2})	η (%)
Blank	30	201	115	99	205	195	-
0.2		547	288	143	125	87	63
0.4		670	497	251	107	84	70
0.6		752	608	302	96	79	73
0.8		1432	1303	763	90	73	86
1.0		1935	1804	914	84	68	89
Blank	35	150	107	85	217	205	-
0.2		371	219	102	127	94	59
0.4		447	284	139	110	88	66
0.6		515	421	215	100	82	70
0.8		956	805	400	94	77	84
1.0		1256	1107	613	87	71	88
Blank	40	141	98	72	221	222	-
0.2		338	215	103	130	100	58
0.4		390	213	107	113	92	64
0.6		444	204	100	104	85	68
0.8		1103	1025	529	97	80	82
1.0		1145	1075	538	91	75	86
Blank	45	105	81	68	230	223	-
0.2		241	105	75	133	104	55
0.4		278	160	83	116	95	62
0.6		301	200	100	107	88	65
0.8		530	402	201	100	81	80
1.0		677	531	264	95	79	84
Blank	50	99	70	55	248	239	-
0.2		210	101	64	137	109	53
0.4		248	124	82	119	99	60
0.6		269	144	94	111	91	63
0.8		464	250	129	106	94	78
1.0		563	311	156	98	98	82

Table 3.101: Electrochemical impedance parameters for the corrosion of AZ31 alloy in 0.05 M Na_2SO_4 in the presence of DC at different temperatures.

Inhibitor Concentration (mmol dm^{-3})	Temperature (°C)	R_{hf} (Ω cm^2)	R_f (Ω cm^2)	R_{dif} (Ω cm^2)	C_{dl} (µF cm^{-2})	C_f (µF cm^{-2})	η (%)
Blank	30	609	471	412	159	102	-
0.2		1931	1775	935	37	80	68
0.4		2680	2531	1308	30	77	77
0.6		3693	3517	1579	28	74	84
0.8		5710	5589	2533	24	71	89
1.0		8713	8588	3979	21	68	93
Blank	35	510	367	303	176	129	-
0.2		1467	1334	689	40	83	65
0.4		1876	1738	913	34	79	73
0.6		2787	2630	1288	31	78	82
0.8		3839	3673	1507	27	73	87
1.0		6452	5321	3434	23	70	92
Blank	40	477	333	288	201	146	-
0.2		1280	1104	525	43	85	63
0.4		1645	1523	790	37	82	71
0.6		2408	2296	1109	33	79	80
0.8		3116	3007	1500	29	76	85
1.0		5002	4901	2390	25	72	90
Blank	45	450	350	275	225	151	-
0.2		1135	1011	501	44	87	60
0.4		1405	1301	651	39	83	68
0.6		1986	1823	909	36	80	77
0.8		2491	2331	1049	30	78	82
1.0		3466	3301	1200	27	75	87
Blank	50	412	354	252	261	168	-
0.2		987	860	450	47	90	58
0.4		1171	1042	538	40	86	64
0.6		1607	1487	750	38	82	74
0.8		2101	2005	1002	35	81	80
1.0		2817	2702	1326	30	78	85

Table 3.102: Electrochemical impedance parameters for the corrosion of AZ31 alloy in 0.10 M Na_2SO_4 in the presence of DC at different temperatures.

Inhibitor Concentration (mmol dm^{-3})	Temperature (°C)	R_{hf} (Ω cm^2)	R_f (Ω cm^2)	R_{dif} (Ω cm^2)	C_{dl} (µF cm^{-2})	C_f (µF cm^{-2})	η (%)
Blank	30	460	343	319	201	188	-
0.2		1079	922	359	37	82	57
0.4		1409	1285	641	32	80	67
0.6		1994	1802	900	25	78	77
0.8		3843	3704	1501	23	72	88
1.0		6534	6377	3129	16	67	93
Blank	35	432	322	293	224	191	-
0.2		876	700	347	69	86	51
0.4		1106	1011	500	53	80	61
0.6		1937	1765	884	41	71	77
0.8		2431	2302	1120	38	67	82
1.0		4810	4702	2295	28	62	91
Blank	40	403	254	227	249	225	-
0.2		839	716	353	72	88	52
0.4		929	811	402	75	81	56
0.6		1622	1478	737	69	75	75
0.8		2011	1912	994	57	72	80
1.0		3911	3756	1629	50	69	90
Blank	45	387	193	160	269	237	-
0.2		766	604	301	78	96	49
0.4		895	763	383	64	90	57
0.6		1666	1504	689	60	87	77
0.8		1860	1706	875	57	80	79
1.0		3846	3703	1501	55	72	90
Blank	50	373	209	161	278	241	-
0.2		721	571	252	90	99	48
0.4		764	589	265	66	85	51
0.6		1276	1123	604	63	80	70
0.8		2097	1894	931	50	74	82
1.0		2985	2831	1095	37	72	87

Table 3.103: Electrochemical impedance parameters for the corrosion of AZ31 alloy in 0.15 M Na_2SO_4 in the presence of DC at different temperatures.

Inhibitor Concentration (mmol dm^{-3})	Temperature (°C)	R_{hf} (Ω cm^2)	R_f (Ω cm^2)	R_{dif} (Ω cm^2)	C_{dl} (µF cm^{-2})	C_f (µF cm^{-2})	η (%)
Blank	30	434	420	383	244	167	-
0.2		981	833	405	45	89	55
0.4		1292	1195	676	39	78	66
0.6		1722	1603	800	33	71	75
0.8		2999	2844	1401	36	67	86
1.0		4833	4701	2100	22	60	91
Blank	35	463	300	280	278	169	-
0.2		1007	916	454	46	92	54
0.4		1300	1188	609	40	79	64
0.6		1719	1605	800	47	74	73
0.8		2851	2733	1357	31	70	83
1.0		4509	4366	2101	26	64	90
Blank	40	380	230	201	299	180	-
0.2		809	722	400	48	95	53
0.4		995	805	450	43	82	61
0.6		1322	1204	589	38	77	71
0.8		2150	2003	993	33	74	82
1.0		3351	3200	1621	30	69	88
Blank	45	273	237	200	307	188	-
0.2		561	460	231	51	97	51
0.4		677	522	250	46	85	60
0.6		883	717	353	49	80	69
0.8		1409	1297	640	36	83	80
1.0		2171	2014	1001	32	71	87
Blank	50	245	200	178	321	200	-
0.2		476	303	147	53	102	48
0.4		589	377	152	47	87	58
0.6		752	614	320	41	81	67
0.8		1107	1008	495	38	84	77
1.0		1653	1511	703	24	75	85

Table 3.104: Electrochemical impedance parameters for the corrosion of AZ31 alloy in 0.20 M Na_2SO_4 in the presence of DC at different temperatures.

Inhibitor Concentration (mmol dm^{-3})	Temperature (°C)	R_{hf} (Ω cm^2)	R_f (Ω cm^2)	R_{dif} (Ω cm^2)	C_{dl} (µF cm^{-2})	C_f (µF cm^{-2})	η (%)
Blank	30	301	226	171	269	179	-
0.2		684	534	261	49	93	56
0.4		843	701	347	46	89	64
0.6		1130	1022	509	42	85	73
0.8		1886	1705	675	39	81	84
1.0		2911	2812	1391	36	77	90
Blank	35	287	224	190	287	186	-
0.2		609	522	264	52	96	53
0.4		755	613	305	49	91	62
0.6		987	815	400	45	88	71
0.8		1633	1513	729	42	84	82
1.0		2411	2300	1145	38	79	88
Blank	40	259	192	163	301	191	-
0.2		530	410	241	55	99	51
0.4		649	531	330	50	93	60
0.6		859	720	444	47	90	70
0.8		1301	1196	629	43	86	80
1.0		1905	1785	886	40	82	86
Blank	45	236	203	167	321	201	-
0.2		472	343	223	57	103	50
0.4		570	469	231	53	96	59
0.6		739	604	300	50	90	68
0.8		1041	905	446	48	88	77
1.0		1461	1307	658	43	85	84
Blank	50	218	187	159	333	219	-
0.2		409	313	170	59	107	47
0.4		493	354	213	55	99	56
0.6		666	523	250	52	93	67
0.8		859	700	348	50	90	75
1.0		1302	1188	601	46	87	83

Table 3.105: Electrochemical impedance parameters for the corrosion of AZ31 alloy in 0.25 M Na_2SO_4 in the presence of DC at different temperatures.

Inhibitor Concentration (mmol dm^{-3})	Temperature (°C)	R_{hf} (Ω cm^2)	R_f (Ω cm^2)	R_{dif} (Ω cm^2)	C_{dl} (µF cm^{-2})	C_f (µF cm^{-2})	η (%)
Blank	30	392	301	280	320	240	-
0.2		834	715	351	53	96	53
0.4		1032	948	452	47	91	62
0.6		1403	1300	650	43	86	72
0.8		2328	2168	1036	40	80	83
1.0		3405	3293	1634	37	76	88
Blank	35	350	250	221	333	259	-
0.2		717	604	301	56	99	51
0.4		883	756	354	49	93	60
0.6		1157	1009	551	46	89	70
0.8		1750	1601	800	43	83	80
1.0		2507	2388	1157	40	78	86
Blank	40	201	114	96	345	267	-
0.2		404	200	100	58	102	50
0.4		469	233	111	52	95	57
0.6		632	502	240	48	92	68
0.8		908	786	371	46	85	79
1.0		1266	1105	552	42	80	84
Blank	45	180	109	80	359	280	-
0.2		345	211	102	63	108	48
0.4		401	210	105	55	94	55
0.6		530	415	208	51	88	66
0.8		784	560	245	48	85	77
1.0		1013	902	450	45	81	82
Blank	50	170	100	64	389	308	-
0.2		322	152	74	66	111	47
0.4		370	169	85	58	96	54
0.6		461	231	115	55	91	63
0.8		686	429	212	51	88	75
1.0		851	744	337	48	84	80

Table 3.106: Activation parameters for the corrosion of AZ31 alloy in NaCl solutions containing different concentrations of DC inhibitor.

Concentration of NaCl (M)	Concentration of inhibitor (mmol dm^{-3})	E_a (kJ mol^{-1})	$\Delta H^{\#}$ (kJ mol^{-1})	$\Delta S^{\#}$ (J mol^{-1} K^{-1})
0.05	Blank	34.00	34.66	-128.69
	0.2	57.14	54.54	-74.24
	0.4	61.01	58.42	-63.85
	0.6	62.00	59.40	-62.10
	0.8	83.43	80.84	1.91
	1.0	102.69	100.01	59.11
0.1	Blank	24.55	20.97	-162.88
	0.2	27.67	25.06	-161.71
	0.4	29.39	26.66	-158.73
	0.6	30.91	28.18	-155.14
	0.8	54.40	50.56	-87.54
	1.0	63.36	62.57	-53.53
0.15	Blank	23.57	18.70	-174.42
	0.2	33.56	30.96	-138.92
	0.4	37.60	35.00	-128.70
	0.6	40.63	38.03	-117.80
	0.8	55.47	52.88	-74.99
	1.0	60.45	57.85	-63.35
0.20	Blank	20.67	18.08	-167.27
	0.2	30.90	28.30	-142.00
	0.4	35.83	33.23	-127.82
	0.6	36.02	33.43	-77.07
	0.8	53.21	50.62	-71.91
	1.0	55.79	53.20	-66.80
0.25	Blank	16.94	15.30	-175.67
	0.2	24.52	21.93	-160.95
	0.4	27.12	24.52	-154.14
	0.6	27.85	25.24	-152.72
	0.8	33.42	30.82	-138.90
	1.0	39.31	36.72	-123.04

Table 3.107: Activation parameters for the corrosion of AZ31 alloy in Na_2SO_4 solutions containing different concentrations of DC inhibitor.

Concentration of Na_2SO_4 (M)	Concentration of inhibitor (mmol dm^{-3})	E_a (kJ mol^{-1})	$\Delta H^{\#}$ (kJ mol^{-1})	$\Delta S^{\#}$ (J mol^{-1} K^{-1})
0.05	Blank	44.17	40.04	−108.74
	0.2	54.07	51.48	-109.16
	0.4	61.49	58.89	-80.22
	0.6	63.73	61.14	-58.77
	0.8	71.57	68.98	-32.08
	1.0	83.18	80.58	1.50
0.1	Blank	39.64	33.78	-126.03
	0.2	46.13	43.71	-101.58
	0.4	49.95	46.71	-98.26
	0.6	54.28	51.86	-76.90
	0.8	57.90	55.64	-74.01
	1.0	73.41	70.60	-48.06
0.15	Blank	35.65	28.33	-137.09
	0.2	41.96	39.37	-108.08
	0.4	44.69	42.10	-101.34
	0.6	47.38	44.79	-94.94
	0.8	54.93	52.33	-74.82
	1.0	60.02	57.43	-58.36
0.20	Blank	35.21	23.87	-149.98
	0.2	46.64	44.04	-92.03
	0.4	48.58	45.90	-95.02
	0.6	48.59	45.98	-87.46
	0.8	59.56	56.96	-58.19
	1.0	63.05	60.45	-50.38
0.25	Blank	24.39	18.81	-164.69
	0.2	28.83	26.23	-146.98
	0.4	32.34	29.74	-137.17
	0.6	35.16	32.57	-130.44
	0.8	38.91	36.32	-121.88
	1.0	45.50	42.90	-103.42

Table 3.108: Thermodynamic parameters for the adsorption of DC inhibitor on AZ31 alloy in NaCl solutions.

Concentration of NaCl (M)	Temperature (°C)	ΔG^0_{ads} (kJ mol^{-1})	ΔH^0_{ads} (kJ mol^{-1})	ΔS^0_{ads} (J mol^{-1} K^{-1})
0.05	30	-34.65	-61.11	-87.4
	35	-34.08		
	40	-33.64		
	45	-33.20		
	50	-32.76		
0.10	30	-33.18	-55.51	-72.0
	35	-32.84		
	40	-32.46		
	45	-32.10		
	50	-31.74		
0.15	30	-31.88	-52.21	-66.4
	35	-31.54		
	40	-31.21		
	45	-30.88		
	50	-30.55		
0.20	30	-29.52	-49.84	-66.8
	35	-29.26		
	40	-28.93		
	45	-28.59		
	50	-28.26		
0.25	30	-30.37	-48.19	58.8
	35	-30.07		
	40	-29.78		
	45	-29.49		
	50	-29.19		

Table 3.109: Thermodynamic parameters for the adsorption of DC inhibitor on AZ31 alloy in Na_2SO_4 solution.

Concentration of Na_2SO_4 (M)	Temperature (°C)	ΔG^0_{ads} (kJ mol^{-1})	ΔH^0_{ads} (kJ mol^{-1})	ΔS^0_{ads} (J mol^{-1} K^{-1})
0.05	30	-32.32	-51.54	-63.4
	35	-32.01		
	40	-31.69		
	45	-31.37		
	50	-31.06		
0.1	30	-32.11	-48.23	-53.2
	35	-31.54		
	40	-31.57		
	45	-31.31		
	50	-31.04		
0.15	30	-30.52	-45.74	-50.2
	35	-30.27		
	40	-30.02		
	45	-29.77		
	50	-29.52		
0.20	30	-29.70	-45.95	-53.6
	35	-29.44		
	40	-29.17		
	45	-28.90		
	50	-28.63		
0.25	30	-29.30	-42.64	-44.0
	35	-29.08		
	40	-28.86		
	45	-28.64		
	50	-28.42		

Table 3.110: Calculated DFT parameters for DC inhibitor.

Parameters	Value
Total energy (KeV)	-2.629
Energy gap (eV)	2.911
E_{HOMO} (eV)	-0.767
E_{LUMO} (eV)	-3.678
Dipole moment (Debye)	66.384
Electronegativity (eV)	2.222
Chemical hardness (eV)	1.455
Electron affinity (eV)	3.678
Ionization potential (eV)	0.767
Softness (eV^{-1})	0.687

3.7 SODIUM 2,2'-(13,22-DIDODECYL-14,21-DIOXO-11,14,17,20-TETRAAZATETRATRIACONTANE-16,19-DIYL)DIACETATE (DD) AS CORROSION INHIBITOR FOR AZ31 MAGNESIUM ALLOY IN SODIUM CHLORIDE AND SODIUM SULFATE MEDIUM SOLUTIONS

3.7.1 Potentiodynamic polarization measurements

Fig. 3.73 shows the potentiodynamic polarization plots for the corrosion of AZ31 magnesium alloy in 0.1 M NaCl and 0.1 M Na_2SO_4 in the presence of different concentrations of DD at 50 °C.

Tables 3.111 to 3.120 list the electrochemical polarization parameters for the corrosion of AZ31 alloy in NaCl and Na_2SO_4 solutions in the presence of different concentrations of DD at different temperatures. Inhibition efficiency increases remarkably as the amount of inhibitor is increased. The inhibition efficiency increases with the increase in the concentration of DD up to an optimum concentration of 0.0005 M, and above which the increase in inhibition efficiency is negligible. Efficient surface coverage could be credited to the increase in inhibition efficiency.

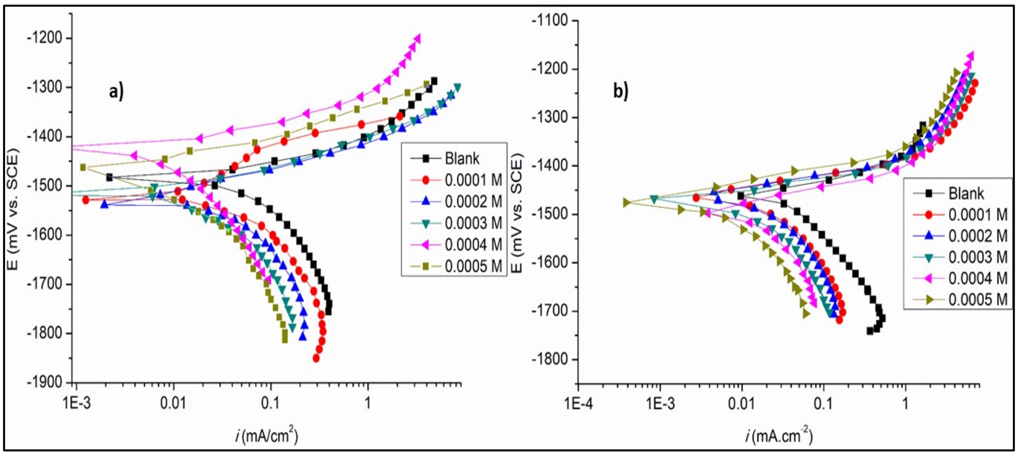

Fig. 3.73: Potentiodynamic polarization curves for the corrosion of AZ31 alloy in the presence of different concentrations of DD in a) 0.1 M NaCl solution and b) 0.1 M Na_2SO_4 solution at 50 °C.

3.7.2 Electrochemical impedance spectroscopy (EIS) studies

Nyquist plots for the corrosion of AZ31 Mg alloy in 0.1 M NaCl and 0.1 M Na_2SO_4 in the presence of different concentration of DD inhibitor are shown in Fig. 3.74. The Nyquist plots are similar to the ones obtained in the presence of inhibitors discussed in the previous sections.

The Electrochemical impedance parameters for the corrosion AZ31 Mg alloy in NaCl and Na_2SO_4 media in the presence of different concentrations of DD have been tabulated in Tables 3.121 to 3.130. All the explanation regarding the electrical equivalent circuit is the same as in the earlier sections.

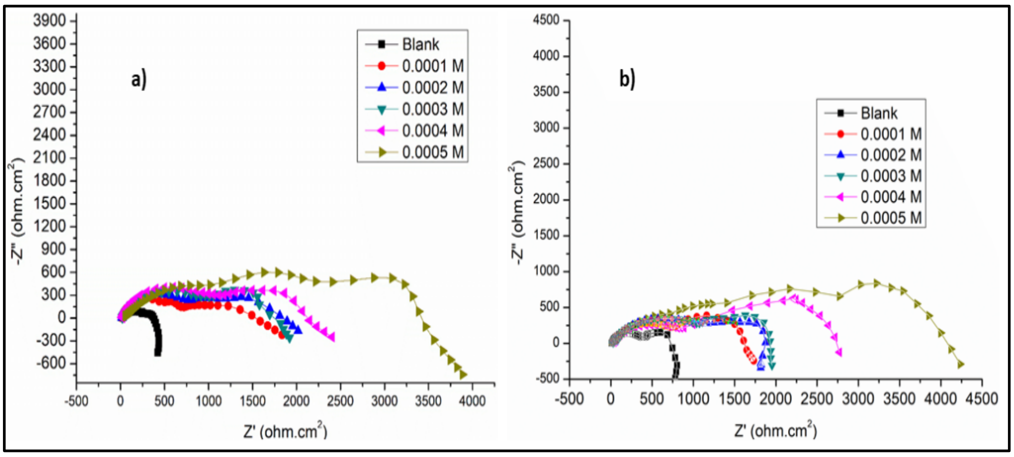

Fig. 3.74: Nyquist plots for the corrosion of AZ31 alloy in a) 0.1 M NaCl and b) 0.1 M Na_2SO_4 in the presence of different concentrations of DD at 50 °C.

Figures 3. 75 and 3.76 show the Bode plots for the corrosion of AZ31 Mg alloy in 0.1 M NaCl and 0.1 M Na_2SO_4 media containing varying concentrations of the inhibitors at 50 °C. The plots indicate that the addition of the inhibitors increases the low-frequency impedance modulus (Z_{mod}) and the medium frequency phase angle maximum (θ_{max}). The values of both Z_{mod} and θ_{max} show that the inhibitor shows good inhibition efficiencies.

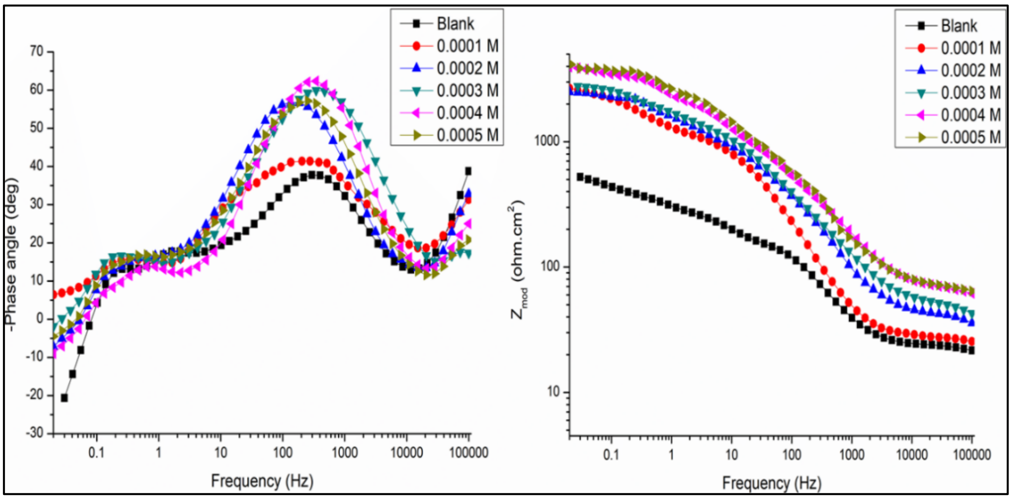

Fig. 3.75: Bode phase angle and amplitude plots for the corrosion of AZ31 in 0.1 M NaCl medium containing different concentrations of DD at 50 °C.

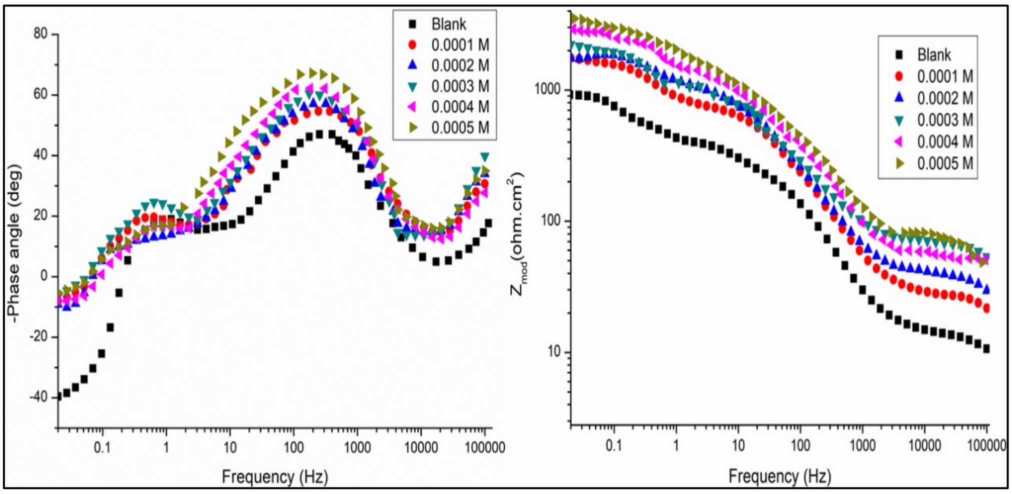

Fig. 3.76: Bode phase angle and amplitude plots for the corrosion of the AZ31 alloy in 0.1 M Na_2SO_4 medium containing different concentrations of DD at 50 °C.

3.7.3 Effect of temperature on inhibitors

It is seen from Tables 3.111 to 3.120 that the inhibition efficiency of DD decreases with the rise in temperature of the medium. Physical adsorption of the inhibition on the alloy surface is predicted due to the decrease in the inhibition efficiency with the increase in temperature (Antropov 1967).

Arrhenius plots for the corrosion of the AZ31 alloy in 0.1 M NaCl and 0.1 M Na_2SO_4 in the presence of the different concentrations of DD are shown in Figure 3.77.

Figure 3.78 represents the plots of $\ln(\upsilon_{corr}/T)$ vs. (1/T) for the corrosion of AZ31 Mg alloy in 0.1 M NaCl and 0.1 M Na_2SO_4 media containing different concentrations of DD. The activation parameters calculated are listed in Tables 3.131 and 3.132. From the tabulated values it is seen that the activation energy (E_a) is higher in the presence of the inhibitor, and it increases with the rise in the concentrations of the inhibitor.

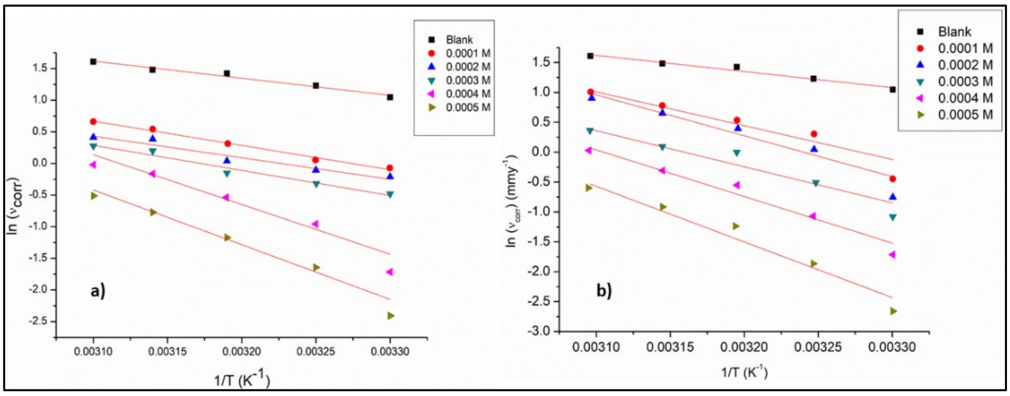

Fig. 3.77: Arrhenius plots for the corrosion of AZ31 magnesium alloy in a) 0.1 M NaCl and b) 0.1 M Na_2SO_4 in the presence of different concentrations of DD.

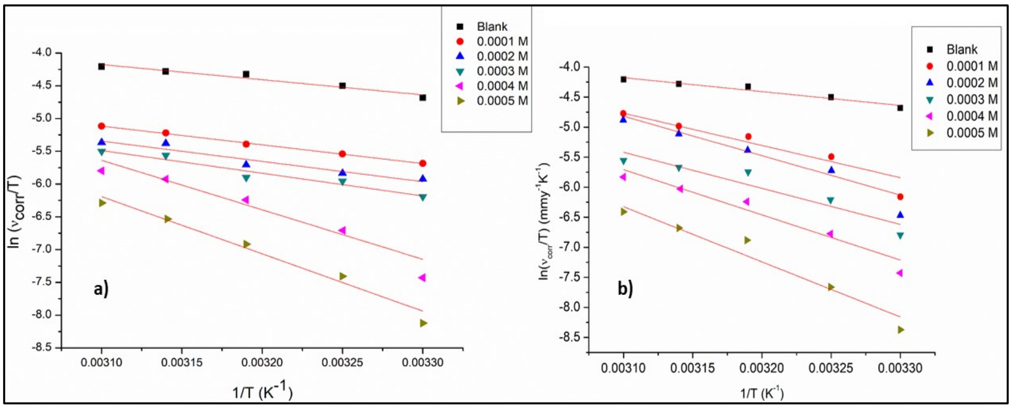

Fig. 3.78: The plots of $\ln(\upsilon_{corr}/T)$ versus $1/T$ for the corrosion of AZ31 magnesium alloy in a) 0.1 M NaCl and b) 0.1 M Na_2SO_4 in the presence of different concentrations of DD.

3.7.4 Adsorption isotherms

Efforts were made to fit the values of θ and C_{inh} graphically, into different adsorption isotherms such as Langmuir, Temkin, Frumkin, Flory-Huggins isotherms, etc. The regression coefficients (R^2) obtained with Langmuir isotherm is close to unity. Figure 3.79 shows the Langmuir adsorption isotherms for the adsorption of DD on AZ31 alloy surface in 0.1 M NaCl and 0.1 M Na_2SO_4 at different temperatures.

The thermodynamic parameters for the adsorption of DD in 0.1 M NaCl and Na_2SO_4 solution are tabulated in Tables 3.133 and 3.134. The linear regression coefficient and slopes of the plots were close to 1 showing a slight deviation from the Langmuir isotherm. This would have been caused due to the mutual interaction of the adsorbed inhibitor molecules on the surface of the alloy (Masel 1996). The values obtained for ΔG^0_{ads} are negative and in between -29.5 kJ mol^{-1} to -36 kJ mol^{-1}, indicating that the adsorption is through both physisorption and chemisorption. The ΔH^0_{ads} is in the range between -19.34 kJ mol^{-1} to -91.77 kJ mol^{-1} implying a predominantly physisorption process.

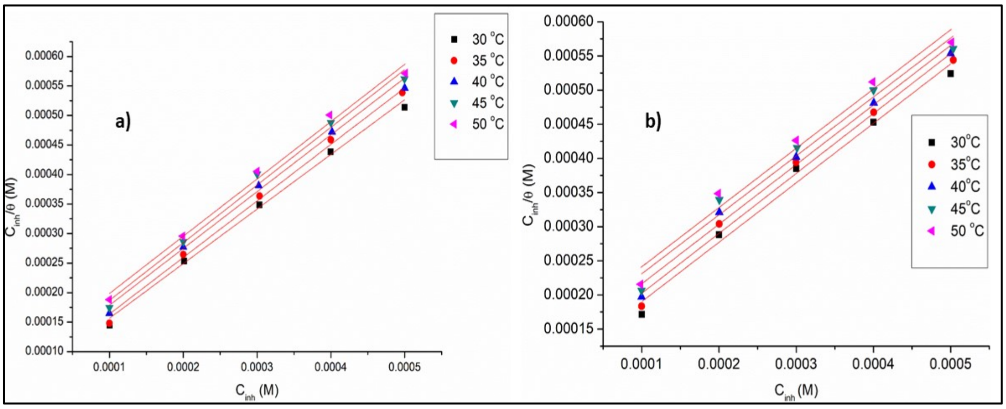

Fig. 3.79: Langmuir adsorption isotherms for the adsorption of DD on AZ31 magnesium alloy in a) NaCl medium and b) Na_2SO_4 medium.

3.7.5 SEM

Fig. 3.80 depicts the SEM image and EDX spectrum of AZ31 Mg alloy surface immersed in 0.1 M NaCl solution in the presence of 0.0002 M DD. Fig. 3.81 presents the SEM image and EDX spectrum of AZ31 Mg alloy surface immersed in 0.1 M Na_2SO_4 solution in the presence of 0.0002 M DD. In the EDX spectra apart from the peaks of Mg, Al, Zn, and Cl, additional small peaks for carbon, oxygen, and nitrogen are observed, which indicate the presence of some organic moieties on the alloy surface, possibly the surface adsorbed DD molecules. It is also observed that the intensity of the Mg peak is reduced.

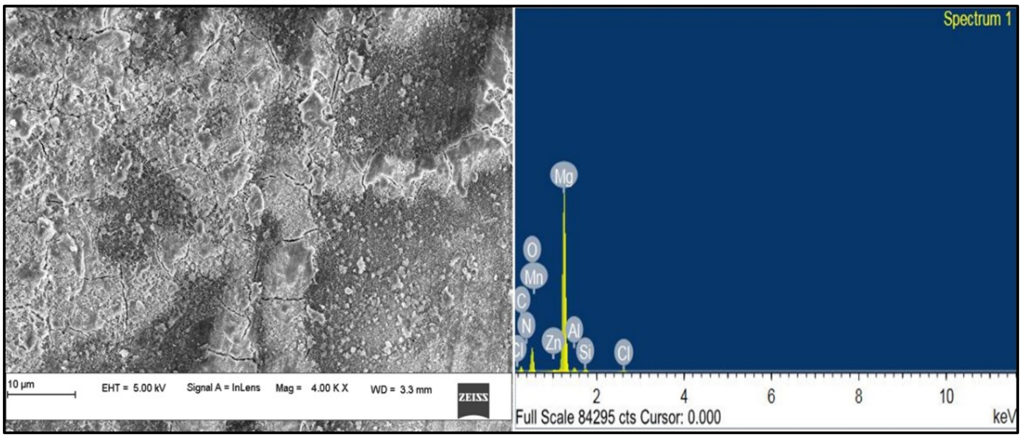

Fig. 3.80: SEM image and EDX spectrum of the AZ31 magnesium alloy surface immersed in 0.1 M NaCl in the presence of DD for 3 h at 30 °C.

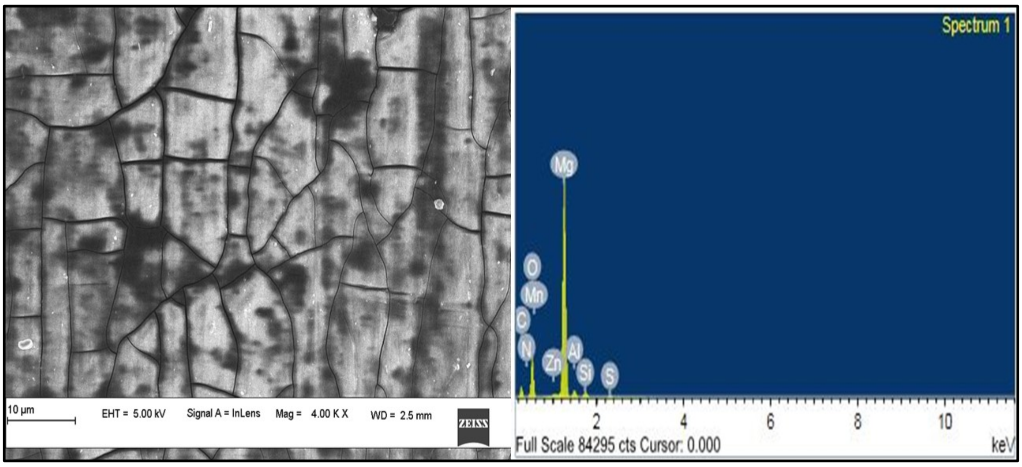

Fig. 3.81: SEM image and EDX spectrum of the AZ31 magnesium alloy surface immersed in 0.1 M Na_2SO_4 in the presence of DD for 3 h at 30 °C.

3.7.6 XPS

Fig. 3.82 and Fig. 3.83 show the XPS survey spectra and individual spectrum corresponding to different elements present on the surface of the AZ31 alloy immersed in 0.1 M NaCl and 0.1 M Na_2SO_4 media for 3 h in the presence of 0.001 M DD at 30 °C.

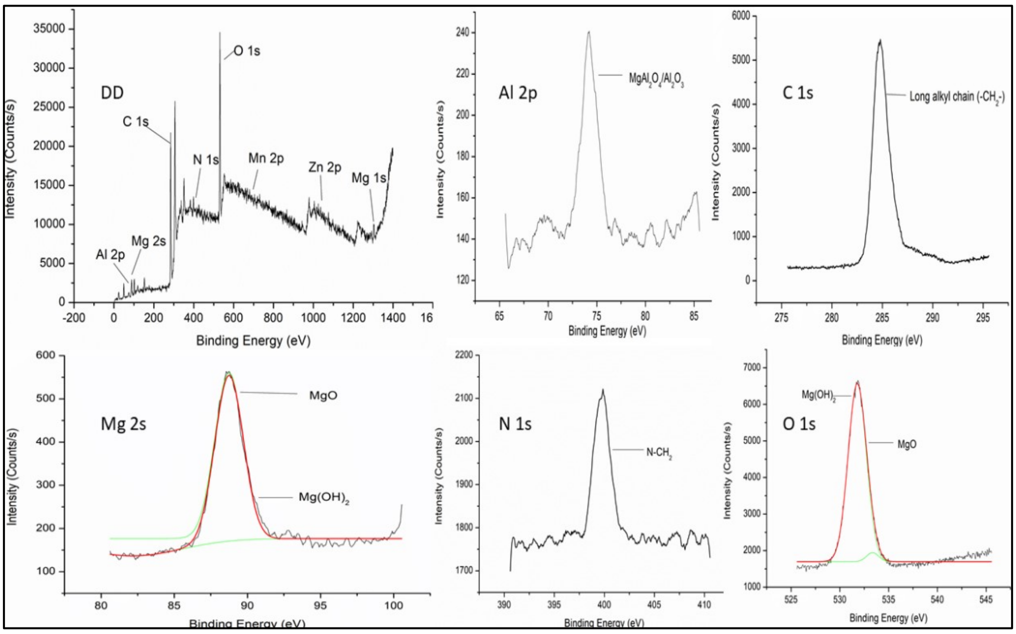

Fig. 3.82: XPS survey spectra and individual spectrum of elements (Mg 1s, Al 2p, C 1s, O 1s and, N 1s) of AZ31 Mg alloy immersed in 0.1 M NaCl medium in the presence of 0.0002 M DD for 3 h at 30 °C.

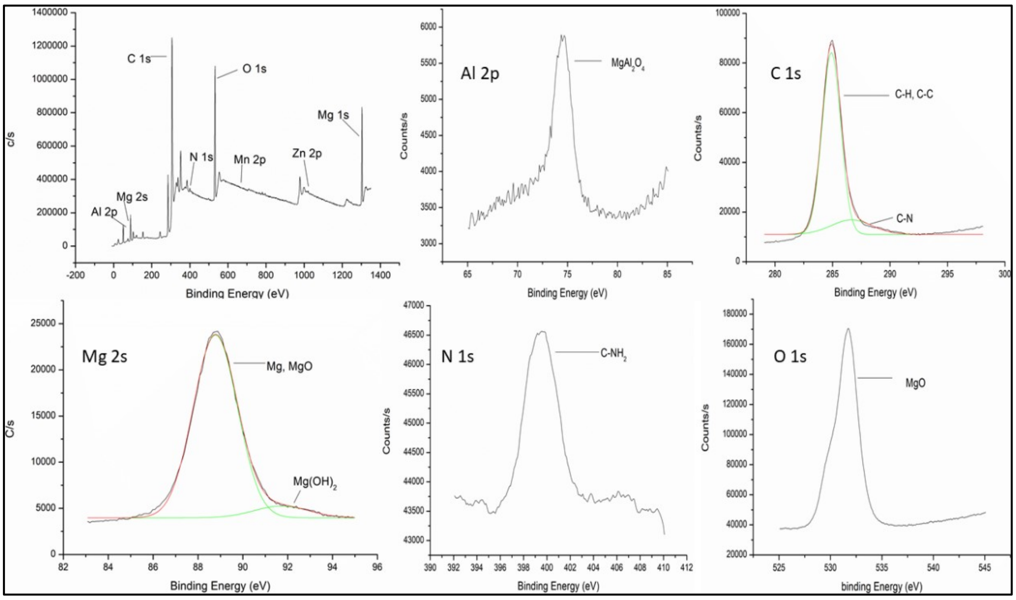

Fig. 3.83: XPS survey spectra and individual spectrum of elements (Mg 1s, Al 2p, C 1s, O 1s and, N 1s) of AZ31 Mg alloy immersed in 0.1 M Na_2SO_4 medium in the presence of 0.0002 M DD for 3 h at 30 °C.

The high-resolution Mg 2s spectrum for magnesium alloys immersed in DD inhibitor has peaks assigned to Mg, MgO, and $Mg(OH)_2$.

The high-resolution Mg 2s spectrum for magnesium alloys immersed in DC inhibitor has peaks assigned to Mg, MgO, and $Mg(OH)_2$. The corrosion is retarded since the peak area of Mg is larger than $Mg(OH)_2$. For O 1s spectrum, the peak ~531.2 corresponds to MgO. The Al 2p spectra show a broad peak centered at 74.7 eV which indicates the co-existence of aluminum oxide or aluminum hydroxide. The C 1s spectra can be fitted to the presence of C-C/C-H groups at peak 284.8 eV. N 1s spectrum shows a peak at 399.2 eV, which shows the presence of C-N bond. The XPS results show that the inhibitor is on the surface.

3.7.7 DFT

The optimized structure for the inhibitor, DD, was obtained using DFT calculations at the B3LYP hybrid functional model with def-TZVP basis set and presented in Fig. 3.84. The calculated parameters are presented in Table 3.135.

The structure of the molecule is optimized and the negative value of the total energy (-2.943 KeV) indicates a thermodynamically stable molecule. E_{HOMO} value of -0.78 eV for the inhibitor DD, indicates the physical adsorption as the basis for the corrosion inhibition action. The low bandgap energy suggests a higher reactivity of the inhibitor molecules, leading to their ready adsorption on AZ31 alloy surface (H. A. Videla; M. F. L. de Mele; G.Brankevich 1988)(Williams et al. 2013)(Liu et al. 2018). The high value of the dipole moment implies a stronger interaction of DD molecules with the AZ31 alloy surface.

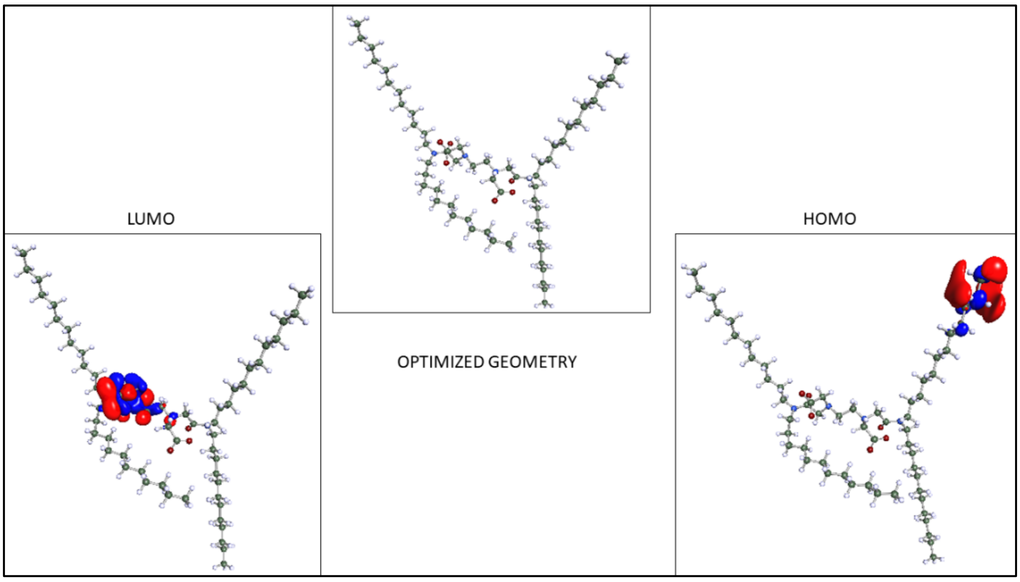

Fig. 3.84: Optimized structure and the frontier molecular orbital density distribution of the DD molecule.

3.7.8 Comparison of inhibitors efficiencies of the inhibitors

The inhibition efficiencies of the five inhibitors vary in the following order in both the media is DD > DC > DO > DH > DB. The surfactants are surface-active agents that exhibit a unique tendency to self-aggregate in solutions and at interfaces, above a definite threshold concentration. The higher inhibition has been observed in DD could be explained with the help of skeletal structure. DD could accumulate on a greater surface area of the alloy due to the presence of large alkyl chain attached to the amine group. The inhibition efficiency decreases with the decrease in the length of the alkyl chain. The inhibition efficiency of DB is least among all the studied inhibitors as it has a small alkyl chain to it compared to other inhibitors.

The examined anionic Gemini surfactants possess both a hydrophilic head and a long alkyl hydrophobic tail. The thermodynamic parameters evaluated in the present study hinted at the possible occurrence of both types of adsorption; physisorption and chemisorption during the interaction of carboxylates with AZ31 alloy surface. At the surface, there can be a strong donor-acceptor interactions might occur between the unshared electrons of the anionic Gemini surfactants and the vacant d-orbitals of the magnesium. The diacetate end of the inhibitor molecules can be chemisorbed along with the secondary phases, most likely blocking the active cathodic reaction sites and hence impede the cathodic hydrogen evolution reaction. The electrostatic interactions are most likely between the anionic head of the surfactants and magnesium ions (Mg^{2+}) confined within the defects of the surface film developed over α-Mg matrix.

The low solubility products of magnesium salts of the surfactant inhibitors are easily exceeded due to the presence of a surplus of dissolved Mg^{2+} ions, and hence the physisorbed diacetates preferentially precipitate as magnesium salts within defects of the surface film over the α-Mg matrix. The precipitates fill up the pores and appreciably rectify the defects of the surface film. The modified surface film, owing to the presence of precipitated film might also acquire hydrophobicity to some extent, which is advantageous given the tendency of the hydrophobic film to repel the aqueous electrolyte. The deviation from ideal Langmuir behavior observed for all the inhibitors hinted at the existence of intermolecular forces which in all likelihood are van der Waals interactions existing between the long alkyl chains of adsorbed inhibitor molecules. Such mutual interactions might further contribute towards the densification of the film. To sum up, the inhibitors are instrumental in the formation of a compact modified surface film over α-Mg matrix, which subsequently impedes the anodic reaction of magnesium dissolution through an enhanced barrier effect against electrolyte ingress. This mechanism suggesting the compaction of the surface film on the addition of inhibitors is corroborated by some results of the study, like the Bode phase angle plots and the impedance parameters such as film resistance, film capacitance whose variations collectively pointed out the augmentation of the barrier effect, the resistance and the thickness of the surface film in the presence of the inhibitors.

To be able to explain the inhibition performance of the investigated anionic Gemini surfactants, we scanned the selectivity descriptors and molecular reactivity for these inhibitors. In this study, some quantum calculations were carried out to explain the mode of adsorption of the five studied compounds. The optimized geometry of the anionic Gemini surfactants and their HOMO and LUMO distributions were shown in each sections. According to the frontier molecular orbital theory, E_{HOMO} is connected with the ability of the molecule to donate the electron to the vacancy d-orbital of the alloy surface. On the other hand, E_{LUMO} is related to the electron-accepting ability of the i.e. lower its value higher would be its electron-accepting tendency from the filled metal orbitals. Based on EIS and potentiodynamic polarization measurements, the order of inhibition efficiency for the investigated surfactants is DD > DC > DO > DH > DB. It is known that E_{HOMO} negative sign has been explained by some authors to be an indication of physisorption rather than chemisorption. As the energy gap values decrease, the reactivity of the molecules increases, leading to an increase in adsorption of inhibitor molecules on the AZ31 alloy surface and consequently an increase in the inhibition efficiency. The dipole moment (μ) is another index that is predominantly utilized for the prediction of the direction of the inhibition of corrosion process. It is related to the distribution of electrons in a molecule and is the measure of polarity in a bond. The compounds with high dipole moment tend to form strong dipole-dipole interactions, intermolecular forces with the AZ31 alloy surface, leading to resulting in strong adsorption on the metal surface and hence resulting in better efficiencies. The theoretical data obtained for the inhibitors are in support of the observed trend.

3.7.9 SUMMARY

Anionic Gemini surfactant, DD, was synthesized and used as a corrosion inhibitor on AZ31 Mg alloy in different concentrations of NaCl solution and Na_2SO_4 solution. The surfactant DD acted as a mixed type of inhibitor and the inhibitor efficiency increased with the increase in the concentration of DD and decreased with the rise in temperature and the increase in the concentration of NaCl and Na_2SO_4 media. The surfactant was adsorbed predominantly through physisorption and obeyed Langmuir adsorption isotherm. The quantum chemical calculation supported the experimental observation.

Table 3.111: Electrochemical polarization parameters for the corrosion of AZ31 alloy in 0.05 M NaCl in the presence of DD at different temperatures.

Inhibitor concentration ($mmol.dm^{-3}$)	Temperature (°C)	E_{corr} vs SCE (mV)	i_{corr} ($\mu A\ cm^{-2}$)	$-\beta_c$ ($mV\ dec^{-1}$)	v_{corr} ($mm\ y^{-1}$)	η (%)
Blank	30	-1514	70.10	99	1.51	-
0.1		-1544	16.00	57	0.42	72
0.2		-1510	14.39	45	0.31	79
0.3		-1503	11.14	37	0.24	84
0.4		-1494	3.24	26	0.07	95
0.5		-1488	1.85	17	0.04	97
Blank	35	-1490	112.81	122	2.43	-
0.1		-1505	33.89	62	0.74	69
0.2		-1510	25.53	49	0.55	77
0.3		-1525	21.35	41	0.46	81
0.4		-1532	9.74	30	0.21	91
0.5		-1523	7.42	22	0.16	93
Blank	40	-1500	168.06	129	3.62	-
0.1		-1513	54.31	65	1.17	67
0.2		-1532	43.64	52	0.94	74
0.3		-1490	36.21	46	0.78	78
0.4		-1481	19.40	34	0.42	88
0.5		-1521	15.78	26	0.34	90
Blank	45	-1503	183.38	134	3.95	-
0.1		-1522	64.06	69	1.38	65
0.2		-1530	51.06	55	1.10	72
0.3		-1513	45.49	49	0.98	75
0.4		-1522	26.92	37	0.58	85
0.5		-1533	21.35	30	0.46	88
Blank	50	-1493	197.77	140	4.26	-
0.1		-1480	71.96	73	1.55	63
0.2		-1537	58.96	58	1.27	70
0.3		-1540	53.39	52	1.15	73
0.4		-1499	33.42	41	0.72	83
0.5		-1512	24.14	35	0.54	87

Table 3.112: Electrochemical polarization parameters for the corrosion of AZ31 alloy in 0.10 M NaCl in the presence of DD at different temperatures.

Inhibitor concentration (mmol.dm^{-3})	Temperature (°C)	E_{corr} vs SCE (mV)	i_{corr} (μA cm^{-2})	$-\beta_c$ (mV dec^{-1})	v_{corr} (mm y^{-1})	η (%)
Blank	30	-1483	154.03	135	3.34	-
0.1		-1531	47.20	35	1.03	69
0.2		-1535	37.40	28	0.81	75
0.3		-1519	28.90	26	0.62	81
0.4		-1471	8.38	27	0.18	94
0.5		-1464	4.42	22	0.09	97
Blank	35	-1489	171.58	141	3.73	-
0.1		-1519	56.24	33	1.21	67
0.2		-1524	42.27	31	0.90	75
0.3		-1521	37.31	28	0.80	78
0.4		-1480	22.00	28	0.47	87
0.5		-1489	11.92	18	0.25	93
Blank	40	-1502	210.77	165	4.54	-
0.1		-1498	60.31	27	1.29	65
0.2		-1491	48.35	23	1.04	72
0.3		-1515	40.16	19	0.86	76
0.4		-1544	27.62	18	0.65	82
0.5		-1483	14.70	15	0.31	91
Blank	45	-1516	225.52	162	4.90	-
0.1		-1543	80.21	21	1.72	64
0.2		-1530	68.34	20	1.47	69
0.3		-1560	57.01	18	1.22	74
0.4		-1500	39.97	17	0.85	82
0.5		-1505	29.12	16	0.62	87
Blank	50	-1490	235.47	173	5.11	-
0.1		-1520	90.20	20	1.94	61
0.2		-1517	70.41	19	1.51	70
0.3		-1532	61.62	17	1.32	74
0.4		-1489	45.81	16	0.98	80
0.5		-1499	27.90	15	0.60	88

Table 3.113: Electrochemical polarization parameters for the corrosion of AZ31 alloy in 0.15 M NaCl in the presence of DD at different temperatures.

Inhibitor concentration ($mmol.dm^{-3}$)	Temperature (°C)	E_{corr} vs SCE (mV)	i_{corr} ($\mu A\ cm^{-2}$)	$-\beta_c$ ($mV\ dec^{-1}$)	v_{corr} ($mm\ y^{-1}$)	η (%)
Blank	30	-1537	233.52	150	5.03	-
0.1		-1540	76.13	46	1.64	67
0.2		-1551	62.21	34	1.34	73
0.3		-1531	51.06	29	1.10	78
0.4		-1513	19.03	25	0.41	92
0.5		-1522	13.92	23	0.30	94
Blank	35	-1500	333.34	155	7.18	-
0.1		-1504	115.13	49	2.48	65
0.2		-1515	95.17	37	2.05	71
0.3		-1521	82.17	31	1.77	75
0.4		-1525	36.67	28	0.79	89
0.5		-1496	29.71	25	0.64	91
Blank	40	-1515	455.90	168	9.82	-
0.1		-1508	171.77	52	3.70	62
0.2		-1512	136.49	40	2.94	70
0.3		-1520	116.06	34	2.50	74
0.4		-1526	68.24	30	1.47	85
0.5		-1530	48.74	28	1.05	89
Blank	45	-1491	478.65	170	10.31	-
0.1		-1498	188.95	55	4.07	60
0.2		-1518	152.27	43	3.28	68
0.3		-1510	132.78	37	2.86	72
0.4		-1522	80.31	33	1.73	83
0.5		-1502	60.35	31	1.30	87
Blank	50	-1475	567.33	194	12.22	-
0.1		-1489	241.41	58	5.20	57
0.2		-1495	192.67	46	4.15	66
0.3		-1502	168.06	40	3.62	70
0.4		-1550	111.42	36	2.40	80
0.5		-1546	83.56	33	1.80	85

Table 3.114: Electrochemical polarization parameters for the corrosion of AZ31 alloy in 0.20 M NaCl in the presence of DD at different temperatures.

Inhibitor concentration ($mmol.dm^{-3}$)	Temperature (°C)	E_{corr} vs SCE (mV)	i_{corr} ($\mu A\ cm^{-2}$)	$-\beta_c$ ($mV\ dec^{-1}$)	v_{corr} ($mm\ y^{-1}$)	η (%)
Blank	30	-1500	432.55	189	9.40	-
0.1		-1515	152.27	49	3.28	65
0.2		-1521	120.70	38	2.60	72
0.3		-1530	109.10	33	2.35	75
0.4		-1525	48.74	28	1.05	89
0.5		-1540	35.28	24	0.76	92
Blank	35	-1485	457.04	214	9.93	-
0.1		-1499	164.81	52	3.55	64
0.2		-1521	147.63	40	3.18	68
0.3		-1526	129.06	36	2.78	72
0.4		-1534	59.42	31	1.28	87
0.5		-1540	45.49	26	0.98	90
Blank	40	-1483	489.13	181	10.63	-
0.1		-1490	196.38	55	4.23	60
0.2		-1498	162.49	42	3.50	67
0.3		-1513	137.88	39	2.97	72
0.4		-1522	83.56	34	1.80	83
0.5		-1536	64.06	29	1.38	87
Blank	45	-1511	687.77	211	14.75	-
0.1		-1520	285.52	57	6.15	58
0.2		-1525	240.49	45	5.18	65
0.3		-1530	204.27	42	4.40	70
0.4		-1527	134.63	37	2.90	80
0.5		-1532	102.13	32	2.20	85
Blank	50	-1497	709.98	171	15.43	-
0.1		-1512	306.41	60	6.60	57
0.2		-1530	263.23	48	5.67	63
0.3		-1524	228.41	44	4.92	68
0.4		-1532	155.52	40	3.35	78
0.5		-1537	120.70	35	2.60	83

Table 3.115: Electrochemical polarization parameters for the corrosion of AZ31 alloy in 0.25 M NaCl in the presence of DD at different temperatures.

Inhibitor concentration ($mmol.dm^{-3}$)	Temperature (°C)	E_{corr} vs SCE (mV)	i_{corr} ($\mu A\ cm^{-2}$)	$-\beta_c$ ($mV\ dec^{-1}$)	v_{corr} ($mm\ y^{-1}$)	η (%)
Blank	30	-1526	520.41	190	11.31	-
0.1		-1538	194.06	70	4.18	63
0.2		-1543	156.45	64	3.37	70
0.3		-1545	134.63	51	2.90	74
0.4		-1504	67.31	43	1.45	87
0.5		-1515	52.46	30	1.13	90
Blank	35	-1515	553.44	192	12.03	-
0.1		-1548	217.27	73	4.68	61
0.2		-1531	188.02	66	4.05	66
0.3		-1528	167.13	53	3.60	70
0.4		-1510	88.21	46	1.90	84
0.5		-1499	71.96	34	1.55	87
Blank	40	-1488	577.18	188	12.54	-
0.1		-1495	243.73	76	5.25	58
0.2		-1522	208.91	68	4.50	64
0.3		-1525	186.63	55	4.02	68
0.4		-1532	104.45	48	2.25	82
0.5		-1538	86.81	36	1.87	85
Blank	45	-1510	706.61	209	15.22	-
0.1		-1515	319.41	78	6.88	56
0.2		-1535	274.84	70	5.92	61
0.3		-1540	245.13	57	5.28	65
0.4		-1544	144.85	51	3.12	79
0.5		-1516	118.38	39	2.55	83
Blank	50	-1494	792.81	186	17.23	-
0.1		-1511	366.77	81	7.90	54
0.2		-1531	333.34	73	7.18	58
0.3		-1550	304.09	60	6.55	62
0.4		-1532	189.88	55	4.09	76
0.5		-1509	150.88	42	3.25	81

Table 3.116: Electrochemical polarization parameters for the corrosion of AZ31 alloy in 0.05 M Na_2SO_4 in the presence of DD at different temperatures.

Inhibitor concentration (mmol dm^{-3})	Temperature (°C)	E_{corr} vs SCE (mV)	i_{corr} (µA cm^{-2})	$-\beta_c$ (mV dec^{-1})	v_{corr} (mm y^{-1})	η (%)
Blank	30	-1483	63.33	93	1.37	-
0.1		-1459	21.35	84	0.46	66
0.2		-1481	16.71	97	0.36	74
0.3		-1461	11.60	88	0.25	82
0.4		-1472	6.03	94	0.13	90
0.5		-1497	1.39	83	0.03	98
Blank	35	-1470	110.24	110	2.39	-
0.1		-1491	39.92	92	0.86	64
0.2		-1493	30.64	107	0.66	72
0.3		-1461	21.82	108	0.47	80
0.4		-1474	14.39	102	0.31	87
0.5		-1487	5.57	104	0.12	95
Blank	40	-1502	164.74	125	3.58	-
0.1		-1542	62.67	71	1.35	62
0.2		-1528	49.67	113	1.07	70
0.3		-1525	38.06	120	0.82	77
0.4		-1530	24.60	104	0.53	85
0.5		-1523	12.99	117	0.28	92
Blank	45	-1465	179.03	154	3.89	-
0.1		-1544	71.96	90	1.55	60
0.2		-1562	58.96	118	1.27	67
0.3		-1535	45.03	95	0.97	75
0.4		-1535	30.64	101	0.66	83
0.5		-1533	17.64	128	0.38	90
Blank	50	-1481	190.03	144	4.13	-
0.1		-1552	80.31	88	1.73	58
0.2		-1552	68.71	142	1.48	64
0.3		-1564	51.06	115	1.10	73
0.4		-1523	36.21	119	0.78	81
0.5		-1528	22.74	114	0.49	88

Table 3.117: Electrochemical polarization parameters for the corrosion of AZ31 alloy in 0.10 M Na_2SO_4 in the presence of DD at different temperatures.

Inhibitor concentration (mmol.dm^{-3})	Temperature (°C)	E_{corr} vs SCE (mV)	i_{corr} (µA cm^{-2})	$-\beta_c$ (mV dec^{-1})	v_{corr} (mm y^{-1})	η (%)
Blank	30	-1482	71.21	117	1.54	-
0.1		-1492	29.71	112	0.64	58
0.2		-1468	21.82	109	0.47	69
0.3		-1462	15.78	111	0.34	77
0.4		-1461	8.35	105	0.18	88
0.5		-1457	3.24	106	0.07	95
Blank	35	-1528	157.60	134	3.42	-
0.1		-1507	74.74	127	1.61	52
0.2		-1498	59.42	120	1.28	62
0.3		-1496	32.49	122	0.70	79
0.4		-1480	25.99	116	0.56	83
0.5		-1450	9.28	111	0.20	94
Blank	40	-1485	191.24	140	4.15	-
0.1		-1519	90.99	131	1.96	52
0.2		-1504	82.17	126	1.77	57
0.3		-1514	46.42	112	1.00	75
0.4		-1513	35.74	110	0.77	81
0.5		-1512	18.57	115	0.40	90
Blank	45	-1481	202.71	150	4.40	-
0.1		-1496	101.21	124	2.18	50
0.2		-1514	89.13	118	1.92	56
0.3		-1519	51.06	112	1.10	75
0.4		-1516	40.85	107	0.88	80
0.5		-1518	18.57	102	0.40	90
Blank	50	-1456	208.41	157	4.53	-
0.1		-1509	106.78	135	2.30	49
0.2		-1514	100.74	130	2.17	52
0.3		-1503	58.03	122	1.25	72
0.4		-1503	44.10	120	0.95	79
0.5		-1530	22.28	101	0.48	89

Table 3.118: Electrochemical polarization parameters for the corrosion of AZ31 alloy in 0.15 M Na_2SO_4 in the presence of DD at different temperatures.

Inhibitor concentration ($mmol.dm^{-3}$)	Temperature (°C)	E_{corr} vs SCE (mV)	i_{corr} ($\mu A\ cm^{-2}$)	$-\beta_c$ ($mV\ dec^{-1}$)	v_{corr} ($mm\ y^{-1}$)	η (%)
Blank	30	-1457	218.14	138	4.74	-
0.1		-1537	98.88	116	2.13	55
0.2		-1521	71.96	151	1.55	67
0.3		-1496	54.78	130	1.18	75
0.4		-1504	32.49	106	0.70	85
0.5		-1485	15.32	134	0.33	93
Blank	35	-1457	322.28	142	7.00	-
0.1		-1491	155.52	120	3.35	52
0.2		-1499	113.74	139	2.45	65
0.3		-1480	87.28	120	1.88	73
0.4		-1505	58.03	140	1.25	82
0.5		-1484	29.24	125	0.63	91
Blank	40	-1469	445.19	151	9.67	-
0.1		-1511	224.24	126	4.83	50
0.2		-1506	169.45	137	3.65	62
0.3		-1500	129.99	143	2.80	71
0.4		-1484	88.21	130	1.90	80
0.5		-1500	48.74	149	1.05	89
Blank	45	-1446	461.63	158	10.03	-
0.1		-1497	241.41	155	5.20	48
0.2		-1519	185.70	141	4.00	60
0.3		-1511	148.56	155	3.20	68
0.4		-1490	102.13	157	2.20	78
0.5		-1500	64.99	158	1.40	86
Blank	50	-1448	546.62	170	11.88	-
0.1		-1493	291.09	161	6.27	47
0.2		-1501	229.81	140	4.95	58
0.3		-1500	191.74	148	4.13	65
0.4		-1498	132.31	153	2.85	76
0.5		-1463	88.21	122	1.90	84

Table 3.119: Electrochemical polarization parameters for the corrosion of AZ31 alloy in 0.20 M Na_2SO_4 in the presence of DD at different temperatures.

Inhibitor concentration (mmol.dm^{-3})	Temperature (°C)	E_{corr} vs SCE (mV)	i_{corr} (µA cm^{-2})	$-\beta_c$ (mV dec^{-1})	v_{corr} (mm y^{-1})	η (%)
Blank	30	-1505	235.63	152	5.12	-
0.1		-1451	109.10	150	2.35	54
0.2		-1481	82.63	151	1.78	65
0.3		-1474	64.06	144	1.38	73
0.4		-1515	40.39	113	0.87	83
0.5		-1494	20.89	127	0.45	91
Blank	35	-1493	354.34	158	7.70	-
0.1		-1513	174.09	154	3.75	51
0.2		-1511	131.85	137	2.84	63
0.3		-1496	103.06	151	2.22	71
0.4		-1476	64.06	152	1.38	82
0.5		-1494	39.46	146	0.85	89
Blank	40	-1489	470.87	164	10.23	-
0.1		-1516	241.41	157	5.20	49
0.2		-1523	183.38	122	3.95	61
0.3		-1507	146.24	158	3.15	69
0.4		-1513	94.24	132	2.03	80
0.5		-1516	61.28	135	1.32	87
Blank	45	-1472	542.13	172	11.23	-
0.1		-1510	276.23	123	5.95	47
0.2		-1529	213.56	132	4.60	59
0.3		-1497	171.77	117	3.70	67
0.4		-1511	119.31	112	2.57	77
0.5		-1548	76.60	111	1.65	85
Blank	50	-1480	672.86	197	14.62	-
0.1		-1533	364.44	135	7.85	46
0.2		-1533	291.09	135	6.27	57
0.3		-1525	236.77	118	5.10	65
0.4		-1530	169.45	122	3.65	75
0.5		-1529	113.74	123	2.45	83

Table 3.120: Electrochemical polarization parameters for the corrosion of AZ31 alloy in 0.25 M Na_2SO_4 in the of DD presence at different temperatures.

Inhibitor concentration (mmol.dm^{-3})	Temperature (°C)	E_{corr} vs SCE (mV)	i_{corr} (µA cm^{-2})	$-\beta_c$ (mV dec^{-1})	v_{corr} (mm y^{-1})	η (%)
Blank	30	-1451	372.80	147	8.10	-
0.1		-1482	180.13	106	3.88	52
0.2		-1486	134.63	145	2.90	64
0.3		-1472	104.45	114	2.25	72
0.4		-1448	71.03	139	1.53	81
0.5		-1493	40.85	136	0.88	89
Blank	35	-1411	497.12	158	10.80	-
0.1		-1500	250.70	138	5.40	50
0.2		-1455	194.99	136	4.20	61
0.3		-1511	149.49	134	3.22	70
0.4		-1499	99.81	143	2.15	80
0.5		-1487	59.42	153	1.28	88
Blank	40	-1438	516.71	170	11.23	-
0.1		-1500	269.27	155	5.80	48
0.2		-1516	213.56	135	4.60	59
0.3		-1501	166.20	140	3.58	68
0.4		-1478	118.38	152	2.55	77
0.5		-1445	71.96	157	1.55	86
Blank	45	-1486	583.03	190	12.67	-
0.1		-1513	316.62	151	6.82	46
0.2		-1505	253.02	149	5.45	57
0.3		-1515	198.70	110	4.28	66
0.4		-1500	146.70	134	3.16	75
0.5		-1489	92.85	181	2.00	84
Blank	50	-1463	727.89	201	15.82	-
0.1		-1492	403.91	163	8.70	45
0.2		-1499	329.62	163	7.10	55
0.3		-1488	262.31	167	5.65	64
0.4		-1482	197.31	164	4.25	73
0.5		-1493	131.38	148	2.83	82

Table 3.121: Electrochemical impedance parameters for the corrosion of AZ31 alloy in 0.05 M NaCl in the presence of DD at different temperatures.

Inhibitor Concentration (mmol dm^{-3})	Temperature (°C)	R_{hf} (Ω cm^2)	R_f (Ω cm^2)	R_{dif} (Ω cm^2)	C_{dl} (μF cm^{-2})	C_f (μF cm^{-2})	η (%)
Blank	30	580	296	225	138	177	-
0.1		2077	1919	1001	89	73	72
0.2		2764	2577	1103	65	67	79
0.3		3706	3589	1556	53	48	84
0.4		8934	8744	3867	44	40	94
0.5		11345	11092	4787	35	35	95
Blank	35	550	255	207	153	181	-
0.1		1794	1611	802	92	76	69
0.2		2389	2195	1085	74	70	77
0.3		2875	2701	1343	59	52	81
0.4		4961	4766	2255	47	45	89
0.5		5533	5412	2201	39	39	90
Blank	40	422	231	184	161	188	-
0.1		1280	1104	766	95	81	67
0.2		1647	1523	843	78	75	74
0.3		1913	1764	887	63	59	78
0.4		3405	3213	1501	53	50	88
0.5		4430	4296	2108	43	44	90
Blank	45	340	191	150	170	192	-
0.1		974	833	415	99	87	65
0.2		1211	1107	559	83	79	72
0.3		1359	1205	600	69	64	75
0.4		2311	2209	1100	56	55	85
0.5		2840	2734	1252	49	49	88
Blank	50	318	160	131	171	198	-
0.1		860	744	352	104	92	63
0.2		1061	940	458	87	83	70
0.3		1200	1101	574	74	69	73
0.4		1915	1810	902	60	58	83
0.5		2507	2302	1177	53	50	87

Table 3.122: Electrochemical impedance parameters for the corrosion of AZ31 alloy in 0.10 M NaCl in the presence of DD at different temperatures.

Inhibitor Concentration (mmol dm^{-3})	Temperature (°C)	R_{hf} (Ω cm^2)	R_f (Ω cm^2)	R_{dif} (Ω cm^2)	C_{dl} (µF cm^{-2})	C_f (µF cm^{-2})	η (%)
Blank	30	507	232	209	166	172	-
0.1		1655	1381	787	116	82	69
0.2		2039	1870	943	67	68	75
0.3		2692	2541	1205	56	50	81
0.4		6923	6701	3104	47	41	93
0.5		9200	8941	3500	32	27	94
Blank	35	380	192	168	181	179	-
0.1		1156	1011	503	131	93	67
0.2		1550	1403	701	77	75	75
0.3		1710	1524	703	69	57	78
0.4		2891	2633	1109	53	48	87
0.5		4912	4781	2116	44	32	92
Blank	40	366	173	142	191	183	-
0.1		1047	938	465	148	99	65
0.2		1318	1202	610	85	83	72
0.3		1510	1400	705	73	79	76
0.4		2011	1903	953	61	63	82
0.5		3610	3477	1561	51	55	89
Blank	45	351	152	115	195	185	-
0.1		980	807	401	157	105	64
0.2		1128	1051	515	93	93	69
0.3		1349	1215	601	81	86	74
0.4		1922	1780	843	69	68	81
0.5		2651	2487	1240	57	59	87
Blank	50	301	139	108	200	191	-
0.1		780	640	318	168	111	61
0.2		1017	916	443	114	102	70
0.3		1161	1033	508	101	93	74
0.4		1533	1406	701	89	77	80
0.5		2510	2395	1159	71	64	88

Table 3.123: Electrochemical impedance parameters for the corrosion of AZ31 alloy in 0.15 M NaCl in the presence of DD at different temperatures.

Inhibitor Concentration (mmol dm^{-3})	Temperature (°C)	R_{hf} (Ω cm^2)	R_f (Ω cm^2)	R_{dif} (Ω cm^2)	C_{dl} (μF cm^{-2})	C_f (μF cm^{-2})	η (%)
Blank	30	358	170	144	172	115	-
0.1		1087	905	450	122	85	67
0.2		1339	1255	621	72	72	73
0.3		1619	1502	750	58	57	77
0.4		3711	3621	1611	50	45	90
0.5		4451	4319	2101	43	33	92
Blank	35	301	161	121	184	128	-
0.1		853	700	346	124	86	64
0.2		1028	915	452	75	75	71
0.3		1210	1099	532	59	60	75
0.4		2711	2603	1288	53	48	89
0.5		3512	3381	1514	46	36	91
Blank	40	288	150	113	197	133	-
0.1		760	613	301	127	89	62
0.2		971	866	418	78	77	70
0.3		1111	997	354	62	64	74
0.4		1981	1806	896	55	51	85
0.5		2711	2600	1279	48	39	89
Blank	45	225	128	100	201	140	-
0.1		567	422	210	130	93	60
0.2		702	600	300	83	79	68
0.3		810	645	318	66	66	72
0.4		1343	1203	601	57	54	83
0.5		1704	1578	665	50	42	87
Blank	50	130	88	73	218	147	-
0.1		301	196	96	132	95	57
0.2		386	207	112	85	82	66
0.3		450	228	119	68	69	70
0.4		651	496	245	59	56	80
0.5		871	711	357	54	45	85

Table 3.124: Electrochemical impedance parameters for the corrosion of AZ31 alloy in 0.20 M NaCl in the presence of DD at different temperatures.

Inhibitor Concentration (mmol dm^{-3})	Temperature (°C)	R_{hf} (Ω cm^2)	R_f (Ω cm^2)	R_{dif} (Ω cm^2)	C_{dl} (μF cm^{-2})	C_f (μF cm^{-2})	η (%)
Blank	30	170	109	95	193	191	-
0.1		488	235	122	125	86	65
0.2		618	503	250	111	77	72
0.3		680	570	261	94	70	75
0.4		1560	1430	710	87	64	89
0.5		2112	2008	1010	72	55	92
Blank	35	166	97	79	190	199	-
0.1		459	222	114	127	89	64
0.2		521	264	129	113	80	68
0.3		600	365	159	96	74	72
0.4		1271	1143	600	90	67	87
0.5		1574	1407	703	76	58	89
Blank	40	158	90	70	212	210	-
0.1		398	202	100	130	92	60
0.2		476	269	134	116	84	67
0.3		564	400	200	99	77	72
0.4		929	797	373	93	70	83
0.5		1241	1115	553	80	63	87
Blank	45	125	78	58	220	219	-
0.1		301	179	95	135	95	58
0.2		358	195	100	118	86	65
0.3		420	330	163	105	80	70
0.4		621	504	251	95	74	79
0.5		838	711	353	84	67	85
Blank	50	103	73	52	243	232	-
0.1		240	105	65	138	98	57
0.2		279	154	77	121	90	63
0.3		327	185	100	108	85	68
0.4		476	242	120	98	78	78
0.5		606	499	274	88	70	83

Table 3.125: Electrochemical impedance parameters for the corrosion of AZ31 alloy in 0.25 M NaCl in the presence of DD at different temperatures.

Inhibitor Concentration (mmol dm^{-3})	Temperature (°C)	R_{hf} (Ω cm^2)	R_f (Ω cm^2)	R_{dif} (Ω cm^2)	C_{dl} (µF cm^{-2})	C_f (µF cm^{-2})	η (%)
Blank	30	201	115	99	205	195	-
0.1		550	422	212	127	88	63
0.2		667	528	252	114	83	70
0.3		776	613	301	101	76	74
0.4		1538	1405	700	90	71	87
0.5		1998	1816	904	81	68	90
Blank	35	150	107	85	217	205	-
0.1		386	238	104	128	91	61
0.2		445	322	163	115	86	66
0.3		501	386	174	104	81	70
0.4		961	800	400	93	77	84
0.5		1193	1066	523	85	72	87
Blank	40	141	98	72	221	222	-
0.1		337	190	88	130	94	58
0.2		390	231	103	117	90	64
0.3		442	228	116	106	85	68
0.4		763	602	300	95	80	82
0.5		930	719	360	87	75	85
Blank	45	105	81	68	230	223	-
0.1		239	105	79	131	96	56
0.2		270	140	84	119	92	61
0.3		300	162	92	109	88	65
0.4		497	188	100	97	83	79
0.5		618	480	249	90	78	83
Blank	50	99	70	55	248	239	-
0.1		215	106	69	134	100	54
0.2		238	121	73	122	97	58
0.3		261	177	87	113	91	62
0.4		419	232	110	101	87	76
0.5		522	340	175	95	82	81

Table 3.126: Electrochemical impedance parameters for the corrosion of AZ31 alloy in 0.05 M Na_2SO_4 in the presence of DD at different temperatures.

Inhibitor Concentration (mmol dm^{-3})	Temperature (°C)	R_{hf} (Ω cm^2)	R_f (Ω cm^2)	R_{dif} (Ω cm^2)	C_{dl} (μF cm^{-2})	C_f (μF cm^{-2})	η (%)
Blank	30	609	471	412	159	102	-
0.1		1809	1688	935	45	81	66
0.2		2363	2216	1102	41	78	74
0.3		3368	3241	1620	38	75	82
0.4		5895	5712	2341	36	70	90
0.5		12913	12765	4990	33	67	98
Blank	35	510	367	303	176	129	-
0.1		1417	1303	650	48	83	64
0.2		1835	1701	887	44	82	72
0.3		2612	2461	1210	40	78	80
0.4		3851	3714	1800	37	74	87
0.5		8913	8766	3977	35	70	95
Blank	40	477	333	288	201	146	-
0.1		1252	1109	501	51	87	62
0.2		1593	1389	663	47	84	70
0.3		2092	1890	975	42	80	77
0.4		3280	3131	1623	39	76	85
0.5		4795	4616	2204	36	73	92
Blank	45	450	350	275	225	151	-
0.1		1137	1004	500	54	91	60
0.2		1384	1209	600	50	88	67
0.3		1825	1611	806	46	85	75
0.4		2617	2457	1144	42	79	83
0.5		4393	4200	2103	38	77	90
Blank	50	412	354	252	261	168	-
0.1		980	806	400	57	95	58
0.2		1147	1056	524	53	90	64
0.3		1522	1402	700	50	88	73
0.4		2074	1833	911	45	83	81
0.5		3381	3219	1503	42	80	88

Table 3.127: Electrochemical impedance parameters for the corrosion of AZ31 alloy in 0.10 M Na_2SO_4 in the presence of DD at different temperatures.

Inhibitor Concentration (mmol dm^{-3})	Temperature (°C)	R_{hf} (Ω cm^2)	R_f (Ω cm^2)	R_{dif} (Ω cm^2)	C_{dl} (µF cm^{-2})	C_f (µF cm^{-2})	η (%)
Blank	30	460	343	319	201	188	-
0.1		1101	956	451	50	89	58
0.2		1500	1307	650	41	82	69
0.3		2027	1866	923	37	79	77
0.4		3340	3221	1510	33	71	86
0.5		7049	6833	3190	26	69	93
Blank	35	432	322	293	224	191	-
0.1		896	923	460	65	90	52
0.2		1146	1002	500	58	84	62
0.3		2204	2100	1081	51	79	80
0.4		2542	2407	1225	46	73	83
0.5		5812	5700	2602	42	70	93
Blank	40	403	254	227	249	225	-
0.1		846	712	348	68	92	52
0.2		935	820	411	60	85	57
0.3		1642	1477	735	53	80	75
0.4		2127	2033	1005	49	76	81
0.5		3822	3710	1502	47	71	89
Blank	45	387	193	160	269	237	-
0.1		776	623	309	77	100	50
0.2		876	700	350	74	88	55
0.3		1576	1377	759	69	82	75
0.4		1968	1781	965	63	77	80
0.5		3810	3644	1222	60	74	90
Blank	50	373	209	161	278	241	-
0.1		732	604	300	89	104	49
0.2		779	731	362	72	98	52
0.3		1327	1206	600	68	90	72
0.4		1808	1674	842	58	83	79
0.5		3396	3230	1810	47	78	89

Table 3.128: Electrochemical impedance parameters for the corrosion of AZ31 alloy in 0.15 M Na_2SO_4 in the presence of DD at different temperatures.

Inhibitor Concentration (mmol dm^{-3})	Temperature (°C)	R_{hf} (Ω cm^2)	R_f (Ω cm^2)	R_{dif} (Ω cm^2)	C_{dl} (µF cm^{-2})	C_f (µF cm^{-2})	η (%)
Blank	30	434	420	383	244	167	-
0.1		970	806	400	54	93	55
0.2		1321	1207	602	50	88	67
0.3		1757	1600	800	45	81	75
0.4		2893	2734	1341	41	77	85
0.5		4512	4301	2100	38	70	90
Blank	35	463	300	280	278	169	-
0.1		966	824	410	68	95	52
0.2		1331	1205	600	61	90	65
0.3		1724	1578	801	54	85	73
0.4		2588	2397	1129	50	81	82
0.5		4182	4001	1989	45	76	89
Blank	40	380	230	201	299	180	-
0.1		765	659	344	73	96	50
0.2		996	811	401	64	92	61
0.3		1323	1204	1101	59	88	71
0.4		1927	1780	955	53	84	80
0.5		3381	3200	1621	47	80	89
Blank	45	273	237	200	307	188	-
0.1		526	411	209	78	99	48
0.2		690	562	251	69	94	60
0.3		860	734	359	60	90	68
0.4		1257	1108	524	56	88	78
0.5		1911	1730	873	50	83	85
Blank	50	245	200	178	321	200	-
0.1		464	308	147	92	102	47
0.2		584	412	204	86	96	58
0.3		708	583	278	81	92	65
0.4		1017	914	456	77	86	75
0.5		1506	1366	685	62	81	83

Table 3.129: Electrochemical impedance parameters for the corrosion of AZ31 alloy in 0.20 M Na_2SO_4 in the presence of DD at different temperatures.

Inhibitor Concentration (mmol dm^{-3})	Temperature (°C)	R_{hf} (Ω cm^2)	R_f (Ω cm^2)	R_{dif} (Ω cm^2)	C_{dl} (µF cm^{-2})	C_f (µF cm^{-2})	η (%)
Blank	30	301	226	171	269	179	-
0.1		653	430	210	57	96	54
0.2		877	687	335	52	91	65
0.3		1124	1015	505	48	87	73
0.4		1818	1676	834	45	80	83
0.5		2892	2751	1234	40	73	86
Blank	35	287	224	190	287	186	-
0.1		586	400	200	61	100	51
0.2		780	665	327	56	93	63
0.3		993	811	402	51	90	71
0.4		1610	1460	728	47	83	82
0.5		2590	2388	1194	42	75	89
Blank	40	259	192	163	301	191	-
0.1		510	322	158	64	102	49
0.2		669	440	224	59	95	61
0.3		843	621	316	54	92	69
0.4		1316	1201	600	50	86	80
0.5		1983	1775	901	45	79	86
Blank	45	236	203	167	321	201	-
0.1		444	217	179	69	105	47
0.2		578	431	218	62	98	59
0.3		716	600	300	58	95	67
0.4		1035	950	477	53	90	77
0.5		1585	1362	741	48	84	85
Blank	50	218	187	159	333	219	-
0.1		406	222	102	71	106	46
0.2		507	251	132	65	100	57
0.3		622	339	147	60	97	64
0.4		875	611	312	56	93	75
0.5		1280	1102	508	51	87	82

Table 3.130: Electrochemical impedance parameters for the corrosion of AZ31 alloy in 0.25 M Na_2SO_4 in the presence of DD at different temperatures.

Inhibitor Concentration (mmol dm^{-3})	Temperature (°C)	R_{hf} (Ω cm^2)	R_f (Ω cm^2)	R_{dif} (Ω cm^2)	C_{dl} (µF cm^{-2})	C_f (µF cm^{-2})	η (%)
Blank	30	392	301	280	320	240	-
0.1		818	688	338	63	100	52
0.2		1093	951	457	60	94	64
0.3		1411	1279	634	56	89	72
0.4		2098	1922	910	53	84	81
0.5		3492	3316	1520	48	80	89
Blank	35	350	250	221	333	259	-
0.1		703	612	301	66	104	50
0.2		896	705	344	62	97	60
0.3		1172	1065	529	59	90	70
0.4		1786	1631	802	55	88	80
0.5		2912	2785	1329	50	82	87
Blank	40	201	114	96	345	267	-
0.1		386	208	102	69	107	48
0.2		494	389	177	64	100	59
0.3		631	517	260	60	93	68
0.4		873	705	351	58	90	77
0.5		1422	1310	605	54	85	86
Blank	45	180	109	80	359	280	-
0.1		332	125	88	72	110	46
0.2		420	319	162	67	94	57
0.3		531	400	200	63	91	66
0.4		722	621	313	60	90	75
0.5		1137	1004	500	57	88	84
Blank	50	170	100	64	389	308	-
0.1		311	188	80	75	108	45
0.2		377	156	88	70	98	54
0.3		477	250	133	66	93	64
0.4		634	489	240	63	92	73
0.5		947	755	371	61	90	82

Table 3.131: Activation parameters for the corrosion of AZ31 alloy in NaCl solutions containing different concentrations of DD inhibitor.

Concentration of NaCl (M)	Concentration of inhibitor (mmol dm^{-3})	E_a (kJ mol^{-1})	$\Delta H^{\#}$ (kJ mol^{-1})	$\Delta S^{\#}$ (J mol^{-1} K^{-1})
0.05	Blank	34.00	34.66	-128.69
	0.1	58.13	55.53	-71.49
	0.2	61.28	58.68	-63.51
	0.3	69.27	66.67	-39.40
	0.4	91.23	88.64	24.94
	0.5	100.30	97.71	41.70
0.1	Blank	24.55	20.97	-162.88
	0.1	28.32	23.74	-166.46
	0.2	31.96	25.72	-162.22
	0.3	32.99	28.80	-153.87
	0.4	65.40	62.81	-49.69
	0.5	71.92	72.63	-23.84
0.15	Blank	23.57	18.70	-174.42
	0.1	34.35	30.23	-106.00
	0.2	35.36	31.75	-96.85
	0.3	41.14	32.77	-87.46
	0.4	62.56	57.99	-73.16
	0.5	63.59	59.96	-29.76
0.20	Blank	20.67	18.08	-167.27
	0.1	31.69	29.09	-91.03
	0.2	33.21	30.62	-86.79
	0.3	40.50	37.91	-82.22
	0.4	51.18	48.58	-66.84
	0.5	53.29	50.69	-41.31
0.25	Blank	16.94	15.30	-175.67
	0.1	23.77	21.18	-143.58
	0.2	28.05	25.46	-135.01
	0.3	30.02	27.42	-133.27
	0.4	39.41	36.82	-120.30
	0.5	40.08	37.48	-106.08

Table 3.132: Activation parameters for the corrosion of AZ31 alloy in Na_2SO_4 solutions containing different concentrations of DD inhibitor.

Concentration of Na_2SO_4 (M)	Concentration of inhibitor (mmol dm^{-3})	E_a (kJ mol^{-1})	$\Delta H^{\#}$ (kJ mol^{-1})	$\Delta S^{\#}$ (J mol^{-1} K^{-1})
0.05	Blank	44.17	40.04	−108.74
	0.1	53.42	50.83	-99.10
	0.2	57.32	54.73	-82.30
	0.3	60.85	58.25	-71.63
	0.4	71.45	68.85	-32.72
	0.5	111.04	107.94	-86.96
0.1	Blank	39.64	33.78	-126.03
	0.1	47.03	44.62	-98.93
	0.2	50.09	49.93	-87.79
	0.3	56.90	54.54	-68.50
	0.4	64.91	62.55	-51.12
	0.5	77.36	76.27	-13.71
0.15	Blank	35.65	28.33	-137.09
	0.1	42.67	40.08	-106.00
	0.2	46.14	43.54	-96.85
	0.3	49.70	47.10	-87.46
	0.4	55.24	52.65	-73.16
	0.5	70.34	63.46	-29.76
0.20	Blank	35.21	23.87	-149.98
	0.1	46.89	44.29	-91.03
	0.2	48.88	46.29	-86.79
	0.3	50.92	48.32	-82.22
	0.4	56.80	54.21	-66.83
	0.5	66.06	63.46	-41.31
0.25	Blank	24.39	18.81	-164.69
	0.1	29.80	19.55	-143.58
	0.2	33.12	27.21	-135.01
	0.3	34.32	30.52	-133.27
	0.4	39.26	36.67	-120.30
	0.5	44.96	42.36	-106.08

Table 3.133: Thermodynamic parameters for the adsorption of DD compound on AZ31 alloy in NaCl solution.

Concentration of Na_2SO_4 (M)	Temperature (°C)	ΔG^0_{ads} (kJ mol^{-1})	ΔH^0_{ads} (kJ mol^{-1})	ΔS^0_{ads} (J mol^{-1} K^{-1})
0.05	30	-34.82	-58.22	-77.2
	35	-34.44		
	40	-34.05		
	45	-33.67		
	50	-33.28		
0.1	30	-34.23	-49.51	-50.4
	35	-33.98		
	40	-33.73		
	45	-33.48		
	50	-33.23		
0.15	30	-30.31	-47.16	-55.6
	35	-30.03		
	40	-29.75		
	45	-29.47		
	50	-29.20		
0.20	30	-31.66	-46.69	-49.6
	35	-31.41		
	40	-31.16		
	45	-30.91		
	50	-30.66		
0.25	30	-30.93	-45.60	-48.4
	35	-30.69		
	40	-30.45		
	45	-30.20		
	50	-29.96		

Table 3.134: Thermodynamic parameters for the adsorption of DD compound on AZ31 alloy in Na_2SO_4 solution.

Concentration of Na_2SO_4 (M)	Temperature (°C)	ΔG^0_{ads} (kJ mol^{-1})	ΔH^0_{ads} (kJ mol^{-1})	ΔS^0_{ads} (J mol^{-1} K^{-1})
0.05	30	-33.49	-58.70	-83.2
	35	-33.07		
	40	-32.65		
	45	-32.24		
	50	-31.82		
0.1	30	-30.80	-46.86	-53.0
	35	-30.53		
	40	-30.27		
	45	-30.00		
	50	-29.74		
0.15	30	-30.01	-40.14	-33.4
	35	-29.85		
	40	-29.68		
	45	-29.51		
	50	-29.35		
0.20	30	-29.57	-39.88	-34.0
	35	-29.40		
	40	-29.23		
	45	-29.06		
	50	-28.89		
0.25	30	-32.87	-38.64	-33.2
	35	-28.58		
	40	-28.24		
	45	-28.08		
	50	-27.91		

Table 3.135: DFT parameters for DD compound.

Parameters	Value
Total energy (KeV)	-2.943
Energy gap (eV)	2.665
E_{HOMO} (eV)	-0.780
E_{LUMO} (eV)	-3.404
Dipole moment (Debye)	91.802
Electronegativity (eV)	2.072
Electron affinity (eV)	3.404
Ionization potential (eV)	0.780

CHAPTER-4

SUMMARY AND CONCLUSIONS

CHAPTER 4

SUMMARY AND CONCLUSION

4.1 SUMMARY

The corrosion behavior of AZ31 Mg alloy in sodium chloride and sodium sulfate media was confirmed. The complete investigation was an electrochemical impedance technique for understanding the overall phenomenon. The environmental factors like ionic concentration of the medium, solution temperature, and pH were varied to grasp the influence of each of these factors on the anodic dissolution of AZ31 Mg alloy. Moreover, studying the AZ31 alloy corrosion in different temperatures was helpful for the evaluation of the activation parameters. The continuance of a partly protective corrosion product surface film, having a remarkable impact on the corrosion behavior of AZ31 alloy was declared from the results of electrochemical and surface analyses studies.

Five long-chain alkyl diacetates; DB, DH, DO, DC, and DD were studied for their efficacy to resist corrosion of magnesium alloy AZ31 Mg alloy in sodium chloride and sodium sulfate solution. The inhibition tests were conducted at various medium concentrations and solution temperatures to find out the effect of ionic concentration of the media and that of temperature on the inhibition efficiency of the diacetates. At every varying inhibitor concentration in a range to establish the optimum concentration for inhibition. The examination involving different inhibitors appears to produce results that helped to comprehend the impact of molecular structure of the inhibitor on the inhibition efficiency. The activation and thermodynamic parameters and DFT (Theoretical) were evaluated to support a complete apprehension of alloy dissolution and interfacial adsorption, respectively. The trends in the variation of all the electrochemical, activation, and thermodynamic parameters reported in the study have been accounted concisely.

Anodic dissolution of magnesium and cathodic hydrogen evolution is inhibited by the addition of anionic Gemini surfactants namely DB, DH, DO, DC, and DD in NaCl and Na_2SO_4 solution. Adsorption of surfactants in the corrosion product is set to form a hydrophobic outer corrosion layer. The efficiency of the inhibitors was demonstrated by potentiodynamic polarization and electrochemical impedance spectroscopy and supported by surface analysis and theoretical calculations.

Potentiodynamic polarization plots indicate that all the five inhibitors used show a mixed-type corrosion inhibitor suppressing both anodic and cathodic reactions. The adsorption film formed after the introduction of the inhibitor is supported by SEM-EDX and XPS. Both adsorption and chemical reaction between the inhibitor and AZ31 Mg alloys result in the formation of a film on the alloy surface. It is in agreement with the XPS and theoretical results. A significant increase in the inhibition efficiency is seen when inhibitors concentration increases to an optimum concentration level, beyond which the increase in the inhibition efficiency is negligible. As the temperature of the system increases, there is a decrease in the inhibition efficiency of surfactant inhibitors. In economic concentration, DD showed the highest inhibition efficiency followed by DC, DO, DH and DB. The difference in aliphatic chains of inhibitors attributes to the change in its inhibition efficiency as it controls over the solubility product of magnesium salts.

The electrochemical results along with SEM-EDX and XPS analysis were taken into consideration for suggesting a credible mechanism for inhibition of AZ31 alloy corrosion by alkyl chains. The chemisorption of the diacetates at the cathodic phases was surmised to block the active reaction sites on the alloy surface, thereby resulting in cathodic inhibition. The anodic inhibition was considered to ensue as a consequence of compaction and thickening of the porous surface film at anodic phases through precipitation of magnesium diacetates. Such densification was supposed to add the barrier effect of the surface film against the electrolyte ingress. The slight deviation from ideal Langmuir behavior was observed and was attributed to intermolecular forces like van der Waals interactions existing between the long alkyl chains of the adsorbed diacetate molecules. Such mutual interactions were believed to further contribute towards the densification of the film. The theoretical studies (DFT) were performed to support the experimental studies which significantly showed the efficiency of diacetate inhibitors.

4.2 CONCLUSIONS

From the above results and discussion, the main conclusions can be summarized in the following points:

1. A higher ionic concentration, higher temperature, and acidic pH bring about destabilization and dissolution of the corrosion product surface film; hence accelerating the rate of AZ31 alloy corrosion.
2. The corrosion kinetics follows Arrhenius law in both the media.
3. The corrosion behavior of AZ31 Mg alloy in sodium chloride and sodium sulfate solutions is strongly influenced by the medium pH. The corrosion rate decreases with the increase in medium pH. The relatively high corrosion resistance in basic solutions is attributed to the formation of the stable $Mg(OH)_2$ barrier film on the alloy surface.
4. The inhibitors, DB, DH, DO, DC, and DD act as mixed-type inhibitors. The increase in inhibition efficiency with the increase in the inhibitor concentration is maximum up to an optimum concentration above which the increase in inhibition efficiency is negligible.
5. The increase in temperature decreases the inhibition efficiency of the inhibitors.
6. The adsorption of the inhibitor molecules on the alloy surface is principally physisorption and complies with the Langmuir adsorption isotherm.
7. The surfactant DD exhibits the highest inhibition efficiency followed by DC, DO, DH, and DB.

4.3 SCOPE FOR FUTURE WORK

1. The corrosion behavior and inhibition of different heat-treated AZ31 Mg alloys can be explored.
2. To carry out electrochemical investigations on AZ31 Mg alloy in media containing living cells and proteins in order to use it in medical implants.
3. The electrochemical studies can be carried out by varying the immersion time, corrosive medium, and deoxygenated environment to understand the efficiency of the surface film during long exposure periods.
4. The negative difference effect (NDE) can be experimentally verified by comparing the results of the present electrochemical study with those derived from weight loss or hydrogen evolution measurements.

REFERENCES

REFERENCES

Abd El Rehim, S. S., Hassan, H. H., and Amin, M. A. (2003). "The corrosion inhibition study of sodium dodecyl benzene sulphonate to aluminium and its alloys in 1.0 M HCl solution." *Mater. Chem. Phys.*, 78(2), 337–348.

Acharya, M. G., and Shetty, A. N. (2019). "The corrosion behavior of AZ31 alloy in chloride and sulfate media – A comparative study through electrochemical investigations." *J. Magnes. Alloy.*, 7(1), 98–112.

Achouri, M. El, Infante, M. R., Izquierdo, F., Kertit, S., Gouttaya, H. M., and Nciri, B. (2001). "Synthesis of some cationic gemini surfactants and their inhibitive effect on iron corrosion in hydrochloric acid medium." *Corros. Sci.*, 43(1), 19–35.

Aiad, I. A., Hafiz, A. A., El-Awady, M. Y., and Habib, A. O. (2010). "Some imidazoline derivatives as corrosion inhibitors." *J. Surfactants Deterg.*, 13(3), 247–254.

Antropov, L. I. (1967). "A correlation between kinetics of corrosion and the mechanism of inhibition by organic compounds." *Corros. Sci.*, 7(9), 607–620.

Ardelean, H., Frateur, I., and Marcus, P. (2008). "Corrosion protection of magnesium alloys by cerium, zirconium and niobium-based conversion coatings." *Corros. Sci.*, 50(7), 1907–1918.

Awad, H. S., and Turgoose, S. (2004). "Influence of hardness salts on the effectiveness of zinc-1 hydroxyethylidene 1, 1 diphosphonic acid (HEDP) mixtures in inhibiting the corrosion of mild steel in neutral oxygen-containing solutions." *Corrosion*, 60(12), 1168–1179.

Ayawei, N., Ebelegi, A. N., and Wankasi, D. (2017). "Modelling and Interpretation of Adsorption Isotherms." *J. Chem.*, (W. Guo, ed.), 2017, 3039817.

Baghni, I. M., Wu, Y.-S., Li, J.-Q., and Zhang, W. (2004). "Corrosion behavior of magnesium and magnesium alloys." *Trans. Nonferrous Met. Soc. China (English Ed.*, 14(1), 1–10.

Baril, G., and Pébère, N. (2001). "The corrosion of pure magnesium in aerated and deaerated sodium sulphate solutions." *Corros. Sci.*, 43(3), 471–484.

Barnartt, S. (1969). "Linear corrosion kinetics." *Corros. Sci.*, 9(3), 145–156.

Beni, G. F. De. (1967). "Magnesium alloys in terphenyls — Corrosion inhibitors." *J. Nucl. Mater.*, 22(2), 158–164.

Bentiss, F., Lebrini, M., and Lagrenée, M. (2005). "Thermodynamic characterization of metal dissolution and inhibitor adsorption processes in mild steel/2,5-bis(n-thienyl)-1,3,4-thiadiazoles/hydrochloric acid system." *Corros. Sci.*, 47(12), 2915–2931.

Bereket, G., Gülec, M., and Yurt, A. (2006). "Inhibition efficiencies of some organic compounds on the corrosion of zinc in alkaline media." *Anti-Corrosion Methods Mater.*

Bezaatpour, D. S. A., and Basharnavaz, A. N. S. H. (2016). "Experimental and Theoretical Studies to Examine the Inhibition Effect of a Schiff Base Against Magnesium Corrosion." *Trans. Indian Inst. Met.*, 69(8), 1545–1555.

Bradford, S. A., and Bringas, J. E. (1993). *Corrosion control*. Springer.

Branzoi, V., Pruna, A., and Branzoi, F. (2008). "Inhibition Effects of Some Organic Compounds on Zinc Corrosion in 3.5% NaCl." *Rev. Chim. Ed.*, 59(5), 540.

Cao, X., Li, Z., Song, X., Cui, X., Wei, Y., Cheng, F., and Wang, J. (2009). "Effects of spacers on surface activities and aggregation properties of anionic gemini surfactants." *J. Surfactants Deterg.*, 12(2), 165–172.

Chen, J., Song, Y., Shan, D., and Han, E.-H. (2015). "Influence of alloying elements and microstructure on the formation of hydrotalcite film on Mg alloys." *Corros. Sci.*, 93, 90–99.

Chen, Y., Li, J., Yang, W., Gao, S., and Cao, R. (2019). "Applied Surface Science Enhanced corrosion protective performance of graphene oxide-based composite fi lms on AZ31 magnesium alloys in 3 . 5 wt % NaCl solution." *Appl. Surf. Sci.*, 493(August 2018), 1224–1235.

CHENG, Y., QIN, T., WANG, H., and ZHANG, Z. (2009). "Comparison of corrosion behaviors of AZ31, AZ91, AM60 and ZK60 magnesium alloys." *Trans. Nonferrous Met. Soc. China*, 19(3), 517–524.

Choi, S., and Pyo, M. (2016). "corrosion inhibition of AZ31 magnesium alloy." *Eval. Program Plann.*, 1–8.

Chou, D.-T., Hong, D., Oksuz, S., Schweizer, R., Roy, A., Lee, B., Shridhar, P., Gorantla, V., and Kumta, P. N. (2019). "Corrosion and bone healing of Mg-Y-Zn-Zr-Ca alloy implants: Comparative in vivo study in a non-immobilized rat femoral fracture model." *J. Biomater. Appl.*, 33(9), 1178–1194.

Cordoba, L. C., Hélary, C., Montemor, F., and Coradin, T. (2019). "Bi-layered silane-TiO2/collagen coating to control biodegradation and biointegration of Mg alloys." *Mater. Sci. Eng. C*, 94, 126–138.

Cui, F., Yang, J., Jiao, Y., Yin, Q., Zhang, Y., and Lee, I.-S. (2008). "Calcium phosphate coating on magnesium alloy for modification of degradation behavior." *Front. Mater. Sci. China*, 2(2), 143–148.

Ćurković, L., Ćurković, H. O., Salopek, S., Renjo, M. M., and Šegota, S. (2013). "Enhancement of corrosion protection of AISI 304 stainless steel by nanostructured sol–gel TiO2 films." *Corros. Sci.*, 77, 176–184.

Dang, N., Wei, Y. H., Hou, L. F., Li, Y. G., and Guo, C. L. (2015). "Investigation of the inhibition effect of the environmentally friendly inhibitor sodium alginate on magnesium alloy in sodium chloride solution." (11), 1354–1362.

Dinodi, N., and Nityananda Shetty, A. (2013). "Electrochemical investigations on the corrosion behaviour of magnesium alloy ZE41 in a combined medium of chloride and sulphate." *J. Magnes. Alloy.*, 1(3), 201–209.

Dinodi, N., and Nityananda Shetty, A. (2014). "Investigation of influence of medium ph and sulfate ion concentrations on corrosion behavior of magnesium alloy ZE41." *Surf. Eng. Appl. Electrochem.*, 50(2), 149–156.

Dinodi, N., and Shetty, A. N. (2014). "Alkyl carboxylates as efficient and green inhibitors of magnesium alloy ze41 corrosion in aqueous salt solution." *Corros. Sci.*, 85, 411–427.

Farhat A. Ansari, M. A. Q. (2010). "Inhibitive Performance of Gemini Surfactants as

Corrosion Inhibitors for Mild Steel in Formic Acid." *Port. Electrochim. Acta*, 28(5), 321–335.

Fawzy, A., Abdallah, M., Zaafarany, I. A., Ahmed, S. A., and Althagafi, I. I. (2018). "Thermodynamic, kinetic and mechanistic approach to the corrosion inhibition of carbon steel by new synthesized amino acids-based surfactants as green inhibitors in neutral and alkaline aqueous media." *J. Mol. Liq.*, 265, 276–291.

Fletcher, S. (1994). "Tables of Degenerate Electrical Networks for Use in the Equivalent-Circuit Analysis of Electrochemical Systems." *J. Electrochem. Soc.*, 141(7), 1823–1826.

Fontana, M. G. (2005). *Corrosion engineering*. New Delhi: Tata McGraw-Hill.

Frignani, A., Grassi, V., Zanotto, F., and Zucchi, F. (2012). "Inhibition of AZ31 Mg alloy corrosion by anionic surfactants." *Corros. Sci.*, 63, 29–39.

Fuchs-Godec, R. (2009). "Effects of surfactants and their mixtures on inhibition of the corrosion process of ferritic stainless steel." *Electrochim. Acta*, 54(8), 2171–2179.

Gad, E. A. M., Azzam, E. M. S., and Halim, S. A. (2018). "Theoretical approach for the performance of 4-mercapto-1-alkylpyridin-1-ium bromide as corrosion inhibitors using DFT." *Egypt. J. Pet.*, 27(4), 695–699.

Gao, G., and Liang, C. (2007). "Electrochemical and DFT studies of β-amino-alcohols as corrosion inhibitors for brass." *Electrochim. Acta*, 52(13), 4554–4559.

Gece, G. (2008). "The use of quantum chemical methods in corrosion inhibitor studies." *Corros. Sci.*, 50(11), 2981–2992.

Ghali, E., Dietzel, W., and Kainer, K.-U. (2004). "General and localized corrosion of magnesium alloys: a critical review." *J. Mater. Eng. Perform.*, 13(1), 7–23.

Gräfen, H., Horn, E., Schlecker, H., and Schindler, H. (2000). "Corrosion, 3. Corrosion Protection and Testing." *Ullmann's Encycl. Ind. Chem.*

Greene, N. D., Bishop, C. R., and Stern, M. (1961). "Corrosion and electrochemical behavior of chromium-noble metal alloys." *J. Electrochem. Soc.*, 108(9), 836.

Gu, X.-N., and Zheng, Y.-F. (2010). “A review on magnesium alloys as biodegradable materials.” *Front. Mater. Sci. China*, 4(2), 111–115.

Gupta, M., and Ling, S. N. M. (2011). *Magnesium, magnesium alloys, and magnesium composites*. John Wiley & Sons.

H. A. Videla; M. F. L. de Mele; G.Brankevich. (1988). “Technical Note: Assessment of Corrosion and Microfouling of Several Metals in Polluted Seawater.” *Corrosion*, 44(7), 423–426.

Hadisaputra, S., Purwoko, A. A., Savalas, L. R. T., Prasetyo, N., Yuanita, E., and Hamdiani, S. (2020). “Quantum Chemical and Monte Carlo Simulation Studies on Inhibition Performance of Caffeine and Its Derivatives against Corrosion of Copper.” *Coatings*, 10(11), 1086.

Hanas, T., Kumar, T. S. S., Perumal, G., and Doble, M. (2016). “Tailoring degradation of AZ31 alloy by surface pre-treatment and electrospun PCL fibrous coating.” *Mater. Sci. Eng. C*, 65, 43–50.

Hassan, R. M., and Ibrahim, S. M. (2021). “Performance and efficiency of methyl-cellulose polysaccharide as a green promising inhibitor for inhibition of corrosion of magnesium in acidic solutions.” *J. Mol. Struct.*, 1246, 131180.

Heakal, F. E. T., Shehata, O. S., and Tantawy, N. S. (2012). “Enhanced corrosion resistance of magnesium alloy AM60 by cerium(III) in chloride solution.” *Corros. Sci.*, 56, 86–95.

Hu, J. Y., Song, X. Q., Zhang, Z., Zeng, D. Z., Shi, T. H., and Gao, J. F. (2015). “The corrosion inhibition behaviors of 2 0 - hydroxy - acetophenone for AZ91D magnesium alloy.” (4), 396–404.

Huang, K., Cai, S., Xu, G., Ye, X., Dou, Y., Ren, M., and Wang, X. (2013). “Preparation and characterization of mesoporous 45S5 bioactive glass–ceramic coatings on magnesium alloy for corrosion protection.” *J. Alloys Compd.*, 580, 290–297.

Idris, M. N., Daud, A. R., Othman, N. K., and Jalar, A. (2013). “Corrosion control by benzyl triethylammonium chloride: effects of temperature and its concentration." *Int. J. Eng. Technol*, 13(03), 47–51.

Ishizaki, T., Masuda, Y., and Sakamoto, M. (2011). "Corrosion resistance and durability of superhydrophobic surface formed on magnesium alloy coated with nanostructured cerium oxide film and fluoroalkylsilane molecules in corrosive NaCl aqueous solution." *Langmuir*, 27(8), 4780–4788.

Iwanaga, K., Tashiro, H., Okamoto, H., and Shimizu, K. (2004). "Improvement of formability from room temperature to warm temperature in AZ-31 magnesium alloy." *J. Mater. Process. Technol.*, 155–156(1–3), 1313–1316.

Jia'an, W., Jiahe, W., and Zhongxiao, S. (2017). "Microstructures and Microsegregation of Directionally Solidified Mg-1.5Gd Magnesium Alloy with Different Growth Rates." *Rare Met. Mater. Eng.*, 46(1), 12–16.

Kaczerewska, O., Leiva-Garcia, R., Akid, R., Brycki, B., Kowalczyk, I., and Pospieszny, T. (2019). "Heteroatoms and π electrons as favorable factors for efficient corrosion protection." *Mater. Corros.*, 70(6), 1099–1110.

Kellou-Kerkouche, F., Benchettara, A., and Amara, S. (2008). "Some imidazoline derivatives as corrosion inhibitors." *Mater. Chem. Phys.*, 110(1), 26–33.

King, A. D., Birbilis, N., and Scully, J. R. (2014). "Accurate Electrochemical Measurement of Magnesium Corrosion Rates; a Combined Impedance, Mass-Loss and Hydrogen Collection Study." *Electrochim. Acta*, 121, 394–406.

Laisa, C. P., Ramesha, R. N., and Ramesha, K. (2017). "Enhanced electrochemical performance of lithium rich layered cathode materials by Ca2+ substitution." *Electrochim. Acta*, 256, 10–18.

Lamaka, S. V, Zheludkevich, M. L., Yasakau, K. A., Montemor, M. F., and Ferreira, M. G. S. (2007). "High effective organic corrosion inhibitors for 2024 aluminium alloy." *Electrochim. Acta*, 52(25), 7231–7247.

Latham, J.-A., Howlett, P. C., MacFarlane, D. R., Somers, A., and Forsyth, M. (2012). "Anodising AZ31 in a phosphonium ionic liquid: corrosion protection through composite film deposition.” *J. Electrochem. Soc.*, 159(11), C539.

Li, L. J., Yao, Z. M., Lei, J. L., Xu, H., Zhang, S. T., and Pan, F. S. (2009). “Adsorption and corrosion inhibition behavior of sodium dodecylbenzenesulfonate on AZ31 magnesium alloy.” *Wuli Huaxue Xuebao/ Acta Phys. - Chim. Sin.*, 25(7), 1332–1336.

Li, X., Weng, Z., Yuan, W., Luo, X., Wong, H. M., Liu, X., Wu, S., Yeung, K. W. K., Zheng, Y., and Chu, P. K. (2016). “Corrosion resistance of dicalcium phosphate dihydrate/poly (lactic-co-glycolic acid) hybrid coating on AZ31 magnesium alloy.” *Corros. Sci.*, 102, 209–221.

Liu, D., Song, Y., Shan, D., and Han, E.-H. (2018). “Comparison of the inhibition effect of four inhibitors on the corrosion behaviour of AM60 magnesium alloy.” *Int. J. Electrochem. Sci.*, 13(3), 2219–2235.

Liu, P., Man, Y., and Bao, Y. (2021). “Bioactive Porous Biocomposites Coated Magnesium Alloy Implant for Bone Rejuvenation Using a Fracture in Rat Model.” *Biotechnol. Bioprocess Eng.*, 26(3), 359–368.

Liu, X., Hou, L., Wang, H., Li, Y., Wei, H., and Liu, B. (2019). “diethyldithiocarbamate and sodium acetate for.” 9(1), 27–41.

Lopez, M. G., and Natta, B. (2001). “No Title.” *Corrosion*, 712, 5006–5015.

Lukovits, I., Kálmán, E., and Zucchi, F. (2001). “Corrosion Inhibitors—Correlation between Electronic Structure and Efficiency.” *Corrosion*, 57(1), 3–8.

Luo, A. A., and Sachdev, A. K. (2012). “Applications of magnesium alloys in automotive engineering.” *Adv. wrought Magnes. Alloy.*, Elsevier, 393–426.

Luo, A., and Shinoda, T. (1998). “Magnesium alloys and their applications.” *Wolfsburg, Ger. Apr*, 151–156.

Lv, J., Qiao, W., and Xiong, C. (2014). “Synthesis and Surface Properties of a pH-Regulated and pH- Reversible Anionic Gemini Surfactant.”

Mansfeld, F., Tsai, C. H., and Shih, H. (1992). “Software for simulation and analysis of electrochemical impedance spectroscopy (EIS) data.” *ASTM Spec. Tech. Publ.*, 186–196.

Marya, M., Hector, L. G., Verma, R., and Tong, W. (2006). "Microstructural effects of AZ31 magnesium alloy on its tensile deformation and failure behaviors." *Mater. Sci. Eng. A*, 418(1–2), 341–356.

Masel, R. I. (1996). *Principles of adsorption and reaction on solid surfaces*. John Wiley & Sons.

Mathaudhu, S. N., and Nyberg, E. A. (2016). "Magnesium alloys in US military applications: past, current and future solutions." *Essent. readings Magnes. Technol.*, Springer, 71–76.

Mathieu, S., Rapin, C., Hazan, J., and Steinmetz, P. (2002). "Corrosion behaviour of high pressure die-cast and semi-solid cast AZ91D alloys." *Corros. Sci.*, 44(12), 2737–2756.

McCafferty, E. (2010). *Introduction to corrosion science*. Springer US.

Medhashree, H., and Shetty, A. N. (2018). "Synergistic inhibition effect of trisodium phosphate and sodium benzoate with sodium dodecyl benzene sulphonate on the corrosion of Mg-Al-Zn-Mn alloy in 30% ethylene glycol containing chloride ions." *J. Adhes. Sci. Technol.*, 1–26.

Mejeha, I. M., Nwandu, M. C., Okeoma, K. B., Nnanna, L. A., Chidiebere, M. A., Eze, F. C., and Oguzie, E. E. (2012). "Experimental and theoretical assessment of the inhibiting action of Aspilia africana extract on corrosion aluminium alloy AA3003 in hydrochloric acid." *J. Mater. Sci.*, 47(6), 2559–2572.

Migahed, M. A., Attya, M. M., Rashwan, S. M., Abd El-Raouf, M., and Al-Sabagh, A. M. (2013). "Synthesis of some novel non ionic surfactants based on tolyltriazole and evaluation their performance as corrosion inhibitors for carbon steel." *Egypt. J. Pet.*, 22(1), 149–160.

Mobin, M., Aslam, R., and Aslam, J. (2017). "Non toxic biodegradable cationic gemini surfactants as novel corrosion inhibitor for mild steel in hydrochloric acid medium and synergistic effect of sodium salicylate: Experimental and theoretical approach." *Mater. Chem. Phys.*, 191, 151–167.

Montemor, M. F. (2014). "Functional and smart coatings for corrosion protection: A review of recent advances." *Surf. Coatings Technol.*, 258, 17–37.

Montemor, M. F., and Ferreira, M. G. S. (2007). "Electrochemical study of modified bis-[triethoxysilylpropyl] tetrasulfide silane films applied on the AZ31 Mg alloy." *Electrochim. Acta*, 52(27), 7486–7495.

Nahlé, A., Abu-Abdoun, I. I., and Abdel-Rahman, I. (2012). "Inhibition of mild steel corrosion by 3-benzoylmethyl benzimidazolium hexafluoroantimonate in acidic solution." *Int. J. Corros.*, 2012.

Niu, J., and Lee, J. Y. (2000). "A new approach for the determination of fish freshness by electrochemical impedance spectroscopy." *J. Food Sci.*, 65(5), 780–785.

Nordlien, J. H., Ono, S., Masuko, N., and Nisancioglu, K. (1997). "A TEM investigation of naturally formed oxide films on pure magnesium." *Corros. Sci.*, 39(8), 1397–1414.

Pakiet, M., Tedim, J., and Kowalczyk, I. (2019). "Functionalised novel gemini surfactants as corrosion inhibitors for mild steel in 50 mM NaCl : Experimental and theoretical insights." 580(June).

Pebere, N., Riera, C., and Dabosi, F. (1990). "Investigation of magnesium corrosion in aerated sodium sulfate solution by electrochemical impedance spectroscopy." *Electrochim. Acta*, 35(2), 555–561.

Pourbaix, M. (1974). "Atlas of electrochemical equilibria in aqueous solutions." Houston, Tex.: National Association of Corrosion Engineers.

R.V. Gadag and A. N. Shetty. (2010). *Engineering Chemistry*. IK International pvt ltd.

Saji, V. S., and Umoren, S. A. (2020). *Corrosion inhibitors in the oil and gas industry*. John Wiley & Sons.

Sastri, V. S. (1998). *Corrosion inhibitors : principles and applications*. Chichester; New York: Wiley.

Schorr, M., and Yahalom, J. (1972). "The significance of the energy of activation for the dissolution reaction of metal in acids." *Corros. Sci.*, 12(11), 867–868.

Shaban, M. M., Eid, A. M., Farag, R. K., Negm, N. A., Fadda, A. A., and Migahed, M. A. (2020). "Novel trimeric cationic pyrdinium surfactants as bi-functional corrosion inhibitors and antiscalants for API 5L X70 carbon steel against oilfield formation water." *J. Mol. Liq.*, 305, 112817.

Shaw, C., and Jones, H. (1997). "The contributions of different alloying additions to hardening in rapidly solidified magnesium alloys." *Mater. Sci. Eng. A*, 226, 856–860.

Solanki, K. N., Orlov, D., Singh, A., and Neelameggham, N. R. (2017). *Magnesium Technology 2017*. Springer.

Song, G., and Atrens, A. (2007). "Recent Insights into the Mechanism of Magnesium Corrosion and Research Suggestions." *Adv. Eng. Mater.*, 9(3), 177–183.

Song, G., Atrens, A., and Dargusch, M. (1998). "Influence of microstructure on the corrosion of diecast AZ91D." *Corros. Sci.*, 41(2), 249–273.

Song, G. L., and Atrens, A. (1999). "Corrosion Mechanisms of Magnesium Alloys." *Adv. Eng. Mater.*, 1(1), 11–33.

Standard, A. (2006). "G102-89, Standard Practice for Calculation of Corrosion Rates and Related Information from Electrochemical Measurements." *Annu. B. ASTM Stand. ASTM Int. West Conshohocken, PA*, 3.

Sun, P., Zhang, S., Pang, J., Tan, Y., Sun, D., Xia, C., Cheng, X., and Xin, X. (2018). "degradation of dye." *J. Mol. Liq.*, 272, 180–187.

Tao, Z., Zhang, S., Li, W., and Hou, B. (2009). "Corrosion inhibition of mild steel in acidic solution by some oxo-triazole derivatives." *Corros. Sci.*, 51(11), 2588–2595.

Thirugnanaselvi, S., Kuttirani, S., and Emelda, A. R. (2014). "Effect of Schiff base as corrosion inhibitor on AZ31 magnesium alloy in hydrochloric acid solution." *Trans. Nonferrous Met. Soc. China*, 24(6), 1969–1977.

Thompson, N. G., and Payer, J. H. (1998). "Corrosion Testing Made Easy—dc Electrochemical Methods." *NACE Int. Houston, TX.*

Tizpar, A., and Ghasemi, Z. (2006). "The corrosion inhibition and gas evolution studies of some surfactants and citric acid on lead alloy in 12.5 M H2SO4 solution." *Appl. Surf.*

Sci., 252(24), 8630–8634.

Tsai, S. T., Yen, K. P., and Shih, H. C. (1998). “The embrittlement of duplex stainless steel in sulfide-containing 3.5 wt% NaCl solution.” *Corros. Sci.*, 40(2), 281–295.

Tunold, R., Holtan, H., Berge, M.-B., Lasson, A., and Steen-Hansen, R. (1977). “The corrosion of magnesium in aqueous solution containing chloride ions.” *Corros. Sci.*, 17(4), 353–365.

Uhlig, H. H. (2011). “Corrosion Handbook.” *Uhlig’s Corros. Handb.*, Wiley Online Books.

Vengatesh, G., and Sundaravadivelu, M. (2019). “Non-toxic bisacodyl as an effective corrosion inhibitor for mild steel in 1 M HCl : Thermodynamic , electrochemical , SEM , EDX , AFM , FT-IR , DFT and molecular dynamics simulation studies.” *J. Mol. Liq.*, 287, 110906.

Wagner, L., Hilpert, M., Wendt, J., and Küster, B. (2003). “On methods for improving the fatigue performance of the wrought magnesium alloys AZ31 and AZ80.” *Mater. Sci. Forum*, Trans Tech Publ, 93–102.

Wang, A.-N., Yu, G.-P., and Huang, J.-H. (2014). “Fracture toughness measurement on TiN hard coatings using internal energy induced cracking.” *Surf. Coatings Technol.*, 239, 20–27.

Wang, N., WangG, R., Peng, C., Feng, Y., and Zhang, X. (2010a). “Corrosion behavior of Mg-Al-Pb and Mg-Al-Pb-Zn-Mn alloys in 3.5% NaCl solution.” *Trans. Nonferrous Met. Soc. China*, 20(10), 1936–1943.

Wang, X., Yang, H., and Wang, F. (2010b). “A cationic gemini-surfactant as effective inhibitor for mild steel in HCl solutions.” *Corros. Sci.*, 52(4), 1268–1276.

Wang, Z., and Guo, Y. (2016). “Corrosion resistance and adhesion of poly (L-lactic acid)/MgF 2 composite coating on AZ31 magnesium alloy for biomedical application.” *Russ. J. Non-Ferrous Met.*, 57(4), 381–388.

Williams, G., Dafydd, H. L., and Grace, R. (2013). “Electrochimica Acta The localised corrosion of Mg alloy AZ31 in chloride containing electrolyte studied by a scanning vibrating electrode technique." *Electrochim. Acta*, 109, 489–501.

Willumeit, R., Fischer, J., Feyerabend, F., Hort, N., Bismayer, U., Heidrich, S., and Mihailova, B. (2011). "Chemical surface alteration of biodegradable magnesium exposed to corrosion media." *Acta Biomater.*, 7(6), 2704–2715.

Yamaguchi, T., Serikawa, T., Henmi, M., Oginuma, H., and Kondoh, K. (2006). "Mg2Si coating technology on magnesium alloys to improve corrosion and wear resistance." *Mater. Trans.*, 47(4), 1026–1030.

Yohai, L., Vázquez, M., and Valcarce, M. B. (2011). "Brass corrosion in tap water distribution systems inhibited by phosphate ions." *Corros. Sci.*, 53(3), 1130–1136.

Zeng, R.-C., Hu, Y., Guan, S.-K., Cui, H.-Z., and Han, E.-H. (2014). "Corrosion of magnesium alloy AZ31: The influence of bicarbonate, sulphate, hydrogen phosphate and dihydrogen phosphate ions in saline solution." *Corros. Sci.*, 86, 171–182.

Zhao, C., Wu, H., Hou, P., Ni, J., Han, P., and Zhang, X. (2016). "Enhanced corrosion resistance and antibacterial property of Zn doped DCPD coating on biodegradable Mg." *Mater. Lett.*, 180, 42–46.

Zhao, M.-C., Liu, M., Song, G.-L., and Atrens, A. (2008a). "Influence of pH and chloride ion concentration on the corrosion of Mg alloy ZE41." *Corros. Sci.*, 50(11), 3168–3178.

Zhao, M., Liu, M., Song, G., and Atrens, A. (2008b). "Influence of pH and chloride ion concentration on the corrosion of Mg alloy ZE41." *Corros. Sci.*, 50(11), 3168–3178.

Zhu, Y., Free, M. L., Woollam, R., and Durnie, W. (2017). "Progress in Materials Science A review of surfactants as corrosion inhibitors and associated modeling." *Prog. Mater. Sci.*, 90, 159–223.

PUBLICATIONS

a) Journals

1. M. G. Acharya and A.N. Shetty, (2018) “The corrosion behavior of AZ31 alloy in chloride and sulfate media – A comparative study through electrochemical investigations.” *J. Magnes. Alloy.*, 7(1), 98–112, https:// doi.org/ 10.1016/ j.jma.2018.09.003.
2. M. G. Acharya and A. N. Shetty, (2021) “Influence of Media pH on corrosion behaviour of AZ31 magnesium alloy in chloride and sulphate media”. Surface engineering and applied electrochemistry, springer, 57, 675-688, DOI 10.3103/S1068375521060065
3. M. G. Acharya and A. N. Shetty, (2021) “Exploring the Corrosion Inhibition Properties of an Anionic Gemini Surfactant Based on an Ethylenediaminetetraacetic Acid Derivative on AZ31 Alloy.” *ChemistrySelect*, 6(32), 8275–8287.
4. M. G. Acharya and A. N. Shetty, “EDTA based gemini surfactant for AZ31 magnesium alloys in sulphate medium”. communicated.

b) Conferences

- M G Acharya, A N Shetty, “Corrosion studies of AZ31 alloy in chloride and sulphate medium”, International Conference On Emerging Trends in Chemical Sciences (ICETCS), 14-16, September 2017, Manipal, India.
- M G Acharya, A N Shetty, “Dibutyl complex as corrosion inhibitor for AZ31 magnesium alloy”, International Conference on Recent Advances in Material Chemistry (ICRAMC-19), 13-15 February, 2019, Chennai, India.
- M G Acharya, A N Shetty, “Influence of media pH in chloride and sulphate ion concentrations on corrosion behaviour of AZ31 Magnesium alloy”, Conference on Electrochemistry in Industry, Health and Environment. January 21-25, 2020, Mumbai, India.
- M G Acharya, A N Shetty, “Study of anionic surfactant as an Effective inhibitor for AZ31 Mg Alloy in 0.1 M NaCl”, Accelerating Innovations in Material Science (AIMS 2020), 4th-7th August 2020, Bengaluru, India.
- M G Acharya, A N Shetty, “Effective inhibitor- anionic dimeric surfactant for AZ31 Alloy in 0.1M NaCl medium”, CRCSA – 2020, 18 and 19th August 2020, Karnataka, India.
- M G Acharya, A N Shetty, “Influence of sodium 2,2'- (7, 16-Dihexyl-8, 15-dioxo-7,10,13,16-tetraazadocosane-10, 13-Diyl) Diacetate in sodium chloride medium on the corrosion inhibition of AZ31 magnesium alloy”, V-ICSEET-2020, 2^{nd}-4^{th} November, 2020.

CURRICULUM VITAE

GURURAJ ACHARYA M

PRESENT ADDRESS

Department of Chemistry
National Institute of Technology Karnataka
Surathkal, Mangalore-575025
Karnataka, India

PERMANENT ADDRESS

#8-11, Eshavasyam, Mundkur
village, Udupi-576121
Karnataka, India

CONTACT DETAILS

Email: mgj1992@gmail.com

Mobile: +918056289150

EDUCATION

Doctor of Philosophy (Ph.D.) Chemistry, National Institute of Technology-Karnataka, (NITK) Surathkal, India	July 2016 - present
Masters of Science (M.Sc.) General Chemistry, Madras University, Tamil Nadu, India	2015 First Class with Distinction (7.57 CGPA)
Bachelor of Science (B.Sc) Physics, Chemistry, Mathematics (PCM) Karnataka University Dharwad, Karnataka, India	2013 First Class with Distinction (7.48 CGPA)
Higher Secondary (10+2) Department of State Board, Tamil Nadu, India	2010 First Class with Distinction (83 %)

RESEARCH EXPERIENCE

07/2015 - 04/2016 (Supervisor: Dr. Geetha Bhaskar, & Dr. Suguna)	CLRI, Chennai	Research Project Assistant	Flame retardant substances
11/2012 - 01/2013 (Supervisor: Dr. Srinivasan)	SGS, Chennai	Summer Intern	Quality Control
07/2016- ongoing (Supervisor: Prof. A. N. Shetty)	National Institute of Technology-Karnataka, (NITK)- Surathkal	Doctoral Student	Corrosion Science

PERSONAL INFORMATION

Sex:	Male
Nationality:	Indian
Languages:	English, Tamil, Hindi, Kannada, French (Elementary)